Adam Mickiewicz University, Poznań, Poland

Faculty of Chemistry

Doctoral School of Exact Sciences, Chemical Sciences

Kamil Jakub Frąckowiak

From amino acids to protein - study of the effect of amino acid photo-oxidation on the model protein

Doctoral dissertation

written in Department of Chemical Physics and Photochemistry

under supervision of

prof. dr. hab. Bronisław Marciniak

dr. Marta Teresa Ignasiak-Kciuk

Poznań 2024

Uniwersytet im. Adama Mickiewicza, Poznań, Polska

Wydział Chemii

Szkoła Doktorska Nauk Ścisłych, Nauki Chemiczne

Kamil Jakub Frąckowiak

Od aminokwasów do białka – badanie wpływu fotoutleniania aminokwasów na modelowe białko

Rozprawa doktorska

napisana w Zakładzie Chemii Fizycznej i Fotochemii

pod kierunkiem

prof. dr hab. Bronisława Marciniaka

dr Marty Teresy Ignasiak-Kciuk

Poznań 2024

Acknowledgements

First and foremost, words cannot express my gratitude to my supervisors, Prof. dr. hab. Bronisław Marciniak and Dr. Marta Ignasiak-Kciuk. It is their invaluable advice, continuous support, and (especially) patience during my PhD study, that culminated in this work. Their immense knowledge and plentiful experience have encouraged me during my academic research and daily life. It is important to emphasize that without Prof. dr. hab. Bronisław Marciniak, not only I would not pursue this scientific path, but also, I would not broaden my knowledge in photochemistry. Tremendous amount of help that I received from Dr. Marta Ignasiak-Kciuk in my everyday struggles in laboratory and in life also deserves special mentioning.

I would also like to thank Prof. UAM dr. hab. Tomasz Pędziński for his knowledge in time resolved techniques and technical support on my study.

I am extremely grateful to all of the members of the Department of Physical Chemistry and Photochemistry, especially Dr. hab. Anna Lewandowska-Andrałojć and M. Eng. Katarzyna Nadzieja Grzyb. It is their kind help and support that have made my study and life in the lab a wonderful time.

This endeavor would not be possible without all scientists that have put their insight into this thesis and provided opportunity for me to further grow. Especially Prof. Michael J. Davies, Prof. Per M. Hagglund, and Dr. Eduardo Fuentes Lemus from Department of Biomedical Sciences; Inflammation, Metabolism and Oxidation; University of Copenhagen; Denmark; and Dr. Łukasz Marczak and Dr. Aleksander Strugała from Laboratory of Mass Spectrometry; Institute of Bioorganic Chemistry; Poznań; Poland.

I would like acknowledge the Department of Chemistry, Adam Mickiewicz University and Centre of Advanced Technology, Poznań, Poland for either financing my scientific endeavors, providing funding for conferences and internships, or for lending the equipment necessary for realization of this thesis.

Finally, I am deeply indebted to my parents, and my wife Anna Wychowaniec. Without their tremendous understanding and encouragement in the past few years, it would be impossible for me to complete my study.

From amino acids to protein - study of the effect of amino acid photo-oxidation on the model protein

Following research that is over a hundred years old on the photo-oxidation of proteins, this thesis provides insight into their anoxic photosensitized oxidation. Despite the considerable amount of work and effort dedicated to this topic, the quest to elucidate both mechanisms and the stable products formed during these processes remains prevalent and highly desired to be accomplished. This effort aims to further substantiate our understanding, which includes, but is not limited to, the pathogenesis of various diseases, research on possible biomarkers of the oxidative stress, and improvements in photodynamic therapies. Anoxic modifications are typically omitted during research due to expectation that they occur in a minor way in living organisms. Nevertheless, they constitute an important element of this process, and their comprehensive study is necessary and may serve as the basis for future research aimed at elucidating the impact of anoxic photosensitized oxidation.

The aim of this work was to investigate the anoxic oxidation of aromatic amino acid residues in model systems and protein – glyceraldehyde-3- phosphate dehydrogenase (GAPDH) in the presence of the sensitizer – 3-carboxybenzophenone (3CB) by examining the mechanisms and stable products. Aromatic amino acids residues in the model compounds were oxidized by 3CB in the presence of different neighboring groups to mimic the environment of the studied protein, GAPDH. The influence of the formed modifications on the activity of the GAPDH was also examined by determining the enzymatic activity assay of the protein.

Analysis of transient products formed during quenching of the 3CB* by the aromatic amino acid residues was carried out using nanosecond flash photolysis technique (LFP). The influence of blocking either amine and/or carboxylic groups on the resulting species was also determined. The resulting stable products were separated by liquid chromatography and characterized by high-resolution mass spectrometry. Results from the model systems were compared to data obtained for GAPDH, with particular emphasis on modifications of tryptophan (Trp), tyrosine (Tyr), histidine (His), and phenylalanine (Phe). The impact of GAPDH photo-oxidation in the presence of 3CB was also investigated using spectroscopic methods. Laser flash photolysis revealed differences in the quenching rate constants and quantum yield for the formation of various transient products. Trends in Tyr, His, and Trp were largely consistent with the literature, showing that the blocking of the amino group significantly affects the two former amino acids but not the latter. Experiments with Phe

demonstrated that reactions with other, more reactive amino acids present in peptide, protect the Phe, as it reacts slower with excited triplet state of the sensitizer. The identified stable products from the model systems could be categorized into three groups: (a) covalently attached CBH-amino acid adduct, (b) amino acid-amino acid dimers, and (c) other products resulting from the processes other than radical recombination following electron transfer. Mass spectrometry was used for the characterization of stable products as this functional analysis technique is most suitable for identification of stable products.

In conclusion, by analyzing various amino acid residues in the model systems, it was demonstrated that dimers are the main product formed during the oxidation of Tyr or Trp, with the number of diTyr/diTrp isomers increasing with the degree of Tyr blockage. The presence of Tyr-3CBH was seen only for some compounds, while Trp-3CBH was only present in peptidic system. Different results were obtained for His and Phe, where unblocked amino group led to the formation of products not assigned to the first two groups, namely Im-CH_2-3CBH and benzyl-Phe/benzyl-3CBH. These products are formed through the recombination of 3CBH radicals with methyl-imidazyl or benzyl radicals (as well as between benzyl radicals and Phe derivatives) generated by the homolytic cleavage of either His or Phe. It is important to note that these compounds are observed only when the amino group is unblocked (i.e., for N-terminal Phe and His compounds). The cleavage of Phe to a benzyl radical has been previously described in the literature by Bent et al. [1]. As of His, it is proposed that energy transfer from the sensitizer to the N-terminal His derivative leads to homolytic cleavage of the derivative into a methyl-imidazole radical. Another product characterized in the third group of compounds was reduced Trp or His (*m/z* -2 Da), exhibiting the formation of a C=C double bond.

The knowledge gathered from the model compounds was then applied to the photosensitized oxidation of a chosen protein, GAPDH, under anoxic conditions. The formation of a ground-state complex between GAPDH and 3CB was confirmed. SDS-PAGE provided information on the relationship between exposure time and the formation of dimers and higher polymers, allowing the selection of an appropriate exposure time for analysis. The characterization of stable products of GAPDH (by timsTOF) digested in solution and in gel after a 5-minute irradiation confirmed the formation of some products identified in the model products, such as 3CBH-amino acid. Amino acid analysis combined with the Ellman test provided insights into the reactivity of selected amino acids that are included in the sequence of GAPDH. Sulfur-containing amino acids were identified as the main source of GAPDH damage, while His and Tyr were considered as secondary targets.

The activity test showed that although GAPDH forms a ground-state complex with 3CB, it does not affect its activity significantly. Moreover, modifications of the available amino acids in solution do not markedly change the activity. The main differences arise when GAPDH is exposed to light for more than 5 minutes, resulting in more dimers and covalent polymers.

The results presented in this work demonstrate that despite over 120 years of research on protein photo-oxidation, new questions arise and there are unresolved issues. Time-resolved experiments require a more in-depth analysis of the transient products, with particular emphasis on His (no reference spectra for individual forms of the histidyl radical). Furthermore, the presented results provide further evidence for the influence of neighboring groups on the photo-oxidation mechanism. Additionally, the results from the analysis of protein stable products enrich the knowledge on the primary products of the described processes and provide evidence that despite the lack of a decrease in its activity, these products are still present.

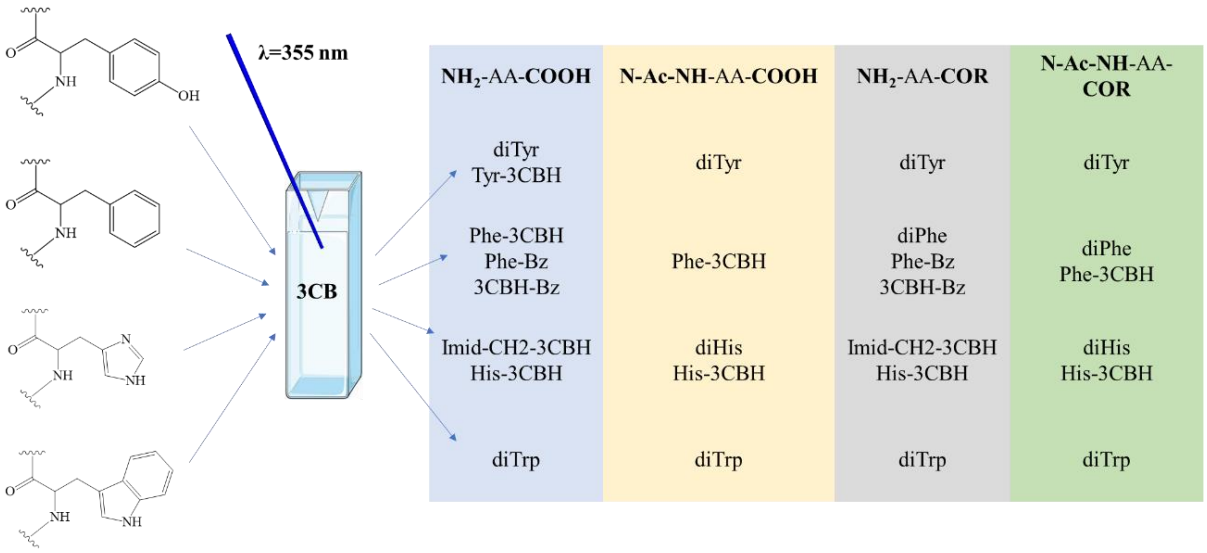

NH_2-AA-COOH	**N-Ac-NH-AA-COOH**	**NH_2-AA-COR**	**N-Ac-NH-AA-COR**
diTyr Tyr-3CBH	diTyr	diTyr	diTyr
Phe-3CBH Phe-Bz 3CBH-Bz	Phe-3CBH	diPhe Phe-Bz 3CBH-Bz	diPhe Phe-3CBH
Imid-CH2-3CBH His-3CBH	diHis His-3CBH	Imid-CH2-3CBH His-3CBH	diHis His-3CBH
diTrp	diTrp	diTrp	diTrp

Figure. *Aromatic amino acids oxidized by ^{3}3CB* under anoxic conditions with identified stable products listed in table*

Od aminokwasów do białka – badanie wpływu fotoutleniania aminokwasów na modelowe białko

Ponad sto lat badań nad fotoutlenianiem białek umożliwiło zdobycie cennych informacji dotyczących mechanizmu fotosensybilizowanego utleniania w warunkach beztlenowych oraz tworzonych produktów trwałych. Jednakże, pomimo wielu prac, nadal istnieją niezbadane jeszcze aspekty. Dlatego też potrzebne są dalsze badania obejmujące m.in. patogenezę różnych chorób, badania nad potencjalnymi biomarkerami stresu oksydacyjnego oraz nad polepszeniem terapii fotodynamicznej. Modyfikacje zachodzące w atmosferze beztlenowej są zazwyczaj pomijane przez większość badaczy ze względu na przekonanie, że zachodzą one w minimalnym stopniu w organizmach żywych. Niemniej jednak, stanowią one ważny element tego procesu, a ich kompleksowa charakterystyka jest niezbędna i może stanowić podstawę dla przyszłych badań mających na celu wyjaśnienie wpływu fotosensybilizowanego utleniania w warunkach beztlenowych.

Celem przedstawionej pracy było zbadanie procesów beztlenowego utleniania aromatycznych reszt aminokwasowych w układach modelowych i białku w obecności fotosensybilizatora, 3-karboksybenzofenonu (3CB) w stanie trypletowym, poprzez zbadanie mechanizmów i produktów trwałych. Aromatyczne reszty aminokwasowe w układach modelowych były utlenianie w obecności różnych grup, które dobrane zostały w sposób odzwierciedlający otoczenie badanego białka, dehydrogenazy aldehydu 3-fosfoglicerynowego (GAPDH). Zbadano również wpływ utworzonych modyfikacji na aktywność GAPDH poprzez wyznaczenie aktywności enzymatycznej białka.

Analiza produktów przejściowych tworzonych podczas wygaszania wzbudzonego stanu trypletowego przez aromatyczne reszty aminokwasowe wykonana została z wykorzystaniem techniki nanosekundowej fotolizy błyskowej (LFP). Określono także wpływ blokady grup funkcyjnych (aminowej, karboksylowej lub obu) na powstałe indywidua przejściowe. Powstałe produkty trwałe rozdzielono z wykorzystaniem metod chromatograficznych i zcharakteryzowano przez wysokorozdzielczą spektrometrię mass. Wyniki z układów modelowych porównano do danych otrzymanych dla GAPDH, ze szczególnym uwzględnieniem modyfikacji na Trp, Tyr, His i Phe. Zbadano także wpływ fotoutleniania GAPDH w obecności 3CB na jego aktywność wykorzystując metody spektrofotometryczne.

Laserowa fotoliza błyskowa wykazała różnice w stałych szybkości wygaszania i wydajności kwantowej tworzenia różnych przejściowych produktów. Pojawiające się trendy w Tyr, His i Trp są w dużej zgodności z literaturą, gdzie blokowanie grupy aminowej ma duży

wpływ na dwa pierwsze aminokwasy (Tyr i His) i brak wpływu na ten ostatni. Eksperymenty z udziałem fenyloalaniny pokazały, że obecność innych, bardziej reaktywnych reszt aminokwasowych w peptydzie chroni ją przed utlenianiem, ze względu ich na większą reaktywność względem trypletu sensybilizatora. W przypadku obecności alifatycznych reszt aminokwasowych obok Phe, jego utleniane wydaje się być szybsze, gdy obie grupy są zablokowane, jednak obniża się wtedy wydajność kwantowa powstawania przejściowych produktów.

Zidentyfikowano produkty trwałe, które dla układów modelowych można podzielić na trzy grupy: (a) kowalencyjnie przyłączony addukt 3CBH-aminokwas, (b) dimery aminokwas-aminokwas oraz (c) pozostałe produkty, które nie przypisano do żadnej z powyższych grup, a wynikają z procesów innych niż rekombinacja rodników powstałych po przeniesieniu elektronu. Do charakterystyki produktów trwałych zastosowano spektrometrię mas, jako że ta technika analizy funkcjonalnej jest najlepsza w przypadku charakterystyki produktów trwałych. W skrócie, analizując kolejne reszty aminokwasowe w układach modelowych wykazano, że głównym produktem tworzonym podczas utleniania Tyr i Trp są dimery, które w zależności od struktury związku mogą występować w różnych formach izomerycznych. Wykazano także, że im bardziej zablokowana struktura Tyr, czy też Trp, tym więcej izomerów diTyr/diTrp jest tworzone. Produkt Tyr-3CBH obserwowany był tylko dla niektórych związków, gdzie produkt Trp-3CBH był obecny wyłącznie w mieszaninie poreakcyjnej peptydu. Odmienne wyniki uzyskano dla His i Phe, gdzie odblokowana grupa aminowa prowadzi do utworzenia produktów nie przypisanych do dwóch pierwszych grup, a mianowicie produkt Im-CH_2-3CBH oraz benzyl-Phe /benzyl-3CBH. Produkty te tworzone są poprzez rekombinację rodników 3CBH z rodnikami metylo-imidazolowym lub benzylowym (oraz pomiędzy rodnikami benzylowymi i pochodnymi Phe), które powstały w wyniku homolitycznego rozpadu tych związków. Należy tutaj podkreślić fakt, że związki te obserwowane są jedynie w przypadku, gdy grupa aminowa jest odblokowana (a więc dla N-końcowych związków Phe i His). Rozpad Phe do rodnika benzylowego został opisany wcześniej w literaturze przez Bent'a et al. [1]. W przypadku His postuluje się przeniesienie energii z sensybilizatora na N-końcową pochodną His prowadzące do homolitycznego rozpadu pochodnej do rodnika metylo-imidazolowego. Innym produktem scharakteryzowanym w trzeciej grupie związków był zredukowany Trp lub His (*m/z* -2 Da), wykazujący tworzenie wiązania podwójnego C=C.

Zwieńczeniem tej pracy było zastosowanie zebranej wiedzy ze związków modelowych do fotosensybilizowanego utleniania w warunkach beztlenowych wybranego białka – GAPDH. Potwierdzono utworzenie kompleksu w stanie podstawowym pomiędzy GAPDH i 3CB. Elektroforeza SDS-PAGE dostarczyła informacji na temat zależności pomiędzy czasem naświetlania, a tworzeniem dimerów i wyższych polimerów, oraz pozwoliła dobrać odpowiedni czas naświetlania do analiz. Charakterystyka produktów trwałych (timsTOF) próbek trawionych w roztworze i próbek trawionych w żelu po analizie SDS 5-minutowego naświetlania roztworu GAPDH potwierdziła tworzenie części produktów zidentyfikowanych w produktach modelowych, takich jak 3CBH-aminokwas. Analiza aminokwasowa w połączeniu z testem Ellmana dostarczyła wglądu w reaktywność wybranych aminokwasów budujących GAPDH. Aminokwasy zawierające siarkę są głównym źródłem uszkodzeń GAPDH, podczas gdy His i Tyr stanowią drugorzędny cel.

Test aktywności wykazał, że chociaż GAPDH tworzy kompleks w stanie podstawowym z 3CB, nie wpływa to na jego aktywność, ponadto modyfikacje dostępnych dla roztworu aminokwasów nie zmieniają znacząco aktywności. Główne różnice występują, gdy GAPDH jest naświetlane przez ponad 5 minut, co skutkuje większą liczbą dimerów i kowalencyjnych polimerów.

Wyniki przedstawione w tej pracy dowodzą, że pomimo 120 lat badań nad fotoutlenianiem białek, wciąż nasuwają się nowe pytania i istnieją nierozwiązane zagadnienia. Eksperymenty czasowo-rozdzielcze wymagają bardziej dogłębnej analizy przejściowych produktów, ze szczególnym naciskiem na His (brak widm wzorcowych dla poszczególnych form rodnika histydylowego). Ponadto przedstawione wyniki dostarczają dalszych dowodów wpływu grup sąsiednich na mechanizm fotoutleniania. Dodatkowo, wyniki z analizy produktów trwałych białka wzbogacają wiedzę na temat pierwotnych produktów opisanych procesów i stanowią dowód na to, że mimo braku spadku jego aktywności, te produkty wciąż są obecne.

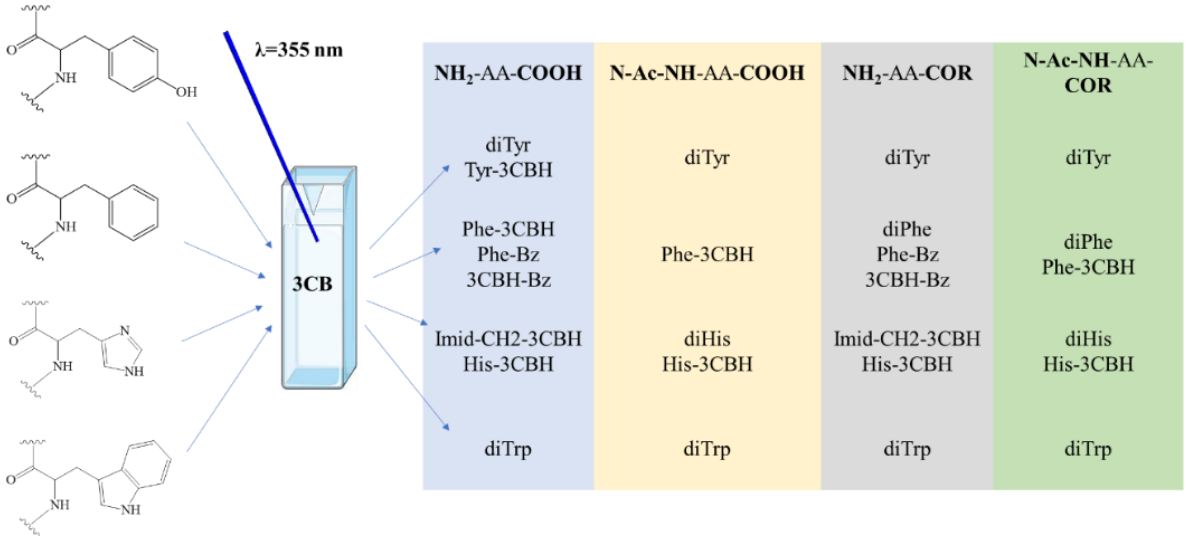

NH_2-AA-COOH	N-Ac-NH-AA-COOH	NH_2-AA-COR	N-Ac-NH-AA-COR
diTyr Tyr-3CBH	diTyr	diTyr	diTyr
Phe-3CBH Phe-Bz 3CBH-Bz	Phe-3CBH	diPhe Phe-Bz 3CBH-Bz	diPhe Phe-3CBH
Imid-CH2-3CBH His-3CBH	diHis His-3CBH	Imid-CH2-3CBH His-3CBH	diHis His-3CBH
diTrp	diTrp	diTrp	diTrp

Rycina. *Aromatyczne aminokwasy, których fotosensibilizowane utlenianie w warunkach beztlenowych było badane w tej pracy. W tabeli obok przedstawiono produkty trwałe powstałe w trakcie tego procesu dla poszczególnych pochodnych*

CONTENT:

Abbreviations:

$\alpha S^{\bullet}$	Methionine radical located on carbon adjacent to sulfur atom
ΔA	Observed absorbance change
ΔA_T^0	Absorption change in the actinometer immediately after the laser pulse at 520 nm, i.e. at the maximum of the triplet absorption
τ_T	Triplet lifetime of the benzophenone or its derivative in a presence of a quencher
τ_T^0	Triplet lifetime of the 3CB without a quencher
Φ	Quantum yield
^{1}3CB*	Excited singlet state of 3-carboxybenzophenon
^{1}AA*	Excited singlet state of amino acid
$^1O_2$	Excited singlet state of oxygen
^{1}PS*	Excited singlet state of photosensitizer
^{3}3CB*	Excited triplet state of 3-carboxybenzophenon
^{3}AA*	Excited triplet state of amino acid
$^3O_2$	Triplet state of oxygen
3CB	3-carboxybenzophenon
$3CB^{\bullet-}$	Carboxybenzophenone radical anion
$3CBH^{\bullet}$	Carboxybenzophenone ketyl radical
^{3}PS*	Excited triplet state of photosensitizer
4CB	4-carboxybenzophenon
AA	Amino acid
$AA^{\bullet+}$	Amino acid radical cation
$AlaC_{\beta}^{\bullet}$	Alanyl radical located on carbon-β in amino acid
$Cys_2SS^{\bullet-}$	Cystine disulfide radical anion
$CysS^{\bullet}$	Cysteine thiol radical
DTT	Dithiothreitol
ET	Electron transfer
ER	Endoplasmic reticulum
FRET	Förster resonance energy transfer
G3P	Glyceralderhyde-3-phosphate
GAPDH	Glyceraldehyde-3-phosphate dehydrogenase

HAT	Hydrogen Atom Transfer
$HisNH^{\bullet+}$	Histydyl radical cation
$HisN^{\bullet}$	Histydyl radical
HPLC	High Performance Liquid Chromatography
IAA	Iodoacetamide
ISC	Inter-system Crossing
k_{obs}	Observed rate constant
k_q	Quenching rate constant
MALDI	Matrix-assisted laser desorption ionization
$Met_2(S\therefore S)^+$	Three electron intermolecular bond located between two sulfur atoms
$MetS^{\bullet+}$	Sulfur radical cation on methionine
$Met(S\therefore N)^+$	Three electron intramolecular bond located between sulfur and nitrogen atoms
MS	Mass spectrometry
MSA	Methanesulfonic acid
NAD^+	Nicotinamide adenine dinucleotide oxidized form
NADH	Nicotinamide adenine dinucleotide reduced form
$O_2^{\bullet-}$	Oxygen radical anion
PDT	Photodynamic therapy
PMT	Photomultiplier
PS	Photo-sensitizer, in this work 3-carboxybenzophenon
$PS^{\bullet-}$	Radical anion of photo-sensitizer, in this work 3-carboxybenzophenone
Q	Quencher
ROS	Reactive oxygen species
RNS	Reactive nitrogen species
TCA	Trichloro acetic acid
TFA	Trifluoro acetic acid
$TrpN^{\bullet}$	Tryptophanyl radical
$TrpNH^{\bullet+}$	Tryptophanyl radical cation
$TyrO^{\bullet}$	Tyrosyl radical
$TyrOH^{\bullet+}$	Tyrosyl radical cation
U	Voltage measured immediately after laser pulse
U_0	Baseline voltage

I. Introduction and the aim of the work

Most studies point to Oscar Raab's 1900 discovery as the first confirmation of suspicions regarding light-induced harm, which trace back to earlier reports in 1883 by Dammann and in 1887 by Wedding (who observed rashes on sheep in areas where they lacked skin pigment) [2]. These findings demonstrated that illuminated cells containing the fluorescent dye eosin began to die, a phenomenon absent without of light or chromophore. Raab's mentor, von Tappeiner, later continued this discovery, leading to the development of the first form of photodynamic therapy in 1904. Despite the initial success, refining this method continued throughout almost the entire 20th century [3].

Tappeiner's research demonstrated that the choice of sensitizer, along with its corresponding wavelength, did not matter. Therefore, research focused on the toxic factor for cells [2]. Initially, the toxicity of these substances was attributed to the presence of oxygen and its reactive forms (reactive oxygen species, ROS), and as a result, research on other possibilities (combined with breakthrough discoveries related to laser technologies in the 1960s) [3]. In the beginning, studies were conducted on complex systems such as cells and tissues [2], thus it is not surprising that to understand the cause of cell death, simpler systems were investigated, with great emphasis on proteins and nucleic acids. Scientists of that time were well aware of a cell's composition, and attention was specifically devoted to its individual macromolecules and components.

Regarding proteins (and consequently peptides and amino acids), as stated in Leopold Weil et al.'s work [4]:

"Previous work of Lieben, Carter, Harris, Gaffron, Weil, and Maher, and Galston has demonstrated the susceptibility of aromatic amino acids to photo-oxidation".

The research conducted by these scientists initiated ongoing efforts to capture the products formed during the photo-oxidation of amino acids. Additionally, in the studies, it was observed that sulfur-containing amino acids are prone to photo-oxidation reactions [4]. Initially, the focus was on aerobic conditions, where attention was directed towards the efficiency of oxygenation of specific amino acids through the analysis of stable products [4]. The current state of knowledge on this matter will be discussed further in **Chapter I.2**.

The abundance of protein in living organisms [5] leads to the assumption that they are major target for oxidizing agents. Oxidation reactions of proteins (and consequently amino acids and peptides) can introduce complications in living organisms due to their conversion into derivatives highly susceptible to proteolytic degradation. Additionally, protein oxidation

may entail the cleavage of polypeptide chains and modification of amino acids, resulting in alterations to the structure and conformation of proteins, thereby contributing to the development of aging and various diseases (e.g. atherosclerosis or Alzheimer's)[6,7].

Extensive research into the damage caused to proteins during oxidative stress has been ongoing since the early 20th century. The identified primary protein modifications include formation of carbonyl groups, modifications to amino acids, the creation of protein-protein cross-links, the formation of sulfur bridges that can yield the loss of catalytic activity, heightened acidity, altered viscosity, reduced thermal stability, changes in fluorescence, fragmentation and an increased susceptibility to proteolysis [7].

Even though the possibility that all probable ways of anoxic photosensitized oxidation were investigated, there are still some aspects that, to some extent, eluded scientists. A comprehensive understanding of processes arising from photosensitized oxidation, with great emphasis on aromatic amino acids, holds the potential to advance various scientific domains. These include, but are not limited to, photodynamic therapy, pathogen inactivation, photocatalytic modifications, and the exploration of species that may emerge during oxidative stress. These processes play pivotal roles in numerous biologically significant phenomena, such as the pathogenesis of disease states. To mitigate biological damage in cells caused by free radicals (generated, for instance, by UV radiation), it is imperative to grasp the reaction pathways leading to such harm. Consequently, the mechanisms of photosensitized oxidation of amino acids and peptides have undergone extensive investigation. However, certain aspects remain contentious and demand further exploration, notably the ultimate fate of transient species. Therefore, the continuation of some earlier studies holds crucial importance from a scientific perspective, particularly considering the advancements in experimental techniques, with modern and more sensitive methods available currently.

I.1. Protein oxidation

Knowledge about oxidative stress continually circulates within the scientific community, and there's a compelling reason behind this interest. The life of a cell involves an ongoing struggle to preserve its equilibrium, referred to as homeostasis - a form of self-regulation within the system [8]. In the various processes involved in maintaining homeostasis in living cell, encompassing ROS or reactive nitrogen species (RNS) [9–12], along with more indirect forms of oxidants, such as the excited triplet states of sensitizers [13–15]. Nevertheless, as their concentration rises, the risk of various diseases, including atherosclerosis,

Alzheimer's, or Parkinson's also increases. Understanding the fundamental processes that occur when various components of the cell undergo oxidation is a significant challenge. ROS, RNS or other factors (e.g. UV-light) interact with amino acids, targeting those most susceptible to oxidation during oxidative stress, as outlined in **Table I.1**. Living cells maintain homeostasis by balancing ROS and antioxidants. Disruption of this balance leads to oxidative stress, that damages all cellular components, including amino acids and, consequently, proteins [16]. ROS include radical species, non-radical compounds, and free radicals generated during interactions with proteins, nucleic acids, and lipids (**Table I.1**). Reaction with proteins causes oxidative cleavage of the polypeptide backbone, modifications of amino acid side chains, and chlorination of terminal α-amino groups [6,7,17].

It has been previously noted that ROS and/or RNS can be formed in different processes including ionizing radiation, ultraviolet light, reactions of endogenous oxidases, inadvertent autoxidation of the reduced forms of electron carriers, oxidative burst during inflammation, metal-catalyzed oxidation, generation from nitric oxide synthase and subsequently the formation of peroxynitrite [18].

Table I.1. *Selectivity of damage to amino acids by different oxidation methods [19–21]*

Oxidant	**Major sites of damage**
$^{\bullet}OH$	most residues
H_2O_2	Cys
$^1O_2$	Cys, His, Met, Trp, Tyr
HOCl/HOBr	α-amino group Lys, Cys, cystine, His, Met, Trp
HOSCN	Cys
$ONOO^-$ / ONOOH	Cys, Trp, Tyr
direct ionization (UVB)	cystine, Trp, Tyr
Photosensitizers	Cys, His, Met, Trp, Tyr

I.1.1. Photo-oxidation and photosensitized oxidation

From facilitating photosynthesis to aiding in the production of vitamin D, light serves as a crucial factor in numerous cellular processes. However, despite its beneficial effects, light can also lead to protein damage [17]. The direct oxidation of proteins, peptides, and amino acids by UV light is only significantly relevant if the light is absorbed by the protein (i.e. the wavelength is below 320 nm).

The appropriate classification of photosensitized oxidation remains a topic of discussion. According to IUPAC, oxidations induced by ultraviolet, visible, or infrared light are called photo-oxidation, while photoinduced reactions in which neither substrate or dioxygen are electronically excited (i.e., photosensitized oxidation) are sometimes called photoinitiated oxidations [22].Commonly, photo-oxidation is categorized into two types referred to as Type I and Type II [23]; however, in contemporary publications, there is an ongoing debate about distinguishing Type III from the others [24] which would be in accordance to IUPAC with one exception, all of them involve oxygen and therefore should be named photo-oxygenations. An argument in favor of this distinction is the fact that in the first two types, the presence of oxygen is acknowledged in the reaction mechanism, whereas in Type III, reaction yields both charged radical species of substrate and photosensitizer, and in the end oxygen radical anion (summary of all processes is present in **Figure I.1**). The difference between Type I and Type II lies in what serves as the primary acceptor of the light quantum, precisely in involvement of oxygen in excited singlet state.

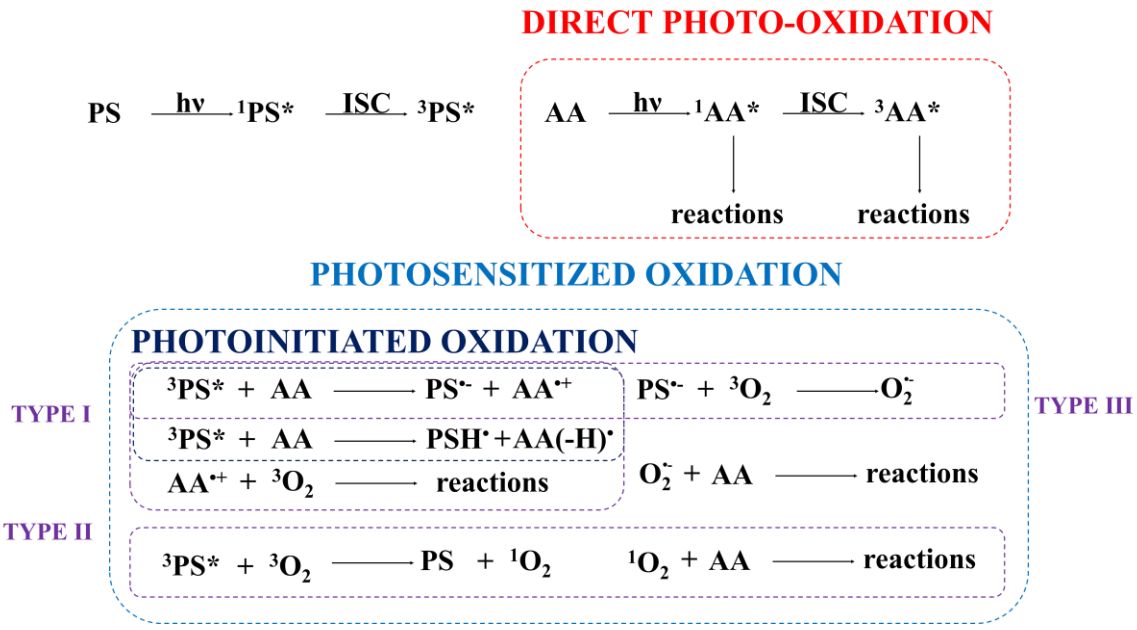

Figure I.1. *Summary of all of the processes involving light*

Chromophores included in side-chains of amino acids have the potential to generate excited states and radicals through photo-ionization. The relative energies of the short-lived excited singlet states of phenylalanine (Phe), tyrosine (Tyr), and tryptophan (Trp) decrease in that sequence, suggesting the possibility of energy transfer from phenylalanine and tyrosine to tryptophan. Amino acids in the first singlet state may undergo an intersystem crossing process, leading to molecules in the triplet state (those susceptible to this type of oxidation include Trp, Tyr, Phe, methionine (Met), cysteine (Cys), cystine (Cys-Cys),). Unlike molecules in the first singlet state, these species can engage in both chemical reactivity and energy transfer processes [14].

Numerous photosensitizers are available, proving their worth in diverse scientific applications. In terms of very basic fundamental description, these molecules absorb a quantum of light, becoming excited singlet state, that undergoes further intersystem crossing (ISC) to an excited triplet state. Chromophores exhibiting a populated excited triplet state find utility in electroluminescence, phosphorescent bioimaging, molecular sensing, photodynamic therapy (PDT), photoinitiated polymerization, and more recently, photocatalytic organic reactions [25]. These substances act as triplet energy donors, instigating photochemical and photophysical processes, including the photo-oxidation of proteins. A noteworthy choice for such purposes is 3-carboxybenzophenon (3CB), a member of the benzophenone family of photosensitizers. This selection is attributed to its enhanced water-solubility, when compared to other benzophenones. It's well-defined transient spectra properties (that have already demonstrated utility in biomolecular research) prove advantageous in both time-resolved and steady-state photochemical experiments. It is also important to mention that, in the presented work, a wavelength of 355 nm will be employed to excite exclusively 3CB and discard any processes that may occur from absorption of light directly by amino acids [26–28].

I.1.1.1. Type I

When considering chromophores other than amino acid backbone employed in the process, Type I photo-oxidation begins with the quenching of the excited triplet state of the sensitizer *via* abstraction of hydrogen or electron in amino acids prone to oxidation. This results in creation of radical couples (in case of hydrogen abstraction) or in radical ion couples (in case of electron transfer, ET) [29,30]. The subsequent fate of radical anion

of photosensitizer in this type of photo-oxidation includes acceptance of a proton (mainly from the radical cation of oxidized substrate) [29], reaction with oxygen, resulting in the formation of oxygen radical anion (named also as Type III photo-oxidation) [24], and reactions with other compounds in its vicinity (since it is a very reactive state).

When the photosensitizer radical reacts with the radical of oxidized product, it may either regenerate the ground state [31], or form a covalent bond between quencher and photosensitizer [29,32]. Two radicals of the photosensitizer could also react, resulting in the formation of covalent bond between them [29,33]. The oxidized radical product (in case of this thesis amino acid or its side-chain) might react with oxygen radical anion, which yields the formation of unstable peroxyl radical. This species further reacts by proton abstraction to create respective hydroperoxide [23]. The emergence of these entities is likely responsible for the oxygen (O_2) dependence observed in Type 1 mechanisms [23,29]. Self-reactions of the oxidized product, may also take place, especially when the concentration of O_2 is low. These reactions have been documented in the photo-oxidation of Trp and Tyr, with diTrp and diTyr suggested as indicators of O_2-independent Type 1 processes [29,34–36].

I.1.1.2. Type II

Type 2 mechanism involves energy transfer from the excited sensitizer to molecular oxygen, resulting in the formation of singlet oxygen, which efficiently oxidizes nearby targets. Sensitizers rarely undergo reactions exclusively through either Type 1 or Type 2 mechanisms due to variations in energy transfer efficiency. Photosensitized reactions typically unfold as a combination of singlet oxygen and radical species. The profile of protein damage is notably influenced by the proportion of each reactive species generated during photosensitization, relying on factors such as the nature of the sensitizer, the excitation wavelength, and the reaction conditions [17].

Regarding amino acids reacting with singlet oxygen (refer to **Table I.2**), proteins are prevalent in most biological systems at high concentrations, leading to their rapid reaction with oxygen. This is further emphasized by the rate constants for side-chain amino acids reacting with $^1O_2$. Notably, among them, only Trp exhibits significant contribution of physical quenching of $^1O_2$ with the rate constant being comparable to chemical reaction [37].

Table I.2. *Selected rate constants for reaction with singlet oxygen with protein side-chains at pH ca. 7 ([a] reaction is pH dependent with k being ca. $10 \cdot 10^7$ for pH above 8 and $0.5 \cdot 10^7$ at lower pH) [37]*

Side-chain amino acid	Rate constant ($x10^7$ $mol^{-1} \cdot dm^3 \cdot s^{-1}$)
Tryptophan	3
Histidine	3.2-9[a]
Tyrosine	0.8
Cysteine	0.9
Methionine	1.6

I.2. GAPDH and amino acid modifications

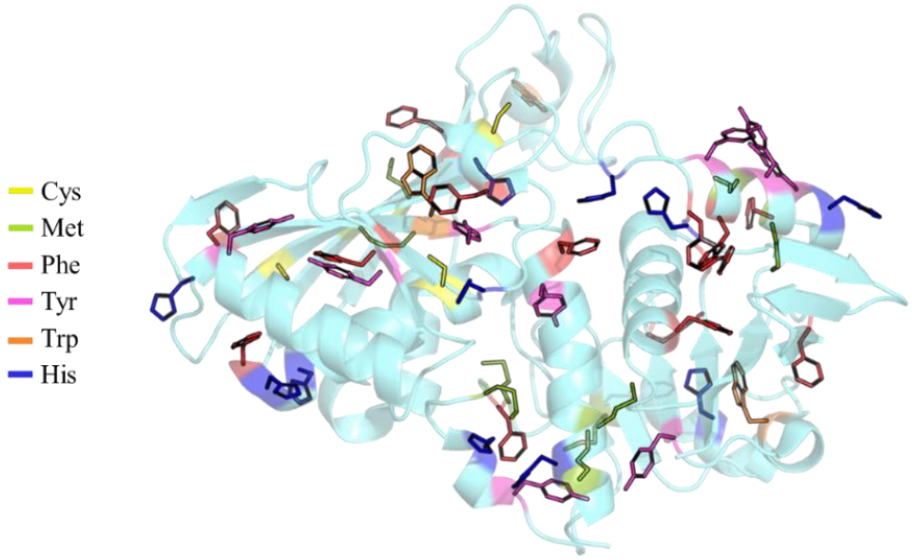

Figure I.2. *Graphical representation of GAPDH with amino acids prone to photoinduced oxidation both highlighted in different colors and represented in said figure*

Glyceraldehyde-3-phosphate dehydrogenase (GAPDH), an enzyme weighing approximately 37 kDa, plays a pivotal role in glycolysis, breaking down glucose to produce energy. Beyond its well-established metabolic function, GAPDH is implicated in various non-metabolic processes including transcription activation, initiation of apoptosis, endoplasmic reticulum (ER) to Golgi vesicle shuttling, and fast axonal or axoplasmic transport [38,39].

Since quantity of different amino acids varies from protein to protein [40], it was essential for this thesis to choose one that has both, enzymatic activity and all amino acids prone to photosensitized oxidation. GAPDH fills that role perfectly as it has all the aforementioned compounds, whether exposed to the solution or hidden in the structure (as presented in **Figure I.2**).

Its catalytic mechanism involves oxidation and phosphorylation steps. Initially, a cysteine residue in the active site attacks the carbonyl group of glyceralderhyde-3-phosphate (G3P). Subsequently, a histidine residue deprotonates the transient, facilitating ejection of the hydride ion. The adjacent oxidized nicotinamide adenine dinucleotide (NAD^+) molecule accepts it, producing reducing nicotinamide adenine dinucleotide (NADH), while the transient undergoes oxidation. In the concluding phase, inorganic phosphate attacks the thioester, forming a tetrahedral intermediate that eventually collapses to release 1,3-bisphosphoglycerate, and the thiol group of the enzyme's cysteine residue [41–44].

GAPDH is often overexpressed in cancers like cutaneous melanoma, promoting tumor proliferation and survival. Its depletion induces senescence in tumor cells, presenting a novel therapeutic strategy [45–48]. In neurodegenerative diseases and disorders, GAPDH interacts with specific proteins implicated in each condition. These interactions may impact energy metabolism and other functions of GAPDH. For instance, interactions with beta-amyloid precursor protein might interfere with its function related to the cytoskeleton or membrane transport. Similarly, interactions with huntingtin could disrupt its role in apoptosis, nuclear tRNA transport, DNA replication, and DNA repair. Notably, nuclear translocation of GAPDH has been reported in Parkinson's disease, and certain anti-apoptotic drugs, such as rasagiline, function by preventing this translocation. It is suggested that hypometabolism could be a contributing factor to Parkinson’s, but the exact mechanisms underlying GAPDH involvement in neurodegenerative diseases remain to be clarified [49–51].

I.2.1. GAPDH oxidation

It is a well-known fact that GAPDH is particularly sensitive to oxidative stress, which leads to damage to this enzyme. Modifications or mechanisms associated with this process include:

- Enzyme aggregation or dissociation;
- Charge or conformational changes resulting from thiol redox modification;
- Decreased active site histidine residues;
- An increased susceptibility to proteolysis [52].

Research on the oxidation of this enzyme has been conducted using various methods. Utilizing femtosecond pulses of UV radiation (257 nm) resulted in detection of protein dimers *in vivo* [53]. On the other hand, there are articles which describe how ROS lead to modifications of the amino acids [54–56]. It is a well-known fact that GAPDH possesses a cysteine in the active center, which is particularly sensitive to oxidation, logically resulting in the deactivation of this enzyme. This cysteine is so reactive that it can also create sulfur bridges with proteins that had their cysteines oxidized *via* singlet oxygen [37].

I.2.2. Photosensitized processes with amino acids side chains

Many sensitizers have been utilized to study photosensitized oxidation of amino acids. Since 3CB is implemented in this thesis, these fundamental processes will be explained based on photophysical and photochemical properties of 3CB. Energy diagram (first published by Jabłoński in 1933, **Figure I.3**) is the most efficient way to lay down fundamentals that are detrimental to photochemistry and photo-physics [57]. The absorption of a light quantum by the chromophore results in exciting it to a singlet state (depending on the wavelength of the light, the appropriate energy level will be reached). Subsequently, there is a rapid transition to the first singlet state (in case of second or higher singlet states, internal conversion (IC) occurs), from which, according to the Kasha's rule, it could undergo a transition to the ground state with the emission of a photon. However, in case of 3CB, the excited singlet state (^{1}3CB*) undergoes intersystem crossing (ISC) with quantum efficiency equal to one yielding formation of the excited triplet state of the 3CB molecule (^{3}3CB*) [58,59].

There are four processes involved in deactivating the excited triplet state: (i) phosphorescence, light emission characterized by a spin-forbidden transition, resulting in a longer lifetime compared to fluorescence, (ii) ISC, (iii) reaction in the excited triplet state, and (iv) quenching. Last three processes belong to non-radiative transitions.

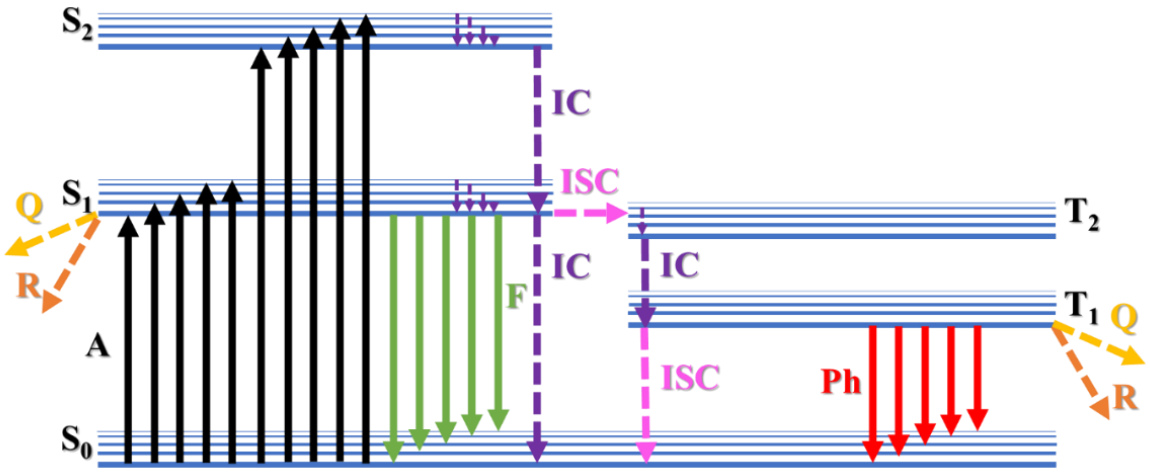

Figure I.3. *Representation of Jablonski diagram. Quenching process can occur both from singlet and triplet state. (S_n – nth singlet state, T_n – nth triplet state, A – absorption, F – fluorescence, Ph – phosphorescence, IC – internal conversion, ISC – intersystem crossing, Q – quenching, R – reaction)*

A quenching process involves the non-radiative deactivation of an excited singlet or triplet state of a molecule by a quencher. The excess energy can be converted into heat and transferred to the surrounding molecules. The excited state can undergo quenching through several processes:

- Energy transfer
- Electron transfer
- Paramagnetic quenching
- Concentration quenching

Energy transfer is a crucial process in photobiology and photochemistry. The donor molecule, absorbs a photon and becomes an excited species. The acceptor molecule is excited by energy transfer. The excited state of 3CB should have higher energy than the excited state of the quencher molecule. Energy can be transferred by either a radiative (also known as trivial case, due to the fact, that excited triplet state emits quantum of light that is absorbed by quencher) or non-radiative mechanism. In the non-radiative process, energy is transferred in one step during interactions between the donor and acceptor. Two mechanisms describe that energy transfer: the Dexter mechanism and Förster resonance energy transfer (FRET). The Dexter model requires donor and acceptor molecules to be in close contact, typically through van der Waals or hard sphere interactions. Electron exchange between chromophore excited state and quencher is possible only due to the overlapping of their orbitals. The overall spin quantum number of the system must be kept constant, allowing energy transfer, in that case, in triplet-triplet systems only. FRET is an energy transfer that may occur over longer distances than the Dexter mechanism, with a distance between donor and acceptor ranging from 5 to 10 nm, transitions should have almost the same energy and pair should interact with each other [58,59].

Electron transfer (ET) is a process of great chemical, physical, and biochemical interest described by Marcus's theory as inner-sphere and outer-sphere ET. Generally, the solvent sphere surrounding the pair of molecules needs to reorganize during ET. According to the inner-sphere model, the interaction between vibrational modes of the donor and acceptor is significant and promotes ET. The second model describes the response of the solvent occurring along the ET coordinate. In photoinduced electron transfer, the transfer of an electron between the excited molecule of photosensitizer (^{3}PS*) and quencher (in case of this thesis amino acid, AA) occurs via an ion pair (k_{el} process on **Figure I.4**). ^{3}PS* is deactivated, and the created ions can return to neutral ground states (back electron transfer) or recombine with another radical. In case of 3CB, the electron transfer from amino acid to 3CB would be expected, which yields 3CB radical anion ($3CB^{\bullet-}$) and amino acid radical cation ($AA^{\bullet+}$) [58,59].

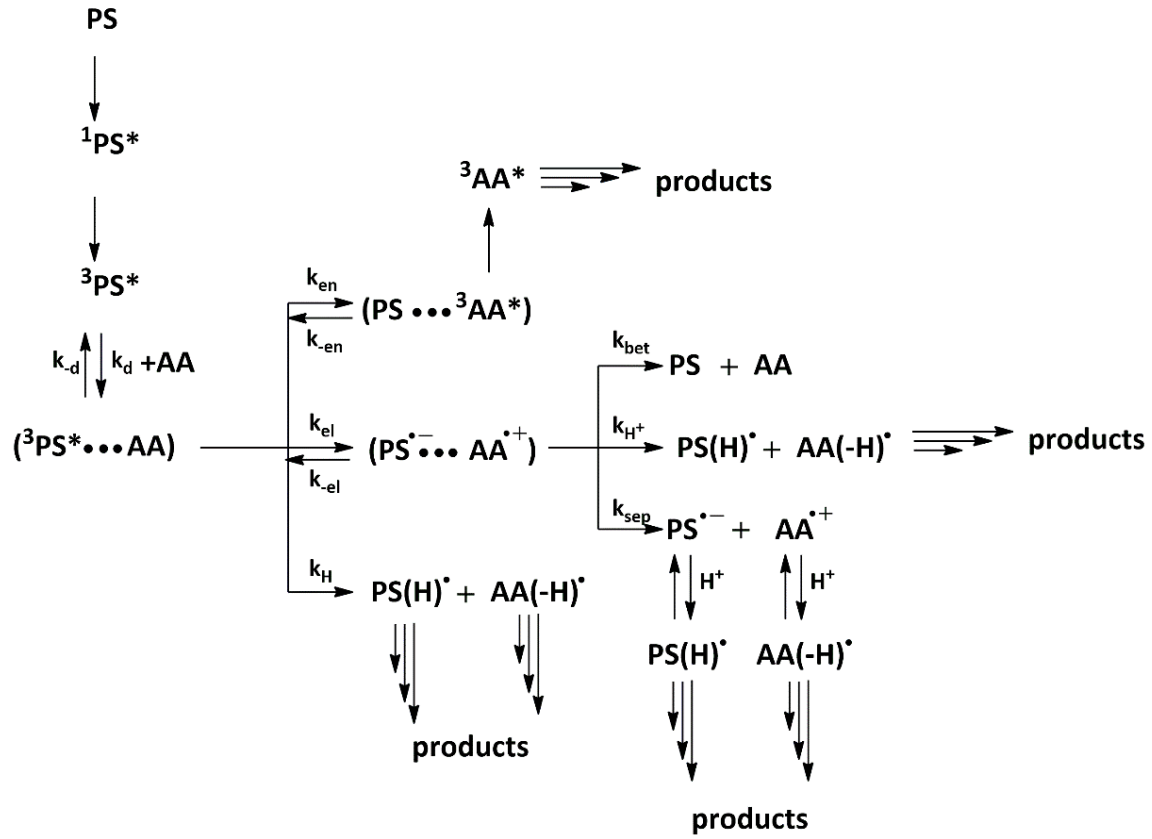

Figure I.4. *Summary of processes that may occur in anoxic photosensitized oxidation of amino acids*

I.2.2.1. Sulfur containing amino acids – Cysteine, cystine and methionine

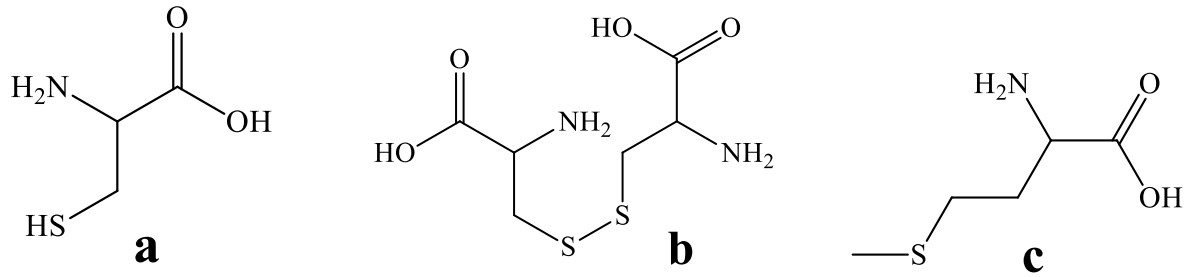

Figure I.5. *Structures of (a) cysteine, (b) cystine and (c) methionine*

There is a competition between Type I and Type II photo-oxidation when it comes to reactions with cysteine (Cys, **Figure I.5 a)** [60]. The photoinduced oxidation of Cys yields the thiol radical ($CysS^{\bullet}$) and respective radical of photosensitizer [61]. Computational methods point towards a possibility that $CysS^{\bullet}$ undergoes further transformation to different forms of radicals (**Figure I.6**) [62]. It was proven that $CysS^{\bullet}$ can either react with radical photosensitizer yielding covalent product [61] or it can react with another $CysS^{\bullet}$. It results in either disproportionation of $CysS^{\bullet}$ or formation of cystine (**Figure I.5 b**). Cystine, is a substantial reaction product when further Cys residues are able to react with the initial intermediate either intra- or inter-molecularly [63]. Cystine has standard reducing potential of -1.38 V ([$Cys_2/Cys_2SS^{\bullet-}$] *vs* NHE, [64]). There are sources in which cystine (or other disulphide compounds) can be reduced yielding cystine disulfide radical anion ($Cys_2SS^{\bullet-}$), however what follows is cleavage of -S-S- bond with consequent formation of Cys anion and $CysS^{\bullet}$. Occurrence of other cross-links in protein (apart from cystine) has also been reported, where these are either products of reaction between oxidized compounds and cysteine [65] or *via* formation of covalent bond between $CysS^{\bullet}$ and other amino acid radicals (namely Tyr, Trp, Lys, His, Phe, or Ser; all of them are presented in **Figure I.6** as $AA^{\bullet}$) [66].

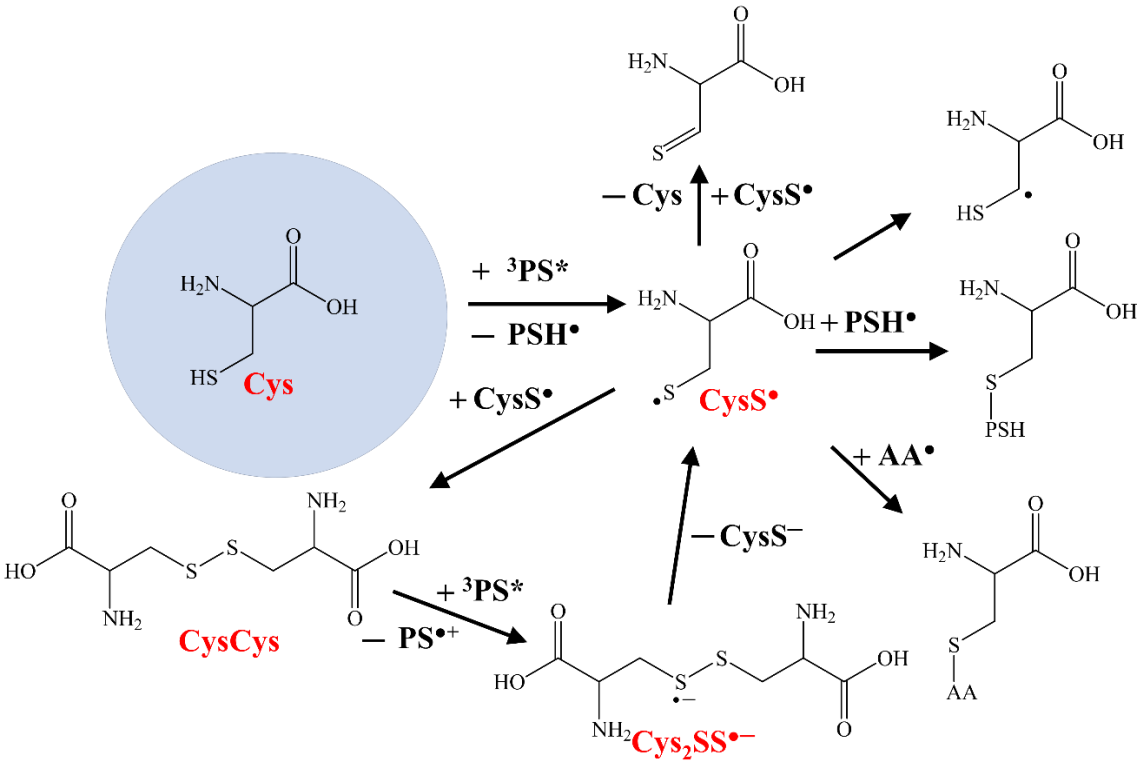

Figure I.6. *Mechanism of formation of stable products from Cys and CysCys anoxic photosensitized oxidation based on [62,64,67]*

Photosensitized reactions of 3CB (and similar 4CB) with methionine (Met, **Figure I.5 c**) has been extensively researched by Marciniak et al [26,27,32,68–70]. The quenching of 3CB by Met derivatives results in the formation of an encounter complex [27] that undergoes decay through three primary reactions:

- Charge separation leading to the formation of $3CB^{\bullet-}$ and $MetS^{\bullet+}$,
- Hydrogen atom transfer from the alpha carbon atom adjacent to sulfur to produce $CBH^{\bullet}$ and $\alpha S^{\bullet}$ radicals,
- Back electron transfer leading to the regeneration of reactants in their ground states.

The mechanism of photo-oxidation of the Met involves electron transfer from the sulfur atom on Met side chain to ^{3}3CB* yielding sulfur radical cation $MetS^{\bullet+}$ and $3CB^{\bullet-}$. Experimental evidence supporting electron transfer has been obtained through the observation of intermediate radicals $3CB^{\bullet-}$ and significant quenching rate constants [68]. The similar values of these rate constants at high pH and close to neutral indicate that they are not influenced by changes in the protonation state of the amino group in the Met derivatives. For comparison, alanine (Ala), an amino acid without an S atom, exhibits a larger quenching rate constant (k_q) at higher pH (at around 11) than in neutral solution. It has been suggested that the quenching by Ala is due to the deprotonated amine group, yet its k_q value remains smaller than that of the Met amino acid. Therefore, the involvement of the amino group in the ^{3}3CB* quenching by Met can be disregarded [71].The $MetS^{\bullet+}$ is stabilized by two centered three electron bonds either intermolecular ($Met_2(S\therefore S)^+$) or intramolecular ($Met(S\therefore N)^+$). The significant yield of the $Met(S\therefore N)^+$ in N-terminal Met-containing peptides at low pH, where the nitrogen in the amino group lacks a free electron pair, confirms the previously mentioned k_{NH} channel [68]. However, some studies have reported the absence of intramolecular $Met(S\therefore N)^+$ due to the delocalization of the lone pair on the nitrogen atom (in an N-acetylated group) [32] The stabilization by $Met(S\therefore N)^+$ leads to decarboxylation when the Met residue is C-terminal. Sulfur-centered radical cations also undergo deprotonation, yielding $\alpha S^{\bullet}$.

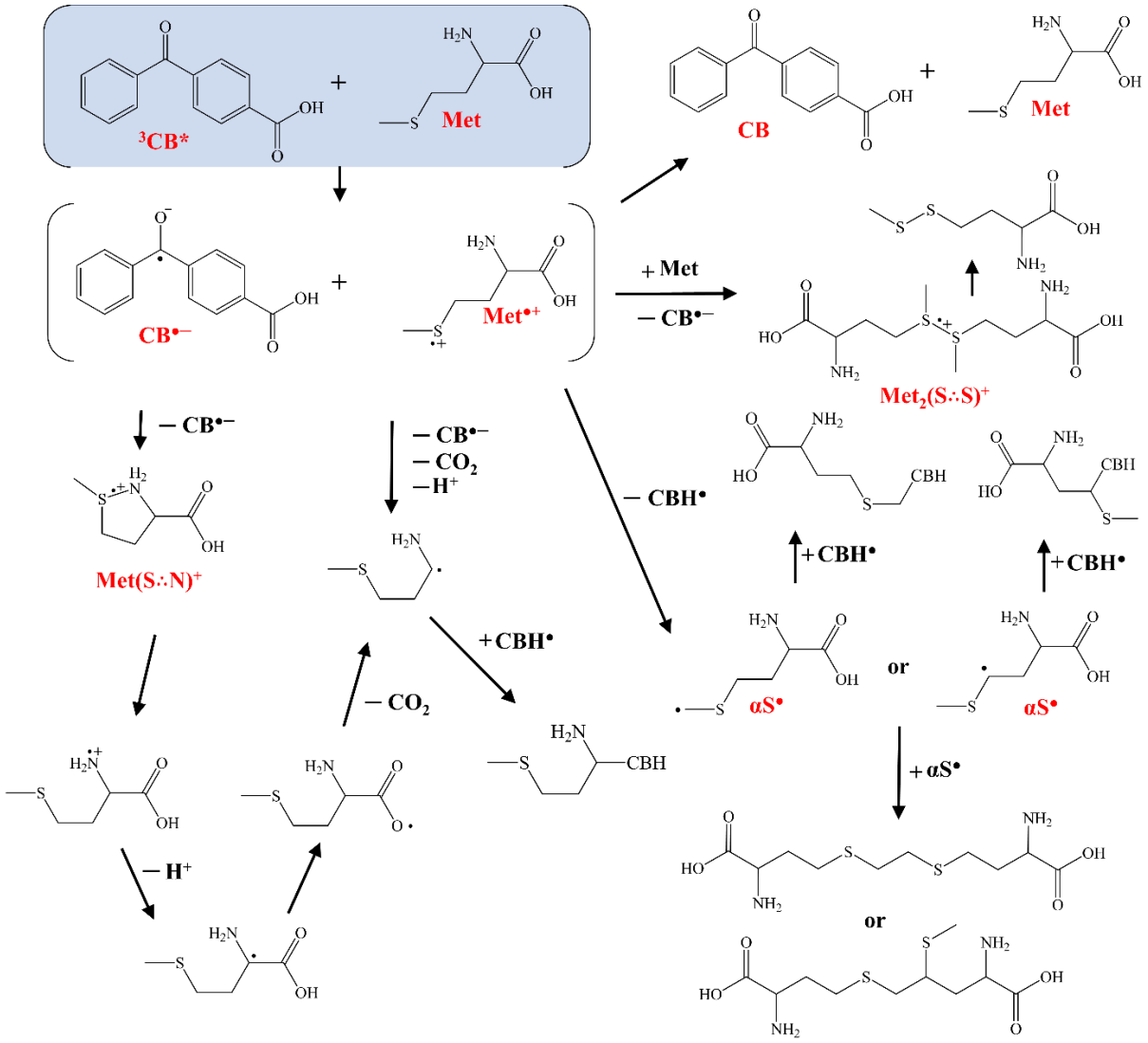

Figure I.7. *Mechanism of formation of stable products from Met anoxic photosensitized oxidation based on, where CB represents either 4CB or 3CB [27,32,68,72]*

An interesting trend regarding the rate constants and the number of Met residues in a peptide has been observed. Peptides containing one Met residue exhibit a k_q value around $2.0 \cdot 10^9$ $M^{-1}s^{-1}$, those with two Met residues have about $k_q = 3.0 \cdot 10^9$ $M^{-1}s^{-1}$, while for three Met residues, the rate constants are $k_q = 3.8 \cdot 10^9$ $M^{-1}s^{-1}$. However, for the peptide Met-Gly-Met-Met, the k_q value is similar to those with two methionine residues [69]. 4CB-sensitized photo-oxidation of Met-Gly (N-methionyl peptides) at pH close to 6 induces the formation of a relatively long-lived (50 μs) $Met(S\therefore N)^+$. The increase in pH induces the decay of $Met(S\therefore N)^+$ in a two-component reaction: the pH-dependent faster one and a pH-independent slower one [70].

Final fate of those processes involves products of formation of covalent bond between two αS•, or αS• and 3CBH•, or finally two 3CBH• [27].

One of the reasons, why so much attention is brought to Met radicals, is the fact that they may react with other amino acids in its presence. They are the very beginning of chain of radicals which usually end on CysS• (**Fig I.8**) [73,74].

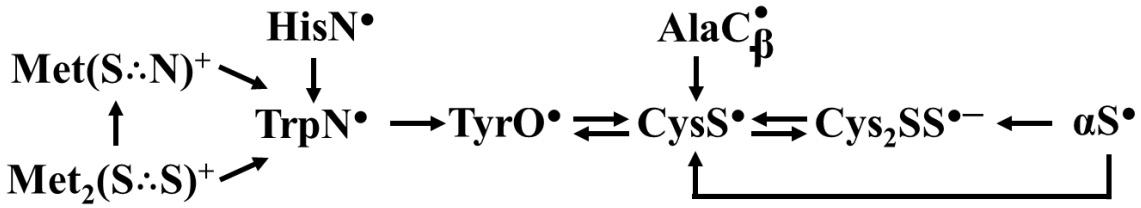

Figure I.8. *Scheme representing flow of electron in radicals occurring from the oxidation of respective amino acids [73–75]*

I.2.2.2. Tyrosine

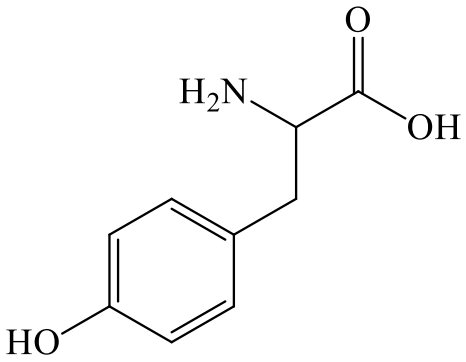

Figure I.9. *Structure of tyrosine*

The mechanisms underlying tyrosine (Tyr, **Figure I.9**) oxidation, including photo-oxidation, and their biological implications have been described in review by Houée-Levin et al. [76], providing an overview of the critical and initial steps in Tyr photosensitized oxidation using various sensitizers, with particular attention to the analysis of end products [76]. In case of excited triplet state of either benzophenone or ^{3}4CB*, it can be quenched by Tyr through an electron transfer mechanism within the encounter complex as the primary reaction step, resulting in the generation of Tyr radical cation

(TyrOH$^{\bullet+}$) and 4CB$^{\bullet-}$ within the same complex (**Figure I.10**) [77,78]. The subsequent destiny of the radical pair can be delineated by three processes: (i) reverse electron transfer (k_{bt}), (ii) radical separation (k_{sep}), (iii) and proton transfer (k_H) within the radical-ion pair, followed by the separation of these neutral radicals. The last one is the major pathway due to the low pKa values of TyrOH$^{\bullet+}$ (pKa= -1) [78,79], and high pKa values of either 4CBH$^{\bullet}$ (pKa = 8.2) or 3CBH$^{\bullet}$ (pKa = 9.5) [26].

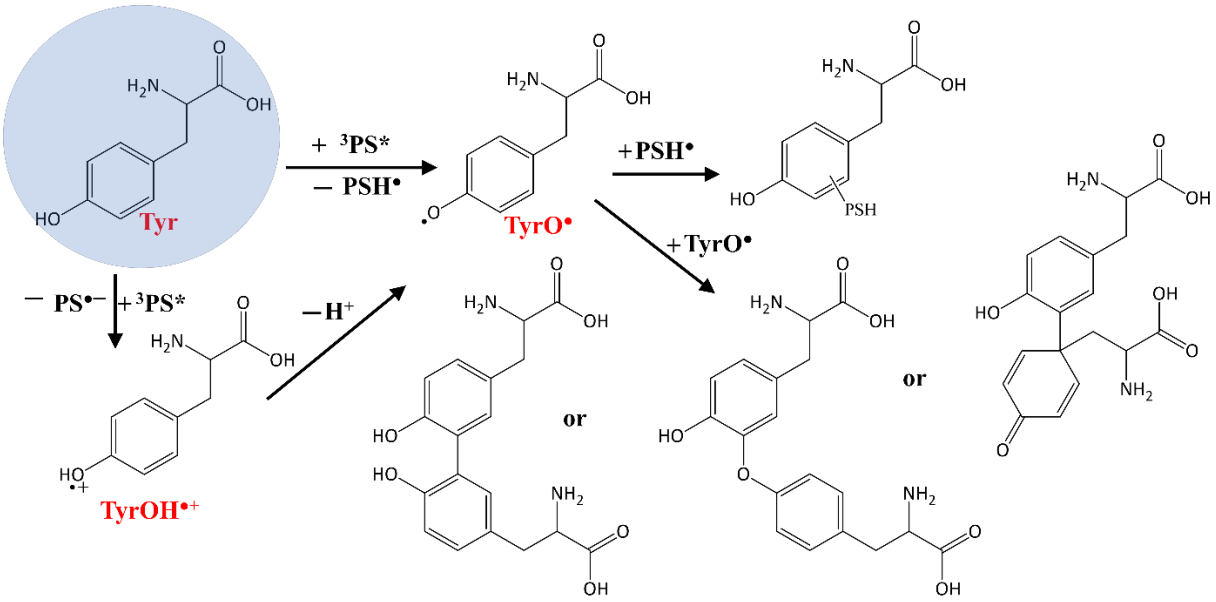

Figure I.10. *Mechanism of formation of stable products from Tyr anoxic photosensitized oxidation based on [78,80–83]*

The phenoxyl radical generated through electron transfer remains in resonance with various structures (**Figure I.11**) overlapping with each other [82,84]. These structures are expected to further react with either sensitizer radical or other TyrO$^{\bullet}$ to produce Tyr-sensitizer adducts or diTyr products [80,82,85,86]. This cross-linking is presumed to be the primary cause of several pathological conditions [67,68].

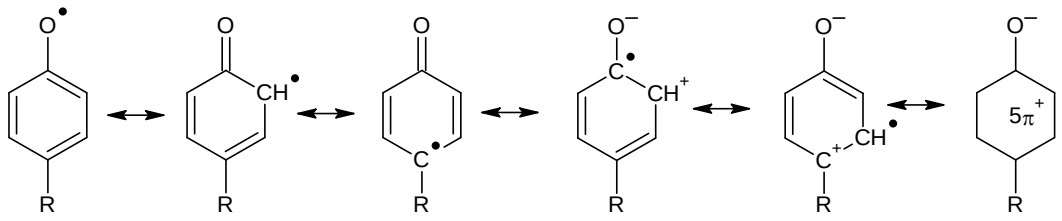

Figure I.11. *Resonance structures of phenoxy radical in tyrosine and its derivatives side-chains (where R is the rest of the amino acid or its derivative)[82,84]*

I.2.2.3. Tryptophan

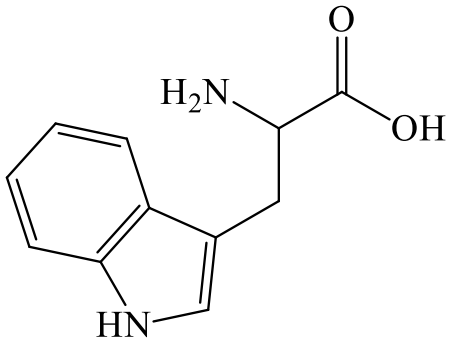

Figure I.12. *Structure of tryptophan*

Mechanistically speaking photo-oxidation of tryptophan (Trp) does not differ that much from Tyr. Main difference lies in the pKa of resulting radical cation - $TrpNH^{\bullet+}$ (pK_a=4.5) [87], which makes concerted proton-coupled electron transfer (PCET) process much slower in comparison to Tyr, but possible at physiological pH. It rapidly deprotonates to give the neutral indolyl radical ($TrpN^{\bullet}$) [14], that has its electron density located on N atom and C atoms with it mostly being present on C-3 atom of Trp (**Figure I.13**) [88].

As mentioned before in **Figure I.8,** this radical possesses the ability to further oxidize Tyr and Cys [73,74], furthermore it would be expected to yield covalent cross-links with Tyr, Cys and Trp radicals with creation of respective dimers [66]. Significant attention was brought to products of Trp photosensitized oxidation (namely various diTrp products [36,89–91] (which seem to appear as main products in anoxic photosensitized oxidation by excited triplet states of kynurenic acid or Trp of age lens proteins) [36] and adducts with sensitizers such as kynurenic acid and 6-thioguanine [36,92,93]).

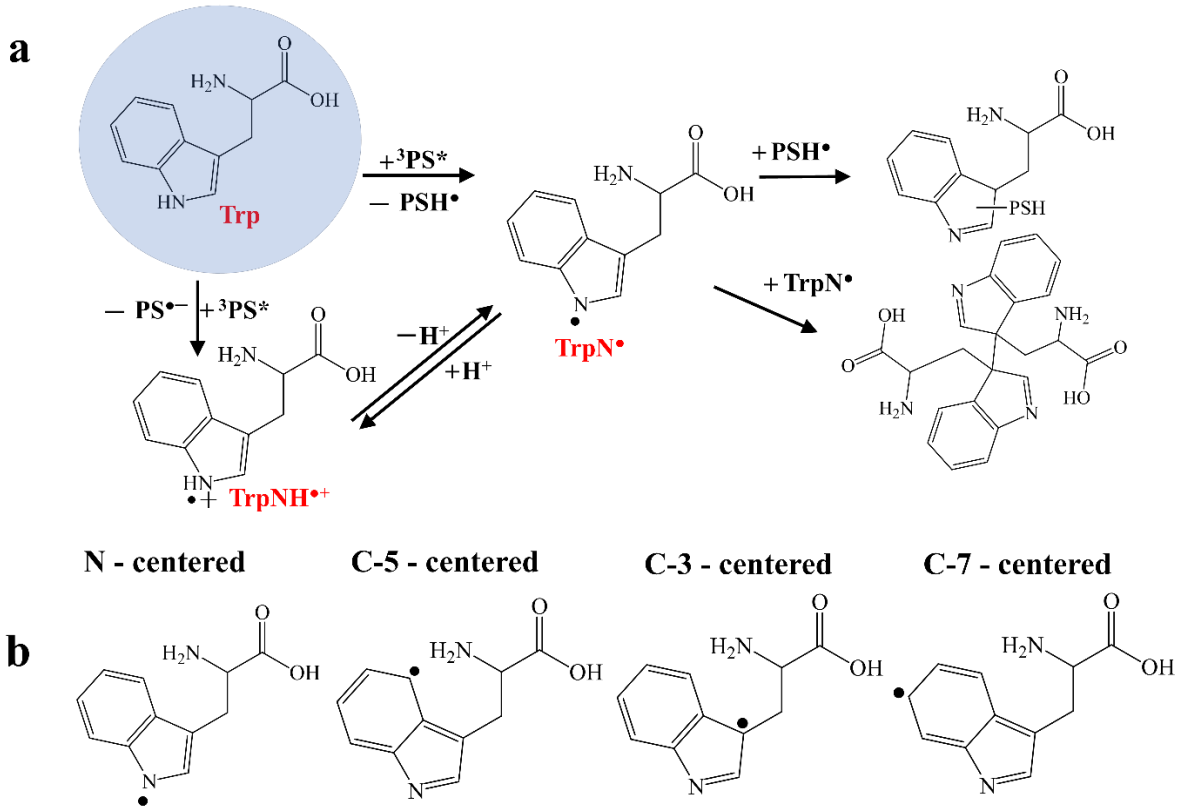

Figure I.13. *Representation of processes involving Trp* ***(a)*** *and structures of different TrpN•radicals* ***(b)*** *[36,88,89,91,92]*

I.2.2.4. Histidine

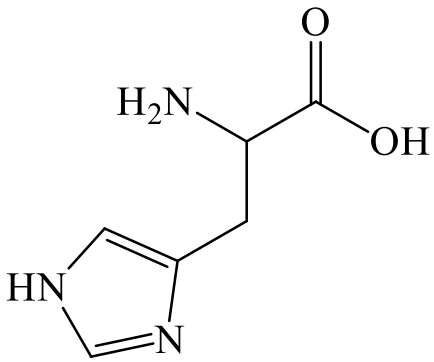

Figure I.14. *Structure of histidine*

Regarding reactions involving histidine (His, **Figure I.14**), it readily reacts with the $^1O_2$* and much more slowly with the excited triplet state of sensitizer directly (however, it may vary tremendously depending on the sensitizer, the excitation wavelength, and the reaction conditions [37]). Studies indicated that His photosensitized oxidation is significantly influenced by the pH of the sample, with the quenching rate constant increasing with pH. Variations in the quenching rate constant can be explained by reduction potential of His as the basicity of the solution rises [94]. Since pK_a of various functional groups in His varies for different derivatives, its values have been arranged in the **Table I.3**.

Table I.3. *pKa values of amine, carboxylic and imidazole group of His and its derivatives*

His derivative	pK_a of -COOH	pK_a of -Im	pK_a of $-NH_3^+$
His[95]	1.8	5.9	9.1
His-OMe[96]	--------	5.2	7.1
His-NH_2[97]	--------	5.8	7.6
N-Ac-His[98]	3.5	7	--------
1-Me-His[96]	1.7	6.5	8.8
His-Ala[99]	3.2	5.8	7.6
Ala-His[100]	2.8	6.8	8.1
His-Phe[98] [a]	---------	6.1	7.8
Gly-His-Gly[101]	3.0	6.5	8.0

His exists in various protonated forms (**Figure I.15**), starting with protonation of the amine group, followed by the imidazole group, and lastly the carboxylic group. Depending on these forms, two possible mechanisms are proposed: PCET or ET [102–106].

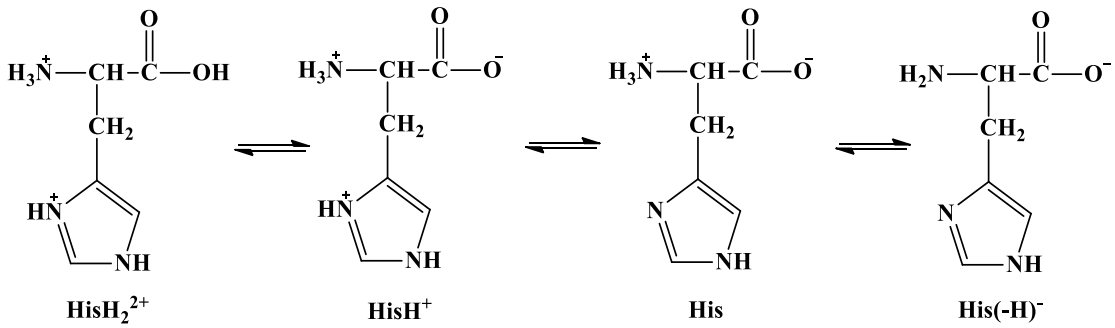

Figure I.15. *Different forms of protonated histidine depending of pH*

In contrast to the scarce literature on photochemical reactions of protonated His, the oxidation pathways of His have been extensively investigated and reviewed [4,107]. Weil et. al. reported [4] that O_2 uptake during the early stages of His photo-oxidation occurs at a 1:1 ratio, which is in agreement with the formation of oxygenated intermediates and products (e.g., hydroperoxides [4,106,108,109]). On the other hand, direct interactions between His and sensitizers are poorly understood. This is because of the complexities associated with the different protonated states of His [108], with recent reports suggesting that the pH of the milieu as well as derivatization of the amino and/or carboxylic group, can have a marked influence on the quenching mechanisms of His, which could include ET and/or PCET (**Figure I.16**) [98,103].

The histidyl radical (HisN$^{\bullet}$) has been studied extensively over many years and remains prominent in research on photosensitized oxidation. This transient molecule exhibits relatively low extinction coefficients in its absorption spectrum, typically around 400 nm [110,111]. As mentioned earlier, two possible entities may emerge, with either protonated or deprotonated nitrogen atoms in the imidazole ring. Structural studies of the HisN$^{\bullet}$, conducted both theoretically and experimentally, indicated its delocalization due to the aromatic character of the imidazole group, resulting in an energetically stable carbon-centered radical [112,113]. Its relatively strong reduction potential aligns with the current trend in scientific inquiry, prompting investigations into whether it may oxidize other amino acids present in proteins [75,94,114].

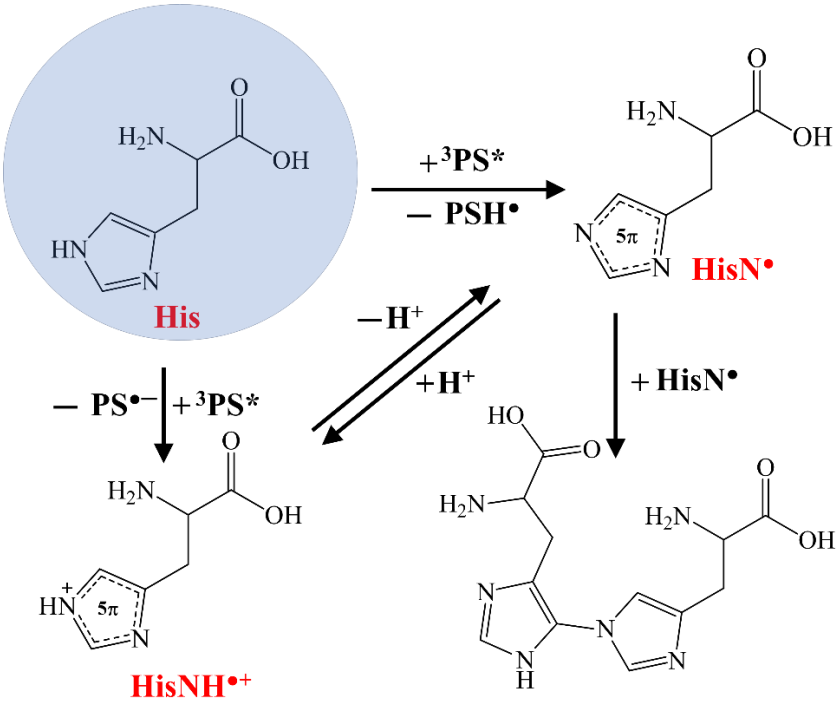

Figure I.16. *Representation of processes involving His [105,113,115]*

I.2.2.5. Phenylalanine

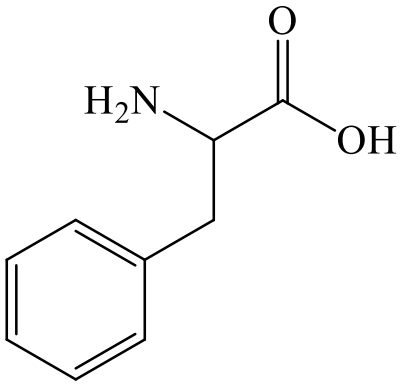

Figure I.17. *Structure of phenylalanine*

First it would be to address the rest of amino acids. Based on research done on excited triplets of anthraquinone-2,6-disulfonate dianion:

"Absolute triplet quenching rate constants at zero ionic strength were in the range of $2 \cdot 10^8$ to $2 \cdot 10^9$ $M^{-1} \cdot s^{-1}$ for R-NH_2 and $2 \cdot 10^7$ to 10^8 $M^{-1} \cdot s^{-1}$ for R-CO_2- type of electron donors, reflecting in principle their standard reduction potentials."[116].

Therefore, it would be expected that in PBS solution due to higher ionic strength and pH, no reaction will occur with amine group (as its quenching rate constants are significantly lower) and quenching rate constants in case of carboxylic group will drop by two orders of magnitude (based on publication [117]).

Not much is known about anoxic photo-oxidation of phenylalanine (Phe, **Figure I.17**). What current state of knowledge provides are facts that phenylalanine in the presence of other, more prone to oxidation amino acids remains intact. Oxidating Phe by excited triplet state of flavins ends with deamination process and uranyl sensitized photodecomposition of this amino acid ends with decarboxylation [102,118–123]. It is known that excitation of Phe to the first singlet state with following intersystem crossing to the first triplet state further results in a simple photo-dissociation reaction that yields a benzyl radical (**Figure I.18**) [1,14].

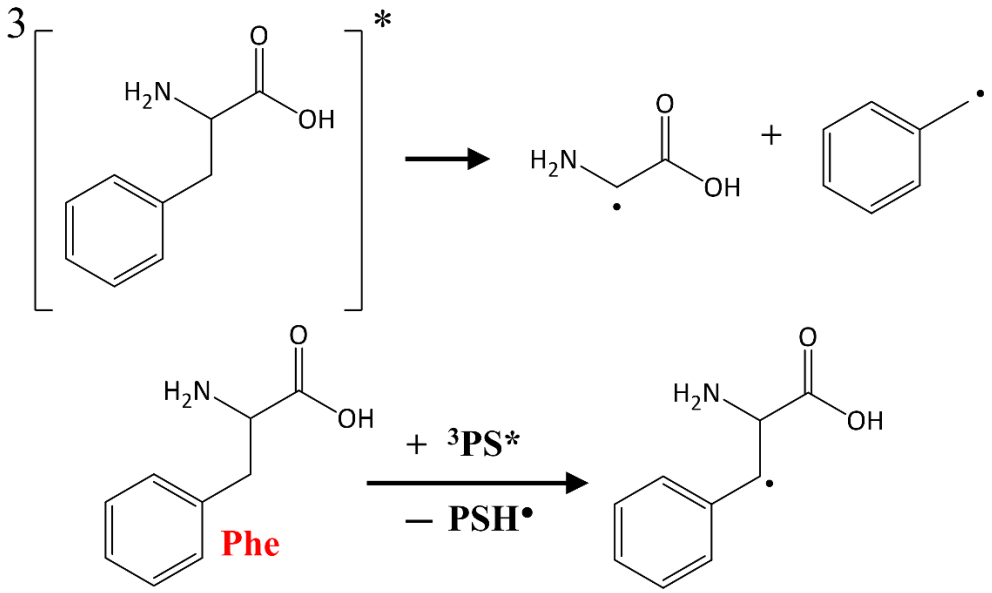

Figure I.18. *Two potential reactions in photo-oxidation of Phe [1,14]*

I.3. The aim of the work

Anoxic modifications are omitted during research because they are expected to occur in minor way in living organisms. However, they can play an important role in further protein functionality. This fact and presented state of the art allowed to formulate the main aim of presented thesis:

The characterization of all stable products of aromatic amino acid side chains induced by UV light and sensitizer (3CB) in model compounds, peptides and GAPDH protein and determination of their influence on GAPDH activity.

In order to fully achieve the goal of presented thesis, it is necessary to answer following questions that also arose after a detailed analysis of the available literature:

1. Does the presence of different neighboring groups influence transient species formed during the oxidation of aromatic side chains (Tyr, Trp, His and Phe)?
2. What effect does the surroundings of an amino acid residue have on stable products?
3. Is there any specific product for 3CB-sensitized photo-oxidation?
4. Does the modification of GAPDH by 3CB induce changes in activity?

Presented results should show possible answers to posed questions and fulfil the mechanism of 3CB sensitized GAPDH photo-oxidation.

II. Materials and methods

II.1. Materials

All model compounds and 3CB (**Figure II.1**) were purchased with the best available grades and used without further purification. Model peptides were purchased from Bachem. GAPDH from rabbit muscle was purchased from Sigma. Water was purified with an EMD Millipore SIMS600CP Millipore Simplicity Personal Ultrapure Water System (resistivity 18.2 μΩ). Hydrochloric acid and potassium hydroxide were purchased from VWR chemicals and used for pH adjustment to around 7 (with Mettler Toledo FiveEasy pH-meter). MS-quality: water, acetonitrile, and formic acid were purchased from Merck. SDS-PAGE using Bolt™ 4–12% Bis-Tris Plus precast gels, NuPAGE MES-SDS running buffer (20x), NuPAGE sample reducing agent (10X) and NuPAGE LDS sample buffer (4X) were obtained from Thermo Fisher. Trypsin Gold was purchased from Promega. Dithiothreitol (DTT), iodoacetamide (IAA), methanesulfonic acid (MSA, 4 M) containing tryptamine (0.2% w/v), tri-chloroacetic acid (TCA) were purchased from Sigma-Aldrich. Amino acid standards were provided courtesy of prof. Davies. GAPDH Activity Assay Kit was purchased from Sigma-Aldrich. All other chemical reagents were purchased from Sigma Aldrich and used as received, unless stated otherwise.

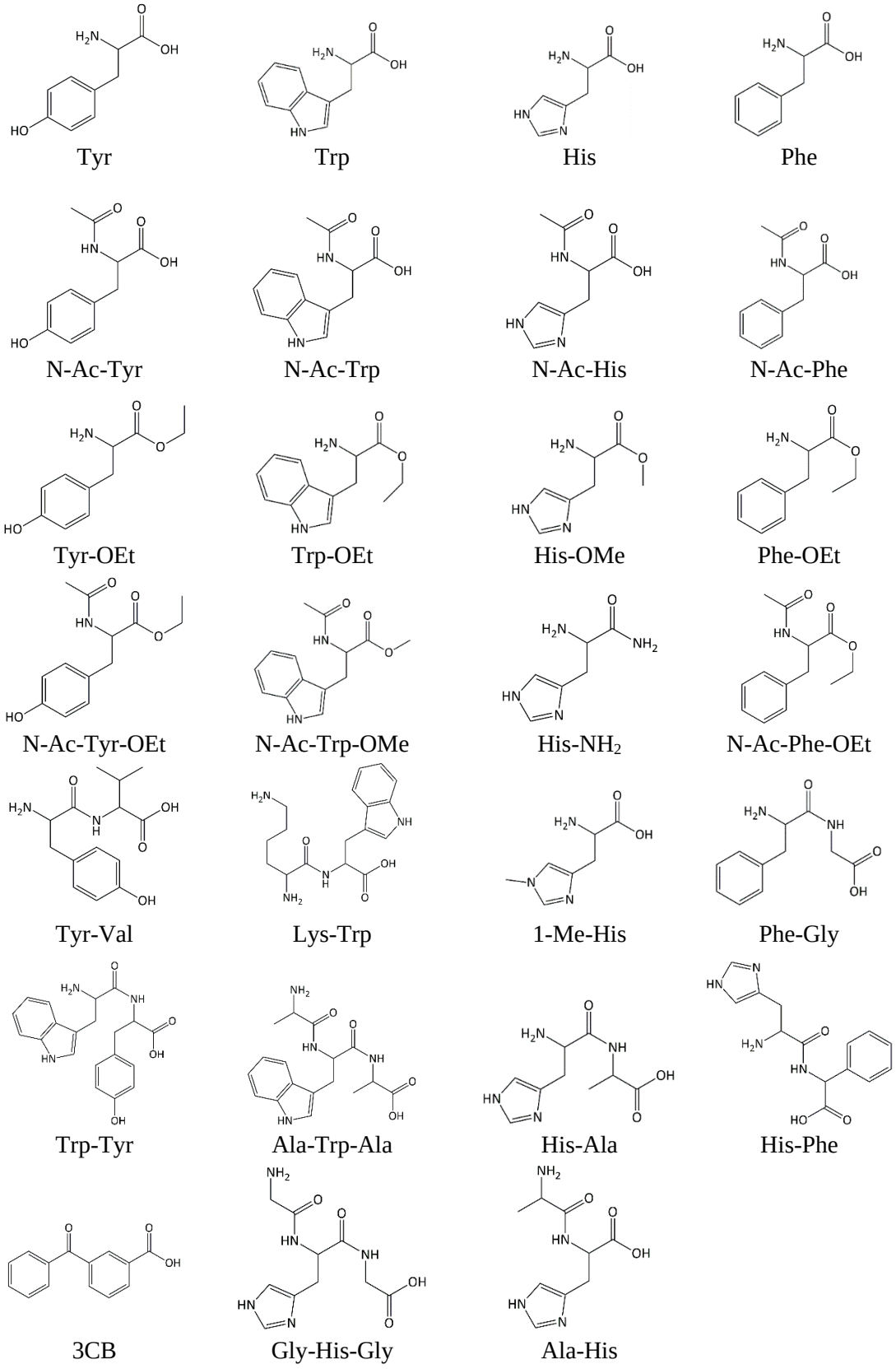

Figure II.1. *Model compounds investigated in this thesis*

II.2. Methods

II.2.1. Laser Flash Photolysis

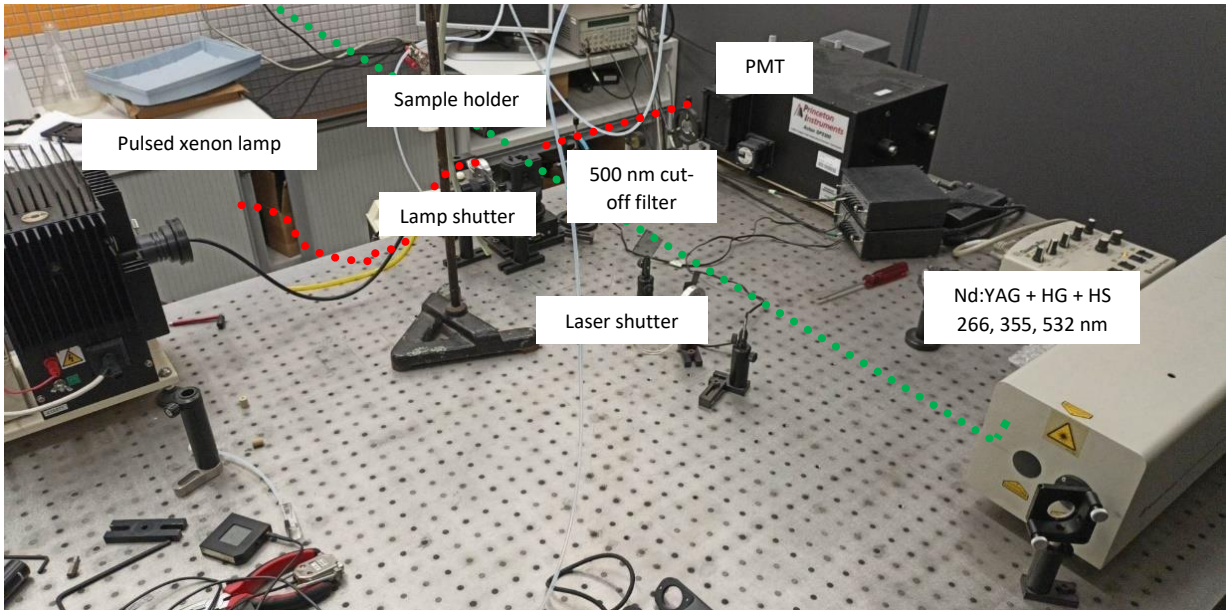

Figure II.2. *The experiment set-up for nanosecond laser flash photolysis*

Neodymium-yttrium aluminum garnet solid state laser (Nd:YAG) is built from Y_3All5O_{12} doped by Nd^{3+} (~1%) and can be excited in a wide spectral range from 480 to 600 nm by e.g. krypton arc lamp. Nd-YAG lasers are widely used (in continuous wavelength or pulsed mode). The 'mineral' used in this laser emits the light in the IR region, 1064 nm. By using special kind of substances having non-linear optical properties (e.g. potassium hydrogen), it is possible to produce other photon frequency e.g. 532 nm (2^{nd} harmonic), 355 nm (3^{rd} harmonic) and 266 nm (4^{th} harmonic) respectively. Nanosecond pulses are generated using the Q-switched mode [124]. The set-up used in this work is presented on **Figure II.2.** The Nd:YAG laser (Spectra-Physics) is operated at 10 Hz repetition rate, and the duration of the pulse is from 6 to 8 ns. The maximum pulse energy at 1064 nm and 355 nm is 450 mJ and 155 mJ respectively. The probe pulse is emitted from a pulsed xenon lamp (Applied Photophysics) with an optical fiber. Signals coming from the sample are analyzed by monochromator (Acton) and a photomultiplier (PMT, Hamamatsu). Besides those elements, a wide variety of electronics, e.g. oscilloscope (LeCroy), photodiode, delay generator, shutters, are required to synchronize the system [32].

Light which reaches PMT from pulsed xenon lamp through cuvette in sample holder is treated as a baseline voltage. Then during short pulses of light from Nd:Yag, molecules

in cuvette become excited and new signal from emission of transient species is given as voltage. Knowing what voltage is applied to PMT *via* oscilloscope, ΔA can be calculated from **Equation 1**, and since this method is time correlated, relation between ΔA and time yields decay curves.

$$\Delta A = \log_{10}\left(\frac{U_0}{U_0 - U}\right) \quad (\mathbf{1})$$

ΔA – observed absorbance change

U_0 – baseline voltage

U – voltage measured immediately after laser pulse

Those experiments provide further opportunities for determination of quenching rate constants and identification of transient species and their quantum yields, described in subchapters below. Kinetic curves were measured from 380-650 nm with 10 nm intervals. Eight laser impulses were averaged for each respective wavelength.

II.2.1.1 Determination of quenching rate constant

To obtain quenching rate constant, k_q, Stern-Volmer equation has been implemented (**Equation 2**). With varying concentration of quencher, it is possible to obtain dependence of it to reciprocal of the lifetime of ^{3}3CB*. Further application of linear regression allows for calculation of k_q of given quencher.

$$k_{obs} = \frac{1}{\tau_T} = \frac{1}{\tau_T^0} + k_q \cdot [Q] \quad (\mathbf{2})$$

Where:

k_{obs} – observed rate constant

τ_T – triplet lifetime of the benzophenone or its derivative in a presence of a quencher

τ_T^0 - triplet lifetime of the 3CB without a quencher

k_q – quenching rate constant

[Q] – concentration of quencher

II.2.1.2 Generation and deconvolution of transient spectra

If decay curves are measured at different wavelengths, utilization of SpectraWin (version 3.6 written by Jäschke and Brede, 2002) allows for generation of transient spectra. The registered transient absorption spectra obtained from LFP are very often a mixture of spectra from several transient species, that in addition can disappear within the formation of new species. To fully understand the investigated process, it is necessary to resolve the spectrum. The qualitative and quantitative analysis by deconvolution is possible with special software, e.g. DECOM (written by J. Mirkowski, Ph.D. and P. Wiśniowski, Ph.D., 2006). The DECOM program uses the additive law of absorption, the reference spectra of transients and least squares method with the **Equation 3**:

$$\Delta A(\lambda_j) = \sum_{i=1}^{n} c_i(t) \cdot \varepsilon_i(\lambda_j) \cdot l, \quad j=1 \ldots r \quad (3)$$

Where:

$\Delta A\ (\lambda_j)$ – observed absorbance change of the composite spectrum at the jth wavelength

λ_j –j^{th} wavelength of the observation

$c_i(t)$ – is the concentration of the i^{th} compound

$\varepsilon_i(\lambda_j)$ – molar absorption coefficient of the i^{th} species at the j^{th} wavelength of the observation

l – optical path length

Some factors influence the correct deconvolution:

- the lack of reference spectra or wrong reference spectra,
- the small difference between the absorption maxima of two species,
- incorrect acquisition of data during LFP or PR experiment,
- wrong selection of transients for deconvolution.

Thus, the DECOM software gives the uncertainty from the sum of all these factors.

Reference spectra of transients implemented in this thesis has been presented in **Figur II.3**. Spectra of transients that arise from 3CB, namely ^{3}3CB*, 3CB$^{\bullet-}$ or 3CBH$^{\bullet}$ (**Figure II.3 a)** has taken from ref. [26]. Spectrum of TyrO$^{\bullet}$ (**Figure II.3 b)** has been taken from the PhD thesis of Kciuk, G. (2011). *"Wpływ grup funkcyjnych aminokwasów na mechanizmy reakcji rodnikowych w peptydach zawierających tyrozynę"*, Institute of Nuclear Chemistry and Technology, Warsaw, Poland. Spectra of TrpN$^{\bullet}$ and TrpNH$^{\bullet+}$ (**Figure II.3 c**) have been published in ref [125],and used as presented there. Due to the fact that HisN$^{\bullet}$ has characterless spectrum with low ε value [94], it has not been utilized in this thesis. The spectra of other transients have not been procured to this day.

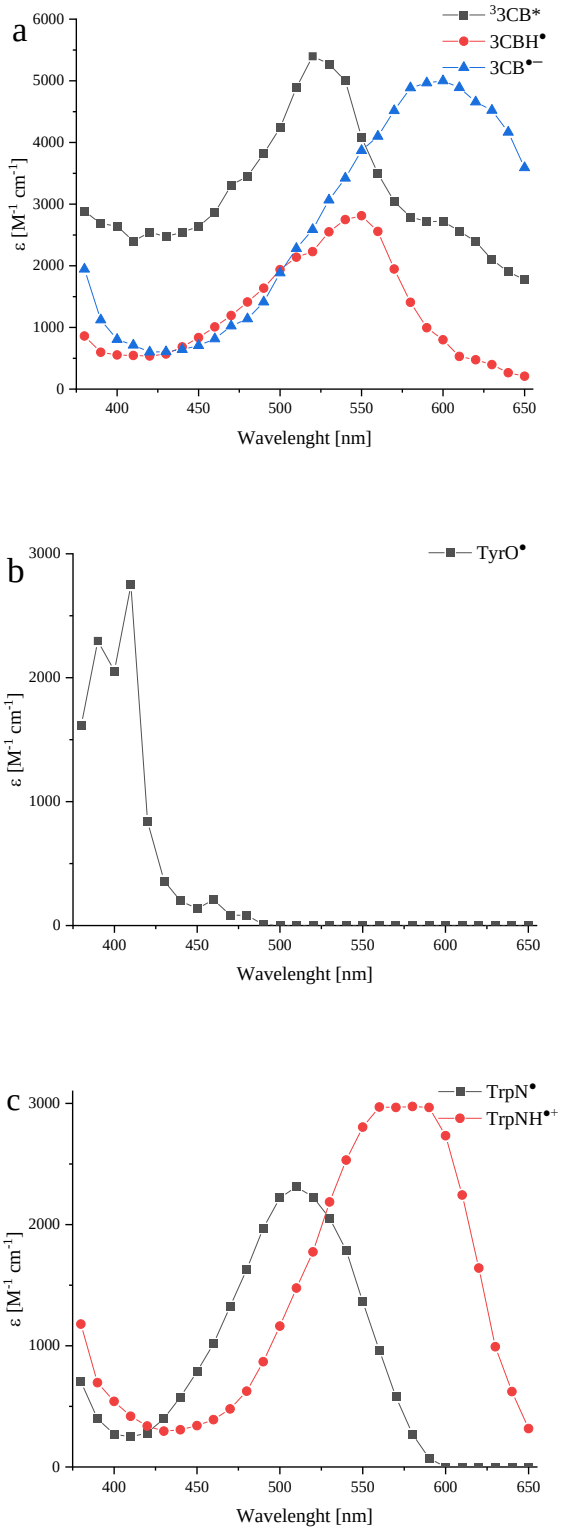

Figure II.3. *Spectra of transients utilized in this thesis during deconvolution of composite spectra*

II.2.1.3 Determination of quantum yield of radicals

The concentration of radicals (e.g. $3CB^{\bullet-}$ or $3CBH^{\bullet}$) were estimated from the concentration profiles, where the $^{3}3CB^{*}$ was quenched by more than 99%. Knowing the absorbance of triplet state and molar absorption coefficient at 520 nm, it is possible to calculate its concentration directly after the flash. Quantum yields of transients were calculated from **Equation 4**:

$$\Phi = \frac{c \cdot \varepsilon_T \cdot l}{\Delta A_T^0} \qquad (4)$$

Where:

Φ – quantum yield of transient

c – concentration of the transient as determined from the concentration profile obtained in spectral deconvolutions

ε_T – molar absorption coefficient of the 3CB triplet at maximum of absorption

l – optical path length

ΔA_T^0 - absorption change in the actinometer immediately after the laser pulse at 520 nm, i.e. at the maximum of the triplet absorption

II.2.2. Steady state photolysis

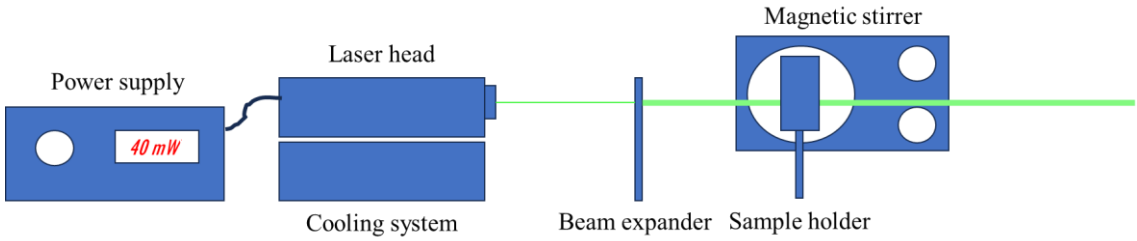

Figure II.4. *Schematic representation of the experiment set-up for steady state photolysis*

Stationary irradiation was employed to excite 3CB and initiate the photo-oxidation reaction. Investigated samples were irradiated using a Genesis CX355STM OPSL laser (Coherent) (**Figure II.4**) with emission wavelength at 355 nm (to selective excitation of the 3CB sensitizer molecule). The power of the laser beam was checked by power meter, which was validated by benzophenone-benzhydrol actinometry. Intensity of incident light was estimated to be $1.5 \cdot 10^{-5}$ $M \cdot s^{-1}$ for 40 mW of the laser power.

II.2.3. High Performance Liquid Chromatography

High-performance liquid chromatography (HPLC) stands as a robust chromatographic technique employed for the detection, separation, quantification, and purification of components within solutions. In this study, HPLC was used to monitor the reaction progress, examining formation of stable radical cross-coupling products initiated during steady-state irradiation of the investigated compounds.

Chromatography encompasses several techniques for separating mixtures. In essence, the components of a mixture distribute between two phases, stationary and mobile, governed by an equilibrium defined by the distribution ratio (or partition ratio). This ratio reflects the concentration of a component in the stationary phase relative to that in the mobile phase, with each component possessing unique values (dependent on the method of elution). The resulting chromatograph illustrates the sample amount versus time dependence, with the retention time of a component representing the interval between sample introduction and the appearance of peak intensity in the chromatogram. The total retention volume indicates the volume of eluent needed to remove a component from the stationary phase [126].

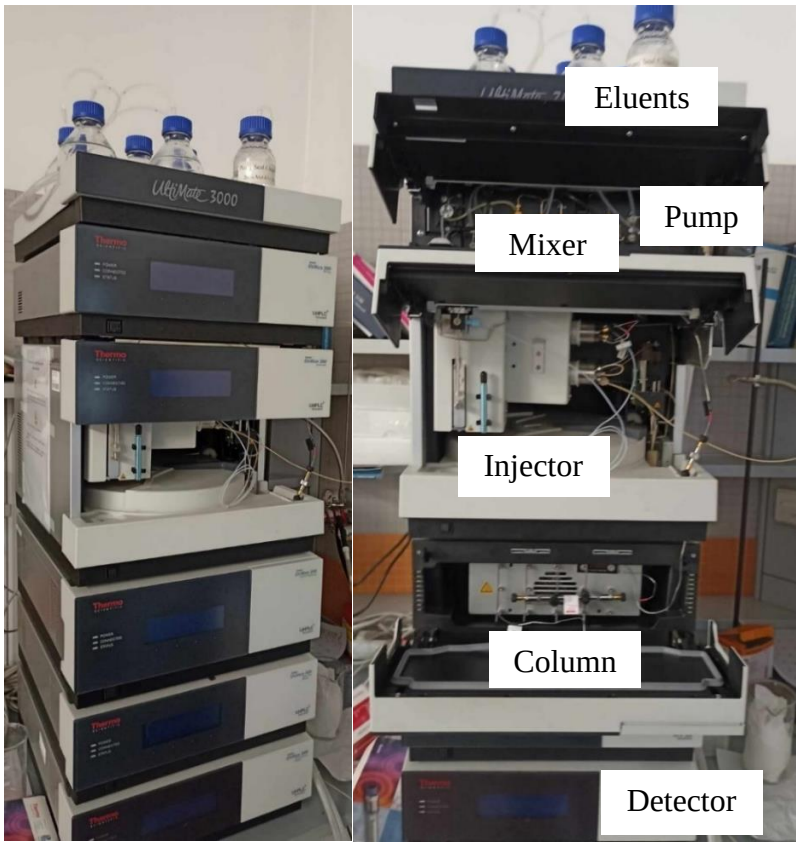

Figure II.5. *HPLC set-up employed in this thesis*

Liquid chromatography has evolved for enhanced precision, exemplified by high-performance liquid chromatography (HPLC), where solvent is forced through a column under high pressures, sometimes reaching hundreds of atmospheres. Here, a liquid sample passes over a solid adsorbent material in the column under the flow of a liquid solvent, facilitating simultaneous interactions between components and the stationary and mobile phases. Different interactions with the adsorbent material result in varying elution times; weak interactions lead to shorter elution times, while stronger interactions prolong retention times. HPLC is often coupled with other instruments, such as mass spectrometers.

In this study, reversed-phase HPLC (RP-HPLC) was employed (**Figure II.5**), featuring a non-polar stationary phase and a moderately polar mobile phase. Columns in RP-HPLC are typically filled with surface-modified silica (R=$C_{18}H_{37}$ or C_8H_{17}). Under these conditions, less-polar molecules exhibit longer retention times, while polar compounds are eluted rapidly. The addition of water to the eluent increases retention time, while the inclusion of TFA (hydrophobic counter ions) forms ion pairs with positively charged solutes, enhancing their affinity for the hydrophobic stationary phase [126–128].

Areas of peaks obtained from chromatograms (absorbance detection at 220 nm) of chosen model compounds and 3CB post irradiation detected were utilized to calculate decrease in concentration of those respective compounds. Given intensity of incident light it was possible to calculate light absorbed by the sample (I_a). With that date quantum yields of photodegradation were calculated based on **Equation 5**. Three sets of experiments were performed for each derivative. Error represents double standard deviation.

$$\Phi = \frac{\Delta c}{I_a \cdot t} \qquad (5)$$

Where:

Φ – quantum yield of photodegradation

Δc – change in concentration

I_a – light absorbed by the sample

t – time of irradiation

II.2.4. Mass Spectrometry

High-performance liquid chromatography coupled with mass spectrometry allows for detailed qualitative analysis of the components of the sample. It provides information about the composition analyzed molecule based on the measurement of the mass-to-charge ratio (*m/z*). This technique serves as a valuable component to liquid chromatography with spectrophotometric detection (HPLC-DAD), which primarily offers quantitative data. In this study, HPLC-MS analysis was followed by a more detailed MS/MS fragmentation of molecular ions, providing straightforward information on the structure of the stable products. The methods implemented in this thesis provided accuracy to the fourth decimal place, and combined with MS/MS fragmentation, they enabled deduction of products.

The basic aim of mass spectrometry is to generate ions, separate and analyze them by their *m/z* in a quantitative and qualitative manners. The sample can be injected directly from a syringe pump or *via* prior chromatographic separation (by GC, HPLC etc.) into an ion source. Subsequently, ions fly to the mass analyzer and then to a detector operated under high vacuum. Mass spectra preparation requires a small amount of the sample.

A mass spectrum consists of two parameters: abundance (signal intensity) on the ordinate and *m/z* on the abscissa. The *m/z* is dimensionless and reflects the ion mass divided by its charge. Ionization occurs via two possible methods: hard and soft ionization. Hard ionization yields ions with large degrees of fragmentation due to the use of significant residual energy, while soft ionization sources (e.g. ESI) form ions with minimal residual energy, allowing for the identification of the molecular ion peak. The mass analyzer is another important component of mass spectrometer. It separates the mixture of ions by *m/z* ratio in order to obtain a mass spectrum. Various types of mass analyzers have been developed depending on the applications.

The final part of the mass spectrometer is the detector, which can record the induced charge or the current produced by the ions. Several detectors have been applied: from the simple ones, such as a Faraday cup to electron multiplier or ion-to-photon detectors. In following subchapters below, ionization method (ESI), ion separation (TIMS) and mass analyzer (TOF) that are utilized in this thesis are describe briefly [129,130].

II.2.4.1 ESI

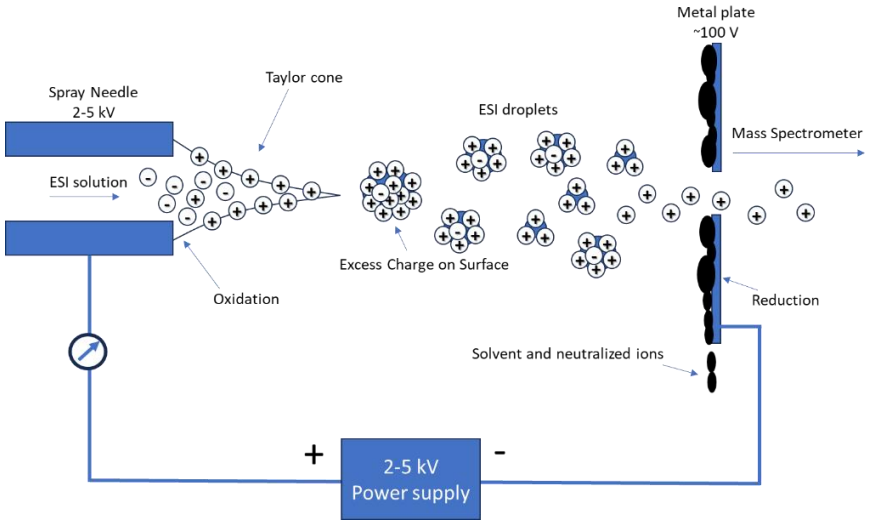

Figure II.6. *Schematic representation of electrospray ionization [131,132]*

Electrospray ionization (ESI) can be operated even at atmospheric pressure. The construction of ions source is quite simple (**Figure II.6**). The stainless-steel capillary has a high potential and produces small, charged droplets. Nebulizer gas directs the aerosol toward the charged plates with small window. Because of high excess of charge in the droplets due to the solvent evaporation, the electrostatic repulsions cause „Coulombic explosions". Those explosions move sample into gas phase. Each molecule can be singly or multiply protonated in the positive mode detection or deprotonated in the negative mode. ESI is widely used in the analysis of nonvolatile and large molecules, such as nucleic acids, polymers or proteins. The samples should be introduced in a polar, volatile solvent to assist protonation. It may create ions with either single or multiple charges [129–132].

II.2.4.2 TIMS

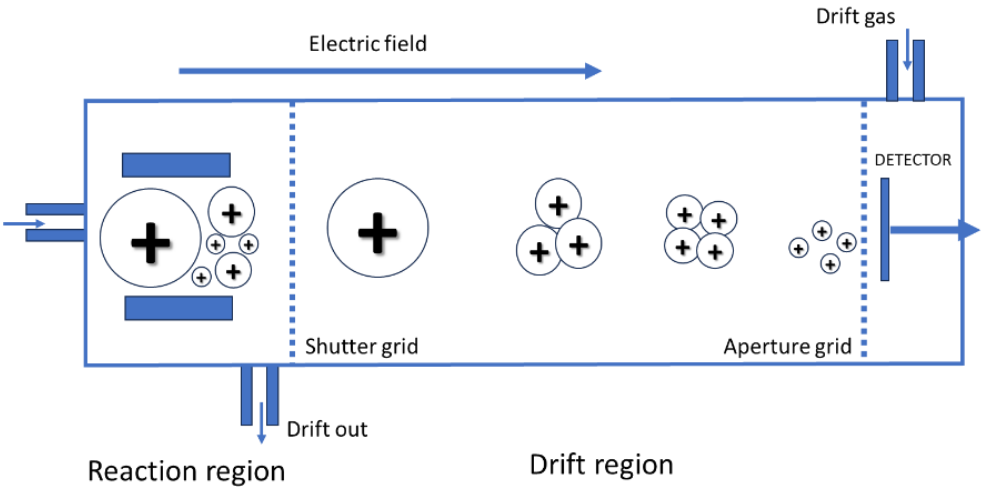

Figure II.7. *Schematic representation of trapped ion mobility spectrometer* [133]

Ion mobility spectrometry–mass spectrometry (IMS-MS) is an analytical chemistry method that separates gas phase ions based on their interaction with a collision gas and their masses. In the first step, the ions are separated according to their mobility through a buffer gas on a millisecond timescale using an ion mobility spectrometer. In the second step, the separated ions are introduced into a mass analyzer, where their *m/z* ratios can be determined on a microsecond timescale. The effective separation of analytes achieved with this method makes it widely applicable in the analysis of complex samples, such as in proteomics and metabolomics.Trapped ion mobility spectrometry (TIMS) is a gas-phase separation method that has been coupled to quadrupole orthogonal acceleration time-of-flight mass spectrometry (Q-TOF). The TIMS analyzer uses an electric field that holds ions stationary against a moving gas (**Figure II.7**), unlike conventional drift tube ion mobility spectrometry where the gas is stationary. Ions are initially trapped, and subsequently eluted from the TIMS analyzer over time according to their mobility.

Effectively, the drift cell is prolonged by the ion motion created through the gas flow. Therefore, TIMS devices do neither require large size nor high voltage in order to achieve high resolution, for instance achieving over 250 resolving power from a 4.7 cm device through the use of extended separation times. However, the resolving power strongly depends on the ion mobility and decreases for more mobile ions. In addition, TIMS can be capable of higher sensitivity than other ion mobility systems because no grids or shutters exist in the ion path, improving ion transmission both during ion mobility experiments and while operating in a transparent MS only mode [133,134].

II.2.4.3 TOF

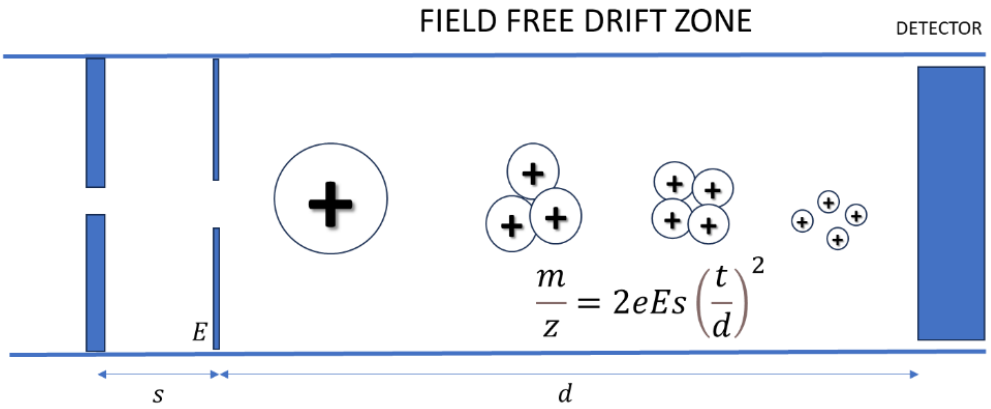

Figure II.8. *Schematic representation of time-of-flight [135]*

It is a method of mass spectrometry in which an ion's mass-to-charge ratio is determined by a time-of-flight measurement. Ions are accelerated by an electric field of known strength. This acceleration results in an ion having the same kinetic energy as any other ion that has the same charge. The velocity of the ion depends on the *m/z* (heavier ions of the same charge reach lower speeds, although ions with higher charge will also increase in velocity, **Figure II.8**). The time that it subsequently takes for the ion to reach a detector at a known distance is measured. This time will depend on the velocity of the ion, and therefore is a measure of its *m/z* ratio. From this ratio and known experimental parameters, one can identify the ion.

Continuous ion sources, most commonly ESI, are generally interfaced to the TOF mass analyzer by "orthogonal extraction". In this method, ions introduced into the TOF mass analyzer are accelerated along an axis perpendicular to their initial direction of motion. Orthogonal acceleration, combined with collisional ion cooling allows for the separation of ion production in the ion source and mass analysis. This technique enables very high resolution for ions produced in MALDI or ESI sources.

Before entering the orthogonal acceleration region or the pulser, the ions produced in continuous (ESI) or pulsed (MALDI) sources are focused (cooled) into a beam of 1–2 mm diameter by collisions with a residual gas in RF multipole guides. A system of electrostatic lenses, mounted in the high-vacuum region before the pulser, makes the beam parallel to minimize its divergence in the direction of acceleration. The combination of ion collisional cooling and orthogonal acceleration TOF has significantly increased the resolution of modern TOF MS from few hundred to several tens of thousands without compromising sensitivity [135–138].

II.2.5. UV-Vis spectroscopy

To determine the equilibrium constant (K) of ground state complex formed between sensitizer and compound/protein, the absorbance changes was monitored while aliquots of compound were titrated to 3CB solution. General procedure consisted of preparation of a constant volume of 3CB solution (1000 μL; 1.25 mM) and titration of the 3CB solution with increasing amounts of the model compound/protein. UV-Vis spectrophotometer (Cary 100 UV-Vis) was employed to measure absorbance. UV-Vis spectrum of CB alone in the range of 220–400 nm was recorded as the reference ("zero") spectrum. After adding each aliquot of 5 μM of the model compound/protein (27.95 μM, 35780 Da, 2 $mg \cdot mL^{-1}$), the mixture was stirred for 1 min, and respective spectra were recorded. Changes of the concentration due to changes in volume has been taken into account. Analytical wavelength at which the largest difference in absorbance occurs between CB alone and the mixture was identified. This difference in absorbance reflected the formation of the complex between CB and the model compound/protein. K was then calculated following formula in **Equation 6** [139,140]:

$$\frac{[sens] \cdot l}{\Delta A_{\lambda}} = \frac{1}{K \cdot \varepsilon_{\lambda}} \cdot \frac{1}{[GAPDH]} + \frac{1}{\varepsilon_{\lambda}} \qquad \textbf{(6)}$$

Where:

[sens] – concentration of sensitizer

l – optical path length

ΔA_{λ} – observed absorbance change of the composite spectrum at the given wavelength

K – equilibrium rate constant

ε_{λ} – molar absorption coefficient of the sensitizer at given wavelength

[GAPDH] – concentration of GAPDH

II.2.6. SDS-PAGE analysis (Sodium dodecyl sulphate–polyacrylamide gel electrophoresis)

Probably the most widely used of techniques for analyzing mixtures of proteins is SDS polyacrylamide gel electrophoresis. In this technique, proteins react with the anionic detergent, sodium dodecyl sulphate (SDS, or sodium lauryl sulphate) to form negatively charged complexes. The amount of SDS bound by a protein, and so the charge on the complex, is roughly proportional to its size.The proteins are generally denatured and solubilized by their binding of SDS, and the complex forms a prolate ellipsoid or rod of a length roughly proportionate to the protein's molecular weight (**Figure II.9**). Thus, proteins of either acidic or basic pl (isoelectric point) form negatively charged complexes that can be separated on the bases of differences in charges and sizes by electrophoresis through a sieve-like matrix of polyacrylamide gel. This thesis follows the procedure from [141,142]. The gel was loaded to the electrophoresis tank. Required volume of sample (mixed with corresponding dye and with/without reducing agent) was loaded it into a sample well through the reservoir buffer. The amount of sample loaded depends upon the method of its detection, in case of this study 12 µl was used. Having loaded all samples without delay, electrophoresis was started by turning on power. On a gel of about 0.5-1 mm thickness and about 14 cm length, an applied voltage of about 200 V gave a current of about 20 mA or so (falling during electrophoresis with constant voltage employed).

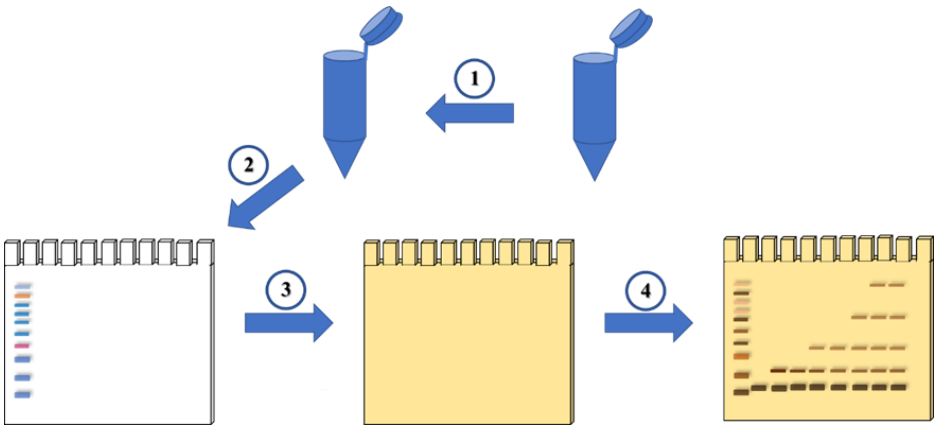

Figure II.9. *Graphical representation of sodium dodecyl sulphate-polyacrylamide gel electrophoresis with silver staining visualization. (1) preparation of the samples, (2) samples are loaded into chambers within the gel, then electrophoresis occurs. (3) gel is washed for the protein fixation, then after detergent is extracted, the gel is subjected to reducing environment, then silver staining, in this step gel changes color, (4) lastly silver ions bounded to proteins are reduced and separated bands are visible*

To visualize low-level proteins separated by gel electrophoresis silver staining was used. Gel taken after electrophoresis was placed in the mixture of 50% methanol and 10% acetic acid for 30 min to denature proteins in the fixative, at the same time detergent is extracted. The diffusion of the protein is thus significantly reduced. We continue the process with 5% methanol water solution for 15 min then wash it three times with water for 5 min for each wash. After that we create a reducing environment by adding a solution of sodium thiosulfate in water (0.2 $g \cdot dm^{-3}$) for 2 min, then wash it again with water for another 2 min. After that we let the gel incubate in silver nitrate solution (2 $g \cdot dm^{-3}$) for 25 min. This allows silver ions to bind to the proteins. Excess amount of silver is washed by another portion of water for 5 min. Then mixture of alkaline formaldehyde (6 g of sodium carbonate, 100 µl of 37% formaldehyde, 4 ml of previously used thiosulfate solution filled up to 200 ml with water) is added to reduce silver ions to metallic silver (this can take up to 2 min, depends on the quality of bands which are visible). After that gel is placed into EDTA solution for 10 min then washed with water for 5 min (14 $g \cdot dm^{-3}$).

II.2.7. Determination of stable products in protein

In order to detect and characterize the main oxidation products of GAPDH, HPLC-MS was applied. Two simultaneous experiments were performed: (i) timsTOF, analysis of in-solution digestion (with non-irradiated GAPDH sample as reference), (ii) in-gel digestion of bands cut from SDS-PAGE gel using the same time of irradiation and analyzed with timsTOF. For first experiment aliquots of protein were dissolved in 50 mM ammonium bicarbonate pH 8, and either directly digested or subjected to reduction (10 mM DTT) and alkylation (30 mM iodoacetamide) prior to digestion. All protein samples were trypsinized at 37 °C overnight using a 1:20 w/w enzyme:protein ratio. Samples were acidified to a final concentration of 0.5% TFA, and 1 µg was desalted on a custom-made micro column comprising Empore C18 disk material (3 M) and Poros R2 50 µm (Thermo Scientific), using 50% AcN, 0.1% TFA and 70% AcN, 0.1% TFA sequentially for elution. Second experiment required in-gel digestion, which was followed exactly from [143], except the gel was silver-stained (described in paragraph II.2.3). All of the aforementioned samples were subjected to LC-MS analysis using a two-column setup on an EASY-nLC™ 1200 System (Thermo Fisher Scientific) coupled to an Orbitrap Exploris 480 mass spectrometer (Thermo Fisher Scientific). The precolumn (3.5 cm, 100 µm ID) was packed with Reprosil-Pur 120 C18-AQ, 5 µm (Dr. A. Maisch, Ammerbuch-Entringen, Germany) and the analytical column

(18 cm, 75 μm ID) with Reprosil-Pur 120C18-AQ, 3 μm (Dr. A. Maisch). For separation of peptides, a gradient of solvent B (95% AcN, 0.1% FA) was applied: 2%–34% B in 30 min, 34%–100% in 10 min and 100% B for 10 min with solvent A being 0.1% FA and the flow set to 250 nl/min. MS data were recorded with a scan range of 350–1600 *m/z* and a resolution of 120K. MS/MS data were recorded as top twelve most abundant peaks with a resolution of 30K, an isolation window of 1.2 *m/z* and 15 s of dynamic exclusion. The spectra were analyzed with Proteome Discoverer (v2.5) and a Sequest HT (v1.17) search engine (Thermo Fisher Scientific). The following search parameters were applied: two missed cleavages; dynamic modifications of CBH on Met, Cys, Tyr, His, Trp, and Phe from experiments on model compounds; the mass tolerance was set to 5 ppm for parent ions and 0.02 Da for fragmented ions.

Calculation of the relative abundance of a modification correlated to a specific type of amino acid was calculated as an average of the particular mass shift of the peptide with well-defined modifications, compared to the area of signals for all of those peptides with given amino acid present in the analysis (with all possible charge states) and normalized to 100%. Only peptides identified in at least three technical replicates were accepted [144]. Areas were determined using Bruker QuantAnalysis software.

II.2.8. Amino Acid Analysis

Amino Acid Analysis was performed to quantify loss of parent amino acids in oxidized sample. There are several possibilities to accurately quantify concentrations of amino acids in given sample. Historically method started as a mean to obtain composition of pure proteins *via* direct hydrolysis of them in 6 M HCl in oxygen-free atmosphere in 110°C for 22 h with subsequent separation of liberated amino acids through ion-exchange chromatography and determination of their presence and quantity using ninhydrin [145]. Method used in this thesis is extensively reported in [146]. To describe it briefly, hydrolysis is improved upon due to usage of methanesulphonic acid with tryptamine to protect the most vulnerable amino acids during acidic hydrolysis. Samples were desalted and hydrolyzed in oven (at 110°C) for 16 hours. Determination and quantification occur simultaneously by HPLC-MS analysis which utilizes internal standards in samples to compare areas of peaks on extracted chromatograms of them with amino acids (and some of their oxidated products) of completely hydrolyzed and purified samples. To accommodate for differences in concentration of amino acids in each sample, they have been normalized to the concentration of alanine.

II.2.9. Ellman's assay

To complement Amino Acid Analysis, Ellman test was implemented to measure concentration of solution accessible cysteines. Method from [147] was used with following changes to allow for usage of microplate reader (Infinite M200, Tecan Corp.). Ellman's reagent (5 mM 5,5-dithiobis-2-nitrobenzoic acid (DTNB), ±5 mM cystamine) was prepared by suspending 38.55 mg DTNB (±28.15 mg cystamine dihydrochloride) in 25 mL of PBS buffer, whereupon all DTNB was dissolved. About 1 mL of water and 0.042 mL of concentrated HCl (37%, 4.5 mmol) were added to 1.811 mg of cysteine (1.5 mmol, zwitterionic form, Sigma C-7755) and stirred for several minutes until all cysteine was dissolved. Subsequently, the solution was diluted to 50 mL with water (0.3 mM cysteine). 0, 2, 4, 6, or 8 µL of 0.3 mM cysteine standard was filled up to 95 µL with PBS, then Ellman's reagent was added (5 µL (concentration 5 mM PBS). Absorbance at 412 nm was read after 5 min to measure formation of product of the reaction (**Figure II.10**). The absorbance values were plotted against the cysteine concentrations. Knowing that GAPDH has a mass of 37 kDa, which translates to 27.027 µM of protein in a 1 mg/ml solution, resulting in 108.108 µM of cysteine (as it has four cysteine residues). Knowing that the calibration curve ranges from 0 to approximately 24 µM cysteine, the experiment was planned as follows: 20 µL of protein was added to 75 µL of PBS and topped with 5 µL Ellman's reagent. The incubation time was set to 20 min in the dark.

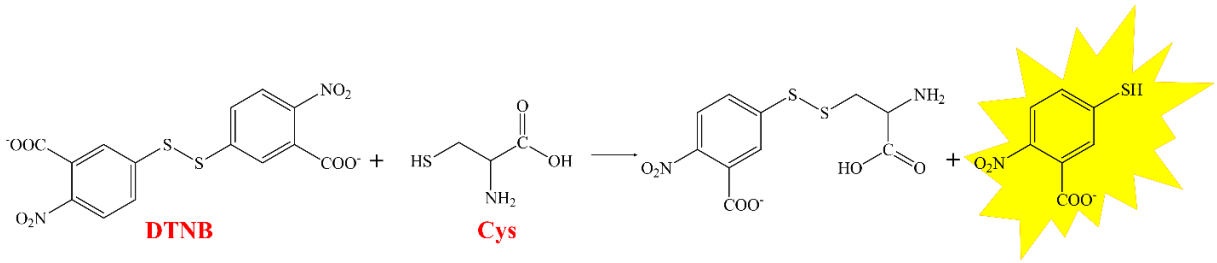

Figure II.10. *Reaction of DTNB with Cys (colorful product of the reaction is highlighted in yellow) [147]*

II.2.10. Activity assay of GAPDH

Glyceraldehyde-3-Phosphate Dehydrogenase (GAPDH) catalyzes the conversion of Glyceraldehyde-3-Phosphate (G3P) to 1,3-Bisphosphate Glycerate (BPG) and plays a key role in glycolysis. GAPDH Activity Assay Kit has been used to measure the enzyme activity of GAPDH before and after irradiation in time to compare how modification influence activity.

The GAPDH Activity Assay Kit provides a simple and sensitive method for monitoring GAPDH activity in various samples. GAPDH activity is determined in a coupled enzyme reaction in which G3P is converted to BPG by GAPDH. This results in a colorimetric (450 nm) product proportional to the enzymatic activity present. The assay is sensitive to 100 mUnits mL^{-1}. One unit of GAPDH activity is the amount of enzyme that will generate 1 mM of NADH per minute at pH 7.2 at 37 °C.

To utilize this assay microplate reader was employed (Infinite M200, Tecan Corp.) set of experiments was conducted to obtain standard curve of concentrations of NADH in nM concentration. All results had blank sample subtracted from them. Then positive sample was run to indicate the correct experimental procedure. No deviations were seen in all of the experiments conducted. Finally, samples of GAPDH either with or without 3CB (to check for possible inhibition of the enzyme in ground state) and with different times of irradiation were measured and presented as kinetic curve. Last measurement at 30 min was utilized to calculate activity of given sample.

III. Results and discussion

As a preliminary remark, each following subsection starts with conditions for each experiment at the very beginning of the paragraph in black box. Each model compound has been subjected to laser flash photolysis and steady state photolysis which is reflected in construction of each subsection. Picking the exact concentration for each sample so that one experiment can provide information for both quenching rate constants and concentration profile, it was detrimental to pick one which suits solubility of given compound and quenches excited triplet state of 3CB substantially. Due to limitations in solubility, given that not 100% triplet state quenching is present (as for Phe compounds, ^{3}3CB* effective quenching was estimated between 10-35%), it was abundantly clear that correction is required. It utilized the reciprocal of **Equation 2** in which whole equation has been multiplied by τ_0 and final result has been subtracted from one as that would give effective quenching of ^{3}3CB* (**Equation 2a)**.

$$\frac{\tau_T}{\tau_T^0} = \frac{1}{1+\tau_T^0 \cdot k_q \cdot [Q]} \quad \textbf{(2a)}$$

Variations in concentrations and times of irradiation in steady state photolysis came from previous optimization *via* HPLC experiments. It was apparent, that if concentration was low then subsequent concentrations of products will be even lower, however higher concentrations resulted in secondary reactions (still present in some chromatograms due to impossibility of stopping further reactions). Unless specified otherwise, all experiments have been conducted at pH 7.

GAPDH experiments followed path during which first experiment answers the question whether the protein-sensitizer complex in the ground state is formed. Secondly, SDS-PAGE provided information on formation of aggregates and allowed for picking suitable time of irradiation of GAPDH. Then, the qualitative and quantitative analysis of GAPDH modification of picked irradiation time should answer additional to those in the aim of the work, questions:

- Do modifications that occur in model compounds are also present in the oxidized protein?
- Which amino acid is modified the most in sample irradiated at chosen time?
- What is the extent of modifications to amino acids?

III.1. Tyrosine

III.1.1. Laser flash photolysis

Concentrations: Tyr, Tyr-OEt, N-Ac-Tyr, N-Ac-Tyr-OEt – 0 mM, 0.25 mM, 0.5 mM, 1 mM, 1.5 mM; Tyr-Val – 0 mM, 0.4 mM, 0.6 mM, 0.8 mM, 1 mM; 3CB – 4 mM and 5 mM in case of Tyr-Val. Ar bubbled for 25 min in rectangular quartz cuvettes with 10 mm optical path.

LFP experiments were performed to monitor the reaction of ^{3}3CB* with Tyr and its derivatives at very early stage of the reaction. The k_q for quenching the ^{3}3CB* by Tyr and other model compounds were measured by monitoring the decay of the absorption of the ^{3}3CB* at 450 nm (to avoid the overlapping of kinetics with 3CBH$^{\bullet}$, **Figure TYR.1 a**). Linear least-squares fits of k_{obs} vs. [Q] plots (Stern-Volmer plot) shown in **Figure TYR.1 b** were used to calculate k_q with pseudo-first-order rate constant. The same was done for other compounds presented in **Figure TYR.SI1-4**. The quenching rate constants are given in **Table TYR.1**. Value for Tyr is within the margin of error for that obtained for ^{3}4CB* quenching [78].

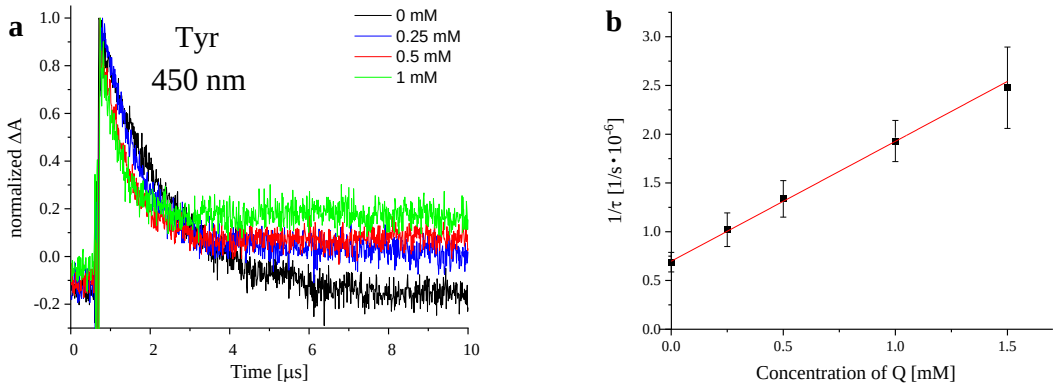

Figure TYR.1 ***(a)*** *Kinetic traces for the ^{3}3CB* decay at 450 nm in the presence of varying concentrations of Tyr at pH 7* ***(b)*** *The Stern-Volmer plots according to* ***Equation 2*** *for the quenching of ^{3}3CB* by Tyr at pH 7 in aqueous solution for 3CB (4 mM)*

Table TYR.1 *Quenching rate constants and corresponding quantum yields of short-lived intermediates formation for Tyr and its derivatives, where Z_Q and Z_{CB} are the net charge of Q and CB at pH 7, respectively*

Quencher	Z_Q	k_q (x10^9 $M^{-1}\cdot s^{-1}$)	$\Phi_{3CBH^\bullet}$	$\Phi_{3CB^{\bullet-}}$	$\Phi_{TyrO^\bullet}$	$Z_Q Z_{3CB}$
Tyr	0	1.2±0.1[a] 1.3±0.3[b]	0.78±0.09	0.17±0.02	0.97±0.11	0
Tyr-OEt	+1	2.3±0.2	0.91±0.24	0.10±0.03	0.96±0.25	-1
N-Ac-Tyr	-1	1.2±0.5	0.79±0.19	0.19±0.05	0.88±0.22	+1
N-Ac-Tyr-OEt	0	2.3±0.2	0.65±0.08	0.20±0.03	0.93±0.10	0
Tyr-Val	0	1.8±0.3	0.75±0.20	0.07±0.03	0.79±0.21	0

[a] value for ^{3}3CB* quenching

[b] value for ^{3}4CB* quenching from [78]

Transient absorption spectra recorded for Tyr and 3CB are presented in **Figure TYR.2**. Quenching of ^{3}3CB* by Tyr resulted in the formation of new absorption bands in transient absorption spectra. The absorption band observed at 550 nm was assigned to the $3CBH^\bullet$, while the absorption band at 410 nm was attributed to $TyrO^\bullet$ based on the previous works [78,148]. Same bands were identified in other Tyr-derivatives with different group blockage (**Figure TYR.SI5).** The deconvolution of recorded transient absorption spectra shown the formation of 3CB*, $3CBH^\bullet$, $3CB^{\bullet-}$ and $TyrO^\bullet$ and provided the concentrations of each individual components based on procedure described in **Chapters II.2.1.2** and **II.2.1.3** [78]. The concentration of each transient was plotted against time after the laser pulse (concentration profiles) and presented in **Figure TYR.2 b**. The concentration of ^{3}CB* (ε_{520} =5400 $dm^3\cdot mol^{-1}\cdot cm$) [26] measured at the end of flash for 3CB samples without quencher (actinometer) were used to determine the quantum yields of intermediate species formed during sensitized photo-oxidation.

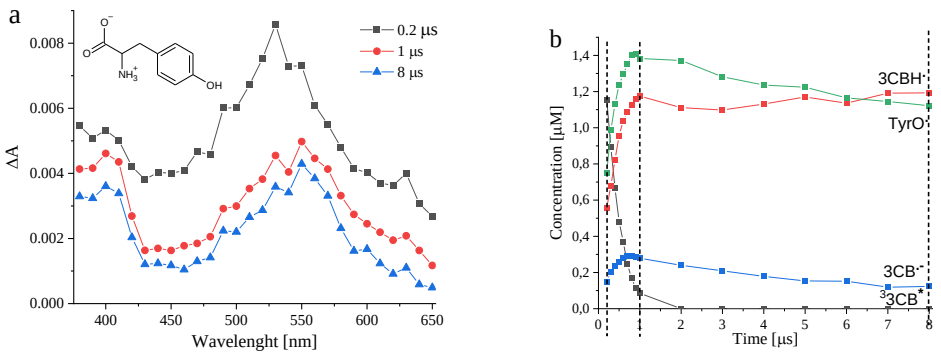

Figure TYR.2 ***(a)*** *Evolution of transient absorption spectra from 3CB-sensitized oxidation of Tyr at pH 7. Spectra were recorded at different delays following laser pulse: 0.2 µs (black ■), 1 µs(red ●), 8 µs (blue ▲).* ***(b)*** *Concentration profiles of transients identified in the laser flash photolysis of an aqueous solution of Tyr (1 mM) and CB (4 mM) at pH 7 where (black ■) is ^{3}3CB*, (red ●) is 3CBH$^\bullet$, (blue ▲) is 3CB$^{\bullet-}$and (green ▼) is TyrO$^\bullet$. Dotted lines represent times at which respective spectra were presented in* ***(a)***

According to those results, it seems that primary step of photosensitized oxidation of Tyr involves electron transfer followed by proton transfer, and is in accordance to proposed mechanism for other sensitizers in the literature [77,78,81]. Large values of quenching rate constants, close to the range of diffusion-controlled processes (10^9 $M^{-1}\cdot s^{-1}$), correspond greatly with the current literature data, and are an indicator of kinetically controlled process.

Three groups contribute to the overall charge of Tyr: carboxylic acid, amine and phenol. At pH equal to 7, the carboxylic group, if unprotected, should be negatively charged, while the amine group should be positively charged. Thus, it can be seen that the molecule with an unprotected carboxylic group has negative charge. This negative charge should lead to the repulsion of negatively charged photosensitizer molecule (Z_{3CB}=-1), indicating that the Coulombic effect described in the introduction is also present here. Consequently, differences in the quenching rate constants for Tyr and its derivatives can be explained by coulombic interaction of 3CB and Tyr ions arising from different groups in Tyr being blocked. Essentially, the net charge of the molecule (see Z_Q values in **Table TYR.1**) results in changes in diffusion-controlled rate constants, with Z_QZ_{3CB} values (**Table TYR.1**) being observed (see ref. [117]). This effect rationalizes the changes observed in k_q values for three derivatives; however, it does not explain higher-than-expected value for N-Ac-Tyr-OEt. It was shown in ref. [98] that application of sensitizer with large charge (Z_Q=-4) (benzophenone with four carboxylic groups) allowed researchers to observe more prevalent differences there.

Presence of $3CB^{\bullet-}$ in all spectra implies that first step must be the electron transfer (ref [149]) followed by second step, proton transfer. Values of quantum yields of the generation of $3CBH^{\bullet}$ and $3CB^{\bullet-}$ presented in **Table TYR.1** (aside from quantum yield of the generation of $3CB^{\bullet-}$ for Tyr-OEt) are in the same range for Tyr and its derivatives. The mechanism of primary steps of sensitized photo-oxidation, based on the presented results, is similar to the mechanism currently known in the literature for another sensitizers [78,98,115,149] and it is presented in **Figure I.10** (with the exception of sensitizer, which in this case would be 3CB). This mechanism for the 3CB-sensitized oxidation of Tyr and its derivatives in aqueous solution is additionally confirmed by the fact that the sum of quantum yields of transients ($3CBH^{\bullet}$ and $3CB^{\bullet-}$) from sensitizer reduction is in 1:1 ratio to quantum yield of $TyrO^{\bullet}$ (**Table TYR.1**), which was also the case in previous study by Wójcik et. al. [78].

III.1.2. Steady state photolysis

Concentrations: Tyr, Tyr-OEt, N-Ac-Tyr, N-Ac-Tyr-OEt, Tyr-Val – 1 mM; 3CB – 4mM and 5 mM in case of Tyr-Val. Ar bubbled for 25 min in rectangular quartz cuvettes with 10 mm optical path; the output power used was set at 40 mW; Gradient elution methods for samples are present in **Table TYR.SI1**

Photodegradation quantum yields were measured by HPLC chromatography from three different sample sets with different irradiation time from 0 to 360 s. The concentration of 3CB was 4 mM, while the concentration of Tyr derivative was 2 mM. It followed the process described in **Chapter II.2.3** based on the **Equation 5** and are presented in **Table TYR.2**. Slope of the linear regression of the concentration over time graphs provided reaction rate (**Figure TYR.SI6**), which further divided by light absorbed by the sample ended in the final results. The value of Φ_{Tyr} for Tyr, Tyr-OEt and N-Ac-Tyr is relatively small probably due to the reaction between $3CBH^{\bullet}$ and $TyrO^{\bullet}$, that yields the regeneration of 3CB and respective Tyr derivative (k_{bH}, **Figure Tyr.7**). Consequences in the formation of stable products (namely their amount **Figure TYR.3**) for N- and C-terminal blocked Tyr can be explained by the increase in quantum yields of photodegradations. Nevertheless, ratio of Φ_{Tyr} and Φ_{3CB} being 1:1 (within the margin of error) in all of the photosensitized anoxic oxidation of Tyr and its derivatives provides further insight into the mechanism.

Table TYR.2. *Quantum yields of Tyr and its derivatives decomposition (Φ_{Tyr}) and quantum yields of 3CB decomposition (Φ_{3CB}) under anaerobic oxidation by ^{3}3CB*.*

	Tyr	**Tyr-OEt**	**N-Ac-Tyr**	**N-Ac-Tyr-OEt**
Φ_{Tyr}	0.12±0.02	0.21±0.06	0.28±0.08	0.52±0.14
Φ_{3CB}	0.14±0.03	0.23±0.08	0.33±0.03	0.74±0.19

Analysis of stable products was carried on with conditions described in the box above. The most crucial part involved separation of products formed during anoxic photo-oxidation of Tyr, and its derivatives, as experiments proved to be different than expected. According to the literature (**Chapter I.2.2.2**) at most four different products of the tyrosine should be present during this process. Number of products present in post reaction mixture grew in the following sequence: Tyr, N-Ac-Tyr, Tyr-OEt, Tyr-Val, N-Ac-Tyr-OEt (**Figure TYR.3** and **Figure TYR.4**). Further mass analyses of stable products unveiled their molecular composition due to their monoisotopic mass (**Table TYR.3**) and possible structure of respective ions due to their fragmentation patterns. Several products shared their respective ion fragments with most important ones being *m/z* 269.13 and *m/z* 209.10, identified as double immonium ion formed from diTyr and fragment represented in blue in **Figure TYR.5**.

Several peaks, that appeared as a result of Tyr and Tyr-derivatives irradiation in the presence of 3CB, were identified. The analysis of monoisotopic mass and fragmentation pattern for each identified products showed the formation of three groups of products: Tyr-CBH adduct, diTyr and Tyr *m/z +2Da*. The first two groups are formed *via* radical recombination of 3CBH$^\bullet$ and TyrO$^\bullet$ radicals or two TyrO$^\bullet$ radicals. The formation of Tyr-3CBH is a characteristic product for this sensitizer, but it was not identified for all Tyr derivatives. However, diTyr has been widely studied since its discovery in 1959 [150]. Many papers focus on two particular diTyr products: 3,3'-diTyr and 3,O'-DiTyr. But looking at the possible structures of TyrO$^\bullet$ radicals [82,84], it is possible that they can recombine to form different diTyr products.

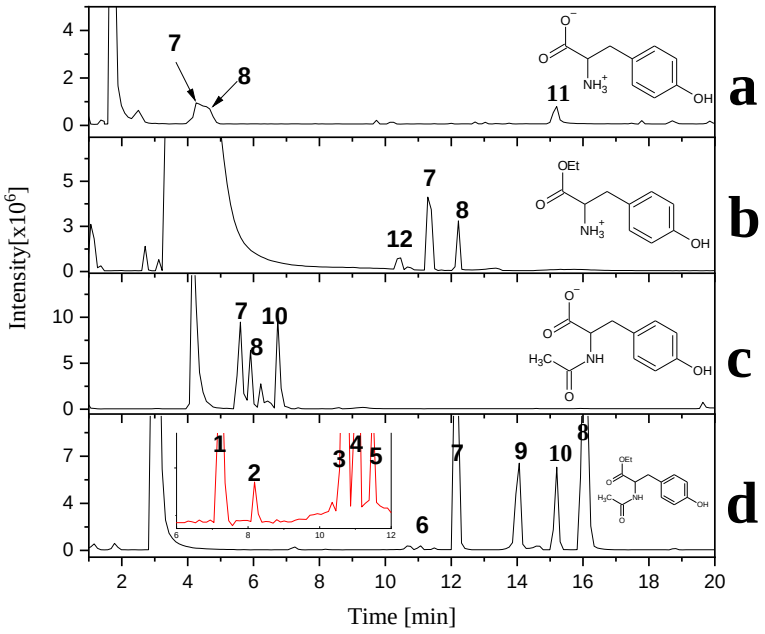

Figure TYR.3 *Comparison of total ion current chromatograms for irradiated samples of 3CB with* ***(a)*** *Tyr,* ***(b)*** *TyrOEt,* ***(c)*** *N-Ac-Tyr,* ***(d)*** *N-Ac-Tyr-OEt, and with identified products listed in* ***Table TYR.3***

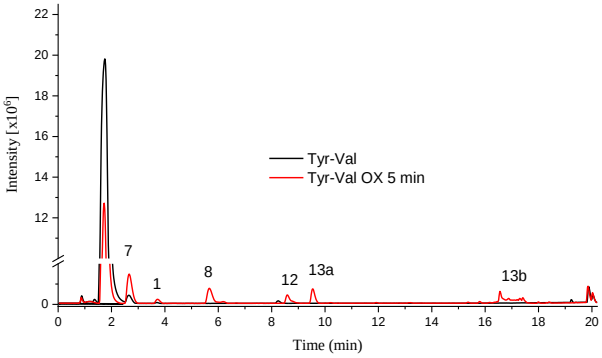

Figure TYR.4 *Comparison of total ion current chromatograms for irradiated samples of 3CB with Tyr-Val with identified products listed in* ***Table TYR.3***

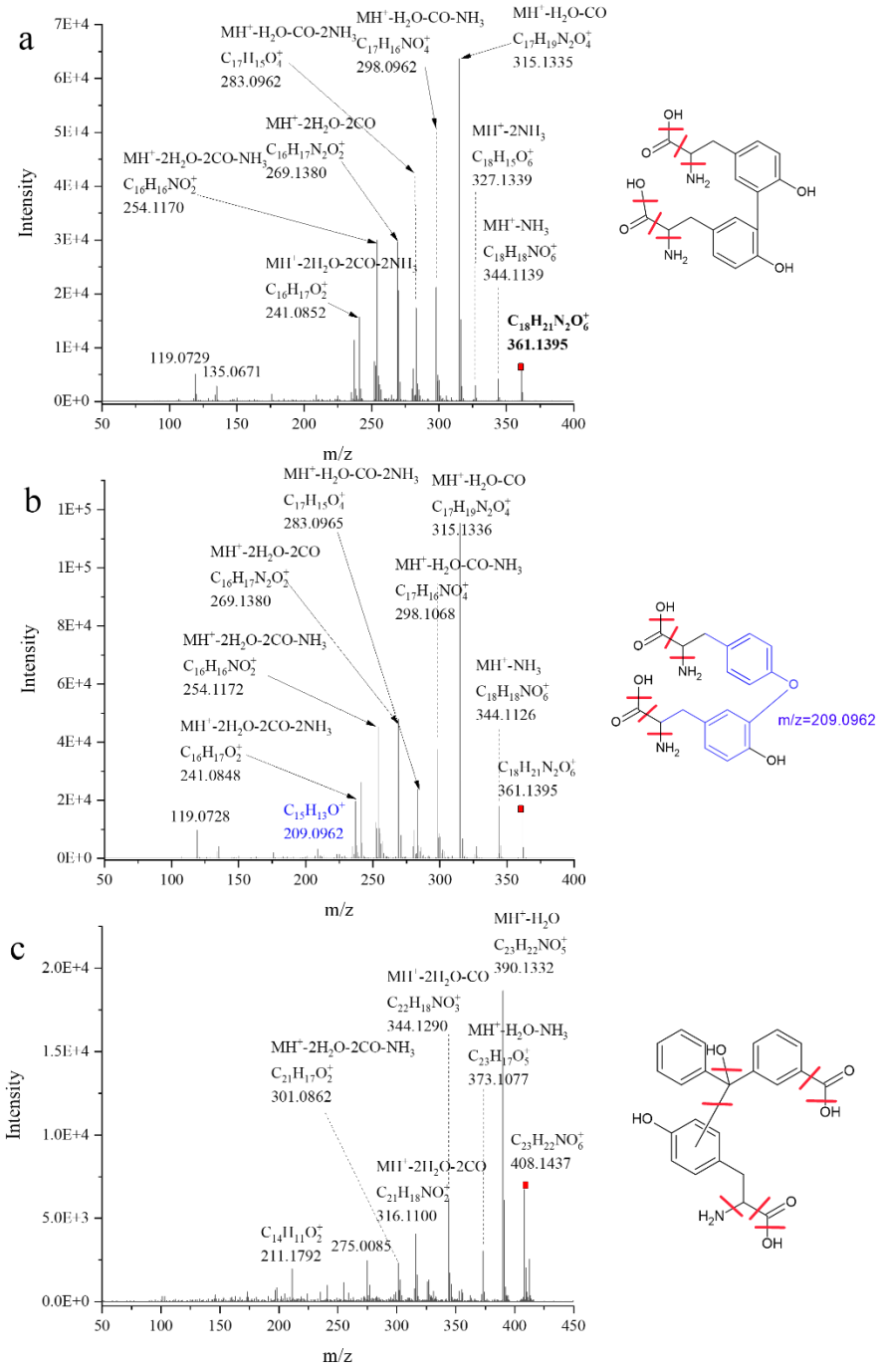

Figure TYR.5 *MS/MS spectrum of products **7**, **8** and **11** derived from Tyr irradiated with 3CB in aqueous solution, Ar-saturated: **(a)** MSMS of m/z = 361.1395 assigned to [diTyr]H$^+$, **(b)** MSMS of m/z = 361.1393 assigned to [diTyr]H$^+$, and **(c)** MSMS of m/z = 408.1437 assigned to [Tyr-3CBH]H$^+$*

For the Tyr-derivative with blocked carboxylic group, Tyr-OEt, four new peaks were eluted after irradiation (**Figure TYR.3**), two dimers (**Figure TYR.SI7**), Tyr-OEt-3CBH adduct, that had lower intensity than Tyr-3CBH and new product, with *m/z 212.12*. This product has *m/z +2 Da* mass higher than the protonated Tyr-OEt. Tyr-CBH like product was not detected in post reaction mixture of each N-acetylated Tyr-derivatives: N-Ac-Tyr and N-Ac-Tyr-OEt. In spite of that, more peaks with diTyr mass were present in the chromatogram, where chromatograms show three products for N-Ac-Tyr (MS/MS spectra present in **Figure SI8** and ten of them for N-Ac-Tyr-OEt (MS/MS spectra present in **Figures TYR.SI9-10**). In addition, the product of radical recombination of 3CBH$^{\bullet}$, 3CBH-3CBH dimers (with *m/z 455.14*) were identified for all Tyr derivatives as it was described previously for other ^{3}3CB* quenchers, e.g. Met compounds [28]. Analysis of diTyr products for all compounds proved itself to be problematic due to limitations presented by method implemented in their identification.

Table TYR.3 *A list of the identified products from sensitized by 3CB photo-oxidation of Tyr-derivatives in aqueous solution in the absence of oxygen. * Different retention time for 3CB were detected for different Tyr derivative due to different separation conditions*

Comp. no	Retention time, min	Identified product	Measured mass	Monoisotopic mass	R [ppm]
	Different*	$[3CB]H^+$	227.0728	227.0708	-8.8
		Tyr			
	1.7	$[Tyr]H^+$	182.0807	182.0817	-5.5
7	**4.3**	$[diTyr]H^+$	361.1395	361.1399	-1.1
8	**4.7**	$[diTyr]H^+$	361.1393	361.1399	-1.7
11	**15.8**	[Tyr-3CBH] H^+	408.1437	408.1447	-2.4
		Tyr–OEt			
	4.0	$[Tyr\text{-}OEt]H^+$	210.1117	210.1130	-6.2
12	**10.4**	$[Tyr\text{-}OEt+2Da]H^+$	212.1275	212.1286	-5.2
7	**11.2**	$[diTyr\text{-}OEt]H^+$	417.2014	417.2025	-2.6
8	**12.3**	$[diTyr\text{-}OEt]H^+$	417.2021	417.2025	-0.9
11	**25.3**	$[Tyr\text{-}OEt\text{-}3CBH]H^+$	436.1738	436.1760	-5.0

N-Ac-Tyr					
	4.3	[N-Ac-Tyr]H^+	224.0907	224.0922	-6.7
7	**4.7**	[diN-Ac-Tyr]H^+	445.1593	445.1610	-3.8
8	**5.6**	[diN-Ac-Tyr]H^+	445.1600	445.1610	-2.2
10	**5.9**	[diN-Ac-Tyr]H^+	445.1588	445.1610	-4.9
N-Ac-Tyr-OEt					
	3.1	[N-Ac-Tyr-OEt]H^+	252.1224	252.1235	-4.4
1	**8.2**	[diN-Ac-Tyr-OEt]H^+	501.2221	501.2226	-1.0
2	**9.6**	[diN-Ac-Tyr-OEt]H^+	501.2203	501.2226	-4.6
3	**10.1**	[diN-Ac-Tyr-OEt]H^+	501.2203	501.2226	-4.6
4	**10.3**	[diN-Ac-Tyr-OEt]H^+	501.2208	501.2226	-3.6
5	**10.6**	[diN-Ac-Tyr-OEt]H^+	501.2213	501.2226	-2.6
6	**11.5**	[diN-Ac-Tyr-OEt]H^+	501.2212	501.2226	-2.8
7	**16.0**	[diN-Ac-Tyr-OEt]H^+	501.2209	501.2226	-2.2
8	**12.1**	[diN-Ac-Tyr-OEt]H^+	501.2215	501.2226	-2.2
9	**14.0**	[diN-Ac-Tyr-OEt]H^+	501.2221	501.2226	-1.0
10	**15.2**	[diN-Ac-Tyr-OEt]H^+	501.2215	501.2226	-3.4
Tyr-Val					
	1.7	[Tyr-Val]H^+	281.1499	281.1501	-0.7
7	**2.7**	[diTyr-Val]H^+	559.2782	559.2762	3.6
1	**3.8**	[diTyr-Val] $2H^{2+}$	280.1420	280.1418	0.7
8	**5.3**	[diTyr-Val]H^+	559.2753	559.2762	-1.6
12	**8.6**	[tetraTyr-Val]$2H^{2+}$	558.2680	558.2684	0.7
13a	**9.6**	[diTyr-Val-2H]H^+	557.2606	557.2606	0
13b	**16.6**	[diTyr-Val-2H]H^+	557.2620	557.2606	2.5

Therefore, formation of ten distinct stable products from the recombination of TyrO$^{\bullet}$ radicals is postulated (**Figure Tyr.6**). The key difference among those products lies in the presence of the peak of the [Compound]H^{+} fragment (**Figure TYR.SI7-11**) in the fragmentation pattern, thus it can be assumed that those with this peak are C-O bonded diTyr, while the others are C-C bonded. Products are most likely the result of different phenoxyl radical resonance structures, as shown in **Figure TYR.6** reacting with each other. Additionally, there is a possibility that diTyr formed under sensitized photo-oxidation may undergo further Micheal addition, as discussed in ref [80]. Products of Micheal addition can exhibit a similar fragmentation pattern to diTyr. Nevertheless, in the same article it is postulated that those products occur after the sample has been incubated. Since samples investigated in this study has been subjected to HPLC-MS analysis right after irradiation, this process can be disregarded.

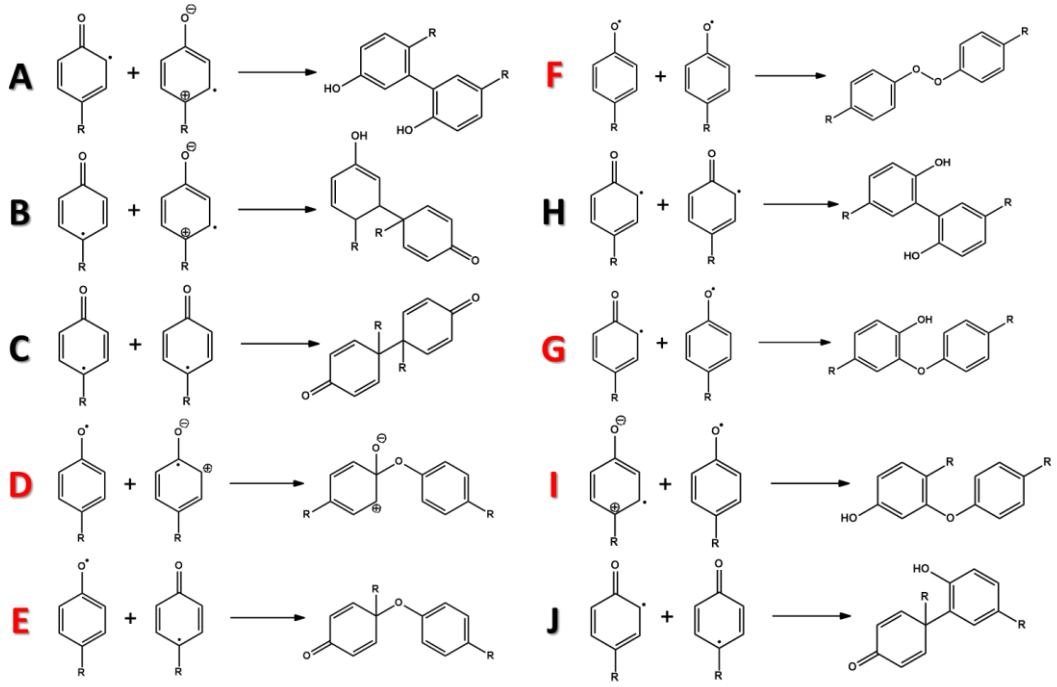

Figure TYR.6 *Proposed structures of diTyr products from reactions of Tyr resonance structures (where black color represents C-C bonded diTyr isomers, red – C-O bonded ones)*

The presence of Tyr-3CBH and 3CBH-3CBH in the products mixture is the direct evidence for a recombination of 3CBH$^{\bullet}$ and TyrO$^{\bullet}$ radicals (**Figure TYR.7**), as well as the recombination of two 3CBH$^{\bullet}$ radicals. Similar radical coupling products were detected in a recent study on 3CB sensitized photo-oxidation of methionine derivatives [27].

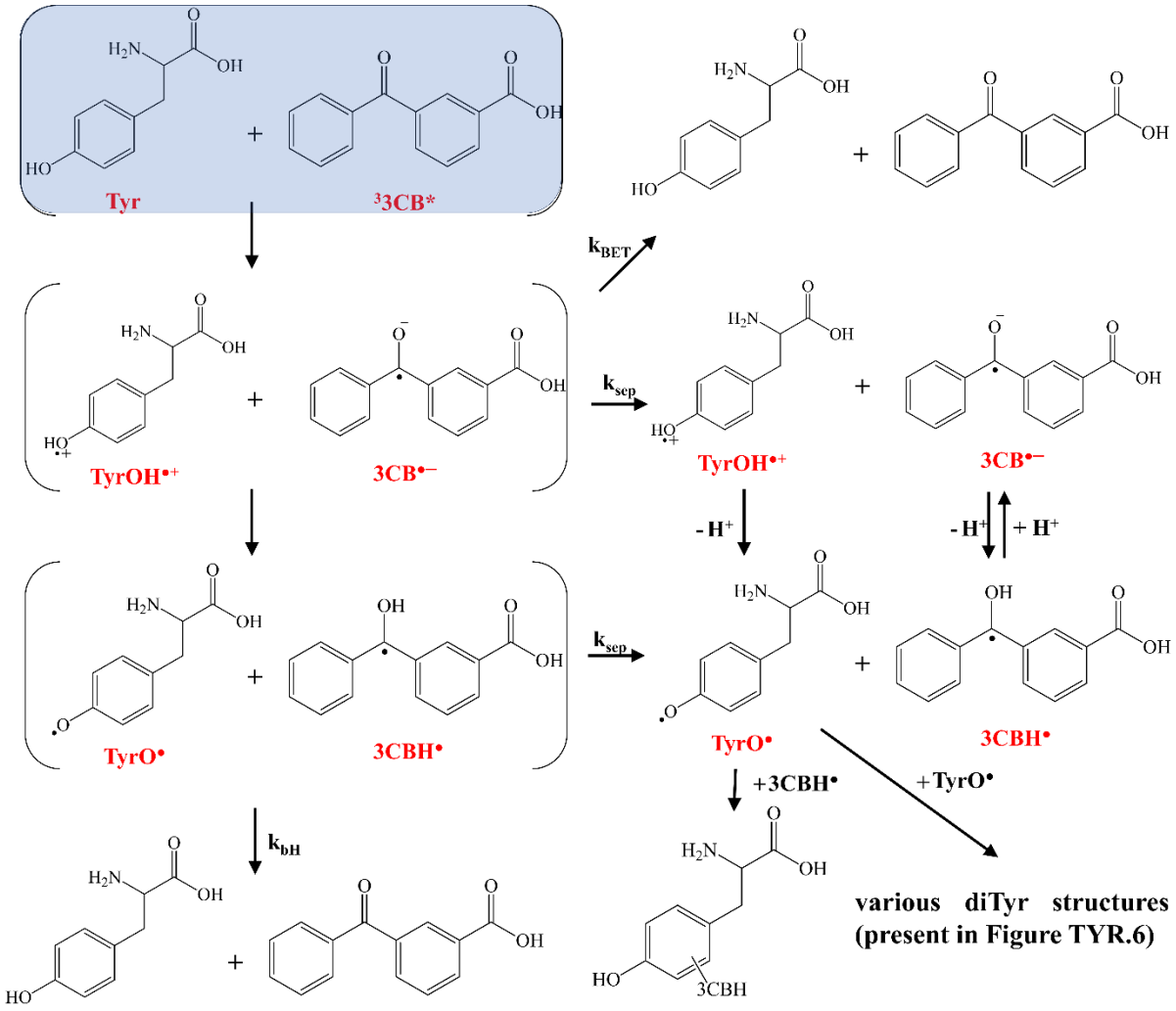

Figure TYR.7 *Mechanism of anaerobic photosensitized oxidation of Tyr based on experiments presented in this thesis*

Two observations emerged from that experiment. Firstly, when Tyr has more blocked groups, a higher number of diTyr products are observed. One possible explanation of this is the increasing hydrophobicity of Tyr molecules. The same experimental conditions were maintained for each individual solution. For photo-oxidated samples of Tyr, only two diTyr compounds were detected being 3,3'-diTyr and 3,O'-diTyr (**Figure TYR.5**). For N-Ac-Tyr and TyrOEt, the same products were identified, with one additional diTyr for the former (**Figure TYR.SI8** and **Figure TYR.SI7**), matching results presented in ref. [85]. Ten different diTyr products are present in the N-Ac-Tyr-OEt solution after the irradiation (**Figure TYR.SI9** and **Figure TYR.SI10**). Tyr-Val products resemble N-Ac-Tyr (**Figure TYR.SI11**) with the exception of product with *m/z -2Da* on dimers. The explanation of this phenomenon is still open for debate.

Secondly, there is a reverse trend in Tyr-3CBH product occurrence in the mixture of products after irradiation of various Tyr derivatives at pH 7. The highest number of Tyr-3CBH product was in Tyr sample, scarcely visible in the Tyr-OEt sample, and undetectable in the rest. One possibility is that the protonation of amine group has a positive effect on the creation of Tyr-CBH products. The possibility of an additional reaction of proton transfer from the protonated amine group to the sensitizer within the [$3CB^{\bullet-}$•••$TyrOH^{\bullet+}$] complex and fast subsequent creation of Tyr-3CBH [68]. It is also possible that steric effect within the encounter complex [$^{3}3CB^{*}$•••TyrOH] may have negative impact on formation of Tyr-3CBH products [86,151]. The presence of steric effect within the encounter complex was recently suggested for the 3CB sensitized oxidation of the derivatives of sulfur -containing amino acids namely methionine and S-methyl-cysteine [28].

III.2. Tryptophan

III.2.1. Laser flash photolysis

Concentrations: Trp, Trp-OEt, N-Ac-Trp, N-Ac-Trp-OMe – 0 mM, 0.25 mM, 0.5 mM, 7.5 mM, 1 mM; Lys-Trp, Trp-Tyr, Ala-Trp-Ala – 0 mM, 0.4 mM, 0.6 mM, 0.8 mM, 1 mM; 3CB – 4 mM and 5 mM in case of Lys-Trp, Trp-Tyr, Ala-Trp-Ala. Ar bubbled for 30 min in rectangular quartz cuvettes with 10 mm optical path.

Following experiments done with Tyr, LFP experiments were implemented to investigate the reaction of $^{3}3CB^{*}$ with Trp and its derivatives at the earliest stages of the reaction. Based on absorption spectra of transients that were expected to emerge (**Figure II.3**), it was difficult to pick suitable wavelength at which the k_q for quenching the $^{3}3CB^{*}$ by the Trp and other model compounds were going to be measured by monitoring the decay of the triplet absorption of the $^{3}3CB^{*}$. Following previous experience done with model compounds 430 nm was chosen. Visible quenching is presented in **Figure TRP.1 a** and **Figure TRP.SI1-6**. To obtain Stern-Volmer plots, linear regression of k_{obs} at given [Q] was used and is shown in section **Figure TRP.1 b** and **Figure TRP.SI1-6**. This allowed to estimate k_q with pseudo-first-order rate constant (**Table TRP.1**).

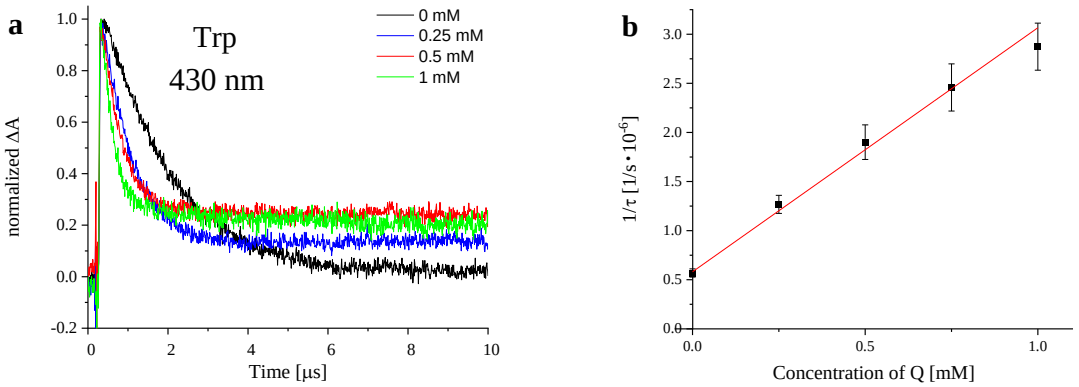

Figure TRP.1 ***(a)*** *Kinetic traces for the ^{3}3CB* decay at 430 nm in the presence of varying concentrations of Trp (0-1 mM) at pH 7* ***(b)*** *The Stern-Volmer plots according to the* ***Equation 2*** *for the quenching of ^{3}3CB* by Trp (0-1 mM) at pH 7 in aqueous solution for 3CB (4 mM)*

Table TRP.1 *Quenching rate constants and corresponding quantum yields of short-lived intermediates formation for Trp and its derivatives. Where Z_Q and Z_{3CB} are the net charge of Q and 3CB at pH 7, respectively*

Quencher	**Z_Q**	***k_q* (x10^9 M^{-1} s^{-1})**	**$\Phi_{3CBH^\bullet}$+ $\Phi_{3CB^{\bullet-}}$**	**$\Phi_{TrpN^\bullet}$**	**$\Phi_{TrpNH^{\bullet+}}$**	**Z_QZ_{3CB}**
Trp	0	2.3±0.2	1.19±0.34	0.39±0.16	----------	0
Trp-OEt	+1	3.3±0.9	1.12±0.13	0.79±0.12	----------	-1
N-Ac-Trp	-1	1.8±0.2	0.86±0.10	0.75±0.08	----------	+1
N-Ac-Trp-OMe	0	1.4±0.2	0.79±0.08	0.76±0.08	----------	0
Lys-Trp	+1	2.3±0.2	0.96±0.33	1.01±0.43	traces	-1
Trp-Tyr	0	2.3±0.1	1.08±0.33	0.22±0.04	----------	0
			$\Phi_{TyrO^\bullet}$ = 0.33±0.04			
Ala-Trp-Ala	0	2.4±0.2	0.93±0.34	0.91±0.29	traces	0

Analyses of transient absorption spectra for Trp and its derivatives had to be taken with special care, due to the fact that they are composite spectra of the most amounts of transients (taking into account all amino acids present in this thesis) that could possibly arise. The most prominent bands are observed at 550 nm and band at 500 nm representing formation of 3CBH$^{\bullet}$ and TrpN$^{\bullet}$ respectively. The same can be said for other Trp-derivatives with different group blockage (**Figure TRP.SI7).** The deconvolution of recorded transient absorption spectra shown the formation of ^{3}3CB*, 3CBH$^{\bullet}$, 3CB$^{\bullet-}$, TrpN$^{\bullet}$, TrpNH$^{\bullet+}$, and in the case of Trp-Tyr - TyrO$^{\bullet}$ and provided the concentrations of each individual components based on procedure described in **Chapters II.2.1.2** and **II.2.1.3** [78]. Concentration profiles are presented in **Figure TRP.2 b**. Resulting values has been presented in **Table TRP.1**.

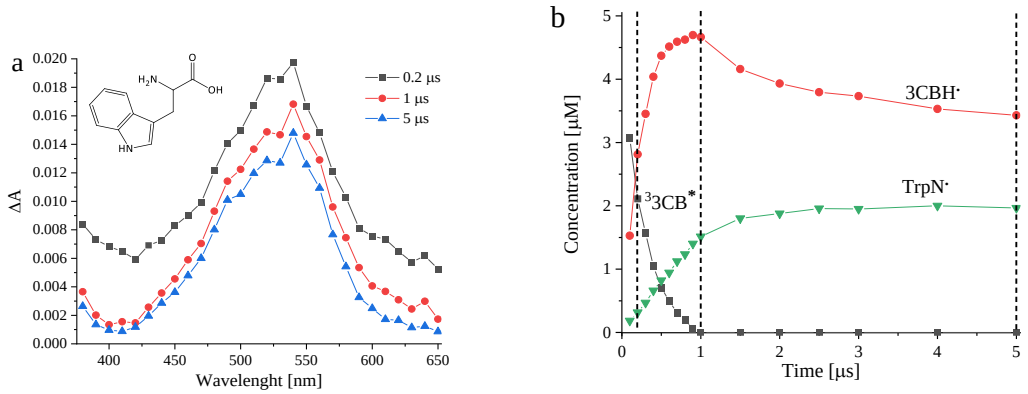

Figure TRP.2 *(a)Evolution of transient absorption spectra from 3CB-sensitized oxidation of Trp (5 mM) at pH 7. Spectra were recorded at different delays following laser pulse 0.2 (black ■), 1 (red ●), 5 µs (blue ▲). (b)Concentration profiles of transients identified in the laser flash photolysis of an aqueous solution of Trp (1 mM) and 3CB (5 mM) at pH 7 where (black ■) is ^{3}3CB*, (red ●) is 3CBH$^{\bullet}$, and (green ▼) is TrpN$^{\bullet}$. Dotted lines represent times at which respective spectra were presented in* ***(a)***

The highest value for quenching rate constant calculated for the Trp-OEt experiment appears to be the highest one (3.3×10^{9} M^{-1} s^{-1}). Nevertheless, it does not show a statistically significant difference from the other quenchers that would provide any insight into the effect of neighboring groups, and therefore structure, on the quenching mechanism. Quenching rate constants for Trp and its derivatives are higher than that of Tyr and similar to those Tyr derivatives with blocked carboxylic groups. This suggests that coulombic interactions and structural dependence on encounter complex formation play a smaller role in photosensitized anaerobic oxidation of Trp. Once again, the large values of k_q close to the range of diffusion-

controlled processes (10^9 $M^{-1}\cdot s^{-1}$) correspond well with current literature data (e.g. $1.09\cdot10^9$ $M^{-1}\cdot s^{-1}$ for 10-(carboxyethyl)flavin excited state quenching by N-Ac-Trp [115]; $1–2\cdot10^9$ $M^{-1}\cdot s^{-1}$ for flavine mononucleotide excited triplet state by Trp [152]) and indicate a kinetically controlled process.

Experimentally determined quantum yields of formation of $3CBH^{\bullet}$ as presented in **Table TRP.1** are equal to unity (within experimental error). It is safe to assume that the process fundamentally starts with concerted PCET from ^{3}3CB* to respective Trp compound in the encounter complex. The presence of the $3CB^{\bullet-}$ in the concentration profile of Trp compounds with a blocked amine group not only further solidifies the theory that quenching encompasses an ET process but also indicates the involvement of the amine group in proton transfer (**Figure TRP.SI7**). $TrpNH^{\bullet+}$ was present only in peptides, which most likely is the result of the presence of Lys or Ala with free amine group that could potentially have had protonated $3CB^{\bullet-}$.

All of the measured compounds (except for Trp and Trp-Tyr) have relatively high value of $\mathbf{\Phi}_{TrpN^{\bullet}}$, which is analogous to Tyr and indicates great efficiency of PCET. Regarding the quenching done by Trp (**Figure TRP.2**), no sign of either $3CB^{\bullet-}$ or $TrpNH^{\bullet+}$ was present. This is in agreement with the commonly known concerted PCET for Trp quenching of sensitizers' triplet states. However, there is two-fold decrease in the value for Trp. For most of them, ratio was 1:1 meaning that for each Trp compound reacted with 3CB yielding either $3CB^{\bullet-}$ or $3CBH^{\bullet}$. Discrepancies can be found in Trp and Trp-Tyr. For Trp additional experiment was made to measure quantum yields of photodegradation.

As for Trp-Tyr, this difference could be explained by careful evaluation of concentration profile (**Figure TRP.SI7**). $TrpNH^{\bullet+}$ concentration rises simultaneously with $TyrO^{\bullet}$ concentration. This resembles two competing reactions occurring, and the higher concentration of $TrpNH^{\bullet+}$ at the beginning is not surprising, as the quenching rate constant for Trp-OEt (with blocked carboxylic group) is greater than that of N-Ac-Tyr (with blocked amine group). However, $TrpNH^{\bullet+}$ decreases without the formation of $TrpN^{\bullet}$ in the process. This phenomenon further substantiates the argument that $TrpNH^{\bullet+}$ has the ability to oxidize $TyrO^{\bullet}$. If that was the case, it would be expected to have higher quantum yields of formation of $TyrO^{\bullet}$, which is also prevalent in the experiment.

III.2.2. Steady state photolysis

Concentrations: Trp, Trp-OEt, N-Ac-Trp, N-Ac-Trp-OMe, Lys-Trp, Trp-Tyr, Ala-Trp-Ala – 1 mM; 3CB – 4mM and 5 mM in case of Lys-Trp, Trp-Tyr, Ala-Trp-Ala. Ar bubbled for 30 min in rectangular quartz cuvettes with 10 mm optical path and magnetic dipole; the output power used was set at 40 mW; Gradient elution methods for samples are present in **Table TRP.SI1**

Since quantum yields of formation of transients was the most prevalent in Trp photodegradation quantum yields of Trp (Φ_{Trp}) and 3CB were determined using method described in previous chapter and the procedure followed the method outlined in **Chapter II.2.3**, based on **Equation 5**. The value of Φ_{Trp} and Φ_{3CB} were calculated (based on **Figure TRP.3**) to be **0.39±0.03** and **0.49±0.06** respectively. Which points to 1:1 ratio of the reaction based on that data, but it also means that there is something that enhances formation of $3CBH^{\bullet}$.

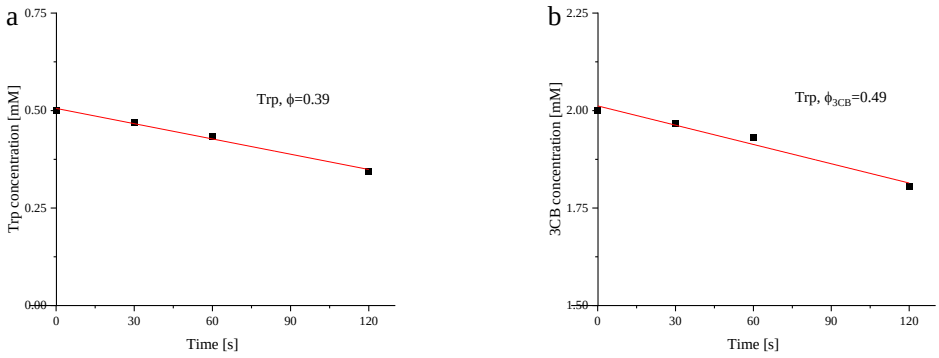

Figure TRP.3. *Graph of decrease in concentration over time for(a) Trp and (b) 3CB. Slopes of the linear regression from that graph provided rate of consumption of given compound*

To unveil the intricacies of stable products formed during anaerobic photo-oxidation of Trp and to reveal the influence of blocking groups and peptide bond on this process, HPLC-MS was implemented using the elution methods described in **Table TRP.SI1** and the conditions presented in the box above. According to the literature (**Chapter I.2.2.3**), a plethora of Trp dimers were expected to arise from this process, with covalent adducts of Trp with relevant sensitizer also prevalent in the post-reaction mixture. Total Ion Current chromatograms are present in **Figure TRP.4** and **Figure TRP.5**.

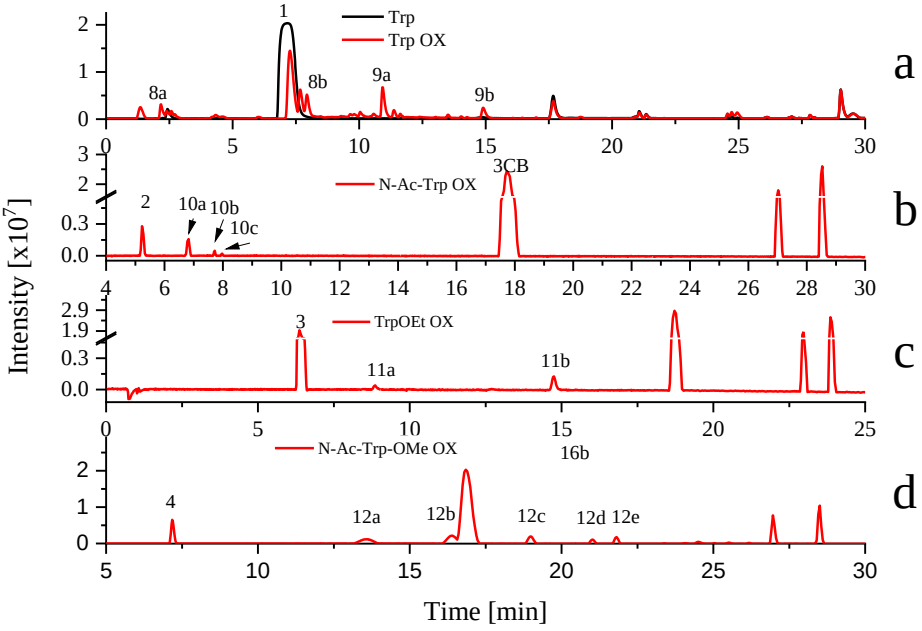

Figure TRP.4 *Comparison of total ion current chromatograms for irradiated samples of 3CB with* ***(a)*** *Trp,* ***(b)*** *N-Ac-Trp,* ***(c)*** *Trp-OEt, and* ***(d)*** *N-Ac-Trp-OMe with identified products listed in* ***Table TRP.2****. Black lines represent blank samples which contain 3CB and respective compound, while red lines are chromatograms of oxidized sample*

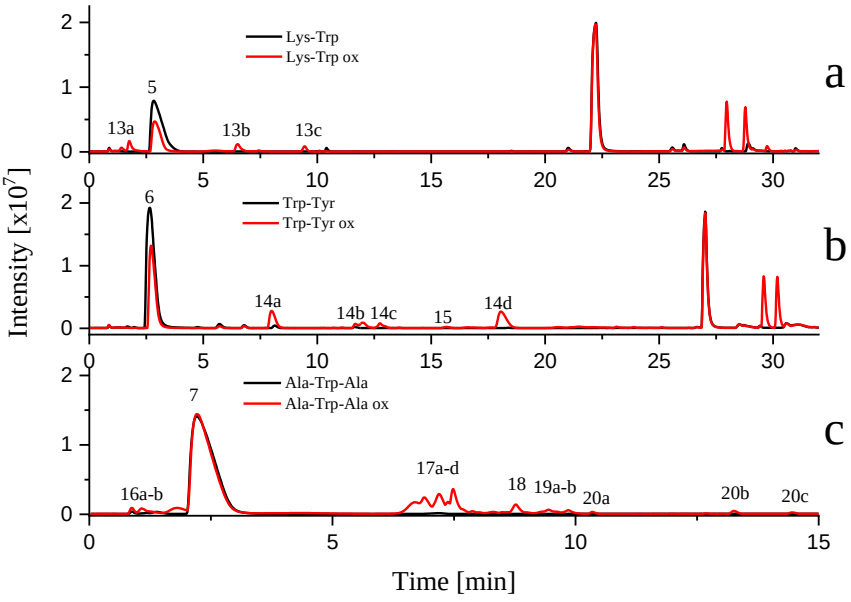

Figure TRP.5 *Comparison of total ion current chromatograms for irradiated samples of 3CB with:* ***(a)*** *Lys-Trp,* ***(b)*** *Trp-Tyr, and* ***(c)*** *Ala-Trp-Ala with identified products listed in* ***Table TRP.2****.* ***Black*** *lines represent blank samples which contains 3CB and respective compound, while* ***red*** *are chromatograms of oxidized samples*

Differentiation between Trp dimers (diTrp) was only possible due to differences in their respective elution times, as the fragmentation patterns were identical for each compound (**Figure TRP.6)**. However, dimers produced during Trp photo-oxidation (**Figure TRP.6**) all possessed *m/z 203.08* corresponding to Trp_{-2Da}, suggesting that they may be C-N connected, as the entire Trp molecule was able to detach during fragmentation. The same can be said about the products of photosensitized oxidation of N-Ac-Trp, to some extent. Two products, namely **10a** and **10b** share fragmentation patterns (**Figure.TRP.SI8 b** and **c** respectively). The fragment with an *m/z 269.11* is a strong indicator of di-N-Ac-Trp formation, as it encompasses the loss of all amine groups and carboxylic groups in its structure. Conversely, product **10c** also has a fragment that implies the loss of N-Ac-Trp. Therefore, whenever this fragment is present, a C-N connection may be assumed, while the presence of the fragment with *m/z 269.11* without any implication of the loss of one of the Trp moiety from the structure implies a C-C connection.

MS/MS analysis of TrpOEt resulted in an uncharacteristic fragmentation pattern, with the base peak, namely the loss of ammonia, dominating over all others (**Figure TRP.SI9 a**). Two products were identified as dimers based on their monoisotopic masses and fragmentation patterns. For product **11a**, two patterns emerge after the loss of the amine group: the subsequent loss of another ammonia or the loss of ester group. Since the rest of the fragments correspond to two indoles with varying attached groups (**Figure.TRP.SI9 b**), the formation of a C-C bond is postulated to occur. In contrast, the same cannot be said about the second product (**11b**, **Figure.TRP.SI9 c**), which has $[Trp\text{-}OEt]H^+$ with the loss of 2Da in its spectrum. Similarly to N-Ac-Trp, this product can be assigned to C-N bonded di-Trp-OEt. The same can be said about N-Ac-Trp-OMe (**Figure.TRP.SI10**), where two distinct groups of spectra are present, and the same logic applies as in previous compounds.

Fragmentation spectra of peptides provided information on their structure. Lys-Trp creates doubly charged species, which is expected as it has additional amine group in this structure, making it easier for it to protonate. The presence of the fragment with an *m/z 269.11* (**Figure.TRP.SI11**) implies formation of the dimer, while Trp_{-2Da} was also present. Therefore, it is reasonable to assume that these dimers were C-N connected, though it could not be determined whether the connection was *via* Lys or Trp. The fragment with an *m/z 269.13* (**Figure.TRP.SI12**) was present in the di-Tyr spectra and also appeared in the fragmentation of one of the MS/MS spectra of the products, meaning that at least one di-Trp-Tyr is Tyr-Tyr connected. Dimers of Ala-Trp-Ala (**Figure.TRP.SI13**) were identified using the same method as for previous peptides.

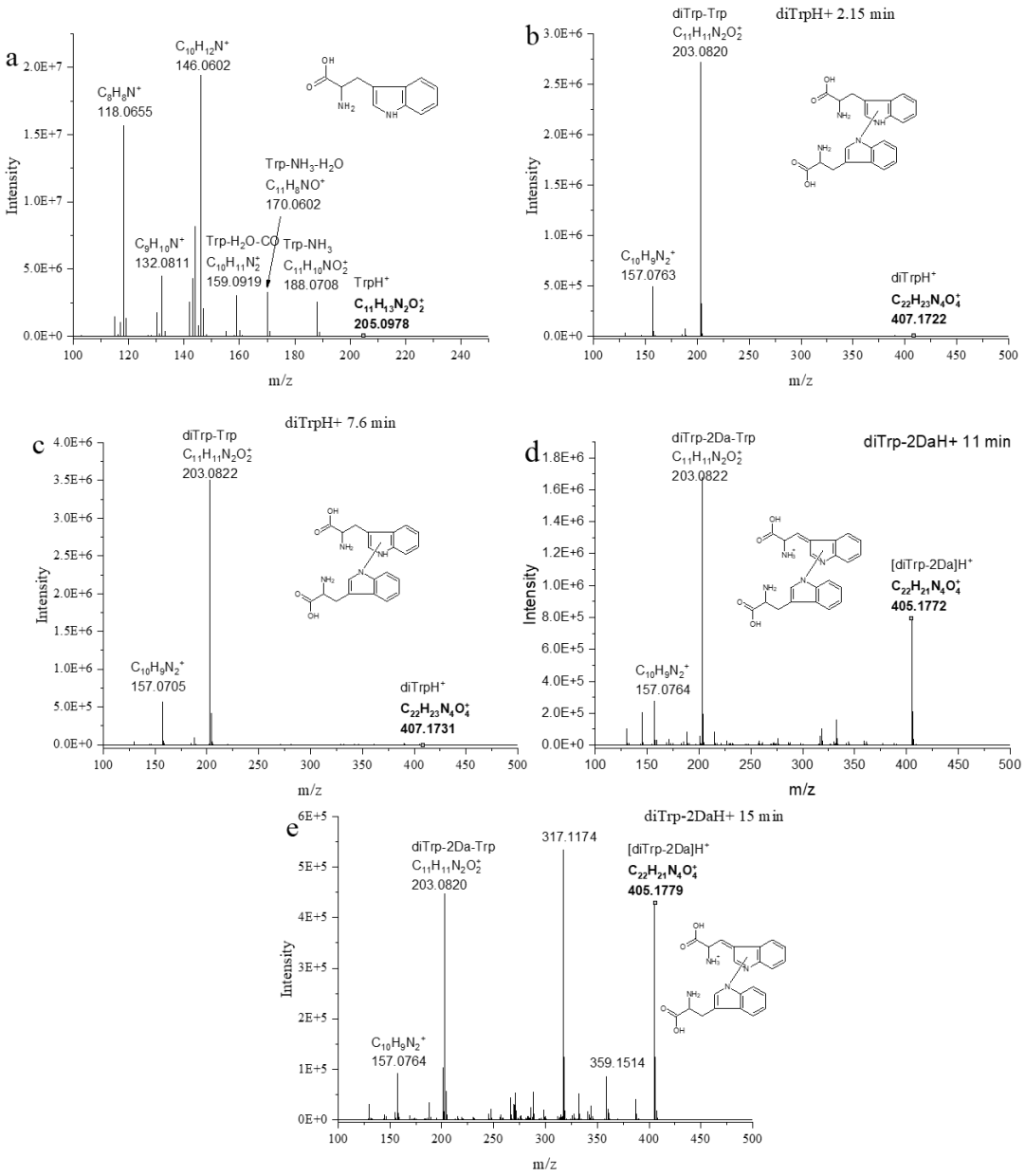

Figure TRP.6 *MS/MS spectrum of Trp* ***(a),*** *and its products* ***8a (b)***, ***8b (c)***, ***9a (d)***, *and* ***9b (e)***, *from Trp irradiated with 3CB in aqueous solution, Ar-saturated*

The formation of 3CB covalent adduct included a fragment of the indole group with an ethylene connected to 3CB, which had lost a water molecule (fragment with *m/z 350.12*) or had undergone a subsequent loss of another water molecule (fragment with *m/z 332.11*). This product was only present in Ala-Trp-Ala (**Figure TRP.SI14**). Additionally, a product present in the post-reaction mixture was classified as this peptide, which had undergone the formation of a double bond in the molecule (**Figure TRP.SI15**). The same process also occurred during the photo-oxidation of Trp. Moreover, products of the radical recombination of 3CBH$^{\bullet}$, 3CBH-3CBH dimers, were identified for all Trp derivatives.

Several peaks that appeared as a result of Trp and Trp-derivative irradiation in the presence of ^{3}3CB* were identified. The analysis of monoisotopic mass and fragmentation pattern for each distinguished product categorized them into three group: Trp-3CBH adduct, tryptophan dimers (diTrp) and Trp$_{-2Da}$ (either as a stable product in Trp or present in dimers of Trp in Ala-Trp-Ala samples). As described earlier, covalent dimers of the sensitizer and Trp model compound result from radical recombination of 3CBH$^{\bullet}$ and TrpN$^{\bullet}$ radicals, whereas two TrpN$^{\bullet}$ radicals yield dimers. The main reaction appears to be dimerization, as it was present in all post-reaction mixtures. Furthermore, as was the case for Tyr, diTrp products undergo further reactions yielding polymeric structures. The formation of Trp-3CBH was only present in Ala-Trp-Ala, pointing towards the hypothesis that either length of the peptide negatively influences formation of dimers and positively formation of Trp-3CBH, or that it favors formation of these covalent adducts.

Table TRP.2 *A list of the identified products from sensitized by 3CB photo-oxidation of Trp and its derivatives in aqueous solution in the absence of oxygen*

Comp. no	Retention time, min	Identified product	Measured mass	Monoisotopic mass	R [ppm]
		Trp			
1	7.2	[Trp]H^{+}	205.0978	205.0972	2.93
8a	2.15	[diTrp]H^{+}	407.1722	407.1714	1.96
8b	7.6	[diTrp]H^{+}	407.1731	407.1714	4.18
9a	11	[diTrp-2Da]H^{+}	405.1580	405.1557	5.68
9b	14.9	[diTrp-2Da]H^{+}	405.1579	405.1557	5.43
		N-Ac-Trp			
2	5.2	[N-Ac-Trp]H^{+}	247.1072	247.1083	-4.45
10a	6.8	[di-N-Ac-Trp]H^{+}	491.1930	491.1931	-0.20
10b	7.7	[di-N-Ac-Trp]H^{+}	491.1915	491.1931	-3.26
10c	8.0	[di-N-Ac-Trp]H^{+}	491.1919	491.1931	-2.44
		Trp-OEt			
3	11.5	[Trp-OEt]H^{+}	233.1279	233.1290	-4.72
11a	8.8	[di-Trp-OEt]H^{+}	463.2332	463.2340	-1.69
11b	14.8	[di-Trp-OEt]H^{+}	463.2330	463.2340	-2.16

N-Ac-Trp-OMe					
4	7.2	[N-Ac-Trp-OMe]H^+	261.1226	261.1239	-4.98
12a	13.6	[di-N-Ac-Trp-OMe]H^+	519.2238	519.2238	0.00
12b	16.4	[di-N-Ac-Trp-OMe]H^+	519.2228	519.2238	-1.93
12c	19.0	[di-N-Ac-Trp-OMe]H^+	519.2225	519.2238	-2.50
12d	21.0	[di-N-Ac-Trp-OMe]H^+	519.2226	519.2238	-2.31
12e	21.9	[di-N-Ac-Trp-OMe]H^+	519.2227	519.2238	-2.12
Lys-Trp					
13a	1.8	[di-Lys-Trp]$2H^+$	332.1839	332.1843	-1.20
5	3.2	[Lys-Trp]H^+	333.1910	333.1927	-5.10
13b	6.5	[di-Lys-Trp]$2H^+$	332.1832	332.1843	-3.31
13c	9.5	[di-Lys-Trp]$2H^+$	332.1832	332.1843	-3.31
Trp-Tyr					
6	3.0	[Trp-Tyr]H^+	368.1583	368.1605	-5.98
14a	8.0	[di-Trp-Tyr]$2H^+$	367.1509	367.1527	-4.90
14b	12.0	[di-Trp-Tyr]$2H^+$	367.1502	367.1527	-6.81
14c	13.0	[di-Trp-Tyr]H^+	733.2965	733.2980	-2.05
15	16	[tri-Trp-Tyr]$3H^+$	366.8165	366.8167	-0.55
14d	18.2	[di-Trp-Tyr]$2H^+$	367.1508	367.1527	-5.17
Ala-Trp-Ala					
16a	1.1	[Ala-Trp-Ala$_{-2Da}$]H^+	345.1556	345.1557	-0.29
16b	1.8	[Ala-Trp-Ala$_{-2Da}$]H^+	345.1566	345.1557	2.61
7	2.5	[Ala-Trp-Ala]H^+	347.1697	347.1714	-4.90
17a	6.7	[di-Ala-Trp-Ala]H^+	691.3206	691.3198	1.16
17b	6.9	[di-Ala-Trp-Ala]H^+	691.3206	691.3198	1.16
17c	7.2	[di-Ala-Trp-Ala]H^+	691.3189	691.3198	-1.30
17d	7.5	[di-Ala-Trp-Ala]H^+	691.3198	691.3198	0.00
18	8.8	[di-Ala-Trp-Ala-CBH]$2H^+$	458.1948	458.1872	16.59
19a	9.4	[di-Ala-Trp-Ala-CBH$_{-H2O}$]$2H^+$	450.1905	450.1898	1.55
19b	9.8	[di-Ala-Trp-Ala-CBH$_{-H2O}$]$2H^+$	450.1879	450.1898	-4.22
20a	10.4	[Ala-Trp-Ala-CBH]H^+	573.2344	573.2344	0.00
20b	12.7	[Ala-Trp-Ala-CBH]H^+	573.2350	573.2344	1.05
20c	14.5	[Ala-Trp-Ala-CBH]H+	573.2343	573.2344	-0.17
21	7.4	[tri-Ala-Trp-Ala]3H+	345.8275	345.8276	-0.29

The dimerization reaction of TrpN• is known to occur rather quickly (with a rate constant of $0.6 – 2 \cdot 10^8$ $M^{-1} \cdot s^{-1}$ [90,153]), with multiple isomeric cross-linked species formed during this process [36,90,91]. The presence of many distinct diTrp products is direct evidence of this fact. This may explain why dimeric structures maybe more prevalent than covalent adduct with the sensitizer.

An unsaturated compound has already been established to arise during the reaction of Trp with hydroxyl radicals in the Fenton system [154]. Therefore, it may be reasonable to assume that this is the result of further H-atom abstraction from TrpN• (as is the case for Ala-Trp-Ala photosensitized oxidation), or it could arise from secondary reactions to diTrp. No reduced products were present in post-reaction mixture. Therefore, it is logical that this product was formed from a reaction with other radical (portrayed as R• in **Figure TRP.7**). Since no information is provided on the redox potential of $TrpN^{\bullet}/Trp_{(-2H)}$, it is impossible to deduce which transient product is responsible for further H-atom abstraction from TrpN•.

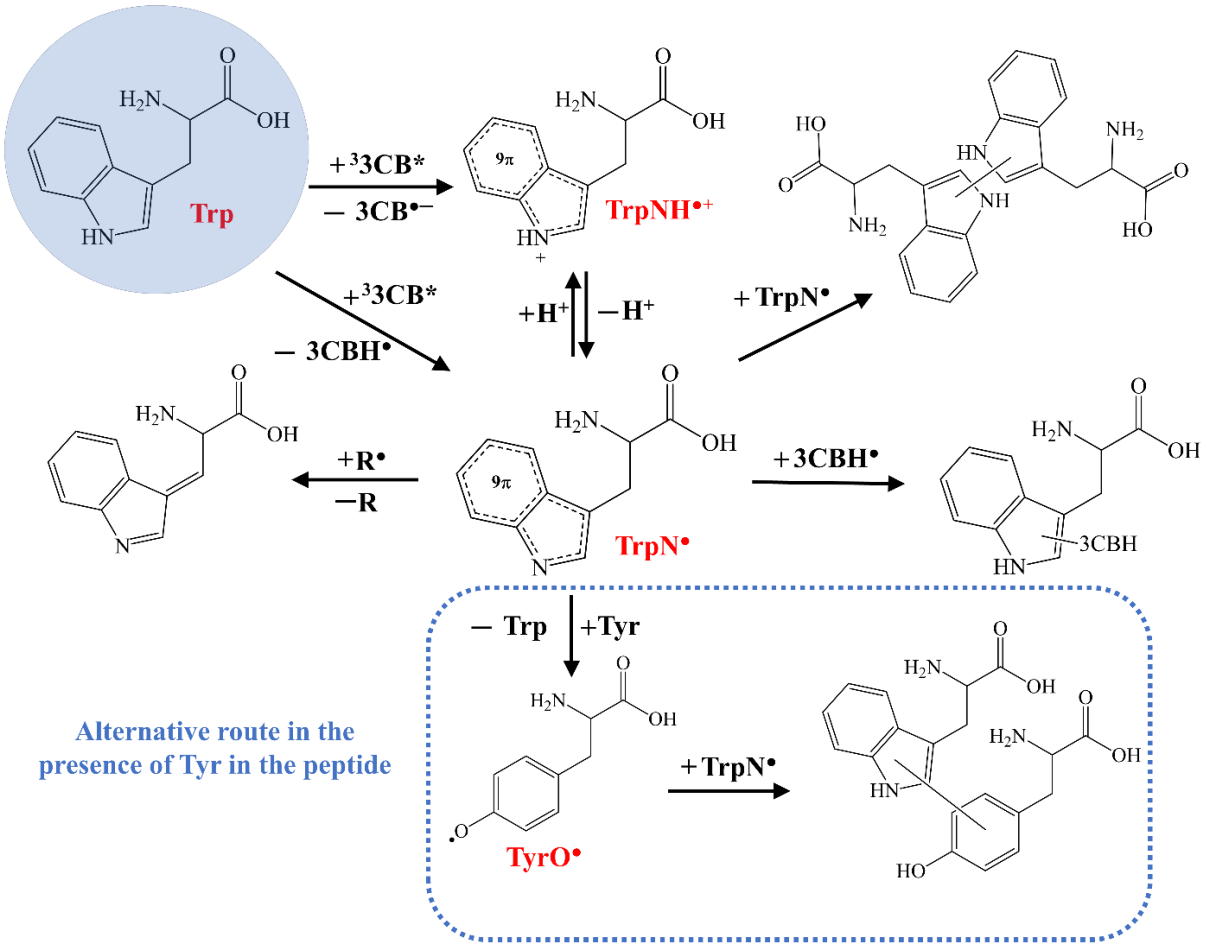

Figure TRP.7 *Mechanism of anaerobic photosensitized oxidation of Trp based on experiments presented in this thesis*

Regardless of the ability to distinguish between different isomers, the analyses of fragmentation patterns of stable products created during anaerobic photosensitized oxidation of all Trp model compounds indicate the presence of several isomers. This observation is supported by experiments conducted by other scientists [36,89–91]. The number of different di-Trp products is affected by the blockage of neighboring groups; the more blocked the Trp, the greater the number of di-Trp products. While the reverse trend was observed in Tyr oxidation regarding Tyr-CBH, , no such trend is visible here (apart of the length of the peptide). For that reason, it cannot be an explanation of formation of more distinct di-Trp products, as there is only one venue of termination of $TrpN^{\bullet}$, namely di-Trp.

Results presented in this chapter provide insight into the involvement of the amine group in the reaction mechanism (likely proton transfer) However, when compared between different model compounds, this effect is negligible. The formation of double bond was observed only when both groups are available or when Trp is blocked by two amino acids. Moreover, the formation of covalent product with sensitizer was only present in Ala-Trp-Ala. This insight leads to a hypothesis that we would expect 3CB covalent adducts to form with the protein. The presence of an additional amine group from lysine did not influence neither quenching rate constant, nor quantum yields of transients, nor stable products formed. The same cannot be said about presence of Tyr. Since Tyr is also an amino acid prone to this type of oxidation, and it has been proven to have capability to reduce $TrpN^{\bullet}$, the reaction mechanism was mostly influenced in that case and this has been included in **Figure TRP.7**.

III.3. Histidine

III.3.1. Laser flash photolysis

Concentrations: His – 0 mM, 5 mM, 10 mM, 15 mM, 20 mM; His-NH_2, His-OMe, N-Ac-His, 1-Me-His – 0 mM, 2.5 mM, 5 mM, 7.5 mM, 10 mM; His-Ala, Ala-His, His-Phe, Gly-His-Gly – 0 mM, 0.4 mM, 0.6 mM, 0.8 mM, 1 mM; 3CB – 10 mM for His, and 5 mM for the rest. Ar bubbled for 25 min in rectangular quartz cuvettes with 10 mm optical path. Time-resolved spectra and concentration profiles were generated using 15 mM His and 10 mM CB, and 7.5 mM concentration of derivative or 1 mM of peptide, and 5 mM of CB for each respective sample.

Kinetic traces for the quenching of ^{3}3CB* were measured at 480 nm for samples of histidine and its derivatives, and at 500 nm for peptide samples. The Stern-Volmer plots for His and its derivatives are presented in **Figure HIS.1** and **Figure HIS.SI1-SI8**). The magnitude of the *kq* values (**Table HIS.1**) suggests kinetically controlled reactions close to diffusion-limited quenching, with some data aligning with literature values for different photosensitizers [98,155–157]. Histidine and derivatives with a free amine group exhibit a higher bimolecular quenching rate constant compared to N-Ac-His and all peptides except for Ala-His. These values are higher than those reported in the literature [98,156]. **Figure HIS.2**, **Figure HIS.SI9**, and **Figure HIS.SI10** represent spectra recorded at different time intervals. All of them show the same shift of ΔA wavelength dependence maxima from 520 nm to 540 nm, assigned to 3CBH$^{\bullet}$, with these spectra corresponding well to previous data [33], indicating the reduction of the photosensitizer.

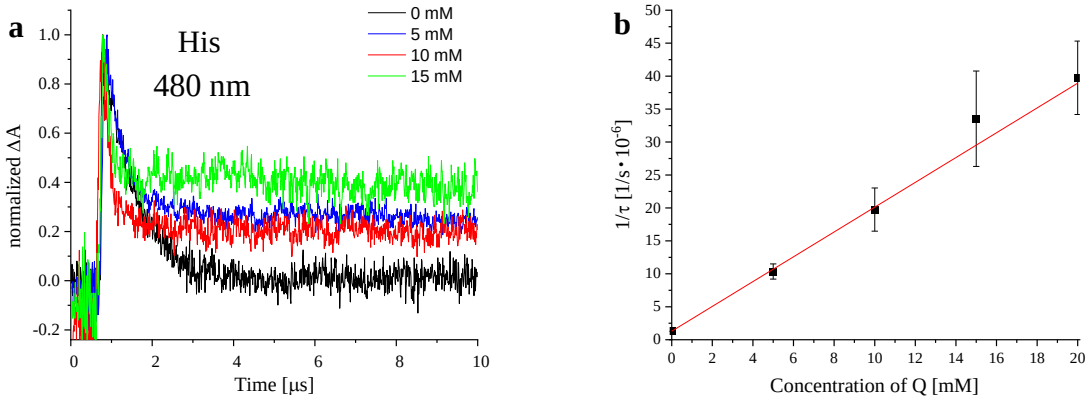

Figure HIS.1 ***(a)*** *Kinetic traces for the ^{3}3CB* decay at 480 nm in the presence of varying concentrations of His at pH 7* ***(b)*** *The Stern-Volmer plots according to* ***Equation 2*** *for the quenching of ^{3}3CB* by His at pH 7 in aqueous solution for 3CB (10 mM)*

The quantum yields of generation of 3CBH• are presented in **Table HIS.1** as $\Phi_{3CBH\bullet}$. They are higher for the three His model compounds with blocked amine or carboxylate group. Quantum yields of formation of 3CBH$^{\bullet}$ for dipeptides were lower (close to 1-Me-His and His itself), which implies some inefficiency in this process.

Table HIS.1 *Quenching rate constants and corresponding quantum yields of short-lived intermediates formation for His and its derivatives, where Z_Q and Z_{3CB} are the net charge of Q and 3CB at pH 7, respectively. Data are mean values from five replicates, with the error values corresponding to two standard deviations*

Quencher	Z_Q	k_q (x10^9 M^{-1} s^{-1})	$\Phi_{3CBH^\bullet}$	$\Phi_{3CB^{\bullet-}}$	Z_QZ_{3CB}
His	0	1.9±0.2	0.61±0.08	Traces	0
His-OMe	+1	2.4±0.2	0.86±0.11	----------	-1
His-NH_2	+1	2.3±0.5	0.91±0.12	Traces	-1
N-Ac-His	-1	1.0±0.1	0.87±0.12	----------	+1
1-Me-His	0	2.1±0.2	0.45±0.06	0.05±0.01	0
His-Ala	0	1.1±0.1	0.54±0.07	0.07±0.01	0
Ala-His	0	1.5±0.2	0.68±0.09	0.11±0.01	0
His-Phe	0	1.3±0.1	0.60±0.06	0.06±0.01	0
Gly-His-Gly	0	1.4±0.2	0.52±0.07	0.11±0.01	0

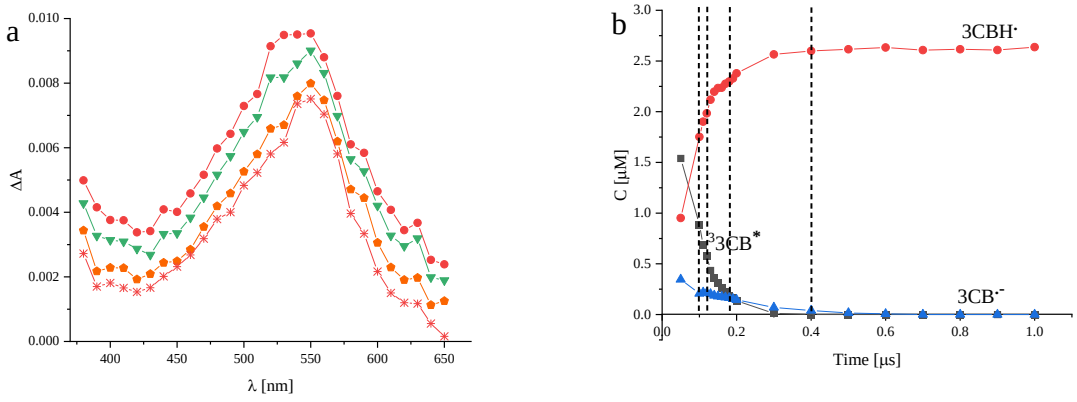

Figure HIS.2 ***(a)*** *Evolution of transient absorption spectra from 3CB-sensitized oxidation of His. Spectra were recorded at different delays following the laser pulse (●) 0.1 μs, (▲) 0.12 μs, (●) 0.18 μs or (*) 0.4 μs.* ***(b)*** *Concentration profiles of transients identified in the laser flash photolysis of an aqueous solution of His and 3CB (5 mM) at pH 7 where (black ■) is ^{3}3CB*, (red ●) is $3CBH^\bullet$, and (blue ▲) is $3CB^{\bullet-}$. Dotted lines represent times at which respective spectra were presented in* ***(a)***

The variation in these values raises questions about the photo-oxidation of His and its derivatives, particularly regarding the early processes when sites on the amino acid are blocked. Another question that could be posed is whether using a sensitizer with a high-energy excited triplet state affects the mechanism of sensitized quenching. The observed reduction of 3CB in these experiments suggests the occurrence ET or PCET within the encounter complex, with the mechanism being dependent on the pH and sensitizer, as it was presented for other sensitizers [98,103]. As mentioned before, the spectrum of the possible transient $HisN^{\bullet}$ is not well characterized [110,111], and literature data indicate that its absorbance bands are very weak (low ε values) [94]. The lack of data on the absorption spectra of other potential transients, such as the excited triplet state of His, posed an additional challenge in the mechanism investigation.

In light of this, deconvolution of the observed spectra was attempted using data for $^{3}3CB^{*}$, $3CB^{\bullet-}$, and $3CBH^{\bullet}$ only. The resulting quantum yields of their respective generation were compared, and no significant differences were found for the different blocked amino acids examined, except for 1-Me-His. However, the values are lower for the peptides, with the exception of Ala-His. The lower value of $\Phi_{3CBH\bullet}$ for 1-Me-His (compared to His) suggests a role for the N-1 nitrogen atom of the imidazole ring in the formation of $3CBH^{\bullet}$. Previous evidence for PCET with analogous sensitizers and other His derivatives (but not 1-Me-His) [98,103] supports this mode of reaction in the current data.

To better understand the observed kinetic differences, a comparison was made between the quantum yields and measured quenching rate constants. It is essential to remember that the k_q values represent a cumulative property encompassing the whole quenching process and can be influenced by many factors, including electron transfer, energy transfer, back electron transfer, pH, environment, and the nature of the sensitizer [158,159]. Bimolecular quenching rate constants for the excited triplet states of different molecules at neutral pH vary between $\leq 10^{5}$ $M^{-1}\cdot s^{-1}$ to the diffusion limit [98,155–157]. The protonation state of amine groups significantly influences *kq* values, which decrease when protonated [98]. A comparison of the *kq* values determined here for the reaction of $^{3}3CB^{*}$ with His or simple derivatives is presented in **Table HIS.1**. Blocking the carboxyl group nullifies its negative charge and enhances potential interactions with the negatively-charged sensitizer, whereas blocking the amine group nullifies its positive charge and decreases interactions. For peptides with an identical overall charge to His, the *kq* values are a bit smaller, possibly due to the increase in their respective size, which in turn influences diffusion that is a limiting factor in this process [158].

However, some of the values presented here are significantly higher than those reported by Saprygina et. al. at the same pH [98]. This discrepancy may be due to back electron transfer (BET) in the previous study, which would decrease the reported *kq* value [159]. Nonetheless, the high Φ_{3CBH}• of N-Ac-His (close to 1) is inconsistent with a low *kq* value (and in good agreement with [98]) for this species and some of the other compounds. It is therefore speculated that this difference might arise from the occurrence of energy transfer that would enhance the *kq* value for other compounds and account for the Φ_{3CBH}• values < 1.

III.3.2. Steady state photolysis

Concentrations: His, His-OMe, N-Ac-His, His-NH_2, 1-Me-His – 6 mM and His-Ala, Ala-His, His-Phe and Gly-His-Gly – 1 mM; 3CB – 4 mM and 5 mM in the case of peptides. Ar bubbled for 25 min in rectangular quartz cuvettes with 10 mm optical path and magnetic dipole; the output power used was set at 40 mW; Gradient elution methods for samples are present in **Table HIS.SI1**

UPLC-MS analysis of the 3CB-sensitized photo-oxidation of His showed the presence of multiple stable products formed during irradiation (**Figure HIS.3**). Based on the analysis of the MS/MS spectra, monoisotopic mass composition and possible fragmentation patterns (**Figure HIS.4 and 5**), the structures of products were proposed. One major category of products appeared to be adducts formed by radical recombination of the $3CBH^{\bullet}$ from the sensitizer with either the histidine side-chain (His-3CBH) or the methyl group of 4-methylimidazole radical (Im-CH_2-3CBH). The latter product had a similar mass to a His-His dimer, but the fragmentation pattern indicated a 3CBH adduct to Me-imidazole fragment. Products with *m/z -2 Da* (compared to the mass of His-3CBH or Im-CH_2-3CBH) were also presented in the MS analysis (**Figure HIS.5**).

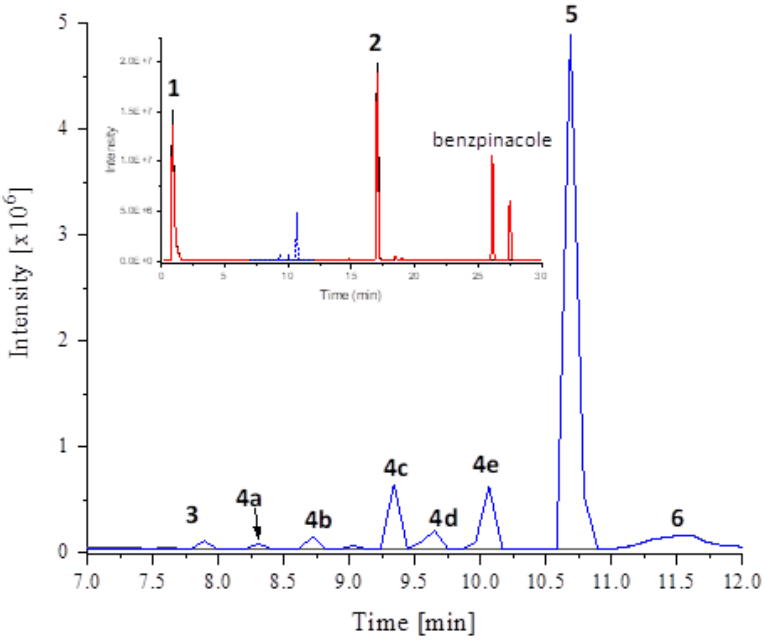

Figure HIS.3 *Expanded total ion chromatogram (TIC) of blank sample containing His (black) or irradiated (blue) for 10 min by 40 mW CW laser. Inset: TIC for non-irradiated His (black) and His irradiated (red) for 10 min with the expanded region marked in blue.*

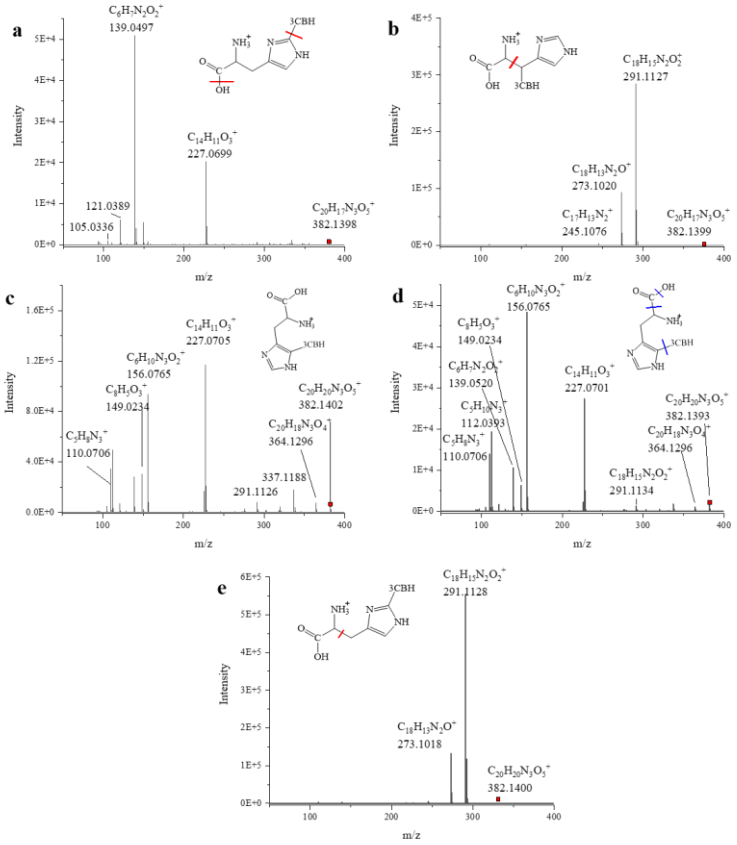

Figure HIS.4 *MS/MS spectra of identified His-3CBH adducts (**4a-e, Table HIS.2**) and their proposed structures*

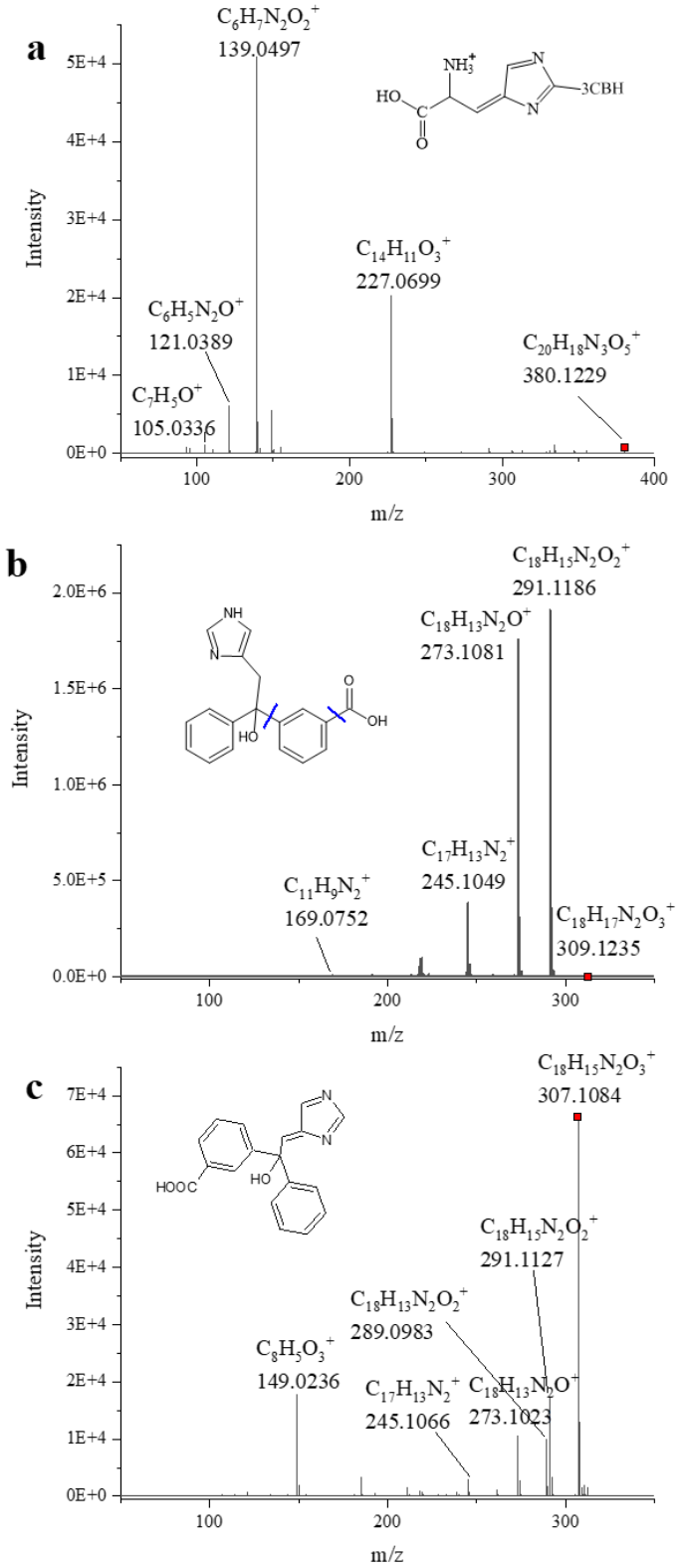

Figure HIS.5 *MS/MS spectra of identified products derived from His oxidation in the presence of 3CB and UVA-light:* ***(a)*** *His-2Da-3CBH,* ***(b)*** *Im-CH2-3CBH, and* ***(c)*** *Im-CH2-2Da-3CBH (products* ***3****,* ***5****, and* ***6****, respectively,* ***Table HIS.2****)*

Chromatograms of stable products formed during the anaerobic sensitized photo-oxidation of His-derivatives, and peptides, along with peak assignments to specific products and their proposed structures, are presented in **Figure HIS.6-7** respectively. When the substrate has a free amine group, similar products were observed, with analogous fragmentation patterns detected from His-NH_2-3CBH (**Figure HIS.SI11**), His-OMe-3CBH (**Figure HIS.14** and **SI15 b**), and 1-Me-His-CBH (**Figure HIS.SI19**). Fragmentation pattern of product **4a** (**Figure His.4**) had loss of whole 3CB and subsequent loss of amine group from the product, therefore providing insight into product structure. Loss of 3CB was also prevalent in products **4c-d**. This could potentially correspond to formation of C-N bond between 3CB and His molecules, or that 3CB hydroxyl group is not protonated first (which was a common theme across all of its products described earlier for Tyr and Trp) making it possible to be lost *via* elimination. Loss of everything apart of methyl-imidazole and 3CB (with loss of water molecule prevalent in those spectra) pointed toward different connection of 3CBH to the His, either to C_β of it or via C-C bond that did not result in elimination of 3CB. Similar behaviour was noted for Im-CH_2-3CBH (**Figure HIS.5**, **SI13**, and **SI15 a**) with the primary products in 1-Me-His oxidation being Me-Im-CH_2-3CBH species (**Figure HIS.SI20 c and SI20 d**). While one of these shares a common fragmentation pattern with other compounds, the second does not.

Alternative products were observed when the amine group is blocked, with no Im-CH_2-CBH species detected; instead, dimeric structures with a new bond between imidazole moieties (di-N-Ac-His, **Figure HIS.16**) were observed. The fragmentation patterns of N-Ac-His-3CBH (**Figure HIS.SI17 a** and **SI17 b**) showed lower intensities compared to the dimer species. Additional minor products, attributed to secondary reactions during longer irradiation times, included species with loss of the carboxylate group on His (**Figure HIS.SI18 a** and **Figure HIS.SI20 a and b**), loss of the amine group (**Figure HIS.SI12**), loss of an ethanol molecule from N-Ac-His-3CBH (**Figure HIS.SI17 c**), and products containing a double bond in His-NH_2-3CBH or 1-Me-His-3CBH (**Figures HIS.SI13 b** and **SI21** respectively).

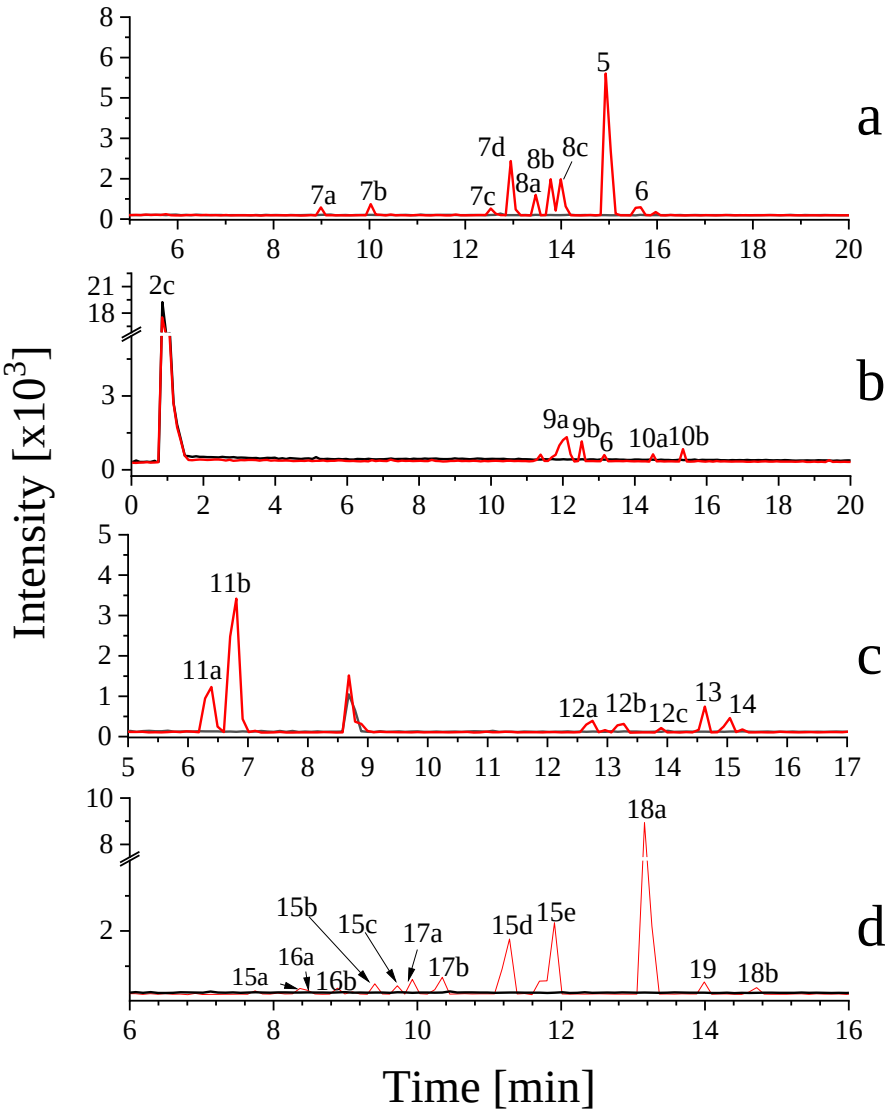

Figure HIS.6 *Chromatogram (TIC) of samples analysis of* ***(a)*** *His-NH_2,* ***(b)*** *His-OMe,* ***(c)*** *N-Ac-His and* ***(d)*** *1-Me-His, non-irradiated (black) and irradiated (red) 10 min by CW laser, 40 mW. Identified compounds (listed in* ***Table HIS.2****):* ***7_{a-d}*** *– [His-NH_2-3CBH]H^+,* ***8_{a-c}*** *– [His-NH_2-3CBH]H^+-NH_3,* ***5*** *– [Im-CH_2-3CBH]H^+,* ***6*** *– [Im-CH_2-3CBH-2Da]H^+,* ***9*** *– [His-OMe-3CBH]H^+,* ***10*** *– [His-OMe-3CBH$_{-NH2/switch/+OH}$]H^+,* ***11*** *– [di-N-Ac-His]H^+,* ***12*** *– [N-Ac-His-3CBH$_{+EtOH}$]H^+,* ***13*** *– [His-NH_2-3CBH$_{-CO2}$]H^+,* ***14*** *– [N-Ac-His-3CBH]H^+,* ***15*** *– [1-Me-His-3CBH]H^+,* ***16*** *– [1-Me-His-3CBH$_{-CO2}$]H^+,* ***17*** *– unidentified,* ***18*** *- [Im-CH_2-3CBH]H^+,* ***19*** *– [Im-CH_2-3CBH$_{-2Da}$]H^+*

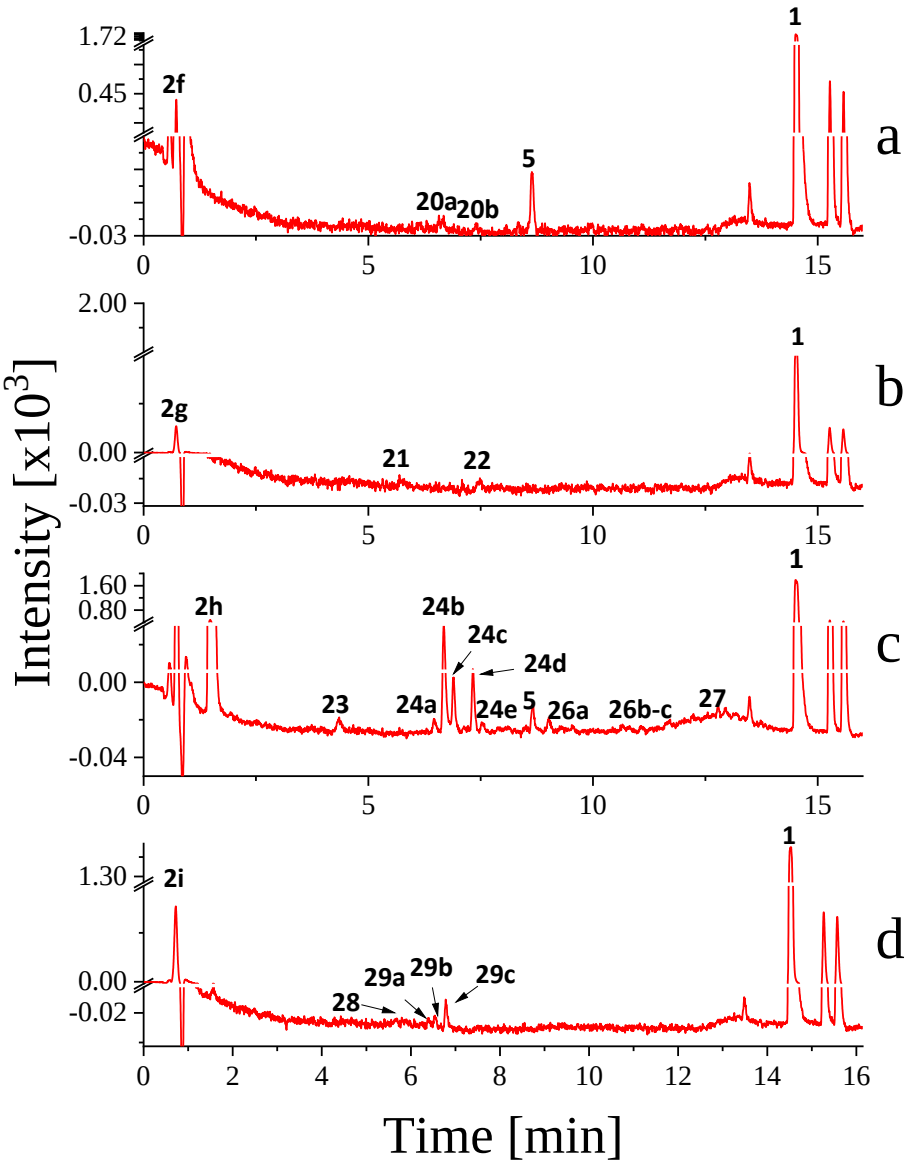

Figure HIS.7 *Chromatogram (UV – 220 nm detection) of analysis of* ***(a)*** *His-Ala* ***(b)*** *Ala-His,* ***(c)*** *– His-Phe, and* ***(d)*** *Gly-His-Gly nonirradiated (black) and irradiated (red) samples (10 min irradiation by CW laser, 40 mW). Identified compounds:* ***5*** *– [Im-CH_2-3CBH]H^+,* ***20*** *– [His-Ala-3CBH]H^+,* ***21*** *- [di-Ala-His]H^+,* ***22*** *- [Ala-His-3CBH]H^+,* ***23****- [Gly-Phe]H^+,* ***24*** *- [di-His-Phe]H^+,* ***25****- unidentified,* ***26*** *- [His-Phe-3CBH]H^+,* ***27*** *– [His-Phe-3CBH$_{-2Da}$]H^+,* ***28*** *– [di-Gly-His-Gly]H^+,* ***29****– [Gly-His-Gly-3CBH]H^+*

The behaviour of His-Ala and Ala-His (**Figure HIS.SI22** and **SI23** respectively) was similar to their His derivative counterparts. Im-CH_2-3CBH species were detected for His-Ala, but no dimers were detected for this peptide, whereas for Ala-His, one dimer was observed. The tri-peptide Gly-His-Gly (**Table HIS.2**) showed only dimer and 3CB products (**Figure HIS.SI25**). Dipeptide containing phenylalanine (e.g., His-Phe) displayed mixed behaviour with both Im-CH_2-3CBH products and dimeric structures identified (**Figure HIS.SI24**). An additional product identified as Gly-Phe was detected in His-Phe samples (**Figure HIS.SI24 b**). Across all compounds, two products from 3CBH$^{\bullet}$ radicals recombination, with the structure similar to benzpinacol, were identified and characterized as described previously [28].

Table HIS.2 *A list of the identified products from sensitized by 3CB photo-oxidation of His and its derivatives in aqueous solution in the absence of oxygen.*

Comp. no	Retention time, min	Identified product	Measured mass	Monoisotopic mass	R [ppm]
1	17.0	$[3CB]H^+$	227.0700	227.0708	-3.52
		His			
2a	1.0	$[His]H^+$	156.0764	156.0773	5.76
3	7.9	$[His\text{-}3CBH_{-2Da}]H^+$	380.1229	380.1246	4.47
4a	8.3	$[His\text{-}3CBH]H^+$	382.1398	382.1403	1.30
4b	8.7	$[His\text{-}3CBH]H^+$	382.1389	382.1403	3.66
4c	9.3	$[His\text{-}3CBH]H^+$	382.1402	382.1403	0.26
4d	9.6	$[His\text{-}3CBH]H^+$	382.1393	382.1403	2.61
4e	10.0	$[His\text{-}3CBH]H^+$	382.1400	382.1403	0.78
5	10.6	$[Im\text{-}CH_2\text{-}3CBH]H^+$	309.1235	309.1239	1.29
6	10.9	$[Im_{-2Da}\text{-}CH_2\text{-}3CBH]H^+$	307.1084	307.1082	0.65

His-NH_2					
2b	1.0	[His-NH_2]H^+	155.0925	155.0933	-5.15
7a	9.0	[His-NH_2-3CBH]H^+	381.1553	381.1562	-2.36
7b	10.0	[His-NH_2-3CBH]H^+	381.1554	381.1562	-2.09
7c	12.7	[His-NH_2-3CBH]H^+	381.1554	381.1562	-2.09
7d	13.4	[His-NH_2-3CBH]H^+	381.1551	381.1562	-2.88
8a	13.5	[His-NH_2-3CBH]H^+ $_{-NH3}$	364.1284	364.1297	-3.57
8b	13.8	[His-NH_2-3CBH]H^+ $_{-NH3}$	364.1290	364.1297	-1.92
8c	14.1	[His-NH_2-3CBH]H^+ $_{-NH3}$	364.1287	364.1297	-2.74
5	15.0	[Im-CH_2-3CBH]H^+	309.1231	309.1239	-2.58
6	15.5	[Im$_{-2Da}$-CH_2-3CBH]H^+	307.1063	307.1082	-6.19
His-Ome					
2c	0.85	[His-OMe]H^+	170.0923	170.0929	-3.53
9a	12.0	[His-OMe-3CBH]H^+	396.1551	396.1559	-2.02
9b	12.5	[His-OMe-3CBH]H^+	396.1556	396.1559	-0.76
6	13.1	[Im-CH_2-3CBH]H^+	309.1227	309.1239	-3.88
10a	14.5	[His-OMe-3CBH]H^+ $_{-NH2 + OH (switch)}$	397.1394	397.1400	-1,51
10b	15.4	[His-OMe-3CBH]H^+ $_{-NH2 + OH (switch)}$	397.1394	397.1400	-1,51
N-Ac-His					
2d	0.85	[N-Ac-His]H^+	198.0873	198.0872	0.50
11a	6.3	[di-N-Ac-His]H^+	393.1518	393.1522	1.01
11b	6.7	[di-N-Ac-His]H^+	393.1523	393.1522	0.25
12a	12.7	[N-Ac-His$_{-EtOH}$-3CBH]H^+	470.1915	470.1927	-2,55
12b	13.3	[N-Ac-His$_{-EtOH}$-3CBH]H^+	470.1915	470.1927	-2,55
12c	13.9	[N-Ac-His$_{-EtOH}$-3CBH]H^+	470.1916	470.1927	-2,34
13	14.6	[N-Ac-His$_{-CO2}$-3CBH]H^+	380.1607	380.1610	-0.79
14a	15.0	[N-Ac-His-3CBH]H^+	424.1503	424.1502	0.23
14b	15.3	[N-Ac-His-3CBH]H^+	424.1496	424.1502	-1.41

1-Me-His					
2e	1.00	[1-Me-His]H^+	170.0925	170.0929	-2,35
15a	8.3	[1-Me-His-3CBH]H^+	396.1546	396.1559	-3.28
16a	8.5	[1-Me-His-3CBH$_{-CO2}$]H^+	352.1652	352.1661	-2.55
16b	8.9	[1-Me-His-3CBH$_{-CO2}$]H^+	352.1656	352.1661	-1.42
15b	9.4	[1-Me-His-3CBH]H^+ - H2O in source	378.1444	378.1453	-2.38
15c	9.7	[1-Me-His-3CBH]H^+	396.1553	396.1559	-1.55
15d	11.4	[1-Me-His-3CBH]H^+	396.1551	396.1559	-2.01
15e	11.8	[1-Me-His-3CBH]H^+	396.1554	396.1559	-1.26
18a	13.2	[1-Me-Im-CH_2-3CBH]H^+	323.1391	323.1395	-1,23
19	14.0	[1-Me-Im$_{-2Da}$-CH_2-3CBH]H^+	321.1233	321.1239	-1.86
18b	14.7	[1-Me-Im-CH_2-3CBH]H^+	323.1388	323.1395	-2.16
His-Ala					
2f	0.72	[His-Ala]H^+	227.1142	227.1144	-0,88
20a	6.56	[His-Ala-3CBH]H^+	453.1773	453.1774	-0,22
20b	7.40	[His-Ala-3CBH]H^+	453.1781	453.1774	1,54
5	8.64	[Im-CH_2-3CBH]H^+	309.1228	309.1239	-3,56
Ala-His					
2g	0.72	[Ala-His]H^+	227.1136	227.1144	-3,52
21	5.70	[di-Ala-His]H^+	451.2025	451.2053	-6,21
22	7.48	[Ala-His-3CBH]H^+	453.1771	453.1774	-0.66
His-Phe					
2h	1.48	[His-Phe]H^+	303.1455	303.1457	-0.66
23	4.35	[Gly-Phe]H^+	223.1067	223.1083	-7.03
24a	6.46	[di-His-Phe]$2H^+$	302.1369	302.1373	-1.32
24b	6.67	[di-His-Phe]$2H^+$	302.1372	302.1373	-0.33
24c	6.89	[di-His-Phe]H^+	603.2683	603.2679	0.66
24d	7.13	[di-His-Phe]H^+	603.2682	603.2679	0.50

24e	7.33	[di-His-Phe]2H^+	302.1375	302.1373	0.66
5	8.65	[Im-CH_2-3CBH]H^+	309.1231	309.1239	-2.59
26a	9.02	[His-Phe-3CBH]H^+	529.2079	529.2087	-1.51
26b	10.65	[His-Phe-3CBH]H^+	529.2094	529.2087	1.32
26c	12.76	[His-Phe-3CBH]H^+	529.2093	529.2087	1.13
27	12.96	[His-Phe-3CBH_{-2Da}]H^+	527.1932	527.1931	0.19
		Gly-His-Gly			
2i	0.72	[Gly-His-Gly]H^+	270.1199	270.1202	-1.11
28	5.80	[di-Gly-His-Gly]H^+	537.2167	537.2170	-0.56
29a	6.40	[Gly-His-Gly-3CBH]H^+	496.1834	496.1832	0.40
29b	6.52	[Gly-His-Gly-3CBH]H^+	496.1831	496.1832	-0.20
29c	6.79	[Gly-His-Gly-3CBH]H^+	496.1833	496.1832	0.20

The Im-CH_2-3CBH adduct appeared in the anaerobic photosensitized oxidation of His and its derivatives only when a free amine group was present, with no detectable dimers in simple model compounds. This is noteworthy as an Im-CH_2-3CBH-like product (without a carboxylate) has been reported as an α2-adrenergic agonist for treating diseases such as sleep disorders, anxiety disorders, and developmental disorders [160]. Therefore, this photo-oxidation method may be a convenient route to candidate His-derived drugs.

A number of aromatic sensitizers have been shown to induce His oxidation in the presence of an appropriate light source (**Figure HIS.8**). Previous experiments have employed sensitizers that have lower energies [98,161,162] than the excited triplet state of $HisH^+$ [$^3(HisH^+)$*], which is 2.58 eV (249 kJ·mol^{-1}) [163]. In the present study, the applied sensitizer 3CB, has an excited triplet state energy of 289 kJ·mol^{-1} [26].

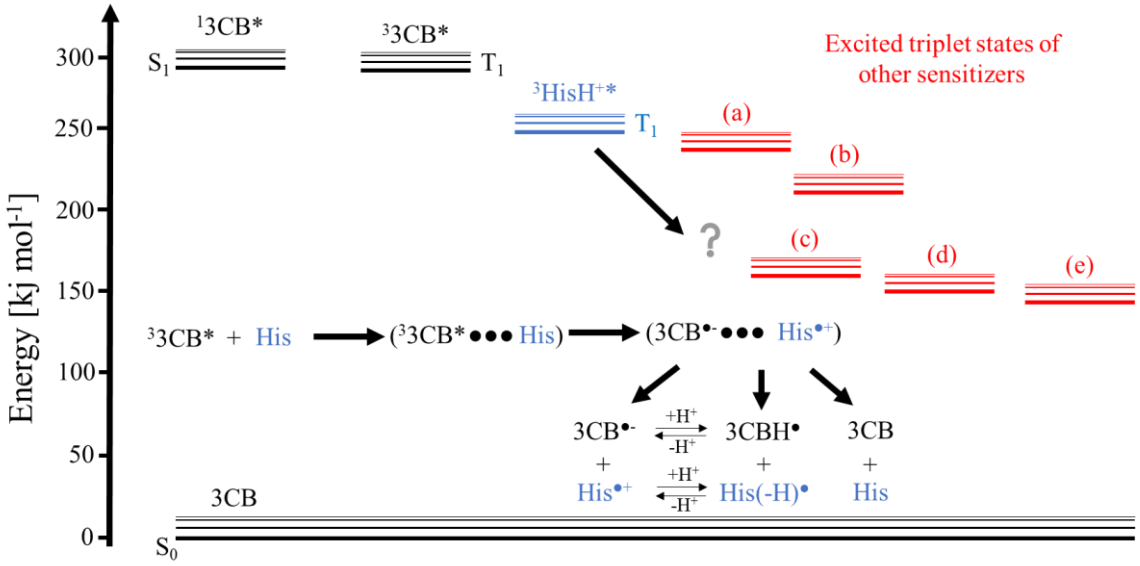

Figure HIS.8. *Energy diagram comparing the energy of ^{3}3CB* to the energy of ^{3}(HisH$^+$)*. The excited triplet states of other sensitizers are also included for comparison ((a) pterin – 236 kJ·mol^{-1} [161]; (b) riboflavin – 208 kJ·mol^{-1} [164]; (c) rose bengal – 169 kJ·mol^{-1} [165,166]; (d) protoporphyrin IX dimethyl ester – 150 kJ·mol^{-1} [165]; (e) methylene blue – 142 kJ·mol^{-1} [167]). The question mark indicates the knowledge gap regarding ^{3}(HisH$^+$)* addressed in this thesis. A general scheme representing the currently known mechanism of action of quenchers (His) on the excited triplet state of ^{3}3CB*, based on analogous processes, is also included [26,32,69,72]*

When the α-amino group of His is blocked, either by acetylation or incorporation into a peptide, significant amounts of dimers are detected. His-Phe showed both dimers and Im-CH_2-CBH in the reaction mixtures. Covalent His dimers have been reported recently [168,169], but the effects of anaerobic photosensitized oxidation have not been previously described (namely stable products). The yield of such dimers is likely maximized in the absence of O_2, minimizing alternative reaction channels. These species most likely arise from dimerization of two HisN$^\bullet$ radicals, with an alternative fate being disproportionation, leading to one product with a double bond and one regenerated parent molecule. Despite the low redox potential of HisN$^\bullet$ [94], these products were not detected in high amounts, possibly due to further reactions of the initial products. The formation of multiple forms of His-CBH and His-His-like products is attributed to the delocalization of electron density across the His structure [170]. The formation of Im-CH_2-CBH and Gly-Phe (from His-Phe) has not been reported previously in anaerobic photosensitized oxidation reactions [168].

A proposed mechanism for the anaerobic ^{3}3CB* sensitized photo-oxidation of His species is presented in **Figure HIS.9** Based on differences in *kq* values, two different quenching processes and additional reactions are proposed. His, with a fluorescence maximum around 360 nm [158], has an excited singlet state energy likely around 350 kJ·mol^{-1}. Given the typical energy difference between the excited singlet and triplet states for ππ* transitions (~100 kJ mol $^{-1}$), the excited triplet state energy of His should be around 250 kJ·mol^{-1}, consistent with literature (249 kJ·mol^{-1}) [163] and lower than that of ^{3}3CB* (289 kJ·mol^{-1}).

The formation of Im-CH_2-3CBH requires an explanation that accounts for differences in quenching rate constants and one specific product (Gly-Phe). The energy transfer from excited ^{3}3CB* to His, forming ^{3}His*, results in C-C bond photodissociation, yielding Im-$CH_2^{\bullet}$ and Gly$^{\bullet}$ radicals. This is consistent with the product analyses and the detection of Im-CH_2-3CBH in model compounds with an unblocked amine group, and in the case of His-Phe, Gly-Phe (**Table HIS.2**). The reactions of His derivatives indicated that a free α-amino group facilitates energy transfer, while its derivatization prevents this channel, leading to the near-exclusive formation of dimers (His-His and His-3CBH). It is postulated that the free amine group promotes energy transfer *via* interaction with the imidazole ring, possibly through an intra-molecular hydrogen bond, lowering the excited triplet state energy. Suppression of the energy transfer pathway increases the yields of His$^{\bullet}$-derived products.

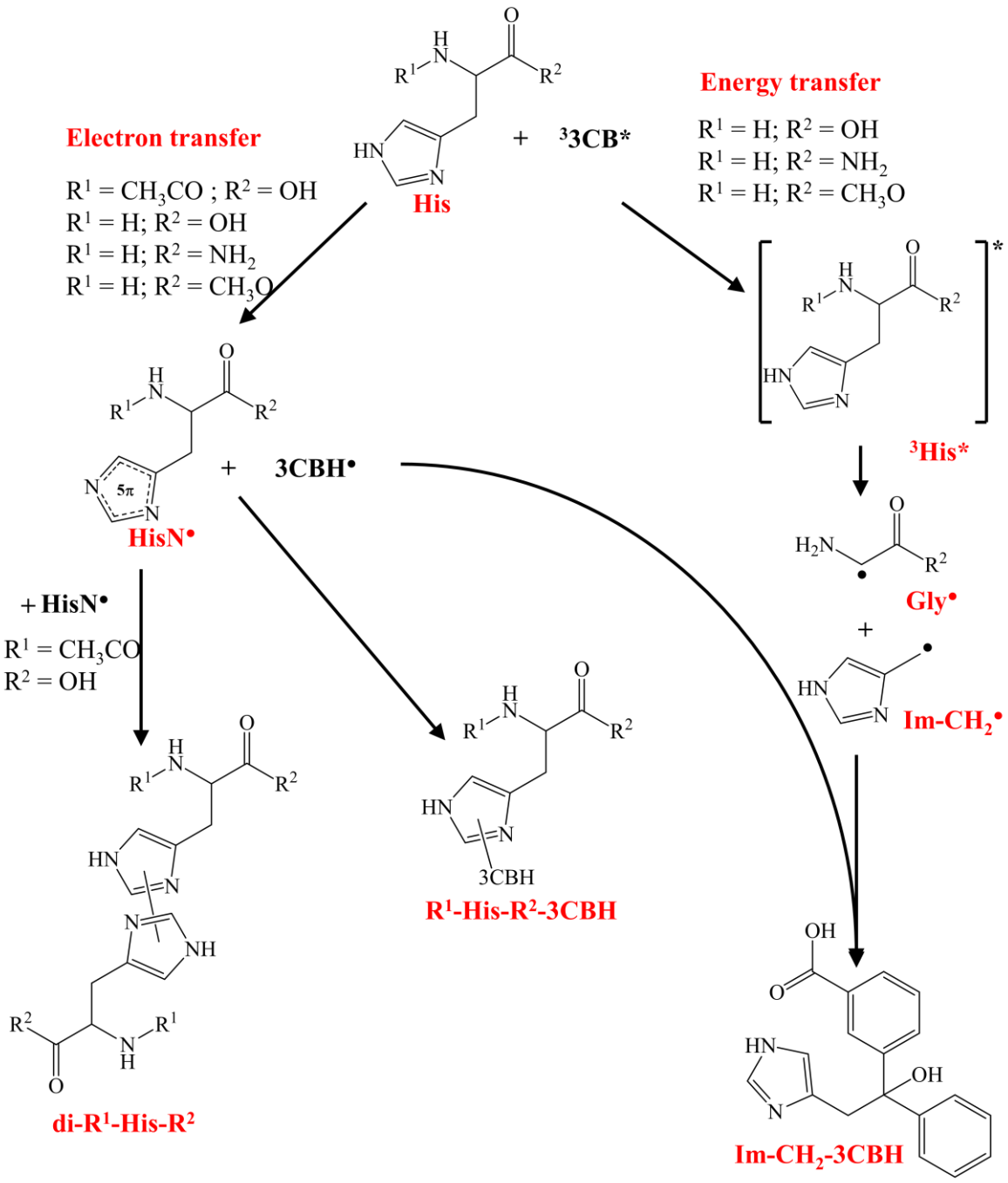

Figure HIS.9. *Proposed mechanism of anaerobic photo-oxidation of His-containing compounds by ^{3}3CB**

III.4. Phenylalanine

III.4.1. Laser flash photolysis

Concentrations: Phe, Phe-OEt, N-Ac-Phe, N-Ac-Phe-OEt, Phe-Gly – 0 mM, 1 mM, 2 mM, 4 mM, 6 mM; Phe-Gly – 0 mM, 0.4 mM, 0.6 mM, 0.8 mM, 1 mM; 3CB – 4mM and 5 mM in case of Phe-Gly. Ar bubbled for 25 min in rectangular quartz cuvettes with 10 mm optical path. Time-resolved spectra and concentration profiles were generated using 1 mM Phe-Gly and 5 mM CB, and 6 mM concentration of the other compounds with 4 mM of CB for each respective sample.

Nanosecond transient absorption spectroscopy for Phe and its derivatives was performed with conditions described above. The average of 8 kinetic traces recorded for every 10 nm at varying concentration of Phe (**Figure PHE.1 a)** were used to create the Stern-Volmer plot (**Figure. PHE.1 b)** and at the highest concentration, the transient absorption spectra presented in **Figure PHE.2 a**. The same was done for other Phe model compounds (**Figure PHE.SI1-4**). The spectra recorded after 0.2, 1, and 2 μs indicated the formation of a broad band with a maximum at 540 nm that decreased with time after the laser pulse, which is in accordance with both literature and previous experiments, however formation of this band was fainter for Phe and its derivatives (**Figure PHE.SI5**). The rate constant for quenching the ^{3}3CB* by Phe was calculated by fitting the pseudo-first order kinetic decays at 450 nm (or 430 nm in case of Phe-Gly) to give a second-order triplet quenching rate constant (**Table PHE.1**).

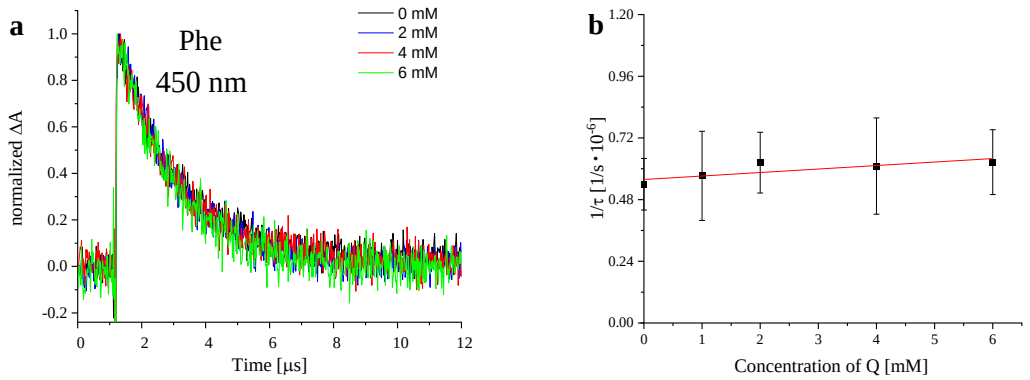

Figure PHE.1 ***(a)*** *Kinetic traces for the ^{3}3CB* decay at 450 nm in the presence varying concentration of Phe at pH 7* ***(b)*** *The Stern-Volmer plot according to* ***Equation 2*** *for the quenching of ^{3}3CB* by Phe at pH 7 in aqueous solution for 3CB (4 mM)*

Quenching rate constants presented a trend in which blocking the carboxyl group resulted in higher k_q values. This phenomenon seems to be prevalent across all amino acids. Therefore, the overall conclusion is that the negative charge located in vicinity of chromophoric side-chain resulted in retardation of process rate. The determined k_q values are generally two orders of magnitude lower than those of other aromatic amino acids. When Phe was incorporated in peptide that also had His in the sequence (**Table HIS.1)**, quenching rate constant increased significantly and resembled that of His itself, indicating that His likely predominated in this process. Such relatively small values of k_q are an indicator of hydrogen atom transfer (HAT) process. The quantum yields of generation of 3CBH$^\bullet$ ($\Phi_{3CBH^\bullet}$) are presented in **Table PHE.1**

Table PHE.1 *Quenching rate constants and corresponding quantum yields of short-lived intermediates formation for Phe and its derivatives, where Z_Q and Z_{3CB} are the net charge of Q and 3CB at pH 7, respectively*

Quencher	**Z_Q**	**k_q (x10^7 M^{-1}·s^{-1})**	**$\Phi_{3CBH^\bullet}$**	**Z_QZ_{3CB}**
Phe	0	1.2±0.6	0.36±0.20	0
Phe-OEt	+1	4.5±0.5	0.44±0.09	-1
N-Ac-Phe	-1	1.4±0.2	0.33±0.13	+1
N-Ac-Phe-OEt	0	3.6±0.2	0.20±0.10	0
Phe-Gly	0	7.0±0.2	0.45±0.23	0

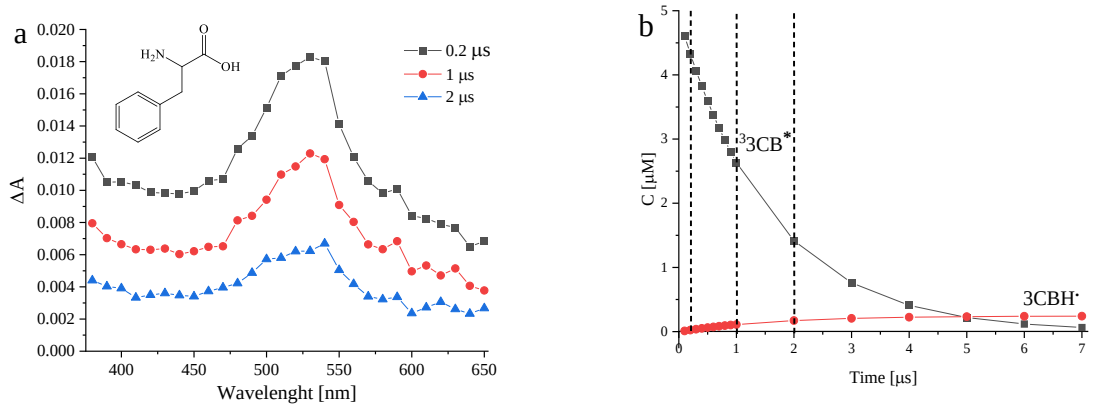

Figure PHE.2 ***(a)*** *Evolution of transient absorption spectra from 3CB-sensitized oxidation of Phe (6 mM). Spectra were recorded at different delays following laser pulse 0.2 (black ■), 1 (red ●) and 2 μs (blue ▲). Concentration profiles of transients identified in the laser flash photolysis of an aqueous solution of* ***(b)*** *Phe and 3CB (4 mM) at pH 7 where (black ■) is* ^{3}*3CB*, and (red ●) is 3CBH*$^\bullet$*. Dotted lines represent times at which respective spectra were presented in* ***(a)***

Deconvolution of the observed spectra was attempted using reference spectra of exclusively ^{3}3CB*, 3CB$^{\bullet-}$ and 3CBH$^\bullet$. That is because transients that could potentially arise absorb in shorter wavelengths (particularly Phe radical cation that has maximum at 310 nm [171]). Keeping that in mind, the shift to longer wavelengths combined with some concentrations of 3CBH$^\bullet$ determined from deconvolution of transient profiles points further into HAT. No concentrations of 3CB$^{\bullet-}$ was present in Phe and its derivatives. The resulting quantum yields of generation of 3CBH$^\bullet$ were compared, revealing no significant differences among the different blocked amino acids examined, except of Phe-OEt and N-Ac-Phe-OEt. The average value of $\Phi_{3CBH^\bullet}$ was 0.35±0.15 which only meant the inefficiency of generation of 3CBH$^\bullet$.

III.4.2. Steady state photolysis

Concentrations: Phe, Phe-OEt, N-Ac-Phe, N-Ac-Phe-OEt, Phe-Gly – 1 mM; 3CB – 1mM and 5 mM in the case of peptide. Ar bubbled for 25 min in rectangular quartz cuvettes with 10 mm optical path and magnetic dipole; the output power used was set at 40 mW; 5 min of irradiation for derivatives, and 10 min for peptide. Gradient elution methods for samples are present in **Table PHE.SI1**

UPLC-MS analysis of the 3CB-sensitized photo-oxidation of Phe showed the presence of multiple stable products after irradiation. Chromatograms of model compounds after photolysis with 3CB in Ar atmosphere re in **Figure PHE.3**. Analysis of the fragmentation patterns (**Figure PHE.4-5** and **Figure PHE.SI6-10**) provided information on potential structures consistent with these spectra.

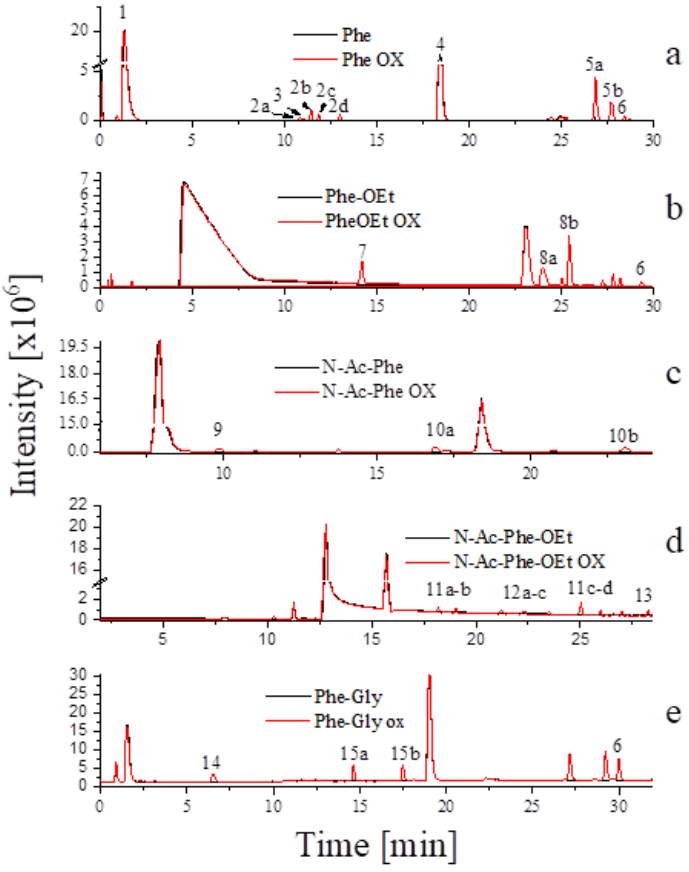

Figure PHE.3 *Comparison of total ion current chromatograms for irradiated samples of 3CB with (in descending order) Phe, Phe-OEt, N-Ac-Phe, N-Ac-Phe-OEt and PheGly with identified products listed in* ***Table PHE.3****.* ***Black*** *lines represent blank sample solutions which contains 3CB and respective compound, in* ***red*** *are chromatograms of oxidized samples*

Products of Phe and its derivatives can be divided into several different categories. First one has been identified as covalent adduct of sensitizer to Phe side-chain. Fragmentation pattern contains ions with the most crucial ones being ions with *m/z 179.08* (**Figure PHE.4**), which suggests that between two benzene rings must be two carbon atoms, presence of *m/z 283.11* proves C-C connection, and lastly loss of two water molecules, one carbon (II) oxide and hydrogen cyanide (between two abundant peaks in **Figure PHE.3**) proves that formation of such bond must occur on C_β, as there is no possibility for hydrogen cyanide to be lost if it were connected *via* C_α. That point towards characteristic place of the formation of the bond between two plausible radicals. The same principles apply to products **13** in **Figure PHE.SI9**, and **15a** in **Figure PHE.SI10**. Products **10a** and **10b** in **Figure PHE.SI7** has been identified as sodium adducts of N-Ac-Phe-3CBH. Presence of this form of ionization implies differences in fragmentation, however it still contained fragment that represented three benzene rings connected *via* two carbon atoms with carboxylic group, and it also had intact ionized amino acid. Existence of utmost four different Phe-3CBH compounds throughout all analyses of stable products further facilitates that claim, as formation of bond in this specific place would yield four stereoisomers, which was also the case in Met oxidation, elaborated further in [28].

An alternative subcategory of this group includes products **12a-c** presented in **Figure PHE.SI9**. The first thing that needs to be addressed regarding these products is the absence of the ethanol moiety form N-Ac-Phe-OEt, with the formation of new ions in the fragmentation patterns. Detailed analysis provided information on the presence of the N-acetyl group and carboxyl group in the molecule and the existence of ion with *m/z 328.11*. The prevalence of that fragment suggests the loss of carboxylic group connected to benzene ring, rather than that of the amino acid. Since fragmentation is constricted in that area, it would be safe to assume that ring formation occurred, rather than double bond in the structure of phenylalanine. If the latter had been the case, it would be logical for the molecule to lose three water molecules during fragmentation, which is not observed. Another argument in favor of this interpretation of data is a well-known phenomenon that displacement of ethanol is easier than that of water molecule from carboxylic group.

The second identified group includes a covalent bond between two Phe side-chains, identified in the stable products of Phe-OEt (**Figure PHE.SI6**), N-Ac-Phe-OEt (**Figure PHE.SI8**), and Phe-Gly (**Figure PHE.SI10**). In all of the fragmentation patterns, functional groups of Phe fragments first and end in formation of tropylium ion. If two benzene ring had been in fact connected, their fragments would be visible. In fact, free immonium

fragment is present, which points toward formation of covalent bond on either C_α or C_β of Phe. The fragmentation pattern of product **14** (**Table PHE.3)** consisted of the loss of two glycine moieties with subsequent loss of phenyl-ethylene, consequently substantiating the argument that two Phe side-chains are covalently bonded *via* C_β. Even though the same argument could be make that existence of four stereoisomers is possible, one of them would result in *meso* form. However, due to limitations of applied method, it is impossible to deduce which products belong into C_β and which not.

Another important group, somewhat unexpected given the current literature, was identified as addition of benzyl group to either Phe or 3CBH (**Figure PHE.5**). MS/MS fragmentation once again provided information on formation of this product on C_β of Phe or its derivative (**Figure PHE.SI6** and **Figure PHE.SI10**). **Table PHE.3** assembles the retention times of products present in **Figure PHE.3**, with respective mass of identified products mentioned in this paragraph. Product **9** has been identified as an oxygen derived side product.

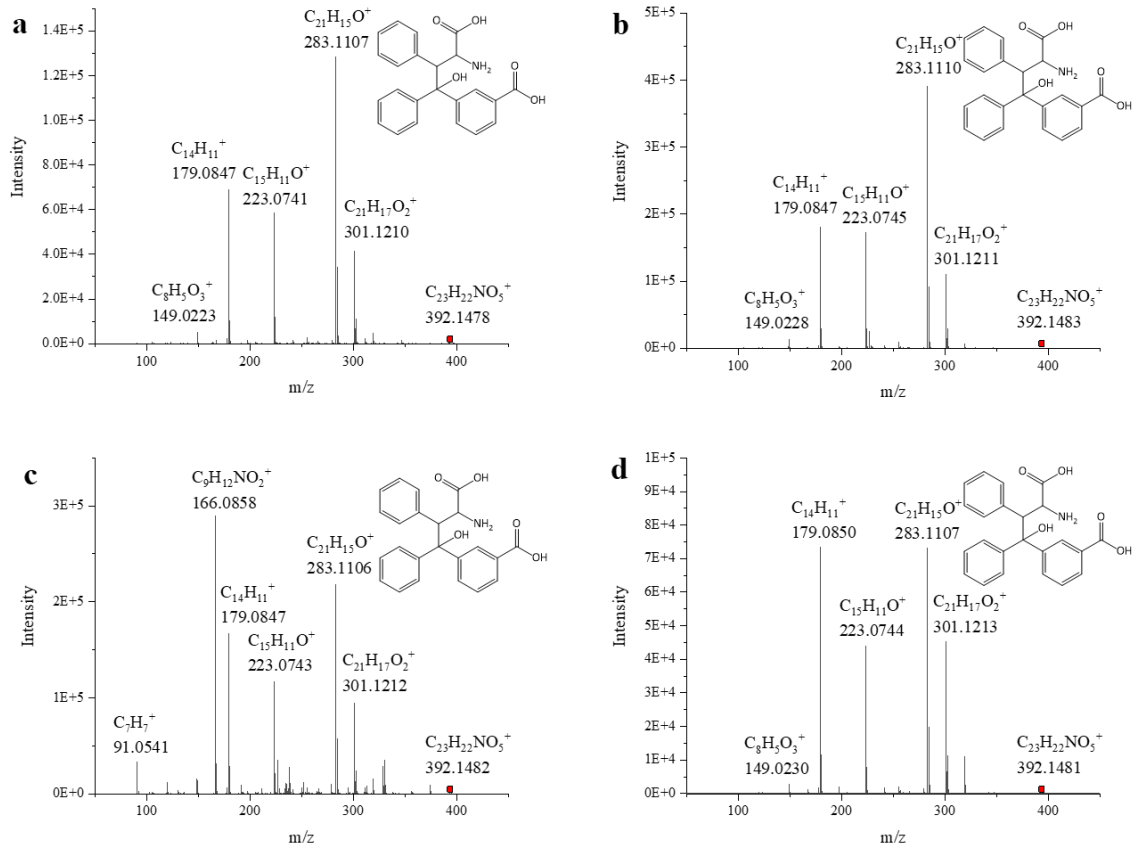

Figure.PHE.4 *MS/MS spectra of identified substances derived from Phe oxidation in the presence of 3CB and UVA-light products* ***2a-d****.*

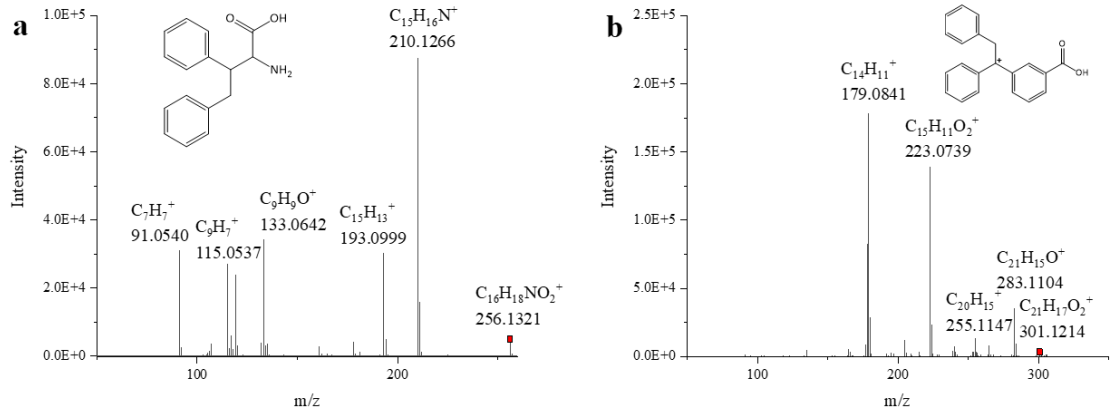

Figure.PHE.5 *MS/MS spectra of identified substances derived from Phe oxidation in the presence of 3CB and UVA-light:* ***(a)*** *product Phe-Bz, and* ***(b)*** *3CBH-Bz*

Table.PHE.3 *A list of the identified products from sensitized by 3CB photo-oxidation of Phe and its-derivatives in aqueous solution in the absence of oxygen.*

Comp. no	Retention time, min	Identified product	Measured mass	Monoisotopic mass	R [ppm]
		Phe			
1	**1.3**	$[Phe]H^+$	166.0857	166.0863	-3.6
2a	**10.8**	$[Phe\text{-}3CBH]H^+$	392.1478	392.1492	-3.6
3	**11.0**	$[Phe\text{-}Bz]H^+$	256.1321	256.1338	-6.5
2b	**11.4**	$[Phe\text{-}3CBH]H^+$	392.1483	392.1492	-2.3
2c	**11.9**	$[Phe\text{-}3CBH]H^+$	392.1482	392.1492	-2.6
2d	**13.0**	$[Phe\text{-}3CBH]H^+$	392.1481	392.1492	-2.8
4	**18.4**	$[3CB]H^+$	227.0692	227.0708	-7.1
5a	**26.9**	$[3CBH\text{-}3CBH]H^+$	455.1472	455.1489	-3.7
5b	**27.7**	$[3CBH\text{-}3CBH]H^+$	455.1475	455.1489	-3.1
6	**28.4**	$[3CBH\text{-}Bz]H^+_{(-H2O\ in\ source)}$	301.1214	301.1223	-3.3
		Phe–OEt			
7	**14.5**	$[Phe\text{-}OEt\text{-}Bz]H^+$	284.1641	284.1629	-1.4
6	**29.0**	$[3CBH\text{-}Bz]H^+$	319.1317	319.1334	-3.7
8a	**24.1**	$[diPhe\text{-}OEt]H^+$	385.2124	385.2127	0.6
8b	**25.4**	$[diPhe\text{-}OEt]H^+$	385.2124	385.2127	0.6

N-Ac-Phe					
9	**9.9**	[N-Ac-Phe-Tyr +H_2]H^+	389.1721	389.1707	3.6
10a	**16.9**	[N-Ac-Phe-3CBH]Na^+	456.1425	456.1423	0.4
10b	**23.2**	[N-Ac-Phe-3CBH]Na^+	456.1427	456.1423	0.9
N-Ac-Phe-OEt					
11a	**18.3**	[diN-Ac-Phe-OEt]H^+	469.2339	469.2333	1.3
11b	**19.0**	[diN-Ac-Phe-OEt]H^+	469.2349	469.2333	3.4
12a	**21.2**	[N-Ac-Phe-OEt-3CBH (-C_2H_5OH)]H^+	416.1505	416.1492	2.1
12b	**22.4**	[N-Ac-Phe-OEt-3CBH (-C_2H_5OH)]H^+	416.1506	416.1492	2.8
12c	**23.5**	[N-Ac-Phe-OEt-3CBH (-C_2H_5OH)]H^+	416.1506	416.1492	2.3
11c	**25.1**	[diN-Ac-Phe-OEt]H^+	469.2348	469.2333	3.2
11d	**26.0**	[diN-Ac-Phe-OEt]H^+	469.2348	469.2333	3.2
13	**28.3**	[N-Ac-Phe-OEt-3CBH]H^+	462.1923	462.1911	2.6
Phe-Gly					
14	**6.5**	[diPhe-Gly]H^+	443.1930	443.1925	1.1
15a	**14.6**	[Phe-Gly-3CBH]H^+	449.1716	449.1707	2.0
15b	**17.5**	[Phe-Gly-3CBH]H^+	449.1723	449.1707	3.5
6	**30.0**	[3CBH-Bz]$H^+_{(-H2O\ in\ source)}$	301.1246	301.1223	7.6

The transient absorption spectra showed the quenching of ^{3}3CB* and the formation of the CBH$^\bullet$. The analysis of stable products allowed to propose the mechanism of sensitized photo-oxidation presented in **Figure PHE.6** [172]. The ^{3}3CB* can be quenched by Phe. Relatively small k_q values combined with the structures of identified products, points toward the fact that irradiation of Phe and its derivatives conducted in the presence of a sensitizer and in the absence of starts with abstraction of hydrogen atom from position C_β yielding a 3CBH$^\bullet$ radical and respective radical of Phe (Phe$^\bullet$) and energy transfer. The latter mechanism, i.e. energy transfer from ^{3}3CB* to Phe (based on energy difference between the energy of an ^{3}3CB* and the energy of an excited triplet state of Phe (^{3}Phe*) molecules estimated

as -12 kJ·mol^{-1} [1]) results in the formation of an ^{3}Phe* followed by homolytic bond dissociation to a benzyl radical (Bz$^\bullet$) and glicyl radical [1]. The analysis of stable products showed that these two processes must occur together, because the identified products are the results of radical recombination. Bz$^\bullet$ could have recombined with 3CBH$^\bullet$ leading to formation of product **6** (**Figure PHE.5**), or it could have recombined with Phe$^\bullet$ to yield product **3**. The Phe$^\bullet$ radicals can also dimerize or recombine with 3CBH$^\bullet$. This last product can also undergo further intramolecular nucleophilic substitution that results in formation of product **12**.

Regarding the influence of blocking group on this process, it seems that the reaction of Phe derivatives resulting in formation of Bz$^\bullet$ occurs exclusively when the amine group is free. This information supports the earlier claim that a free α-amino group allows for the energy transfer, while its derivatization prevents this channel, leading to the near-exclusive formation of products of recombination of Phe$^\bullet$. Blocking C- end of the Phe results in greater degradation of 3CB with underlying processes unknown, nevertheless ending in the formation of 3CBH-3CBH product.

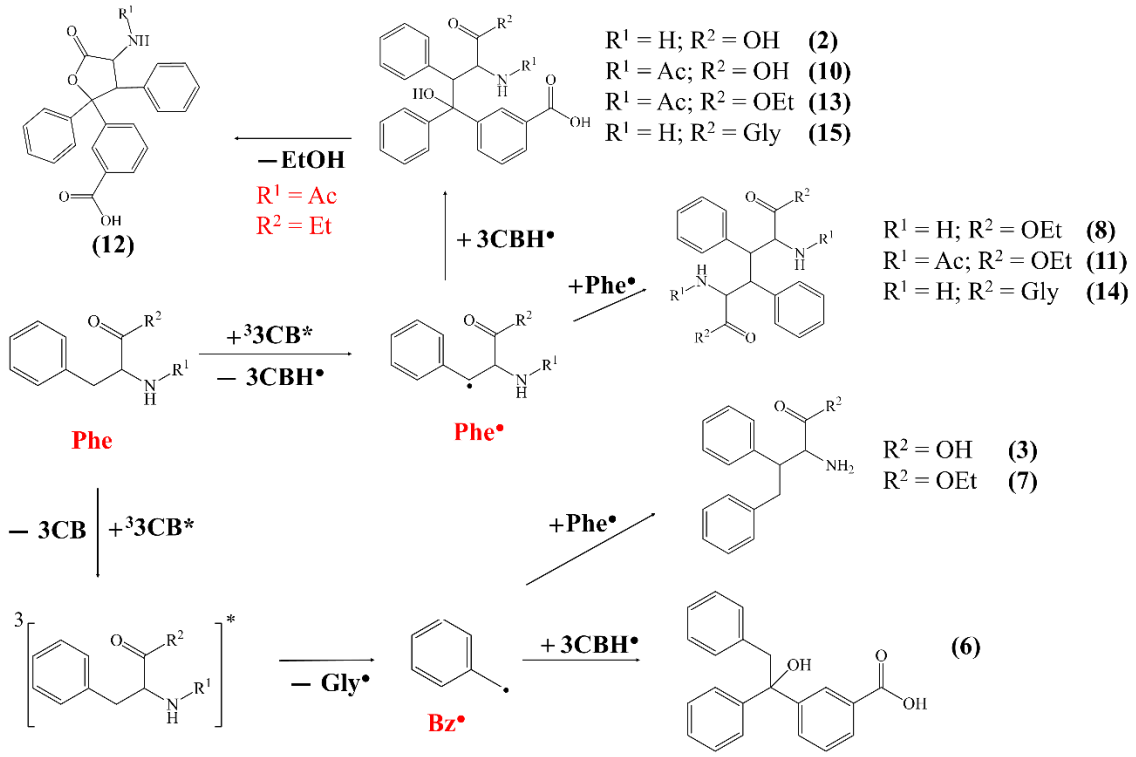

Figure PHE.6 *Proposed mechanism of anaerobic photo-oxidation of Phe-containing compounds by ^{3}3CB**

III.5. GAPDH

III.5.1. Ground state complexation

Formation of ground state complex was investigated using the method explained in **Chapter II.2.5**. In **Figure GAPDH.1,** isosbestic points are visible and serve as a strong indicator of formation of ground state complex. The final solution, which was consisted of maximum concentration of GAPDH in the mixture, was filtered using commercially available filters, resulting in the loss of roughly one-third of the initial 3CB in the solution.

The requirement for an isosbestic point to occur is that the two species involved are related linearly by stoichiometry, such that the absorbance is invariant at a certain wavelength. Thus, ratios other than 1-to-1 are possible. The presence of an isosbestic point typically indicates that only two species that vary in concentration contribute to the absorption around the isosbestic point. If a third species is involved in the process, the spectra typically intersect at varying wavelengths as concentrations change, creating the impression that the isosbestic point is 'out of focus' or that it will shift as conditions change. This is because it would be very unlikely for three compounds to have extinction coefficients linked in a linear relationship by chance for one particular wavelength. However, due to low concentrations of both GAPDH and 3CB, it was impossible to deduce whether that point was changing or staying in the same place (**Figure GAPDH.2**).

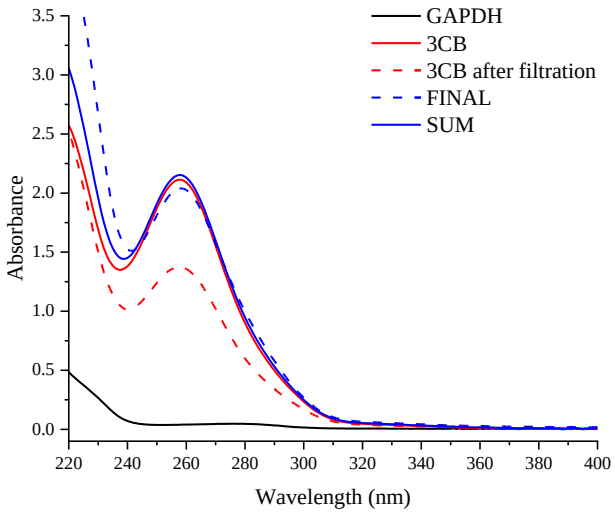

Figure GAPDH.1 *Absorbance spectra of GAPDH at given concentration, 3CB at given concentration, 3CB after filtration, at final concentration, and sum of absorbance spectra of 3CB and GAPDH*

Calculated value of *K* (according to the **Equation 6** in **Chapter II.2.5**) was (**143000±9010) M^{-1}** (slopes for three distinct experiments are in **Figure GAPDH.SI1**). This result differs tremendously from that obtained for complexation of the same sensitizer with a different protein (MtN13, [172]) which was 4 orders of magnitude lower. This phenomenon can be explained through two possibilities. One, there is something in the structure of GAPDH that makes 3CB bind stronger. This rather naïve view was disregarded, as there are no sensitizers known to bind that strongly. Thus, second option was opted to be the best explanation, namely formation of more than one complexes of 3CB with GAPDH.

For the reasons presented above, when we take into account amount of 3CB relatively to GAPDH it is safe to assume that multiple sensitizer molecules bind to the protein. This phenomenon has been explored by scientists and has even been conducted in case of 3CB with different protein [172]. There is a study in which sensitizer (porphyrin complex) binds to a protein in a cooperative manner [173]. That means that first binding of that complex enables further binding with greater ease (like a positive feedback loop). Therefore, an important question arises: would the activity of the enzyme drop significantly in the presence of 3CB? This aspect was researched further and is presented in **Chapter III.5.5**.

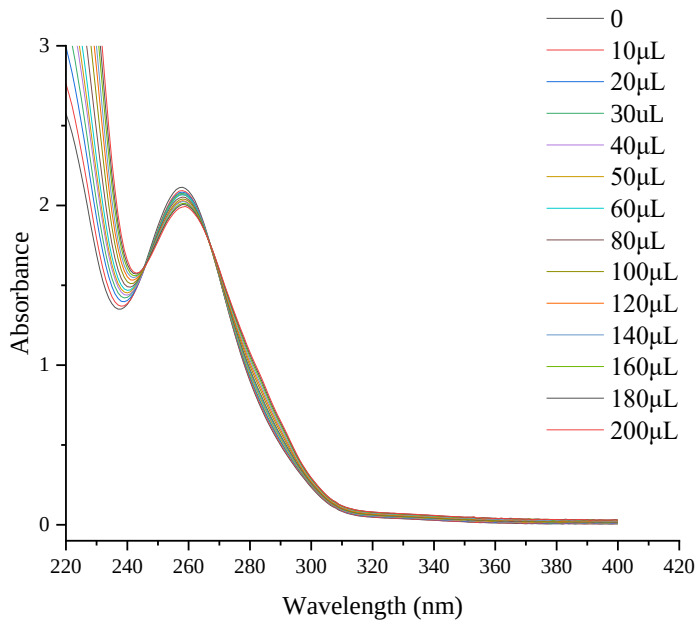

Figure GAPDH.2 *Absorbance spectra measured at different concentrations of GAPH in the solution*

III.5.2. SDS-PAGE gel electrophoresis

The structural consequence of ^{3}3CB* sensitized oxidation in anaerobic solution was studied by SDS-PAGE in both reducing and non-reducing environment. As shown in **Figure GAPDH.3**, irradiation in the presence of 3CB induced significant formation of cross-linked products (dimers and higher aggregates), with smearing of the band from GAPDH and its oligomers (as indicated in **Figure GAPDH.3** 10 and 20 minutes of irradiation), indicating changes in the protein monomer. This analysis provided information that either there are modifications that resemble scission products of GAPDH or charge of the proteins has been modified [174]. However, since their intensity rises in reducing environment, an argument is to be made that they are connected *via* sulfur-bridges, and their cleavage allows for detection of them. For that reason, in-gel digestion was performed to localize amino acids, that belong to the structure of those peptides.

Number	1	2	3	4	5	6	7	8	9	10
Time of irr.	0	1	5	10	20	0	1	5	10	20

Figure GAPDH.3 *SDS-PAGE profiles of the GAPDH subjected to ^{3}3CB*-mediated photo-oxidation subsequently developed using silver staining. Lanes **1-5** contain reduced samples, lanes **6-10** include non-reduced ones. Lane 1: GAPDH control sample, subsequent lanes represent samples with corresponding time of irradiation in minutes. The same principle applies to non-reduced samples. Molecular mass markers (SeeBluePlus2 pre-stained) are provided at the left-hand side of the gel*

III.5.3. Analysis of stable products

A study done on the photosensitized oxidation of ubiquitin by pterin revealed that under anaerobic conditions, formation of adducts between pterin and ubiquitin is oxygen independent, whereas formation of diTyr crosslinks or fragmentation of the protein occurs when oxygen is present in the mixture [175]. To align this hypothesis with findings from model compounds, an analysis of in-solution and in-gel digestion of samples chosen from SDS-PAGE electrophoresis was conducted, focusing on those oxidized to a sufficient extent (5-minute samples). It is necessary to see whether conclusions formed in ref .[175] can be extended to other photosensitizers. This claim is already supported by other experiments done with tiaprofenic acid with BSA [176].

Results presented in this work include changes to amino acids that are most prone to this type of oxidation (His, Tyr, Trp, highlighted in **Figure GAPDH.3** along with Phe), with changes manifesting as either protein cross-linking or sensitizer-protein adducts. The amount of amino acid loss with samples containing oxygen being definitely more oxidized than those in argon atmosphere [176]. Studies conducted on in-solution digested samples should allow for a detailed identification of modifications, which were included in the analyses of in-gel digested samples. These analyses, in turn, will provide information on peptides with a smaller mass than GAPDH and will also help identify the amino acids most susceptible to this type of oxidation.

MVKVGVNGFG RIGRLVTRAA FNSGKVDVVA INDPFIDLHY MVYMFQYDST
HGKFHGTVKA ENGKLVINGK AITIFQERDP ANIKWGDAGA EYVVESTGVF
TTMEKAGAHL KGGAKRVIIS APSADAPMFV MGVNHEKYDN SLKIVSNASC
TTNCLAPLAK VIHDHFGIVE GLMTTVHAIT ATQKTVDGPS GKLWRDGRGA
AQNIIPASTG AAKAVGKVIP ELNGKLTGMA FRVPTPNVSV VDLTCRLEKA
AKYDDIKKVV KQASEGPLKG ILGYTEDQVV SCDFNSATHS STFDAGAGIA
LNDHFVKLIS WYDNEFGYSN RVVDLMVHMA SKE

Figure GAPDH.3 *Sequence of GAPDH with highlighted aromatic amino acids.*

III.5.3.1. In solution digestion

Eluted peptides were detected on a timsTOF mass spectrometer (BRUKER) in positive ion mode using data-dependent acquisition. The identification of modified side chains was done by BYOS software with manual validation using the Bruker DataAnalysis software. Modifications were searched for on Cys (alkylation *m/z +57 Da*, fixed modifications), on His, Trp, Tyr, Phe, Met and Cys residues with variable modification like addition of 3CBH$^{\bullet}$ (*m/z +227.07* Da mass shift), addition of 3CBH with water loss on the source (*m/z +208.05 Da*), addition of either one oxygen atom (*m/z +15.99 Da*) or two atoms (*m/z +31.99 Da*), and the formation of a double bond (mass shift *m/z -2.01 Da*). The formation of dimers such as: His-His, Trp-Trp, Cys-Trp, Tyr-Tyr, Cys-Tyr, His-Trp, His-Tyr, and Tyr-Trp was also investigated. Chromatographic separation of the oxidized solution containing GAPDH with 3CB at 5 minutes of irradiation indicated the formation of products, with examples listed in **Table GAPDH.1**, which were analyzed by MS/MS. The fragmentation spectra of chosen products are presented in **Figure GAPDH.SI2-42**. Analyses consisted of finding corresponding a, b, and y fragments as shown in **Figure GAPDH.4,** with a representative spectrum from the MS/MS analysis.

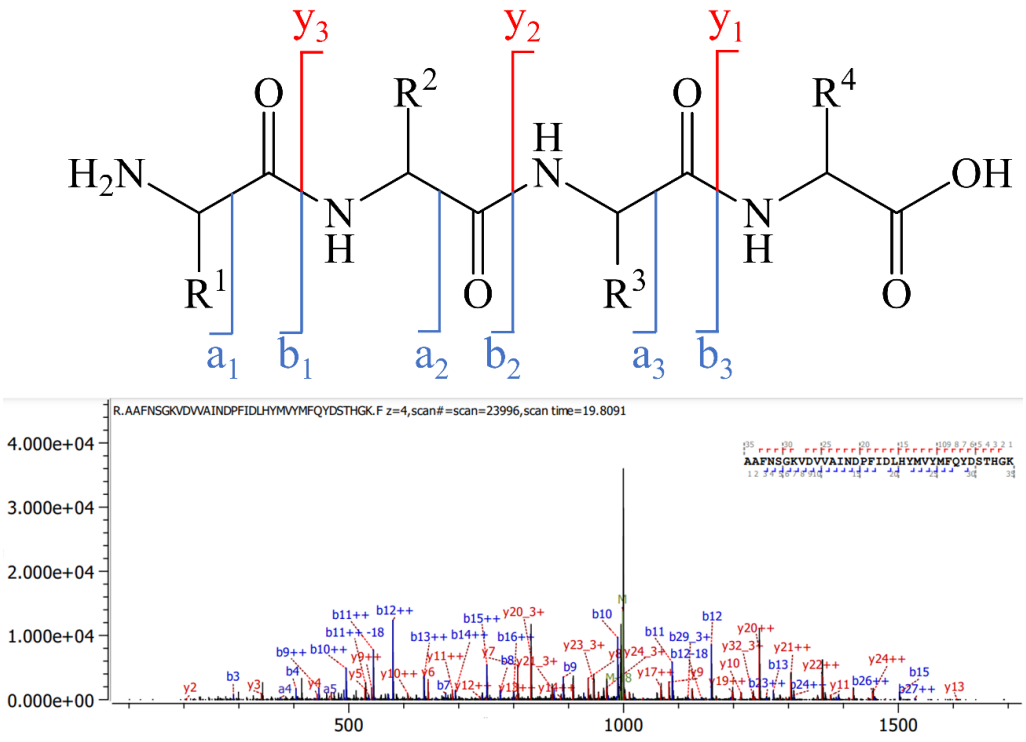

Figure GAPDH.4 *Fragmentation of peptide (above) with fragments a, b and y representing respective mass of ion fragment. Below, representative MS/MS spectrum of intact peptide form this analysis*

Table GAPDH.1 *Modified residues from the 5 min oxidized samples, after in-solution digestion*

No.	Sequence	Modifications	Score	Z	Observed *m/z*	Calculated *m/z*	Ppm error
P1	19-AAFNSGKVDVVAINDPFI DLHYMVYMFQYDSTHGK-53	H^{39} (-2H)	819.69	4	998.4750	998.4762	-1.21
P2	26-VDVVAI NDPFIDLHYMVYMFQYDSTHGK-53 185-TVDGPSGKLWRDGR-198	Y^{43}-W^{194}	425.65	5	972.4713	972.4737	-2.41
P3	26-VDVVAINDPFIDLHYMVYMF QYDSTHGKFHGTVK-59	F^{54} (3CBH)	977.41	5	843.4028	843.4033	-0.59
P4	26-VDVVAINDPFIDLHYMV YMFQYDSTHGKFHGTVK-59	H^{51} (3CBH)	929.40	5	843.4040	843.4033	0.85
P5	26-VDVVAINDPFIDLHYMV YMFQYDSTHGKFHGTVK-59	H^{55} (3CBH)	913.64	5	843.4037	843.4033	0.48
P6	26-VDVVA INDPFIDLHYMVYMFQYDSTHGK-53 193-LWRDGR-198	Y^{40}-W^{194}	817.60	5	824.1998	824.2005	-0.92
P7	26-VDVVAINDPFIDLH YMVYMFQYDSTHGK-53 193-LWRDGR-198	Y^{43}-W^{194}	644.53	5	824.1989	824.2005	-1.98
P8	26-VDVVAINDPFIDLH YMVYMFQYDSTHGK-53 253-YDDIKK-258	Y^{43}-Y^{253}	604.94	5	819.9951	819.9960	-1.04
P9	26-VDVVAINDPFIDLHYMV YMFQYDSTHGKFHGTVK-59	H^{55} (-2H)	912.56	5	797.7866	797.7876	-1.27
P10	26-VDVVAINDPFIDLH YMVYMFQYDSTHGK-53 193-LWR-195	Y^{40}-W^{194}	769.85	4	947.9615	947.9615	0.00
P11	26-VDVVAINDPFIDLH YMVYMFQYDSTHGK-53	F^{35} (3CBH)	1086.27	4	886.6614	886.6624	-1.06
P12	26-VDVVAINDPFIDLH YMVYMFQYDSTHGK-53	Y^{40} (3CBH)	909.22	4	886.6632	886.6624	0.97
P13	26-VDVVAINDPFIDLH YMVYMFQYDSTHGK-53	H^{39} (-2H)	972.85	4	829.6463	829.6427	4.30
P14	26-VDVVAINDPFIDLH YMVYMFQYDSTHGK-53	M^{41} (-2H)	869.17	3	1105.8542	1105.8545	-0.30
P15	71-AITIFQERDPANIK-84	F^{75} (3CBH)	405.87	3	614.6519	614.6526	-1.10
P16	116-RVIISAPSADAPMF VMGVNHEKYDNSLK-143	M^{131} (3CBH)	724.65	4	829.6557	829.6599	-5.04
P17	116-RVIISAPSADAPMF VMGVNHEKYDNSLK-143	M^{128} (3CBH)	520.95	4	829.6646	829.6599	5.72
P18	116-RVIISAPSADAPMF VMGVNHEKYDNSLK-143	M^{131} (3CBH) H^{135} (-2H)	951.64	4	829.1563	829.1560	0.45
P19	116-RVIISAPSAD APMFVMGVNHEK-137	M^{128} (3CBH)	717.17	3	865.7637	865.7627	1.19
P20	116-RVIISAPSAD APMFVMGVNHEK-137	M^{131} (3CBH)	699.06	3	865.7654	865.7627	3.14
P21	116-RVIISAPSAD APMFVMGVNHEK-137	M^{128} (-2H) F^{129} (3CBH)	897.53	4	649.0701	649.0699	0.27
P22	116-RVIISAPSAD APMFVMGVNHEK-137	M^{128} (3CBH)	965.15	4	645.0697	645.0712	-2.35

P23	117-VIISAPSADAPMF VMGVNHEKYDNSLK-143	M^{131} (3CBH)	780.17	4	790.6358	790.6346	1.49
P24	117-VIISAPSADAPMF VMGVNHEKYDNSLK-143	M^{128} (3CBH)	410.26	4	790.6318	790.6346	-3.56
P25	117-VIISAPSADAPMF VMGVNHEKYDNSLK-143	F^{129} (3CBH) M^{131} (-2H)	953.74	4	790.1309	790.1307	0.32
P26	117-VIISAPSADAPMF VMGVNHEK-137	F^{129} (3CBH) M^{131} (3CBH)	439.04	3	889.0855	889.0833	2.45
P27	117-VIISAPSADAPMF VMGVNHEK-137	F^{129} (3CBH)	755.97	3	813.7268	813.7290	-2.60
P28	117-VIISAPSADAPMF VMGVNHEK-137	M^{128} (3CBH)	623.35	3	813.7285	813.7290	-0.53
P29	117-VIISAPSADAPMF VMGVNHEK-137	M^{131} (3CBH)	571.56	3	813.7323	813.7290	3.15
P30	117-VIISAPSADAPMF VMGVNHEK-137	M^{128} (-2H) F^{129} (3CBH)	787.99	3	813.0592	813.0571	2.65
P31	117-VIISAPSADAPMF VMGVNHEK-137	F^{129} (3CBH) M^{131} (-2H)	641.96	3	813.0602	813.0571	3.81
P32	117-VIISAPSADAPMF VMGVNHEK-137	M^{129} (3CBH)	879.33	3	807.7308	807.7254	6.60
P33	117-VIISAPSADAPMF VMGVNHEK-137	M^{129} (-2H)	749.95	3	737.7036	737.7027	1.14
P34	144-IVSNASCT TNCLAPLAK-160	C^{150}-C^{154}	833.76	2	909.4517	909.4479	4.20
P35	161-VIHDHFGIVEGL MTTVHAITATQK-184	H^{177} (-2H)	1050.53	4	654.8453	654.8455	-0.42
P36	186-VDGPSG KLWRDGR-198	W^{194} (3CBH)	531.00	3	590.6237	590.6250	-2.24
P37	226-LTGMAFRVPT PNVSVVDLTCR-246	F^{231} (3CBH)	786.67	3	853.7671	853.7627	5.22
P38	226-LTGMAFRVPT PNVSVVDLTCR-246	M^{229} (-2H) F^{231} (3CBH)	641.83	3	853.0871	853.0908	-4.33
P39	233-VPTPNVSV VDLTCRLEK-249	C^{245} (3CBH)	514.52	3	718.3680	718.3698	-2.44
P40	322-VVDLM VHMASKE-333	H^{328} (3CBH)	511.25	2	792.8780	792.8755	3.21
P41	322-VVDLM VHMASKE-333	M^{326} (3CBH)	439.24	2	792.8759	792.8755	0.60

Analyses provided information on the modification of sample containing GAPDH and 3CB after 5 minutes of irradiation in argon atmosphere. Even though the formation of oxygen on methionines was detected, it has been disregarded from further analysis due to the fact that experiments were conducted in anaerobic conditions, and methionine is known to be readily oxidized either during sample storage [177] or during ESI [178]. Another dubious modification was addition of 3CBH to Phe, as every peptide that contained it had other reactive amino acid also. **P3** from **Table GAPDH.1** had y fragments that share His (**Figure GAPDH.SI4**), **P21** shared it with Met (**Figure GAPDH.SI22**), while **P26**, **P27**, **P30**, and **P31** once again shared it with His (**Figure GAPDH.SI27-SI28 and SI31-32** respectively). The same cannot be said about **P11**, **P15**, **P25**, **P37**, and **P38,** which suggest that this modification may have actually occurred.

The remining modifications included the addition of 3CBH, either with or without the loss of water (presumably in source), on all other aromatic and sulfur-containing amino acids. Interestingly, the modification on sulfur in **P39** (**Figure GAPDH.SI40**) was also alkylated. That potentially indicates the formation of C_β radical on Cys residue with subsequent recombination with 3CBH$^\bullet$. This novel product deserves some further study with complementary research on model compounds. The loss of hydrogen from amino acids was detected in Trp, His, and Met, corresponding to the same types of modifications that occur in model compounds. The formation of dimers was detected only for Cys (intermolecular), Trp or Tyr. However, definitive confirmation of their existence would require more sophisticated methods such as O^{18} labelling. Nevertheless, no intramolecular Cys-Cys was detected, which is the first clue, that modifications to lower bands (**Figure GAPDH.3**) could be caused by some different interaction. Presumably, the formation of intramolecular Cys-Cys resulted in changes in protein conformation, which in turn caused it to behave differently during electrophoresis.

It is best to keep in mind that even though those products exist inside the protein and resemble those in model compounds, mechanistically speaking, there is a possibility that they might not have risen in the same way as those in model compounds have. The complex environment of radicals that may arise during photosensitized oxidation of proteins is still being researched. These modifications prove that those amino acids are indeed the most vulnerable ones in this process, and an argument can be made that they may have emerged from the same mechanisms. This analysis was conducted to qualitatively answer the first question that was brought at the very beginning of **Chapter 3**, namely *"Do modifications that occur in model compounds are also present in oxidized protein?"*. Short answer is yes; however, another method of sample treatment was implemented to further substantiate that claim.

III.5.3.2. In-gel digestion

Respective bands from reduced sample of GAPDH protein from SDS-PAGE silver-stained gel has been cut and subjected to further preparation as described in **Chapter II.2.7**. Keeping in mind the results from previous analysis, samples were treated with the same method of analysis. Eluted peptides were detected on a timsTOF mass spectrometer (BRUKER) in positive ion mode using data-dependent acquisition. The identification of modified side chains was done using BYOS software with manual

validation using the Bruker DataAnalysis software. The same modifications (with exclusion of Phe and dimers) has been presented in **Table GAPDH.2**. Repeatedly, addition of 3CBH has been detected in all amino acids of interest with loss of hydrogen visible on His, Met, and Trp. Extent of those modifications has been investigated further in **Chapters III.5.3.3 and III.5.4**. All bands had high coverage of protein sequence, meaning that could mean structural modifications, rather than scission of GAPDH. However, MALDI of intact protein would be required to be performed to provide direct evidence of this phenomenon. All further analyses and calculations were performed for the most abundant gel fragment (**Figure GAPDH.3**) as it had the most reproducible results.

Table GAPDH.2 *Modified residues from the 5 min oxidized samples from GAPDH the most abundant band*

No.	Modified Sequence	Modifications
M1	AAKYDDIK	Y^{253} (3CBH)
M2	DPANIKWGDAGAEYVVESTGVFTTMEK	W^{85} (O) M^{103} (O)
M3	FHGTVKAENGK	H^{55} (3CBH)
M4	LTGMAFR	M^{229} (3CBH)
M5	RVIISAPSADAPMFVMGVNHEK	M^{128} (3CBH)
M6	TVDGPSGKLWR	W^{194} (-2H)
M7	TVDGPSGKLWRDGR	W^{194} (3CBH)
M8	VIHDHFGIVEGLMTTVHAITATQK	M^{173} (3CBH)
M9	VIISAPSADAPMFVMGVNHEK	M^{131} (3CBH)
M10	VIISAPSADAPMFVMGVNHEK	M^{128} (O) M^{131} (O) H^{135} (3CBH)
M11	VIISAPSADAPMFVMGVNHEK	M^{128} (O) M^{131} (3CBH)
M12	VIISAPSADAPMFVMGVNHEK	M^{128} (3CBH) M^{131} (O)
M13	VIISAPSADAPMFVMGVNHEK	M^{128} (3CBH) M^{131} (O) H^{135} (3CBH)
M14	VIISAPSADAPMFVMGVNHEK	M^{128} (3CBH)
M15	VIISAPSADAPMFVMGVNHEK	M^{128} (3CBH) M^{131} (O)
M16	VIISAPSADAPMFVMGVNHEK	M^{128} (3CBH) M^{131} (3CBH)
M17	WGDAGAEYVVESTGVFTTMEK	M^{103} (3CBH)
M18	WGDAGAEYVVESTGVFTTMEK	W^{85} (O) M^{103} (3CBH)

III.5.3.3. Occupancy

Following the analysis presented in **Chapter III.5.3.2,** the relative abundance of a particular mass shift has been calculated as described in **Chapter II.2.7** and presented in **Table GAPDH.3** below.

Table GAPDH.3 *Results of occupancy calculations for the most abundant band in silver-stained gel of GAPDH sample irradiated at 5 min*

	[-2.0157]	**[15.9949]**	**[208.0524]**	**[226.0630]**
H55	----------	----------	----------	97.9±0.8 %
W85	----------	11.6±4.5 %	----------	----------
M103	----------	24.1±7.2 %	3.4±1.9 %	5.5±4.2 %
M128	----------	35.4±11.6 %	1.5±0.8 %	2.1±0.9 %
M131	----------	43.5±7.1 %	0.7±0.6 %	3.5±1.4 %
H135	----------	----------	1.3±0.5 %	0.6±0.2 %
M173	----------	----------	----------	0.3±0.2 %
W194	8.3±4.5 %	----------	----------	7.3±2.3 %
M229	----------	----------	----------	0.2±0.1 %
Y253	----------	----------	----------	42.7±5.5 %

From that data it can be deduced with certainty that first amino acids that are modified during anaerobic photosensitized oxidation are solution accessible ones (**Figure GAPDH.5**). As mentioned before, modifications that are present resemble strongly those present in model compounds. Once again, some amount of oxygenation was present, nevertheless it can be seen here that without the doubt it includes mostly Met which further substantiates the hypothesis that they were oxygenated during sample preparation. Trp follows the *m/z -2Da* modification that was also present in model compounds. Therefore, argument that redox potentials of its radicals and respective reduced states could be of interest to future research on protein modifications. Tyr amino acid backbones were not reduced, however, as established earlier they were prone to creating covalent product with 3CB and so were other active amino acids. Also worth mentioning is the fact that active site of GAPDH was left intact, however whether modifications to other amino acids may result in changes of activity was explored in **Chapter III.5.5**.

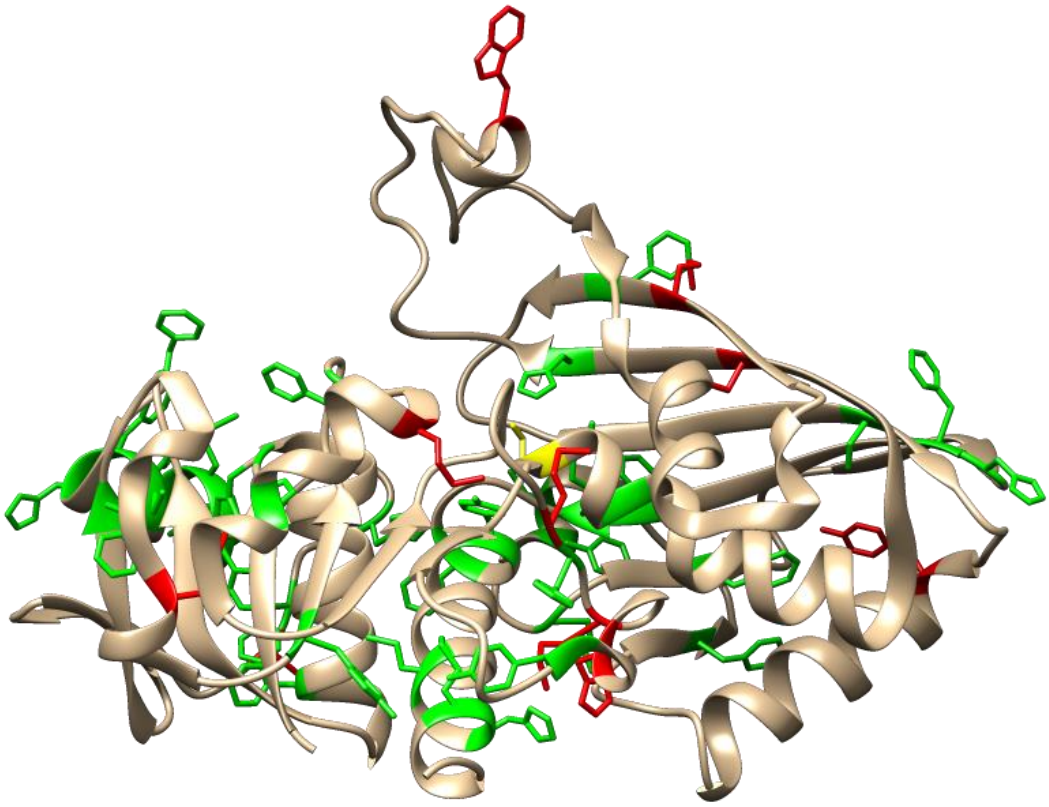

Figure GAPDH.5 *Modified residues (represented in red) from the 5 min oxidized samples, mapped on the three-dimensional structure of GAPDH based on occupancy calculations. Cys from active site is represented in yellow while intact amino acids are represented in green*

III.5.4. Amino Acid Analysis and Ellman's assay

To investigate the extent of modifications of amino acids present in the GAPDH, amino acid analysis with Ellman's assay was performed. Variations in the concentration of Trp did not allow for statistically significant analysis (ANOVA $p>0.05$, **Figure GAPDH.8**). There are three potential reasons that could explain this phenomenon. Trp could have been oxidized during sample hydrolysis. If that was the case, the same could be applied to the results of this paper [146]. Since authors reported both, good protection of Trp and good recovery of it, then it is safe to assume that there was some sort of interaction with 3CB. For the other amino acids, four repetitions were done for amino acid analysis and six for the Ellman's assay for solution accessible thiols. After ANOVA analysis with a post-hoc Dunnet test, it was revealed that there were significant modifications on sulfur containing amino acids (**Figure GAPDH.6**), Tyr (**Figure GAPDH.7**) and other aromatic amino acids (**Figure GAPDH.8**).

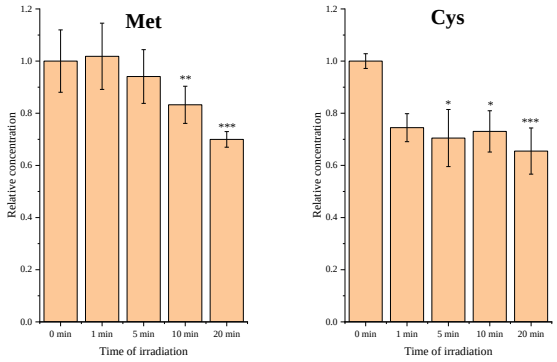

Figure.GAPDH.6 *Relative concentrations of Met as estimated in Amino Acid Analysis assay, and Cys as estimated in Ellmans Assay (* p<0.05; ** p<0.01; *** p<0.005)*

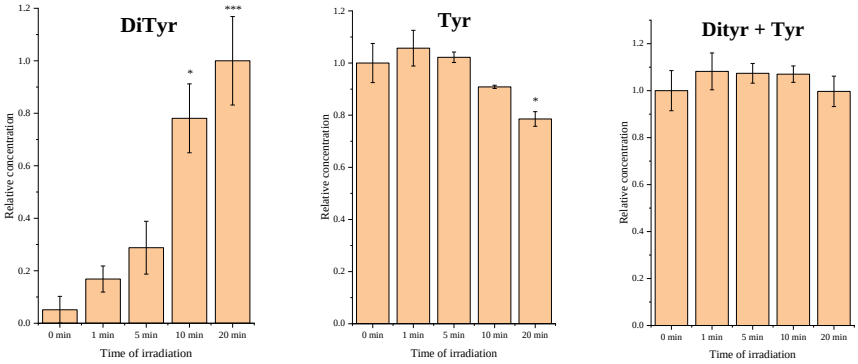

Figure.GAPDH.7 *Relative concentrations of diTyr, Tyr, and sum of both of them as estimated in Amino Acid Analysis assay (* p<0.05; *** p<0.005)*

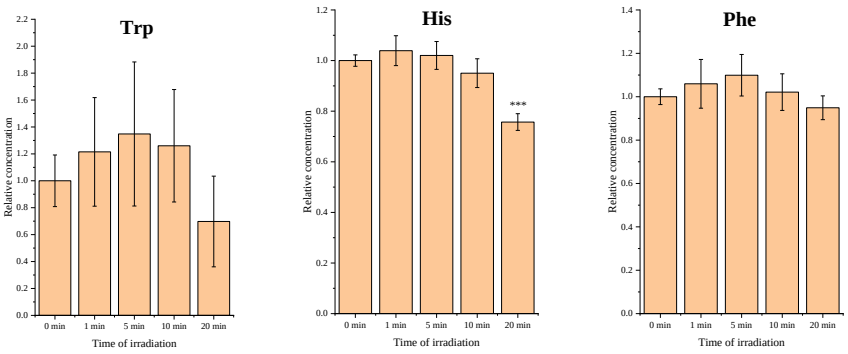

Figure.GAPDH.8 *Relative concentrations of Trp, His, and Phe as estimated in Amino Acid Analysis assay (*** p<0.005)*

A visible trend emerges from the results presented in **Figures GAPDH.6-8**. The first amino acids that indicated modifications are the sulfur containing ones. It is uncertain whether these modifications resulted from oxidation during anaerobic photo-oxidation. Resulting decrease in concentration of Met suggests that it is the first to be oxidized in this process. There are also noticeable differences for solution-accessible Cys, which, when combined with the occupancy results, would further explain that most of the modifications occur on the surface of GAPDH. Significant modifications to the investigated amino acids (except Trp and Phe) began to occur at 10 minutes of irradiation. Therefore, the main hypothesis is that relevant differences in activity should occur at that time. Insignificancy of Phe oxidation supports the rationality of exclusion of Phe from in-gel digestion analyses, as it could potentially result in false positives. Its main role seems to be creation of ground state complex with the protein as demonstrated in ref. [172]. The detection of diTyr, further proves its existence. Interestingly, when concentration of Tyr had been added to concentration of diTyr detected, with consequent normalization to the concentration of blank sample, it resulted in nearly 100% consistency across all samples. Consequently, it can be deduced that this is the main form of damage cause by anaerobic photosensitized oxidation of Tyr and matches perfectly results from model compounds.

III.5.5. Activity

Following the procedure for the GAPDH activity test described in **Chapter II.2.10**, measurements were taken for blank sample, blank sample with 3CB, and samples after varying irradiation times (1-20 min), with four replicates each. ANOVA analysis with post-hoc Dunnet test indicated that the samples irradiated for 10 and 20 minutes showed a statistically significant loss of activity at $p<0.005$.

Firstly, it was important to deterine whether 3CB (since it exhibits potent complex formation) influences the activity of GAPDH without irradiation. As shown in **Figure GAPDH.9**, the formation of this complex did not diminish the enzymatic activity of GAPDH. No changes in activity were observed after one minute of irradiation. Some difference in enzyme kinetics were seen at five minutes (**Figure.GAPDH.9 a**), but there was no relevant difference in the value of activity. This observation can be explained by qualitative and quantitative analysis of protein oxidation at five min. Qualitatively, solution-accessible amino acids were modified, and this was confirmed by quantitative analysis of Cys.

Therefore, amino acids that have been oxidized do not impediment activity in any relevant form. A different pattern was observed at ten- and twenty-minutes of irradiation, with the longest irradiation time resulting in a lack of enzymatic activity. Not only did the activity drop at these irradiation times, but also the relative concentration of non-modified amino acids decreased.

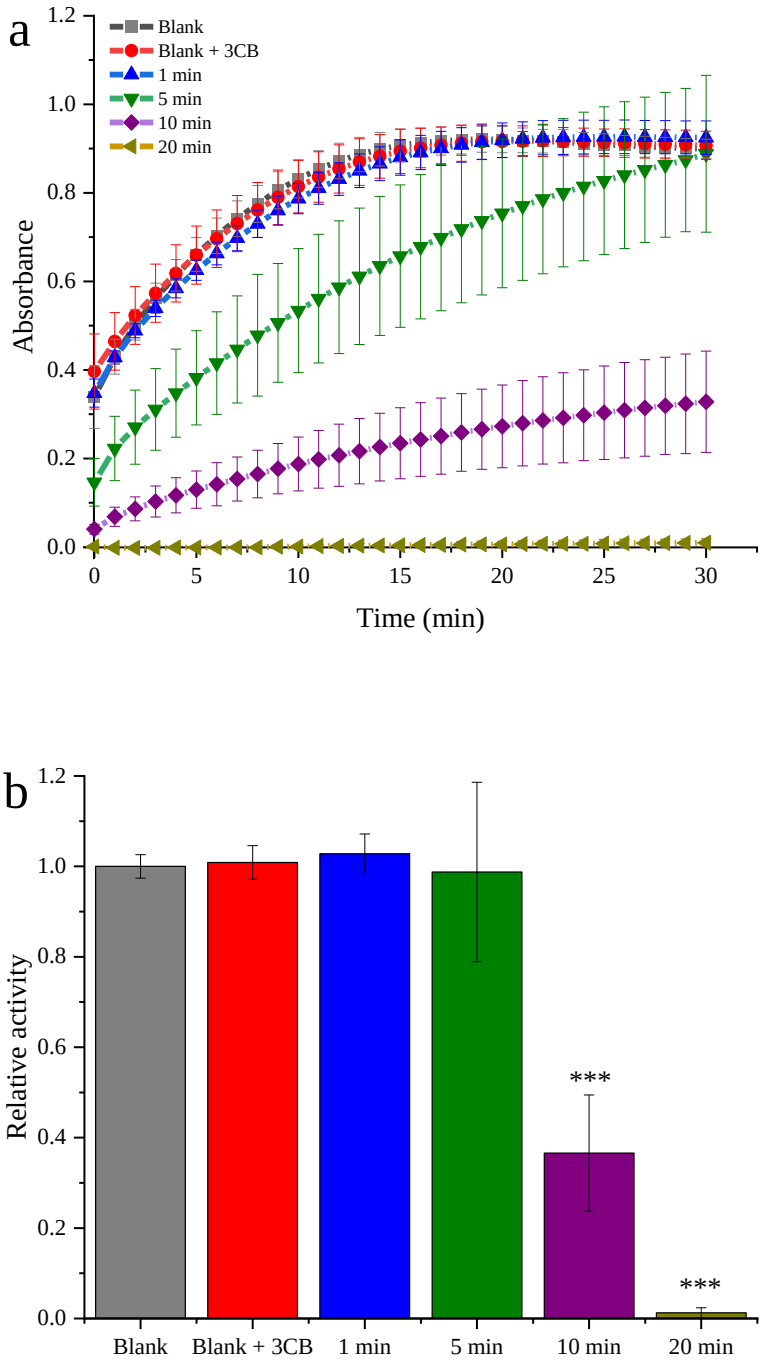

Figure GAPDH.9 ***(a)*** *progress curve of enzyme reaction as measured during activity of GAPDH,* ***(b)*** *relative activity of GAPDH samples (*** $p<0.005$)*

IV. Conclusions

The doctoral dissertation presents the characterization of model compounds in terms of transient species and final products of the photosensitized anaerobic oxidation of aromatic amino acids. Following sections provide brief summary of experiments on model compounds and answer to the question present in the Aim of the work and at the beginning of GAPDH chapter.

TYROSINE (Tyr):

Experimental data presented two notable observations. Firstly, the presence of more blocked groups on Tyr correlates with a higher number of diTyr products, potentially due to the increase in hydrophobicity of Tyr molecules. Under consistent experimental conditions, photo-oxidized Tyr samples produced two diTyr compounds: 3,3'-diTyr and 3,O'-diTyr. The same products, along with an additional diTyr compound, were detected in N-Ac-Tyr and TyrOEt samples, aligning with previous research (ref. [82]). Notably, the N-Ac-Tyr-OEt solution yielded ten different diTyr products post-irradiation. The Tyr-Val products were similar to those of N-Ac-Tyr, except for a *m/z - 2Da* loss in dimers with unclear mechanism of formation (but it counts rather as a secondary product).

Secondly, a reverse trend was observed in the occurrence of Tyr-3CBH products across irradiated Tyr derivatives at pH 7. The highest Tyr-3CBH product count was found in the Tyr sample, with minimal presence in the Tyr-OEt sample and none in the others. This suggests that the protonation of the amine group may facilitate Tyr-3CBH product formation, possibly through a proton transfer from the protonated amine group to the sensitizer within the [$3CB^{\bullet-}$•••$TyrOH^{\bullet+}$] complex, followed by rapid Tyr-3CBH creation (see **Figure TYR.7**) Alternatively, steric effects within the [^{3}3CB*•••TyrOH] encounter complex might hinder Tyr-3CBH formation, a phenomenon observed in the 3CB-sensitized oxidation of sulfur-containing amino acids like methionine and S-methyl-cysteine.

TRYPTOPHAN (Trp):

Interestingly, the formation of $3CB^{\bullet-}$ in the presence of blocked amine groups suggests that the quenching mechanism (see **Figure TRP.7**) involves ET and PCET. The presence of $TrpNH^{\bullet+}$ in peptides only, indicates a more complex reaction pathway, potentially involving competing reactions (such as the proton transfer from amine group) and the influence of neighboring amino acids such as Tyr. Stable product analysis through HPLC-MS revealed several peaks corresponding to Trp-3CBH adducts, diTrp, and Trp-2Da. These products indicate the presence of radical recombination and dimerization reactions, where the second seems to be the main process, that is affected by the neighboring groups. The more blocked Trp is, the number of di-Trp rises. Notably, covalent adduct formation was observed only in the Ala-Trp-Ala peptide suggesting a possible influence of peptide length on product formation.

Overall, the study provides insights into the anaerobic photosensitized oxidation of Trp and its derivatives, highlighting the role of structural factors and the involvement of amine groups in the reaction mechanisms. The results underscore the complex interplay between different reaction pathways and the potential for forming various transient and stable products, offering a deeper understanding of Trp's photochemical behavior and its interactions with sensitizer.

HISTIDINE (His):

When the α-amino group of His is blocked, either by acetylation or incorporation into a peptide, the sensitized photo-oxidation yielded mostly dimers as stable products. Although covalent His dimers have been reported recently [66], the effects of anaerobic photosensitized oxidation on stable products have not been previously described. The yield of such dimers is likely maximized in the absence of O_2, minimizing alternative reaction channels. These species most likely arise from the dimerization of two $HisN^{\bullet}$ radicals, with an alternative fate being disproportionation, leading to one product with a double bond and one regenerated parent molecule. Despite the low redox potential of $HisN^{\bullet}$, these products were not detected in high amounts, possibly due to further reactions of the initial products. The formation of multiple forms of His-3CBH and His-His-like products is attributed to the delocalization of electron density across the $HisN^{\bullet}$ structure.

Interestingly, His-His dimers were not detected for His and its derivatives with free amine group. The formation of unreported in the literature product, Im-CH_2-3CBH, for these compounds was observed and it could be attributed to second channel of ^{3}3CB* quenching, i.e. to energy transfer. The energy transfer from ^{3}3CB* to His, forming ^{3}His*, may result in C-C bond photodissociation, yielding Im-$CH_2^\bullet$ and Gly$^\bullet$ radicals (for mechanism see **Figure HIS.9**). This is consistent with the product analyses and the detection of Im-CH_2-3CBH in model compounds with an unblocked amine group, and Gly-Phe from His-Phe. The reactions of His derivatives indicate that a free α-amino group facilitates the energy transfer, while its derivatization prevents this channel, leading to the near-exclusive formation of dimers (His-His) and His-3CBH adduct. It is postulated that the free amino group promotes energy transfer *via* interaction with the imidazole ring, possibly through an intra-molecular hydrogen bond, lowering the excited triplet state energy. Suppression of the energy transfer pathway increases the yields of HisN$^\bullet$-derived products.

PHENYLALANINE (Phe):

The quenching rate constants showed a trend where blocking the carboxylic group resulted in higher k_q values. This phenomenon appears prevalent across all derivatives, suggesting that the negative charge near the chromophoric side-chain slows the process. The determined k_q values are generally two orders of magnitude lower than those of other aromatic amino acids. This suggests a hydrogen atom transfer (HAT) process, as expected in the anoxic photo-oxidation of Phe. The resulting $\Phi_{3CBH\bullet}$ values showed no significant differences among the different blocked amino acids examined, except for Phe-OEt and N-Ac-Phe-OEt. The average value of $\Phi_{3CBH\bullet}$ was 0.35±0.15, indicating lower efficiency in generating 3CBH$^\bullet$ or additional process, namely energy transfer.

UPLC-MS analysis of 3CB-sensitized photo-oxidation of Phe revealed multiple stable products after irradiation. MS/MS spectra of Phe and its derivatives were categorized into several groups. The first identified group included covalent adducts of the sensitizer to the Phe side-chain, an alternative subcategory included secondary products of cyclization of this adduct. Second group consisted of Phe dimers, and lastly addition of benzyl to either Phe or 3CB was detected. The analysis of stable products proposed a mechanism of sensitized photo-oxidation (see **Figure PHE.6**) in which the ^{3}3CB* can be quenched by Phe. The relatively small k_q values and identified product structures indicate that irradiation in the presence of a sensitizer and absence of oxygen starts with hydrogen atom abstraction

from C_β, yielding 3CBH$^\bullet$ and Phe$^\bullet$ radicals, with competing energy transfer, as indicated by the formation of Bz$^\bullet$ and its recombination with 3CBH$^\bullet$ or Phe$^\bullet$. Blocking the amine group affects this process, supporting the claim that a free α-amino group facilitates energy transfer, while derivatization prevents this, leading to predominant formation of Phe$^\bullet$ recombination products.

GAPDH:

The research conducted as part of the doctoral dissertation indicates that photosensitized oxidation of aromatic amino acids under anaerobic conditions primarily leads to the formation of covalent adducts of the sensitizer and amino acid or dimers. This was necessary not only to better understand fundamental processes that occur in the photosensitized oxidation of protein, but also to correctly assign modifications that were present in the protein. In this thesis, GAPDH was chosen as it is a well-researched one with well-defined characteristics. Ground state complexation was proven to occur with multiple molecules of sensitizer bound to the protein structure. SDS-PAGE electrophoresis followed by silver staining provided information on formation of dimers and structurally different fragments of GAPDH. In solution digested samples of the irradiation time chosen from previous experiments proved that all modifications that were present in model compounds occur in the protein, whereas in-gel digested samples of the most abundant band have shown that amino acids that are the most susceptible to anaerobic photosensitized oxidation of GAPDH, are those that are solution accessible. Even though, His and Tyr manifested themselves as the most prominent targets for this type of oxidation (when it comes to aromatic amino acids), lower times of irradiation did not hinder the activity of the enzyme.

To summarize the doctoral dissertation the answers for questions from the Aim of the work and GAPDH chapter are presented below:

Does the presence of different neighboring groups influence transient species formed during the oxidation of aromatic side chains (Tyr, Trp, His and Phe)?

The detected transients were qualitatively similar for all detected compounds, however their yields varied when different groups were blocked.

What effect does the surroundings of an amino acids residue have on stable products?

Amino group facilitates energy transfer between ^{3}3CB* and either His or Phe procuring products of photodissociation of those amino acids. Blocking that group enhances formation of covalent dimers in all amino acids, where blocking carboxylic groups enhances the number of different dimers in Trp and Tyr.

Is there any specific product for 3CB-sensitized photo-oxidation?

Specific products would be a covalent adduct of 3CB to the respective amino acid, formation of double bond in His and Trp, and formation of Im-CH_2-3CBH or Bz-3CBH (as a result of the energy transfer). Formation of covalent dimers were expected to be detected based on the literature.

Do modifications that occur in model compounds are also present in the oxidized protein?

The analyses provided detailed information on the modifications of samples containing GAPDH and 3CB after five minutes of irradiation in an argon atmosphere. Despite detecting oxygen formation on methionines, this was disregarded due to the anaerobic conditions of the experiment and methionine's known propensity for oxidation during sample storage or ESI. Modifications of Phe has not been detected in sufficient manner. Other products matched model compounds. The alteration to Cys side-chain involved alkylation and addition of 3CBH, indicating the formation of a C_β radical on the Cys residue with subsequent recombination with 3CBH$^{\bullet}$. This product deserves further study with complementary research on model compounds. Dimerization in this researched occurred exclusively in Trp, Tyr or Cys. It is crucial to note that while these products exist within the protein and resemble those in model compounds, the exact mechanisms may differ due to the complex radical environment during photosensitized oxidation of proteins. The modifications indicate the vulnerability of these amino acids, supporting the argument that they might arise from similar mechanisms. This analysis aimed to qualitatively answer whether modifications occurring in model compounds are also present in oxidized proteins, and the answer is affirmative.

Which amino acid is modified the most in the sample irradiated at chosen time?

Based on the amino acid analysis and Ellman's assay it seems like modifications follow the trend of Cys>Met>His>Tyr>>>Phe with insufficient evidence against Trp. Results provided in this thesis suggest that from all of the aromatic amino acids, His is the most prominent target for anaerobic photo-oxidation of GAPDH.

What is the extent of modifications to amino acids?

Based on the data, it can be conclusively deduced that the first amino acids modified during anaerobic photosensitized oxidation are those that are solution accessible. As previously mentioned, the observed modifications closely resemble those seen in model compounds. Trp exhibits the -2Da modification, similar to the model compounds, suggesting that the redox potentials of its radicals and respective reduced states could be of interest for future research on protein modifications. Sulfur-containing amino acids are the first to be modified. Whether these modifications are due to the oxidation during sample handling or anaerobic photo-oxidation is unclear. However, assuming the modifications from occupancy to be accurate, it makes sense that Met is the first to be modified. DiTyr is the main form of damage caused by anaerobic photosensitized oxidation of Tyr, aligning perfectly with results from model compounds.

Does the modification of GAPDH by 3CB induce changes in the activity?

As the extent of those modification relies on solution accessible amino acids, this trend shows that lower times of irradiation (< 5 min) do not change the activity of GAPDH. Increasing irradiation time causes larger damage of protein, including active-site, that yields decrease in activity.

Perspectives:

Results presented in this thesis provide copious amounts of opportunities to enhance knowledge in this field. Discovery of variety of dimers that may occur during oxidative stress require further investigation into their occurrence *in vivo*. Therefore, necessary experiments need to be conducted. However, it is crucial to reevaluate methods such as detection of diTyr with antibodies and fluorescence assays that detect dimers.

It is posed that different isomers of diTyr may not react the same way with the antibody. Since it has been proven that existence of different forms of diTyr in products is dependent on the structure of model compound, it is assumed that restrictive environment of the protein may result in different ratios of those products formed. This combined with structural differences in isomers require further investigation into antigen method.

Different dimers of Tyr, Trp, and His may have fluorescence properties that intertwine with each other. Which is why necessity arises for reevaluation of detection of dimers based on their fluorescent characteristics.

This work proved that there is a scientific gap in transients, especially when it comes to His photo-oxidation. Necessary experiments require definitive identification of transient spectra, especially those of Im-$CH_2^{\bullet}$ and variety of $HisN^{\bullet}$ that may be either protonated or deprotonated.

Lastly, information provided in this research shows that activity of GAPDH is not hindered by changes to solution accessible amino acid side-chains. Effort should be made to check the extent of modifications that result in structural and conformational changes to GAPDH, but still allow it to retain its enzymatic properties.

V. References

[1] D. V Bent, E. Hayon, Excited state chemistry of aromatic amino acids and related peptides. II. Phenylalanine, J Am Chem Soc. 97 (1975) 2606–2612. https://doi.org/10.1021/ja00843a003.

[2] P.E. Hockberger, A History of Ultraviolet Photobiology for Humans, Animals and Microorganisms ¶, Photochem Photobiol. 76 (2002) 561–579. https://doi.org/10.1562/0031.

[3] A.C. Kübler, Photodynamic therapy, Medical Laser Application. 20 (2005) 37–45. https://doi.org/10.1016/j.mla.2005.02.001.

[4] L. Weil, W.G. Gordon, A.R. Buchert, Photoöxidation of amino acids in the presence of methylene blue, Arch Biochem Biophys. 33 (1951) 90–109. https://doi.org/https://doi.org/10.1016/0003-9861(51)90084-7.

[5] G.E. Neurohr, A. Amon, Relevance and Regulation of Cell Density, Trends Cell Biol. 30 (2020) 213–225. https://doi.org/10.1016/j.tcb.2019.12.006.

[6] E.R. Stadtman, Protein Oxidation and Aging, Free Radical Research . 40 (2006) 1250–1256. https://doi.org/https://doi.org/10.1080/10715760600918142.

[7] B.S. Berlett, E.R. Stadtman, Protein oxidation in aging, disease, and oxidative stress, Journal of Biological Chemistry. 272 (1997) 20313–20316. https://doi.org/10.1074/jbc.272.33.20313.

[8] J.S. Torday, Homeostasis as the mechanism of evolution, Biology (Basel). 4 (2015) 573–590. https://doi.org/10.3390/biology4030573.

[9] P.D. Ray, B.W. Huang, Y. Tsuji, Reactive oxygen species (ROS) homeostasis and redox regulation in cellular signaling, Cell Signal. 24 (2012) 981–990. https://doi.org/10.1016/j.cellsig.2012.01.008.

[10] X.-W. Zhang, A. Oleinick, H. Jiang, Q.-L. Liao, Q.-F. Qiu, I. Svir, Y.-L. Liu, C. Amatore, W.-H. Huang, al Electrochemical, Electrochemical Monitoring of ROS/RNS Homeostasis Within Individual Phagolysosomes Inside Single Macrophages, Angewandte Chemie International Edition. 58 (2019). https://doi.org/10.1002/anie.201902734ï.

[11] A.I. Yemets, Y. V. Karpets, Y.E. Kolupaev, Y.B. Blume, Emerging technologies for enhancing ROS/RNS homeostasis, in: Reactive Oxygen, Nitrogen and Sulfur Species in Plants: Production, Metabolism, Signaling and Defense Mechanisms, Taylor and Francis, 2019: pp. 873–922. https://doi.org/10.1002/9781119468677.ch39.

[12] T. Maliński, Nitric Oxide and Nitroxidative Stress in Alzheimer's Disease, Journal of Alzheimer's Disease. 11 (2007) 207–218. https://doi.org/10.3233/jad-2007-11208.

[13] S. Kim, E. Kim, M. Park, S. Ho Kim, B.-G. Kim, W. Bhashini Wijesinghe, Y.-G. Eom, G. Yoon, C. Lee, H. Jeong, C. Un Kim, K. Myung, J.-M. Choi, S. Kyu Min, H. Kwon, D. Min, Hidden route of protein damage through confined 2 oxygen gas 3 4, (n.d.). https://doi.org/10.1101/2024.01.03.574110.

[14] M.J. Davies, R.J.W. Truscott, Photo-oxidation of proteins and its role in cataractogenesis, J Photochem Photobiol B. 63 (2001) 114–125. https://doi.org/10.1016/s1011-1344(01)00208-1.

[15] M.J. Davies, Singlet oxygen-mediated damage to proteins and its consequences, Biochem Biophys Res Commun. 305 (2003) 761–770. https://doi.org/10.1016/S0006-291X(03)00817-9.

[16] G. Pizzino, N. Irrera, M. Cucinotta, G. Pallio, F. Mannino, V. Arcoraci, F. Squadrito, D. Altavilla, A. Bitto, Oxidative Stress: Harms and Benefits for Human Health, Oxid Med Cell Longev. 2017 (2017). https://doi.org/10.1155/2017/8416763.

[17] D.I. Pattison, A.S. Rahmanto, M.J. Davies, Photo-oxidation of proteins, Photochemical and Photobiological Sciences. 11 (2012) 38–53. https://doi.org/10.1039/c1pp05164d.

[18] E.R. Stadtman, B.S. Berlett, Reactive oxygen-mediated protein oxidation in aging and disease, Drug Metab Rev. 30 (1998) 225–243. https://doi.org/10.3109/03602539808996310.

[19] M.J. Davies, Oxidative Damage to Proteins, in: A. Studer (Ed.), Encyclopedia of Radicals in Chemistry, Biology and Materials, John Wiley & Sons, Ltd, 2012. https://doi.org/10.1002/9781119953678.rad045.

[20] J.D. Spikes, Photosensitization, in: K.C. Smith (Ed.), The Science of Photobiology, Second, Springer New York, NY, Stanford, California, 1989: pp. 79–110. https://doi.org/10.1007/978-1-4615-8061-4.

[21] M.J. Davies, Protein oxidation and peroxidation, Biochemical Journal. 473 (2016) 805–825. https://doi.org/10.1042/BJ20151227.

[22] S.E. Braslavsky, Glossary of terms used in photochemistry 3rd edition: (IUPAC Recommendations 2006), Pure and Applied Chemistry. 79 (2007) 293–465. https://doi.org/10.1351/pac200779030293.

[23] M.S. Baptista, J. Cadet, P. Di Mascio, A.A. Ghogare, A. Greer, M.R. Hamblin, C. Lorente, S.C. Nunez, M.S. Ribeiro, A.H. Thomas, M. Vignoni, T.M. Yoshimura, Type I and Type II Photosensitized Oxidation Reactions: Guidelines and Mechanistic Pathways, Photochem Photobiol. 93 (2017) 912–919. https://doi.org/10.1111/php.12716.

[24] M.R. Hamblin, H. Abrahamse, Oxygen-independent antimicrobial photoinactivation: Type III photochemical mechanism?, Antibiotics. 9 (2020). https://doi.org/10.3390/antibiotics9020053.

[25] J. Zhao, W. Wu, J. Sun, S. Guo, Triplet photosensitizers: From molecular design to applications, Chem Soc Rev. 42 (2013) 5323–5351. https://doi.org/10.1039/c3cs35531d.

[26] T. Pedzinski, K. Bobrowski, M. Ignasiak, G. Kciuk, G.L. Hug, A. Lewandowska-Andralojc, B. Marciniak, 3-Carboxybenzophenone (3-CB) as an efficient sensitizer in the photooxidation of methionyl-leucine in aqueous solutions: Spectral, kinetic and acid-base properties of 3-CB derived transients, J Photochem Photobiol A Chem. 287 (2014) 1–7. https://doi.org/10.1016/j.jphotochem.2014.04.004.

[27] T. Pędzinski, K. Grzyb, K. Skotnicki, P. Filipiak, K. Bobrowski, C. Chatgilialoglu, B. Marciniak, Radiation-and photo-induced oxidation pathways of methionine in model peptide backbone under anoxic conditions, Int J Mol Sci. 22 (2021). https://doi.org/10.3390/ijms22094773.

[28] T. Pedzinski, K. Grzyb, F. Kaźmierczak, R. Frański, P. Filipiak, B. Marciniak, Early Events of Photosensitized Oxidation of Sulfur-Containing Amino Acids Studied by Laser Flash Photolysis and Mass Spectrometry, Journal of Physical Chemistry B. 124 (2020) 7564–7573. https://doi.org/10.1021/acs.jpcb.0c06008.

[29] E. Fuentes-Lemus, C. López-Alarcón, Photo-induced protein oxidation: Mechanisms, consequences and medical applications, Essays Biochem. 64 (2020) 33–44. https://doi.org/10.1042/EBC20190044.

[30] C.S. Foote, Mechanisms of Photosensitized Oxidation, Science (1979). 162 (1968) 963–970. https://doi.org/10.1126/science.162.3857.963.

[31] S. Narra, Y. Nishimura, H.A. Witek, S. Shigeto, Mechanism of Back Electron Transfer in an Intermolecular Photoinduced Electron Transfer Reaction: Solvent as a Charge Mediator, ChemPhysChem. 15 (2014) 2945–2950. https://doi.org/10.1002/cphc.201402411.

[32] T. Pedzinski, A. Markiewicz, B. Marciniak, Photosensitized oxidation of methionine derivatives. Laser flash photolysis studies, Res. Chem. Intermed. 35 (2009) 497–506. https://doi.org/10.1007/s11164-009-0046-4.

[33] M.T. Ignasiak, T. Pedzinski, F. Rusconi, P. Filipiak, K. Bobrowski, C. Houée-Levin, B. Marciniak, Photosensitized oxidation of methionine-containing dipeptides. from the transients to the final products, Journal of Physical Chemistry B. 118 (2014) 8549–8558. https://doi.org/10.1021/jp5039305.

[34] E. Silva, P. Barrias, E. Fuentes-Lemus, C. Tirapegui, A. Aspee, L. Carroll, M.J. Davies, C. López-Alarcón, Riboflavin-induced Type 1 photo-oxidation of tryptophan using a high intensity 365 nm light emitting diode, Free Radic Biol Med. 131 (2019) 133–143. https://doi.org/10.1016/j.freeradbiomed.2018.11.026.

[35] E. Fuentes-Lemus, E. Silva, F. Leinisch, E. Dorta, L.G. Lorentzen, M.J. Davies, C. López-Alarcón, α- and β-casein aggregation induced by riboflavin-sensitized photo-oxidation occurs via di-tyrosine cross-links and is oxygen concentration dependent, Food Chem. 256 (2018) 119–128. https://doi.org/10.1016/j.foodchem.2018.02.090.

[36] E.D. Sormacheva, P.S. Sherin, Y.P. Tsentalovich, Dimerization and oxidation of tryptophan in UV-A photolysis sensitized by kynurenic acid, Free Radic Biol Med. 113 (2017) 372–384. https://doi.org/10.1016/j.freeradbiomed.2017.10.007.

[37] M.J. Davies, Reactive species formed on proteins exposed to singlet oxygen, Photochemical and Photobiological Sciences. 3 (2004) 17–25. https://doi.org/10.1039/b307576c.

[38] D. Zala, M.V. Hinckelmann, H. Yu, M.M. Lyra Da Cunha, G. Liot, F.P. Cordelières, S. Marco, F. Saudou, Vesicular glycolysis provides on-board energy for fast axonal transport, Cell. 152 (2013) 479–491. https://doi.org/10.1016/j.cell.2012.12.029.

[39] A. Tarze, A. Deniaud, M. Le Bras, E. Maillier, D. Molle, N. Larochette, N. Zamzami, G. Jan, G. Kroemer, C. Brenner, GAPDH, a novel regulator of the pro-apoptotic mitochondrial membrane permeabilization, Oncogene. 26 (2007) 2606–2620. https://doi.org/10.1038/sj.onc.1210074.

[40] M.E. Brosnan, J.T. Brosnan, Histidine metabolism and function, Journal of Nutrition. 150 (2020) 2570S-2575S. https://doi.org/10.1093/jn/nxaa079.

[41] D. Moras, K.W. Olsen, M.N. Sabesan, M. Buehner, G.C. Ford, M.G. Rossmann, Studies of Asymmetry in the Three-dimensional Structure of Lobster D-Glyceraldehyde-3-phosphate Dehydrogenase, J Biol Chem. 250 (1975) 9137–9162. https://doi.org/10.2210/pdb1gpd/pdb.

[42] P.J. Harrigan, D.R. Trentham, Kinetic Studies of the Acylation of Pig Muscle D-Glyceraldehyde 3-Phosphate Dehydrogenase by 1,3-Diphosphoglycerate and of Proton Uptake and Release in the Overall Enzyme Mechanism, 1973.

[43] N.W. Seidler, Basic biology of GAPDH, Adv Exp Med Biol. 985 (2013) 1–36. https://doi.org/10.1007/978-94-007-4716-6_1.

[44] R.G. Duggleby, D.T. Dennis, Nicotinamide Adenine Dinucleotide-specific Glyceraldehyde 3-Phosphate Dehydrogenase from Pisum sativum, Journal of Biological Chemistry. 249 (1974) 162–166. https://doi.org/10.1016/S0021-9258(19)43106-2.

[45] J.Y. Zhang, F. Zhang, C.Q. Hong, A.E. Giuliano, X.J. Cui, G.J. Zhou, G.J. Zhang, Y.K. Cui, Critical protein GAPDH and its regulatory mechanisms in cancer cells, Cancer Biol Med. 12 (2015) 10–22. https://doi.org/10.7497/j.issn.2095-3941.2014.0019.

[46] D. Wang, D.R. Moothart, D.R. Lowy, X. Qian, The Expression of Glyceraldehyde-3-Phosphate Dehydrogenase Associated Cell Cycle (GACC) Genes Correlates with Cancer Stage and Poor Survival in Patients with Solid Tumors, PLoS One. 8 (2013). https://doi.org/10.1371/journal.pone.0061262.

[47] M. Phadke, N. Krynetskaia, A. Mishra, E. Krynetskiy, Accelerated cellular senescence phenotype of GAPDH-depleted human lung carcinoma cells, Biochem Biophys Res Commun. 411 (2011) 409–415. https://doi.org/10.1016/j.bbrc.2011.06.165.

[48] C. Nicholls, H. Li, J.P. Liu, GAPDH: A common enzyme with uncommon functions, Clin Exp Pharmacol Physiol. 39 (2012) 674–679. https://doi.org/10.1111/j.1440-1681.2011.05599.x.

[49] M. Allen, C. Cox, O. Belbin, L. Ma, G.D. Bisceglio, S.L. Wilcox, C.C. Howell, T.A. Hunter, O. Culley, L.P. Walker, M.M. Carrasquillo, D.W. Dickson, R.C. Petersen, N.R. Graff-Radford, S.G. Younkin, N. Ertekin-Taner, Association and heterogeneity at the GAPDH locus in Alzheimer's disease, Neurobiol Aging. 33 (2012) 203.e25-203.e33. https://doi.org/10.1016/j.neurobiolaging.2010.08.002.

[50] C. Tristan, N. Shahani, T.W. Sedlak, A. Sawa, The diverse functions of GAPDH: Views from different subcellular compartments, Cell Signal. 23 (2011) 317–323. https://doi.org/10.1016/j.cellsig.2010.08.003.

[51] J.L. Mazzola, M.A. Sirover, Alteration of Intracellular Structure and Function of Glyceraldehyde-3-Phosphate Dehydrogenase: A Common Phenotype of Neurodegenerative Disorders?, Neurotoxicology. 23 (2002) 603–609. https://doi.org/10.1016/S0161-813X(02)00062-1.

[52] J. Jedziniak, Photo-oxidative Damage to Lenticular GAPDH and its Relationship to Aldehyde Metabolism, Exp. Eye Res. 50 (1990) 589–595. https://doi.org/10.1016/0014-4835(90)90099-g.

[53] F. Itri, D.M. Monti, B. Della Ventura, R. Vinciguerra, M. Chino, F. Gesuele, A. Lombardi, R. Velotta, C. Altucci, L. Birolo, R. Piccoli, A. Arciello, Femtosecond UV-laser pulses to unveil protein-protein interactions in living cells, Cellular and Molecular Life Sciences. 73 (2016) 637–648. https://doi.org/10.1007/s00018-015-2015-y.

[54] A.L. Samson, A.S. Knaupp, I. Kass, O. Kleifeld, E.M. Marijanovic, V.A. Hughes, C.J. Lupton, A.M. Buckle, S.P. Bottomley, R.L. Medcalf, Oxidation of an exposed methionine instigates the aggregation of glyceraldehyde-3-phosphate dehydrogenase, Journal of Biological Chemistry. 289 (2014) 26922–26936. https://doi.org/10.1074/jbc.M114.570275.

[55] A.S. Rahmanto, P.E. Morgan, C.L. Hawkins, M.J. Davies, Cellular effects of photogenerated oxidants and long-lived, reactive, hydroperoxide photoproducts, Free Radic Biol Med. 49 (2010) 1505–1515. https://doi.org/10.1016/j.freeradbiomed.2010.08.006.

[56] P.E. Morgan, R.T. Dean, M.J. Davies, Inhibition of glyceraldehyde-3-phosphate dehydrogenase by peptide and protein peroxides generated by singlet oxygen attack, Eur J Biochem. 269 (2002) 1916–1925. https://doi.org/10.1046/j.1432-1033.2002.02845.x.

[57] A. Jabłoński, Efficiency of Anti-Stokes Fluorescence in Dyes., Nature. 131 (1933) 839–840.

[58] B. Marciniak, Metody badania mechanizmów reakcji fotochemicznych, Wydawnictwo Naukowe UAM, Poznań, 1999.

[59] Nicholas J. Turro, V. Ramamurthy, Juan C. Scaiano, Principles of Molecular Photochemistry: An Introduction, University Science Books, 2009.

[60] L. Pecci, M. Costa, A. Antonucci, G. Montefoschi, D. Cavallini, Methylene blue photosensitized oxidation of cysteine sulfinic acid and other sulfinates: The involvement of singlet oxygen and the azide paradox, Biochem Biophys Res Commun. 270 (2000) 782–786. https://doi.org/10.1006/bbrc.2000.2489.

[61] M.E. Brow, J. Dai, G. Park, M.W. Wright, I.G. Gillman, R.A. Manderville, Photochemically Catalyzed Reaction of Ochratoxin A with D- and L-cysteine, Photochem Photobiol. 76 (2002) 649. https://doi.org/10.1562/0031-8655(2002)076<0649:pcrooa>2.0.co;2.

[62] T. Nauser, W.H. Koppenol, C. Schöneich, Protein thiyl radical reactions and product formation: A kinetic simulation, Free Radic Biol Med. 80 (2015) 158–163. https://doi.org/10.1016/j.freeradbiomed.2014.12.006.

[63] S. Jiang, P. Hägglund, L. Carroll, L.M. Rasmussen, M.J. Davies, Crosslinking of human plasma C-reactive protein to human serum albumin via disulfide bond oxidation, Redox Biol. 41 (2021). https://doi.org/10.1016/j.redox.2021.101925.

[64] Q. Zhu, C. Costentin, J.A. Stubbe, D.G. Nocera, Disulfide radical anion as a super-reductant in biology and photoredox chemistry, Chem Sci. 14 (2023) 6876–6881. https://doi.org/10.1039/d3sc01867a.

[65] L. Doblas, P.M. Hägglund, E. Fuentes-Lemus, M.J. Davies, The cysteine residue in beta-lactoglobulin reacts with oxidized tyrosine residues in beta-casein to give casein-lactoglobulin dimers, Arch Biochem Biophys. 733 (2023). https://doi.org/10.1016/j.abb.2022.109482.

[66] E. Fuentes-Lemus, P. Hägglund, C. López-Alarcón, M.J. Davies, Oxidative Crosslinking of Peptides and Proteins: Mechanisms of Formation, Detection, Characterization and Quantification, Molecules. 27 (2022). https://doi.org/10.3390/molecules27010015.

[67] Z. Zhao, M.M. Poojary, L.H. Skibsted, M.N. Lund, Cleavage of Disulfide Bonds in Cystine by UV-B Illumination Mediated by Tryptophan or Tyrosine as Photosensitizers, J Agric Food Chem. 68 (2020) 6900–6909. https://doi.org/10.1021/acs.jafc.0c01760.

[68] G.L. Hug, K. Bobrowski, H. Kozubek, B. Marciniak, Photooxidation of Methionine Derivatives by the 4-Carboxybenzophenone Triplet State in Aqueous Solution. lntracomplex Proton Transfer Involving the Amino Group, Photochem Photobiol. 68 (1998) 785–796. https://doi.org/10.1111/j.1751-1097.1998.tb05285.x.

[69] K. Bobrowski, B. Marciniak, G.L. Hug, 4-Carboxybenzophenone-Sensitized Photooxidation of Sulfur-Containing Amino Acids. Nanosecond Laser Flash Photolysis and Pulse Radiolysis Studies, J. Am. Chem. Soc. 14 (1992) 10279–10288. https://doi.org/https://doi.org/10.1021/ja00052a025.

[70] G.L. Hug, B. Marciniak, K. Bobrowski, Acid-Base Equilibria Involved in Secondary Reactions Following the 4-Carboxybenzophenone Sensitized Photooxidation of Methionylglycine in Aqueous Solution. Spectral and Time Resolution of the Decaying (S∴N) + Radical Cation, J Phys Chem. 100 (1996) 14914–14921. https://doi.org/10.1021/jp960367j.

[71] K. Bobrowski, G.L. Hug, B. Marciniak, H. Kozubek, 4-Carboxybenzophenone-Sensitized Photooxidation of Sulfur-Containing Amino Acids in Alkaline Solutions. Secondary Photoreactions Kinetics, J. Phys. Chem. 98 (1994) 537–544. https://pubs.acs.org/sharingguidelines.

[72] B. Marciniak, K. Bobrowski, Photo-and Radiation-Induced One-Electron Oxidation of Methionine in Various Structural Environments Studied by Time-Resolved Techniques, Molecules. 27 (2022) 1028. https://doi.org/10.3390/molecules27031028.

[73] W.A. Prütz, J. Butler, E.J. Land, A.J. Swallow, The role of sulphur peptide functions in free radical transfer: a pulse radiolysis study, Int. J. Radiat. Biol. 55 (1989) 539–556. https://doi.org/10.1080/09553008914550591.

[74] C. Houée-Levin, K. Bobrowski, The use of the methods of radiolysis to explore the mechanisms of free radical modifications in proteins, J Proteomics. 92 (2013) 51–62. https://doi.org/10.1016/j.jprot.2013.02.014.

[75] O.B. Morozova, A. V. Yurkovskaya, Reduction of transient histidine radicals by tryptophan: influence of the amino group charge, Physical Chemistry Chemical Physics. 23 (2021) 5919–5926. https://doi.org/10.1039/d0cp06366e.

[76] C. Houée-Lévin, K. Bobrowski, L. Horakova, B. Karademir, C. Schöneich, M.J. Davies, C.M. Spickett, Exploring oxidative modifications of tyrosine: An update on mechanisms of formation, advances in analysis and biological consequences, Free Radic Res. 49 (2015) 347–373. https://doi.org/10.3109/10715762.2015.1007968.

[77] S. Canonica, B. Hellrung, J. Wirz, Oxidation of phenols by triplet aromatic ketones in aqueous solution, Journal of Physical Chemistry A. 104 (2000) 1226–1232. https://doi.org/10.1021/jp9930550.

[78] A. Wojcik, A. Łukaszewicz, O. Brede, B. Marciniak, Competitive photosensitized oxidation of tyrosine and methionine residues in enkephalins and their model peptides, J Photochem Photobiol A Chem. 198 (2008) 111–118. https://doi.org/10.1016/j.jphotochem.2008.02.027.

[79] R.I. Teixeira, J.S. Goulart, R.J. Corrêa, S.J. Garden, S.B. Ferreira, J.C. Netto-Ferreira, V.F. Ferreira, P. Miro, M.L. Marin, M.A. Miranda, N.C. De Lucas, A photochemical and theoretical study of the triplet reactivity of furano- and pyrano-1,4-naphthoquionones towards tyrosine and tryptophan derivatives, RSC Adv. 9 (2019) 13386–13397. https://doi.org/10.1039/c9ra01939a.

[80] A. Gatin, P. Duchambon, G. van der Rest, I. Billault, C. Sicard-Roselli, Protein Dimerization via Tyr Residues: Highlight of a Slow Process with Co-Existence of Numerous Intermediates and Final Products, Int J Mol Sci. 23 (2022). https://doi.org/10.3390/ijms23031174.

[81] M.T. Zhang, T. Irebo, O. Johansson, L. Hammarström, Proton-coupled electron transfer from tyrosine: A strong rate dependence on intramolecular proton transfer distance, J Am Chem Soc. 133 (2011) 13224–13227. https://doi.org/10.1021/ja203483j.

[82] H. Eickhoff, G. Jung, A. Rieker, Oxidative phenol coupling - Tyrosine dimers and libraries containing tyrosyl peptide dimers, Tetrahedron. 57 (2001) 353–364. https://doi.org/https://doi.org/10.1016/S0040-4020(00)00942-X.

[83] E.D. Keyes, K. Kauser, K.S. Warner, A.G. Roberts, Photosensitized Oxidative Dimerization at Tyrosine by a Water-Soluble 4-Amino-1,8-naphthalimide, ChemBioChem. 22 (2021) 2703–2710. https://doi.org/10.1002/cbic.202100193.

[84] T.K. Dalsgaard, M. Triquigneaux, L. Deterding, F. Summers, K. Ranguelova, G. Mortensen, R.P. Mason, Site-specific detection of radicals on α-lactalbumin after a riboflavin-sensitized reaction, detected by immuno-spin trapping, ESR, and MS, J Agric Food Chem. 61 (2013) 418–426. https://doi.org/10.1021/jf303973b.

[85] H.-R. Shen, J.D. Spikes, C.J. Smith, J. Kopeček, Photodynamic cross-linking of proteins V. Nature of the tyrosine-tyrosine bonds formed in the FMN-sensitized intermolecular cross-linking of N-acetyl-l-tyrosine, J Photochem Photobiol A Chem. 133 (2000) 115–122. https://doi.org/https://doi.org/10.1016/S1010-6030(00)00228-8.

[86] A. Gatin, I. Billault, P. Duchambon, G. Van der Rest, C. Sicard-Roselli, Oxidative radicals (HO• or N3•) induce several di-tyrosine bridge isomers at the protein scale, Free Radic Biol Med. 162 (2021) 461–470. https://doi.org/10.1016/j.freeradbiomed.2020.10.324.

[87] L. Olshansky, B.L. Greene, C. Finkbeiner, J. Stubbe, D.G. Nocera, Photochemical Generation of a Tryptophan Radical within the Subunit Interface of Ribonucleotide Reductase, Biochemistry. 55 (2016) 3234–3240. https://doi.org/10.1021/acs.biochem.6b00292.

[88] R. Pogni, M.C. Baratto, C. Teutloff, S. Giansanti, F.J. Ruiz-Dueñas, T. Choinowski, K. Piontek, A.T. Martínez, F. Lendzian, R. Basosi, A tryptophan neutral radical in the oxidized state of versatile peroxidase from Pleurotus eryngii: A combined multifrequency EPR and density functional theory study, Journal of Biological Chemistry. 281 (2006) 9517–9526. https://doi.org/10.1074/jbc.M510424200.

[89] Y.S. Zhuravleva, P.S. Sherin, Influence of pH on radical reactions between kynurenic acid and amino acids tryptophan and tyrosine. Part I. Amino acids in free state, Free Radic Biol Med. 172 (2021) 331–339. https://doi.org/10.1016/j.freeradbiomed.2021.06.015.

[90] L. Carroll, D.I. Pattison, J.B. Davies, R.F. Anderson, C. Lopez-Alarcon, M.J. Davies, Superoxide radicals react with peptide-derived tryptophan radicals with very high rate constants to give hydroperoxides as major products, Free Radic Biol Med. 118 (2018) 126–136. https://doi.org/10.1016/j.freeradbiomed.2018.02.033.

[91] L. Carroll, D.I. Pattison, J.B. Davies, R.F. Anderson, C. Lopez-Alarcon, M.J. Davies, Formation and detection of oxidant-generated tryptophan dimers in peptides and proteins, Free Radic Biol Med. 113 (2017) 132–142. https://doi.org/10.1016/j.freeradbiomed.2017.09.020.

[92] J. Dong, C. Huang, S. Guo, Y. Xia, Y. Hou, C. Yang, X. Zhang, J. Jie, B.Z. Zhu, H. Su, Free-Radical-Mediated Photoinduced Electron Transfer between 6-Thioguanine and Tryptophan Leading to DNA–Protein-Like Cross-Link, Journal of Physical Chemistry B. 126 (2022) 14–22. https://doi.org/10.1021/acs.jpcb.1c03380.

[93] E.D. Savina, Y.P. Tsentalovich, P.S. Sherin, UV-A induced damage to lysozyme via Type I photochemical reactions sensitized by kynurenic acid, Free Radic Biol Med. 152 (2020) 482–493. https://doi.org/10.1016/j.freeradbiomed.2019.11.017.

[94] S. Navaratnam, B.J. Parsons, Reduction potential of histidine free radicals : a pulse radiolysis study, Journal of the Chemical Society, Faraday Transactions. 94 (1998) 2577–2581. https://doi.org/10.1039/A803477J.

[95] B.P. Dey, S.C. Lahiri, Studies on the dissociation constants and solubility of amino acids in water + urea mixtures at 298 K, interaction of urea with amino acids and the role of urea in the denaturation of proteins in terms of structural aspects of water, J. Indian Chem. Soc. 87 (2010) 29–41. https://doi.org/10.5281/zenodo.5775371.

[96] R. Williams, pKa Data Compiled by R. Williams, [(Accessed on 12 May 2024)]; Available Online: Https://Www.Chem.Wisc.Edu/Areas/Reich/Pkatable/PKa_compilation-1-Williams.Pdf. (2022).

[97] J.A. Dean, N.A. Lange, Lange's handbook of chemistry, McGraw-Hill, 1999.

[98] N.N. Saprygina, O.B. Morozova, G. Grampp, A. V. Yurkovskaya, Effect of amino group charge on the photooxidation kinetics of aromatic amino acids, Journal of Physical Chemistry A. 118 (2014) 339–349. https://doi.org/10.1021/jp4097919.

[99] R.P. Reddy, S.K. Mohan, Interaction of zinc with cysteinylglycine and histidine containing di-peptides: Relevance to zinc binding sites in transcription factor IlIA, Indian J Chem. 41A (2002) 1816–1820.

[100] K. Elvingson, M. Fritzsche, D. Rehder, L. Pettersson, Speciation in Vanadium Bioinorganic Systems. 1. A Potentiometric and 51V NMR Study of Aqueous Equilibria in the H+--Vanadate(V)--L-alpha-Alanyl-L-histidine System., Acta Chem Scand. 48 (1994) 878–885. https://doi.org/10.3891/acta.chem.scand.48-0878.

[101] H.A. Azab, K.M. Abou El-Nour, S.H. Sorror, Metal ion complexes containing dipeptides, tripeptides, and biologically important zwitterionic buffers, J Chem Eng Data. 52 (2007) 381–390. https://doi.org/10.1021/je060319k.

[102] O.B. Morozova, M.S. Panov, N.N. Fishman, A. V. Yurkovskaya, Electron transfer: Vs. proton-coupled electron transfer as the mechanism of reaction between amino acids and triplet-excited benzophenones revealed by time-resolved CIDNP, Physical Chemistry Chemical Physics. 20 (2018) 21127–21135. https://doi.org/10.1039/c8cp03591a.

[103] Y.P. Tsentalovich, O.B. Morozova, A. V. Yurkovskaya, P.J. Hore, R.Z. Sagdeev, Time-resolved CIDNP and laser flash photolysis study of the photoreactions of N-acetyl histidine with 2,2′-dipyridyl in aqueous solution, Journal of Physical Chemistry A. 104 (2000) 6912–6916. https://doi.org/10.1021/jp000019o.

[104] P.F. Heelis, B.J. Parsons, G.O. Phillips, The pH dependence of the reactions of flavin triplet states with amino acids. A laser flash photolysis study, Biochim Biophys Acta. 587 (1979) 455–462. https://doi.org/10.1016/0304-4165(79)90449-5.

[105] C. Castaño, E. Oliveros, A.H. Thomas, C. Lorente, Histidine oxidation photosensitized by pterin: PH dependent mechanism, J Photochem Photobiol B. 153 (2015) 483–489. https://doi.org/10.1016/j.jphotobiol.2015.10.026.

[106] V. V. Agon, W.A. Bubb, A. Wright, C.L. Hawkins, M.J. Davies, Sensitizer-mediated photooxidation of histidine residues: Evidence for the formation of reactive side-chain peroxides, Free Radic Biol Med. 40 (2006) 698–710. https://doi.org/10.1016/j.freeradbiomed.2005.09.039.

[107] J. Moro, D. Tomé, P. Schmidely, T.C. Demersay, D. Azzout-Marniche, Histidine: A systematic review on metabolism and physiological effects in human and different animal species, Nutrients. 12 (2020) 1414. https://doi.org/10.3390/nu12051414.

[108] R. Matsukawa, M. Yamane, M. Kanai, Histidine Photooxygenation Chemistry: Mechanistic Evidence and Elucidation, Chemical Record. 23 (2023) e202300198. https://doi.org/10.1002/tcr.202300198.

[109] R.B. (Robert B. Woodward, D.H.R. Barton, R.B. Woodward remembered : a collection of papers in honour of Robert Burns Woodward, 1917-1979, Pergamon Press, 1982.

[110] G.E. Adams, J.E. Aldrich, R.H. Bisby, R.B. Cundall, J. Lo Redpath, R. Lo Willson, Selective Free Radical Reactions with Proteins and Enzymes: Reactions of Inorganic Radical Anions with Amino Acids, Radiat Res. 49 (1972) 278–289. https://doi.org/10.2307/3573266.

[111] M.S. Sule, J. Butler, Electron Transfer from Azide Radical to Histidine Generates Histidinyl Radical, Biokemistri. 13 (2003) 16–22.

[112] A. Mukhopadhyay, L. Jacob, S. Venkataramani, Dehydro-oxazole, thiazole and imidazole radicals: insights into the electronic structure, stability and reactivity aspects, Physical Chemistry Chemical Physics. 19 (2017) 394–407. https://doi.org/10.1039/c6cp05677f.

[113] G. Lassmann, L.A. Eriksson, F. Himo, F. Lendzian, W. Lubitz, Electronic Structure of a Transient Histidine Radical in Liquid Aqueous Solution: EPR Continuous-Flow Studies and Density Functional Calculations, Journal of Physical Chemistry A. 103 (1999) 1283–1290. https://doi.org/10.1021/jp9843454.

[114] O.B. Morozova, Reduction of Transient Histidine Radicals by Tyrosine: Influence of the Protonation State of Reactants, ChemPhysChem. 21 (2020) 43–50. https://doi.org/10.1002/cphc.201901020.

[115] Karol A. Muszkat, Tmima Wismontski-Knittel, Reactivities of Tyrosine, Histidine, Tryptophan, and Methionine in Radical Pair Formation in Flavin Triplet Induced Protein Nuclear Magnetic Polarization, Biochemistry. 24 (1985) 5416–5421. https://doi.org/https://doi.org/10.1021/bi00341a020.

[116] P. Tarábek, M. Bonifačić, D. Beckert, Time-resolved FT EPR and optical spectroscopy study on photooxidation of aliphatic α-amino acids in aqueous solutions; electron transfer from amino vs carboxylate functional group, Journal of Physical Chemistry A. 110 (2006) 7293–7302. https://doi.org/10.1021/jp060764m.

[117] Tomasz Pedzinski, Bronislaw Marciniak, Gordon L. Hug, Quenching of the excited singlet state of acridine and 10-methylacridinium cation by thio-organic compounds in aqueous solution, J Photochem Photobiol A Chem. 150 (2002) 21–30. https://doi.org/https://doi.org/10.1016/S1010-6030(02)00028-X.

[118] A. Posadaz, A. Biasutti, C. Casale, J. Sanz, F. Amat-Guerri, N.A. García, Rose Bengal–Sensitized Photooxidation of the Dipeptides l-Tryptophyl-l-Phenylalanine, l-Tryptophyl-l-Tyrosine and l-Tryptophyl-l-Tryptophan: Kinetics, Mechanism and Photoproducts¶, Photochem Photobiol. 80 (2004) 132. https://doi.org/10.1562/2004-03-03-ra-097.1.

[119] O.B. Morozova, P.S. Sherin, A. V. Yurkovskaya, Competition of singlet and triplet recombination of radical pairs in photoreactions of carboxy benzophenones and aromatic amino acids, Physical Chemistry Chemical Physics. 21 (2019) 2017–2028. https://doi.org/10.1039/c8cp06760k.

[120] M.Y. Jung, S.K. Kim, S.Y. Kim, Riboflavin-sensitized photooxidation of ascorbic acid: kinetics and amino acid effects, Food Chem. 53 (1995) 397–403. https://doi.org/10.1016/0308-8146(95)99834-M.

[121] P. Byrom, J.H. Turnbull, Excited states of flavine coenzymes. II. Anaerobic oxidation of amino acids by excited riboflavine derivatives, Photochem Photobiol. 6 (1967) 125–131. https://doi.org/10.1111/j.1751-1097.1967.tb08797.x.

[122] R.R. Yettella, D.B. Min, Effects of Trolox and ascorbic acid on the riboflavin photosensitised oxidation of aromatic amino acids, Food Chem. 118 (2010) 35–41. https://doi.org/10.1016/j.foodchem.2009.04.022.

[123] I. Volodyaev, Y.A. Vladimirov, Free Radicals in Biology, in: I. Volodyaev, E. van Wijk, M. Cifra, Y.A. Vladimirov (Eds.), Ultra-Weak Photon Emission from Biological Systems, 1st ed., Springer Cham, 2023: pp. 107–122. https://doi.org/10.1007/978-3-031-39078-4_8.

[124] N. V. Tkachenko, Optical Spectroscopy: Methods and Instrumentation, 1st ed., Elsevier Science, 2006. https://doi.org/10.1016/B978-0-444-52126-2.X5024-2.

[125] P. Müller, E. Ignatz, S. Kiontke, K. Brettel, L.O. Essen, Sub-nanosecond tryptophan radical deprotonation mediated by a protein-bound water cluster in class II DNA photolyases, Chem Sci. 9 (2018) 1200–1212. https://doi.org/10.1039/c7sc03969g.

[126] W. Szczepaniak, Metody instrumentalne w analizie chemicznej , Wydawnictwo Naukowe PWN SA, 2002.

[127] Witkiewicz Z., Podstawy Chromatografii, Wydawnictwo Naukowo-Techniczne, Warszawa, 2000.

[128] A. Braithwaite, F.J. Smith, Chromatographic Methods, Springer Netherlands, Dordrecht, 1999. https://doi.org/10.1007/978-94-011-0599-6.

[129] R.M. Silverstein, F.X. Webster, D.J. Kiemle, Spectrometric identification of organic compounds, John Wiley & Sons, Inc., 2005.

[130] J.H. Gross, Mass spectrometry. A textbook, Springer, 2004.

[131] P.K. So, B. Hu, Z.P. Yao, Mass spectrometry: Towards in vivo analysis of biological systems, Mol Biosyst. 9 (2013) 915–929. https://doi.org/10.1039/c2mb25428j.

[132] N.B. Cech, C.G. Enke, Practical implications of some recent studies in electrospray ionization fundamentals, Mass Spectrom Rev. 20 (2001) 362–387. https://doi.org/10.1002/mas.10008.

[133] M. Mäkinen, M. Nousiainen, M. Sillanpää, Ion spectrometric detection technologies for ultra-traces of explosives: A review, Mass Spectrom Rev. 30 (2011) 940–973. https://doi.org/10.1002/mas.20308.

[134] K. Michelmann, J.A. Silveira, M.E. Ridgeway, M.A. Park, Fundamentals of trapped ion mobility spectrometry, J Am Soc Mass Spectrom. 26 (2014) 14–24. https://doi.org/10.1007/s13361-014-0999-4.

[135] W.C. Wiley, I.H. McLaren, Time-of-flight mass spectrometer with improved resolution, Review of Scientific Instruments. 26 (1955) 1150–1157. https://doi.org/10.1063/1.1715212.

[136] R.J. Cotter, Time-of-Flight Mass Spectrometry for the Structural Analysis of Biological Molecules, Anal Chem. 64 (1992) 1027A-1039A. https://doi.org/doi.org/10.1021/ac00045a726.

[137] M. Guilhaus, Special feature: Tutorial. Principles and instrumentation in time-of-flight mass spectrometry. Physical and instrumental concepts, Journal of Mass Spectrometry. 30 (1995) 1519–1532. https://doi.org/10.1002/jms.1190301102.

[138] B.A. Mamyrin, V.I. Karataev, D. V Shmikk, V.A. Zagulin, The mass-reflectron, a new nonmagnetic time-of-flight mass spectrometer with high resolution, Zhurnal Ehksperimental'noj i Teoreticheskoj Fiziki. 64 (1973) 82–89.

[139] R.L. Scott, Some comments on the Benesi-Hildebrand equation, Recueil Des Travaux Chimiques Des Pays-Bas. 75 (1956) 787–789. https://doi.org/10.1002/recl.19560750711.

[140] M. Steblecka, M. Wolszczak, E. Szajdzinska-Pietek, Interaction of 1-pyrene sulfonic acid sodium salt with human serum albumin, J Lumin. 172 (2016) 279–285. https://doi.org/10.1016/j.jlumin.2015.12.038.

[141] H.A. Goldberg, K.J. Warner, The Staining of Acidic Proteins on Polyacrylamide Gels: Enhanced Sensitivity and Stability of "'Stains-All'" Staining in Combination with Silver Nitrate, Anal Biochem. 251 (1997) 227–233. https://doi.org/10.1006/abio.1997.2252.

[142] G. Degendorfer, C.Y. Chuang, H. Kawasaki, A. Hammer, E. Malle, F. Yamakura, M.J. Davies, Peroxynitrite-mediated oxidation of plasma fibronectin, Free Radic Biol Med. 97 (2016) 602–615. https://doi.org/10.1016/j.freeradbiomed.2016.06.013.

[143] S. Jiang, L. Carroll, M. Mariotti, P. Hägglund, M.J. Davies, Formation of protein cross-links by singlet oxygen-mediated disulfide oxidation, Redox Biol. 41 (2021). https://doi.org/10.1016/j.redox.2021.101874.

[144] M. Rykær, B. Svensson, M.J. Davies, P. Hägglund, Unrestricted Mass Spectrometric Data Analysis for Identification, Localization, and Quantification of Oxidative Protein Modifications, J Proteome Res. 16 (2017) 3978–3988. https://doi.org/10.1021/acs.jproteome.7b00330.

[145] S.M. Rutherfurd, G.S. Gilani, Amino acid analysis, Curr Protoc Protein Sci. 58 (2009) 11.9.1-11.9.37. https://doi.org/10.1002/0471140864.ps1109s58.

[146] L.F. Gamon, C. Guo, J. He, P. Hägglund, C.L. Hawkins, M.J. Davies, Absolute quantitative analysis of intact and oxidized amino acids by LC-MS without prior derivatization, Redox Biol. 36 (2020). https://doi.org/10.1016/j.redox.2020.101586.

[147] C.K. Riener, G. Kada, H.J. Gruber, Quick measurement of protein sulfhydryls with Ellman's reagent and with 4,4′-dithiodipyridine, Anal Bioanal Chem. 373 (2002) 266–276. https://doi.org/10.1007/s00216-002-1347-2.

[148] R. V. Bensasson, E.J. Land, T.G. Truscott, Flash photolysis and pulse radiolysis : contributions to the chemistry of biology and medicine, Pergamon, 1983.

[149] B. Marciniak, K. Bobrowski, G.L. Hug', Quenching of Triplet States of Aromatic Ketones by Sulfur-Containing Amino Acids in Solution, Evidence for Electron Transfer, J. Phys. Chem. 97 (1993) 11937–11943. https://doi.org/https://doi.org/10.1021/j100148a015.

[150] A.J. Gross, I.W. Sizer, The oxidation of tyramine, tyrosine, and related compounds by peroxidase., J Biol Chem. 234 (1959) 1611–1614. https://doi.org/10.1016/s0021-9258(18)70059-8.

[151] S. Criado, A.T. Soltermann, J.M. Marioli, N.A. Garcia, Sensitized photooxidation of Di- and tripeptides of tyrosine, Photochem Photobiol. 68 (1998) 453–458. https://doi.org/10.1111/j.1751-1097.1998.tb02499.x.

[152] Y.P. Tsentalovich, J.J. Lopez, P.J. Hore, R.Z. Sagdeev, Mechanisms of reactions of flavin mononucleotide triplet with aromatic amino acids, Spectrochimica Acta Part A. 58 (2002) 2043–2050. https://doi.org/10.1016/s1386-1425(01)00652-7.

[153] X. Fang, F. Jin, H. Jin, C. Von Sonntag, Reaction of the superoxide radical with the N-centered radical derived from N-acetyltryptophan methyl ester, J. Chem. Soc., Perkin Trans. 2 (1998) 259–264. https://doi.org/10.1039/A706979K.

[154] S. Bellmaine, A. Schnellbaecher, A. Zimmer, Reactivity and degradation products of tryptophan in solution and proteins, Free Radic Biol Med. 160 (2020) 696–718. https://doi.org/10.1016/j.freeradbiomed.2020.09.002.

[155] C.K. Remucal, K. McNeill, Photosensitized amino acid degradation in the presence of riboflavin and its derivatives, Environ Sci Technol. 45 (2011) 5230–5237. https://doi.org/10.1021/es200411a.

[156] C. Castaño, M.P. Serrano, C. Lorente, C.D. Borsarelli, A.H. Thomas, Quenching of the Singlet and Triplet Excited States of Pterin by Amino Acids, Photochem Photobiol. 95 (2019) 220–226. https://doi.org/10.1111/php.13046.

[157] I. Kraljic, L. Lindqvist, Laser photolysis study of triplet eosin and thionine reactions in photosensitized oxidations, Photochem Photobiol. 20 (1974) 351–355. https://doi.org/10.1111/j.1751-1097.1974.tb06587.x.

[158] M.O. Iwunze, The characterization of the fluorescence of l-histidine in simulated body fluid, J Photochem Photobiol A Chem. 186 (2007) 283–289. https://doi.org/10.1016/j.jphotochem.2006.05.034.

[159] G.L. Hug, B. Marciniak, Quenching of Triplet States of Organic Compounds by Copper(II) and Nickel(II) 1,3-Diketonates in Acetonitrile Solution. Energy and/or Electron Transfer, J. Phys. Chem. 98 (1994) 7523–7532. https://doi.org/10.1021/j100082a022.

[160] T.A. Armer, R.O. Cook, T. Alfredson, A. Sun, Inhalation delivery methods and devices, US 2010/196286 A1, 2010.

[161] K.V. Neverov, E.A. Mironov, T.A. Lyudnikova, A.A. Krasnovskij, M.S. Kritskij, Phosphorescence analysis of triplet state of pterins in connection with their photoreceptor function in biochemical systems, Biochemi. (Mosc.). 61 (1996) 1627–1636. https://www.researchgate.net/publication/279539411.

[162] M. D'Auria, A DFT study of the photochemical dimerization of methyl 3-(2-furyl)acrylate and allyl urocanate, Molecules. 19 (2014) 20482–20497. https://doi.org/10.3390/molecules191220482.

[163] W.D. Cooke, S.L. Fortner, S.M. Jahan, Radiation Damage in Single Crystal L-Histidine as Studied by Low-Temperature Thermoluminescence Techniques, J Lumin. 26 (1982) 319–328.

[164] C.B. Martin, M.L. Tsao, C.M. Hadad, M.S. Platz, The reaction of triplet flavin with indole. A study of the cascade of reactive intermediates using density functional theory and time resolved infrared spectroscopy, J Am Chem Soc. 124 (2002) 7226–7234. https://doi.org/10.1021/ja0123711.

[165] S.J. Chantrell, C.A. Mcauliffe, R.W. Munn, A.C. Pratt, E.J. Land, THE EXCITED STATES OF PROTOPORPHYRIN IX, J Lumin. 12 (1976) 887–891. https://doi.org/https://doi.org/10.1016/0022-2313(76)90193-9.

[166] J.M. Larkin, W.R. Donaldson, T.H. Foster, R.S. Knox, Reverse intersystem crossing from a triplet state of rose bengal populated by sequential 532-q1064-nm laser excitation, Chem Phys. 244 (1999) 319–330. https://doi.org/https://doi.org/10.1016/S0301-0104(99)00130-5.

[167] P.B. Merkel, J.P. Dinnocenzo, Thermodynamic energies of donor and acceptor triplet states, J Photochem Photobiol A Chem. 193 (2008) 110–121. https://doi.org/10.1016/j.jphotochem.2007.06.014.

[168] C.F. Xu, Y. Chen, L. Yi, T. Brantley, B. Stanley, Z. Sosic, L. Zang, Discovery and Characterization of Histidine Oxidation Initiated Cross-links in an IgG1 Monoclonal Antibody, Anal Chem. 89 (2017) 7915–7923. https://doi.org/10.1021/acs.analchem.7b00860.

[169] T. Powell, M.J. Knight, J. O'Hara, W. Burkitt, Discovery of a Photoinduced Histidine-Histidine Cross-Link in an IgG4 Antibody, J Am Soc Mass Spectrom. 31 (2020) 1233–1240. https://doi.org/10.1021/jasms.0c00076.

[170] B. Fan, J. Wan, A. McKay, Z. Qu, S.H. Thang, Facile synthesis of well-controlled poly(1-vinyl imidazole) by the RAFT process, Polym Chem. 11 (2020) 5649–5658. https://doi.org/10.1039/d0py00985g.

[171] C. Gaosheng, Z. Shujuan, Y. Side, H. Zhenhui, D. Zhiwen, Z. Zhicheng, Spectroscopic characterization of mechanisms of oxidation of Phe by SO4●− − radical: A pulse radiolysis study, Sci China Chem. 45 (2002) 398–406. https://doi.org/10.1360/02YB9051.

[172] M. Ignasiak-Kciuk, K. Nowicka-Bauer, M. Grzechowiak, T. Ravnsborg, K. Frąckowiak, O.N. Jensen, M. Jaskólski, B. Marciniak, Does the presence of ground state complex between a PR-10 protein and a sensitizer affect the mechanism of sensitized photo-oxidation?, Free Radic Biol Med. 198 (2023) 27–43. https://doi.org/10.1016/j.freeradbiomed.2023.01.022.

[173] V. Bogoeva, L. Petrova, P. Kubát, Binding of palladium (II) 5, 10, 15, 20-tetrakis (4-sulfonatophenyl) porphyrin to a lectin for photosensitizer targeted delivery, J Photochem Photobiol B. 153 (2015) 276–280. https://doi.org/10.1016/j.jphotobiol.2015.10.010.

[174] P. Tiwari, P. Kaila, P. Guptasarma, Understanding anomalous mobility of proteins on SDS-PAGE with special reference to the highly acidic extracellular domains of human E- and N-cadherins, Electrophoresis. 40 (2019) 1273–1281. https://doi.org/10.1002/elps.201800219.

[175] L.O. Reid, M.L. Dántola, G. Petroselli, R. Erra-Balsells, M.A. Miranda, V. Lhiaubet-Vallet, A.H. Thomas, Chemical Modifications of Globular Proteins Phototriggered by an Endogenous Photosensitizer, Chem Res Toxicol. 32 (2019) 2250–2259. https://doi.org/10.1021/acs.chemrestox.9b00286.

[176] M.A. Miranda, J. V Castell, D. Herná Ndez, M.J. Gómez-Lechón, F. Bosca, I.M. Morera, Z. Sarabia, Drug-Photosensitized Protein Modification: Identification of the Reactive Sites and Elucidation of the Reaction Mechanisms with Tiaprofenic Acid/Albumin as Model System †, Chem. Res. Toxicol. 11 (1998) 172–177. https://doi.org/https://doi.org/10.1021/tx970082d.

[177] H.K. Khor, M.E. Jacoby, T.C. Squier, G.C. Chu, D. Chelius, Identification of methionine sulfoxide diastereomers in immunoglobulin gamma antibodies using methionine sulfoxide reductase enzymes, MAbs. 2 (2010) 299–308. https://doi.org/10.4161/mabs.2.3.11755.

[178] K. Morand, G. Talbo, M. Mann, Oxidation of Peptides During Electrospray Ionization, RAPID COMMUNICATIONS IN MASS SPECTROMETRY. 7 (1993) 738–743. https://doi.org/10.1002/rcm.1290070811.

VI. Supplementary Information

Tyrosine:

Table TYR.SI1 *Gradient elution methods for samples*

Tyr (20°C oven) Flow = 0.3 [ml/min]		**Tyr-OEt (25°C oven) Flow = 0.3 [ml/min]**		**N-Ac-Tyr (30°C oven) Flow = 0.4 [ml/min]**		**N-Ac-Tyr-OEt (45°C oven) Flow = 0.3 [ml/min]**		**Tyr-Val (40°C oven) Flow = 0.3 [ml/min]**	
time	%B	**time**	**time**	%B	%B	**time**	%B	**time**	%B
-1.00	1	**-1.00**	5	**-1.00**	3	**-1.00**	15	**-1.00**	5
0.00	1	**0.00**	5	**0.00**	3	**0.00**	15	**0.00**	5
5.00	1	**4.00**	5	**1.00**	15	**6.00**	15	**1.50**	5
10.00	18	**10.00**	15	**7.00**	15	**7.00**	23	**6.00**	8
20.00	30	**20.00**	15	**10.00**	20	**20.00**	23	**12.00**	8
23.00	40	**23.00**	40	**20.00**	30	**23.00**	40	**15.00**	25
30.00	40	**30.00**	40	**23.00**	40	**30.00**	40	**20.00**	70
31.00	60	**31.00**	60	**30.00**	40	**31.00**	60	**28.00**	70
36.00	60	**36.00**	60	**31.00**	60	**36.00**	60	**30.00**	5
37.00	5	**37.00**	5	**36.00**	60	**37.00**	3	**32.00**	5
42.00	5	**42.00**	5	**37.00**	3	**42.00**	3		
				42.00	3				

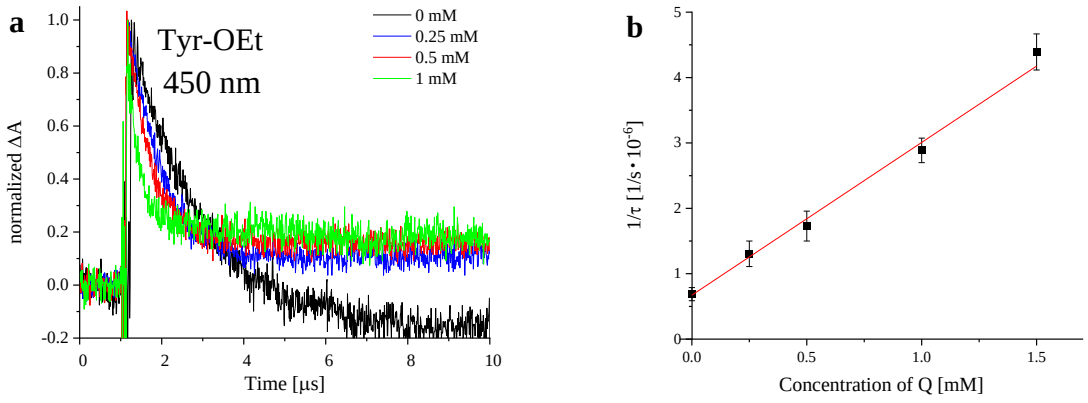

Figure TYR.SI1 ***(a)*** *Kinetic traces for the ^{3}3CB* decay at 450 nm in the presence of varying concentrations of Tyr-OEt (0-1 mM) at pH 7* ***(b)*** *The Stern-Volmer plots according to* ***Equation 2*** *for the quenching of ^{3}3CB* by Tyr-OEt at pH 7*

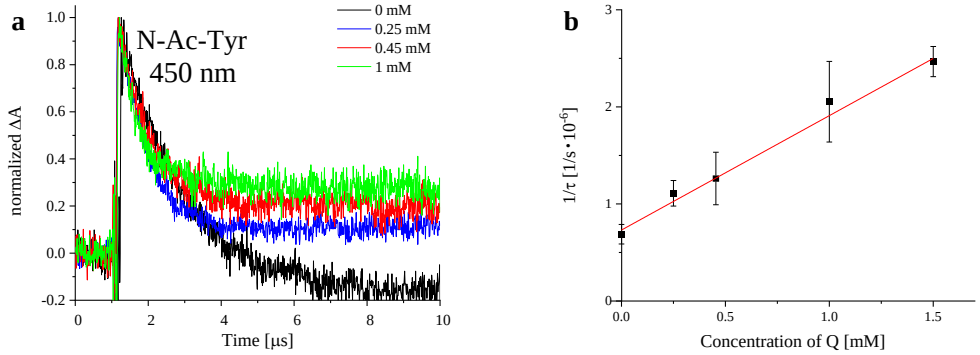

Figure TYR.SI2 ***(a)*** *Kinetic traces for the* ^{3}*3CB* decay at 450 nm in the presence of varying concentrations of N-Ac-Tyr (0-1 mM) at pH 7* ***(b)*** *The Stern-Volmer plots according to* ***Equation 2*** *for the quenching of* ^{3}*3CB* by N-Ac-Tyr at pH*

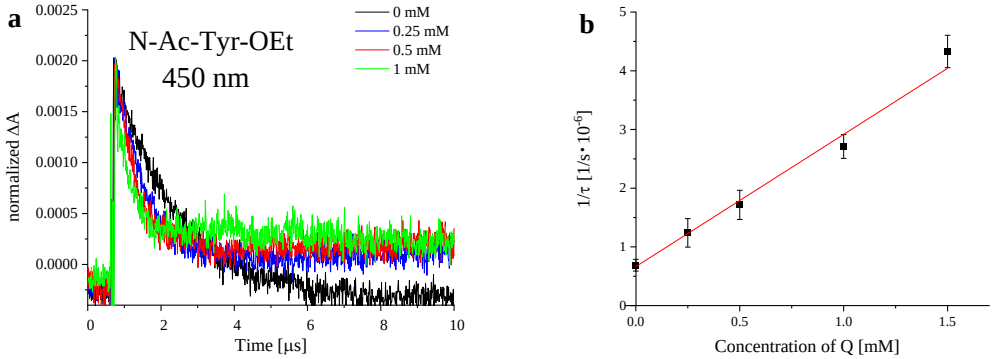

Figure TYR.SI3 ***(a)*** *Kinetic traces for the* ^{3}*3CB* decay at 450 nm in the presence of varying concentrations of N-Ac-Tyr-OEt (0-1 mM) at pH 7* ***(b)*** *The Stern-Volmer plots according to* ***Equation 2*** *for the quenching of* ^{3}*3CB* by N-Ac-Tyr-OEt at pH 7*

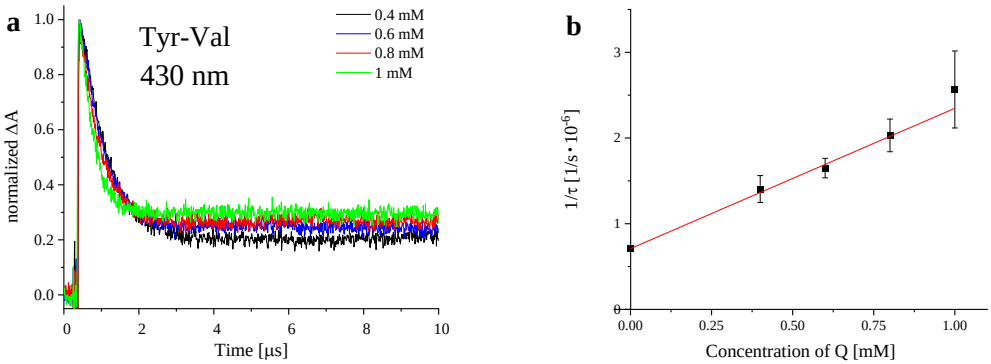

Figure TYR.SI4 ***(a)*** *Kinetic traces for the* ^{3}*3CB* decay at 430 nm in the presence of varying concentrations of Tyr-Val at pH 7* ***(b)*** *The Stern-Volmer plots according to* ***Equation*** *2 for the quenching of* ^{3}*3CB* by Tyr-Val at pH 7*

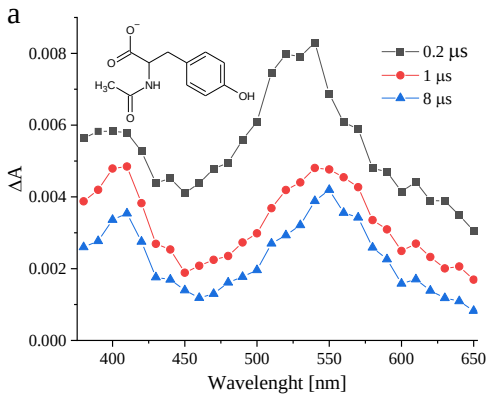
a
0.2 µs
1 µs
8 µs
ΔA
Wavelenght [nm]

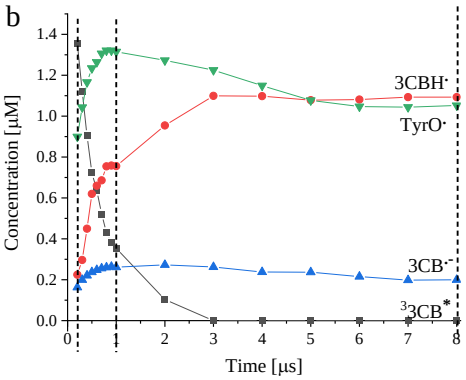
b
3CBH·
TyrO·
3CB·-
3CB*
Concentration [µM]
Time [µs]

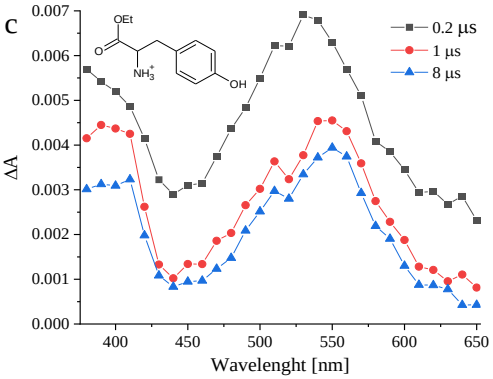
c
0.2 µs
1 µs
8 µs
ΔA
Wavelenght [nm]

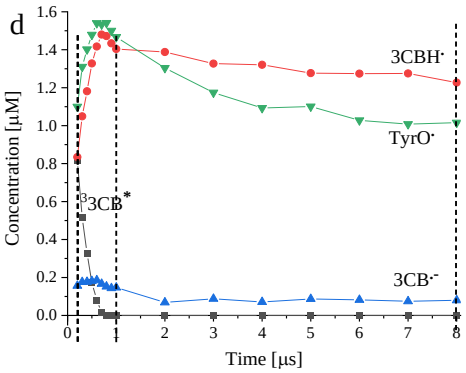
d
3CBH·
TyrO·
3CB*
3CB·-
Concentration [µM]
Time [µs]

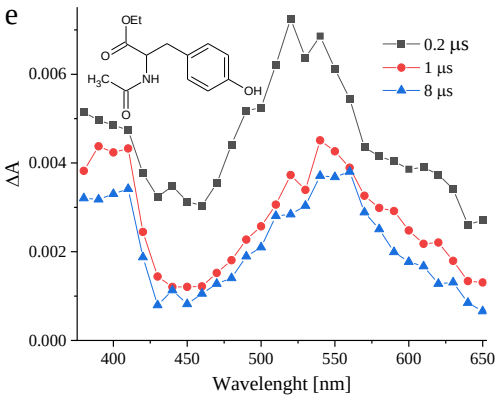
e
0.2 µs
1 µs
8 µs
ΔA
Wavelenght [nm]

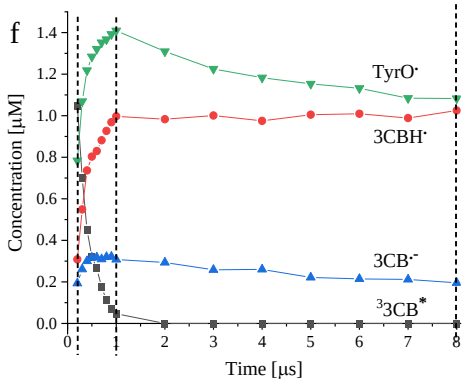
f
TyrO·
3CBH·
3CB·-
3CB*
Concentration [µM]
Time [µs]

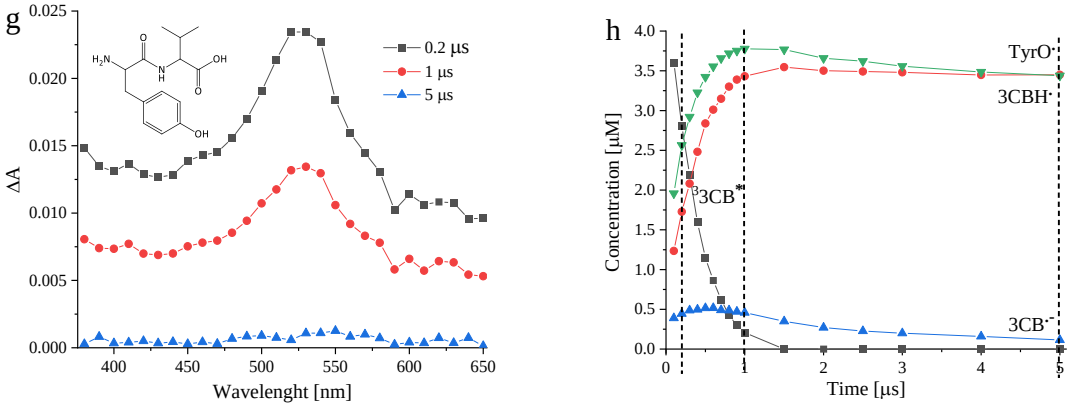

Figure TYR.SI5 *Evolution of transient absorption spectra from CB-sensitized oxidation of* ***(a)*** *N-Ac-Tyr;* ***(c)*** *Tyr-OEt;* ***(e)*** *N-Ac-Tyr-OEt;* ***(g)*** *Tyr-Val all at pH 7. Spectra were recorded at different delays following laser pulse 0.2 (black ■), 1 (red ●), 8 or 5 µs (blue ▲). Concentration profiles of transients identified in the laser flash photolysis of an aqueous solution of* ***(b)*** *N-Ac-Tyr;* ***(d)*** *Tyr-OEt;* ***(f)*** *N-Ac-Tyr-OEt;* ***(h)*** *Tyr-Val (1 mM) and CB (4 mM and 5 mM in case of Tyr-Val) at pH 7 where (black ■) is* ^{3}*3CB*, (red ●) is 3CBH*$^\bullet$*, (blue ▲) is 3CB*$^{\bullet-}$ *and (green ▼) is TyrO*$^\bullet$*. Dotted lines represent points at which concentrations were measured on spectra represented in respective figure to the left. Dotted lines represent times at which respective spectra in were presented in* ***(a)****,* ***(c)****,* ***(e)****, and* ***(g)***

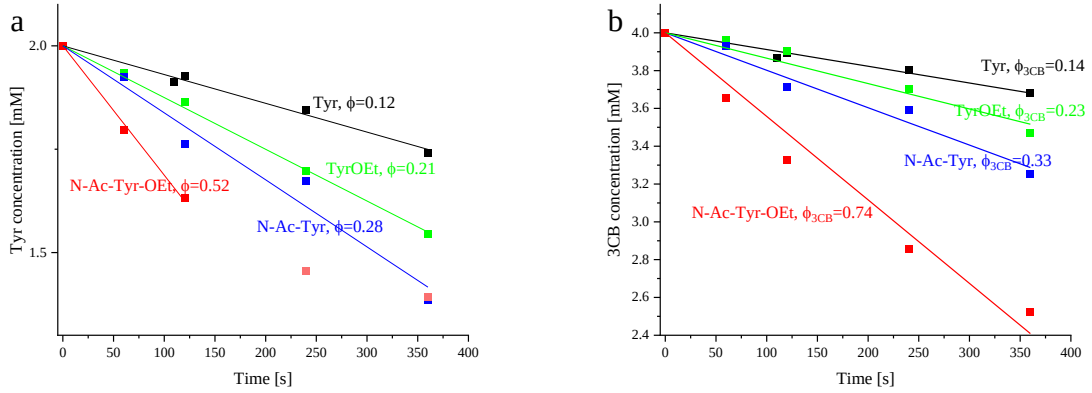

Figure.TYR.SI6. *Graph of decrease in concentration over time for Tyr and its derivatives* ***(a)*** *and 3CB* ***(b)*** *for each respective experiment. Slope of those graphs provided rate of consumption of given compound*

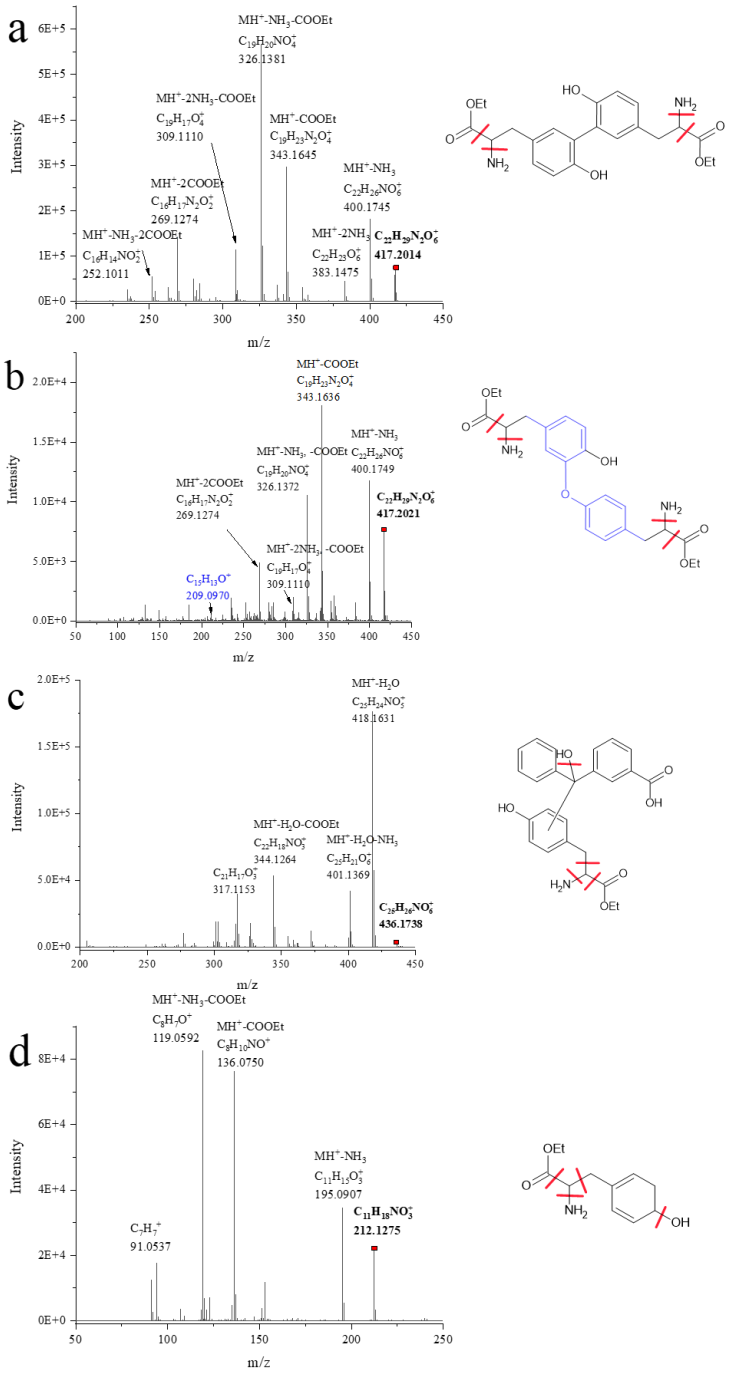

Figure TYR.SI7 *MS/MS spectra of products **7**, **8**, **11** and **12** derived from TyrOEt irradiated with ^{3}3CB* in aqueous solution, Ar-saturated: **(a)** MSMS of m/z = 417.2014 assigned to [diTyrOEt]H^{+}, **(b)** MSMS of m/z = 417.2021 assigned to [diTyrOEt]H^{+}, **(c)** MSMS of m/z = 436.1738 assigned to **11** [TyrOEt-3CBH]H^{+} and d) MSMS of m/z = 212.1275 assigned to **12** [TyrOEt+2Da]H^{+}*

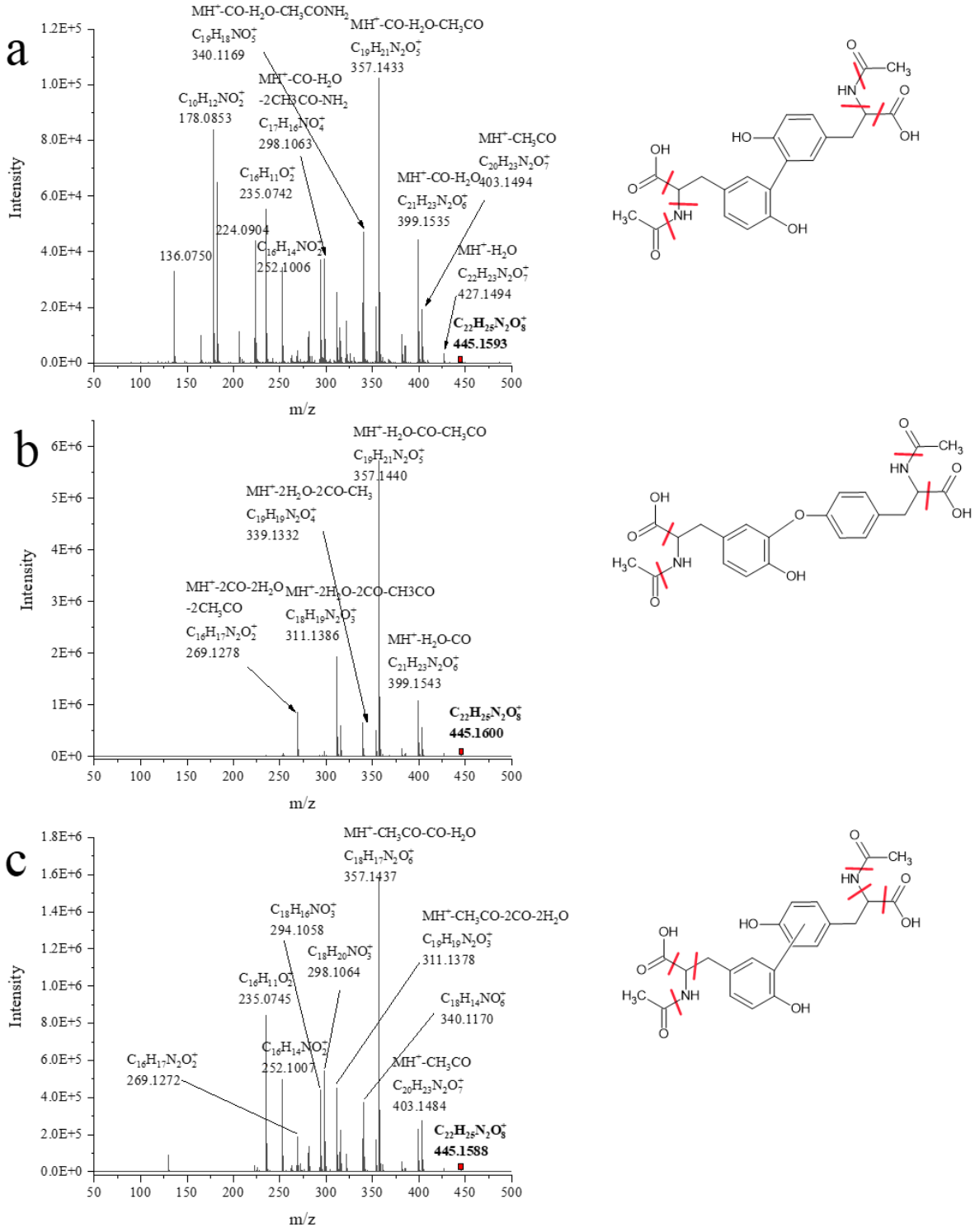

Figure TYR.SI8 *MS/MS spectra of products **7**, **8**, and **10** derived from N-Ac-Tyr irradiated with ^{3}3CB* in aqueous solution, Ar-saturated: **(a)** MSMS of m/z = 445.1593 assigned to [diN-Ac-Tyr]H$^+$, **(b)** MSMS of m/z = 445.1600 assigned to [diN-Ac-TyrTyr]H$^+$ and **(c)** MSMS of m/z = 445.1588 assigned to [diN-Ac-Tyr]H$^+$ with undefined structure*

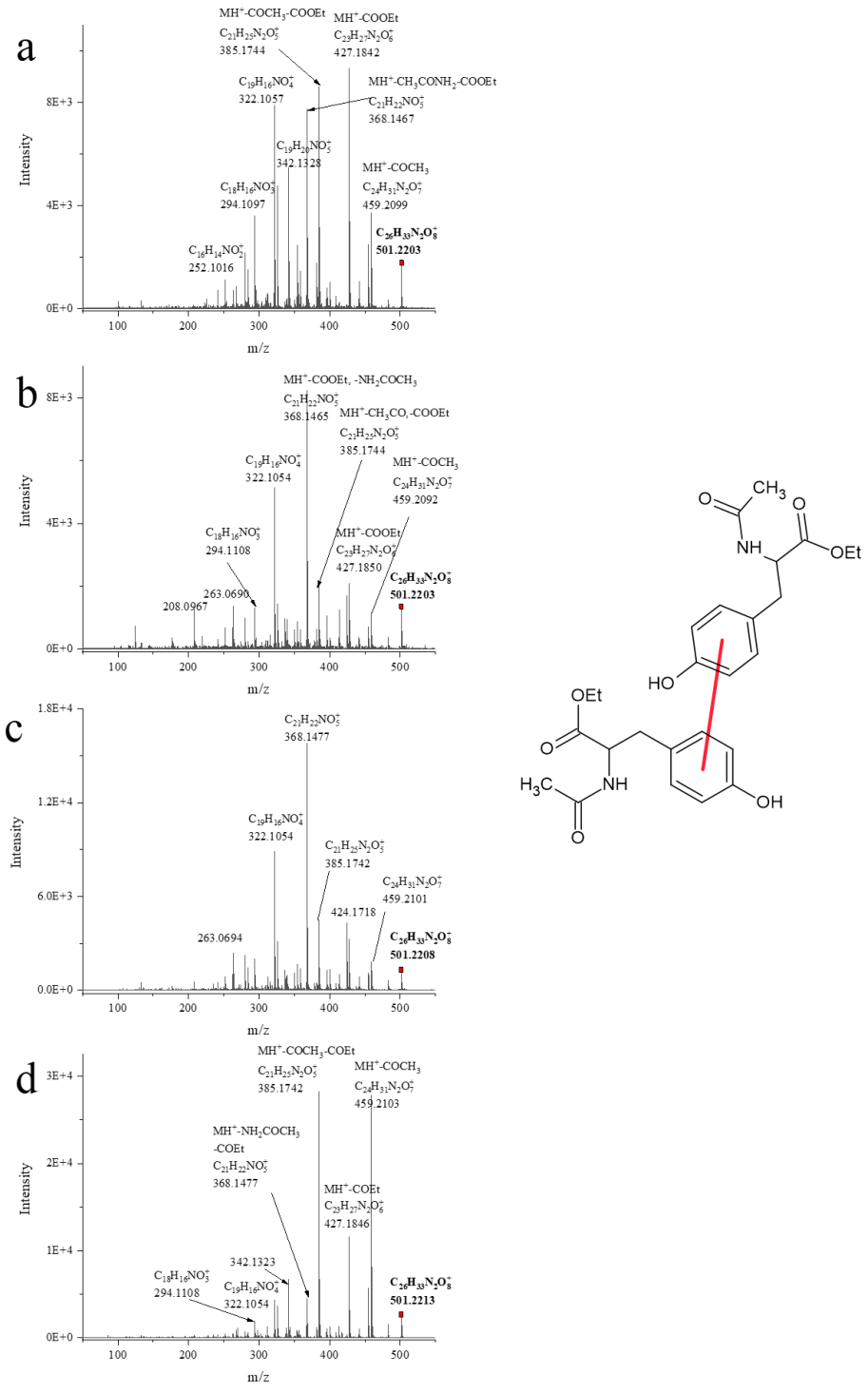

Figure TYR.SI9 *MS/MS spectra of products* ***2***, ***3***, ***4,*** *and* ***5*** *derived from N-Ac-Tyr-OEt irradiated with* ^{3}*3CB* in aqueous solution, Ar-saturated:* ***(a)*** *MSMS of m/z = 501.2203 assigned to [diN-Ac-Tyr-OEt]H*$^+$*,* ***(b)*** *MSMS of m/z = 501.2203 assigned to [diN-Ac-Tyr-OEt]H*$^+$*,* ***(c)*** *MSMS of m/z = 501.2208 assigned to [diN-Ac-Tyr-OEt]H*$^+$ *and* ***(d)*** *MSMS of m/z = 501.2213 assigned to [diN-Ac-Tyr-OEt]H*$^+$ *with structures difficult to precisely defined by high resolution MS*

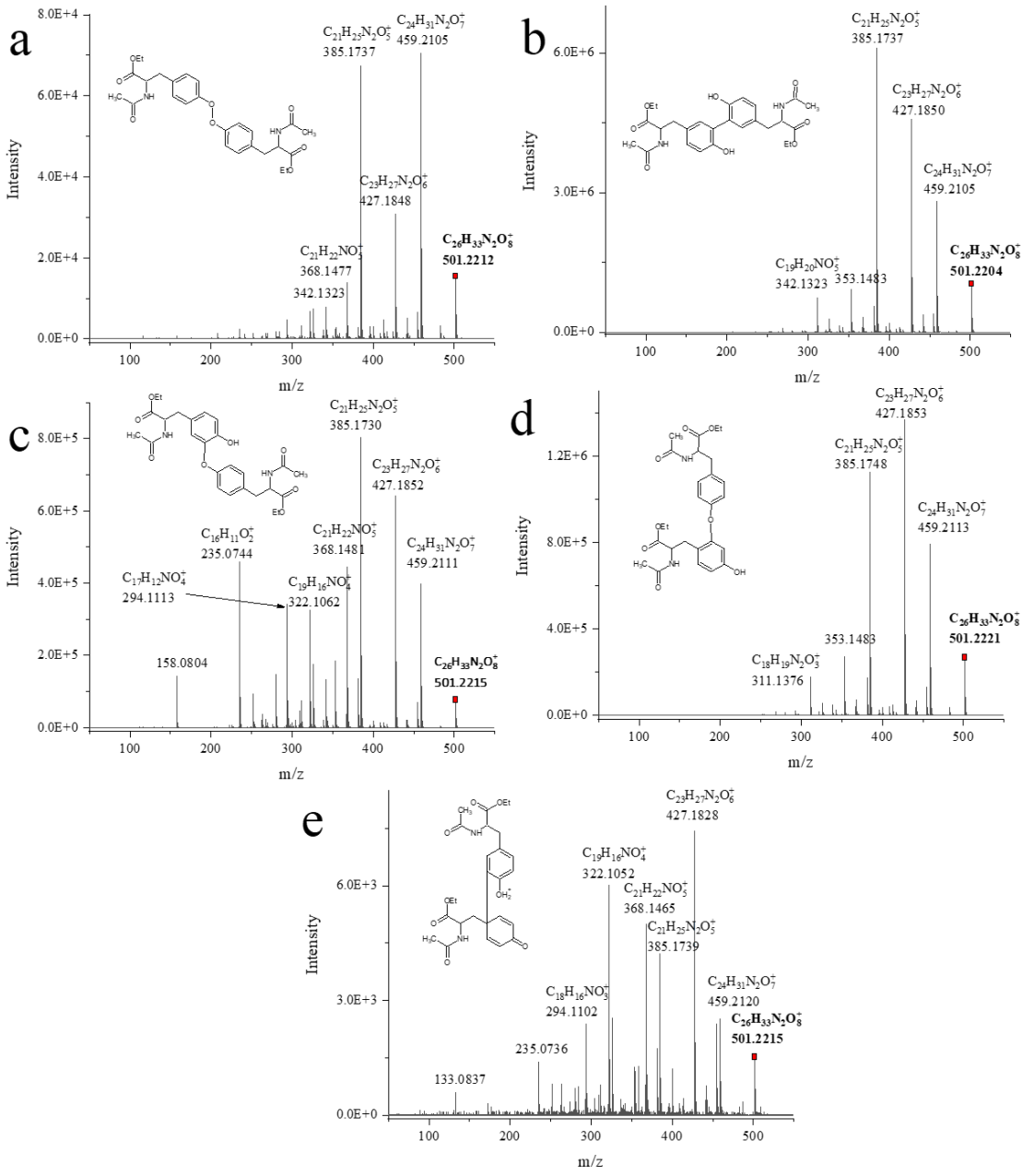

Figure TYR.SI10 *MS/MS spectra of products **6**, **7**, **8**, **9,** and **10** derived from N-Ac-Tyr-OEt irradiated with 3CB in aqueous solution, Ar-saturated: **(a)** MSMS of m/z = 501.2212 assigned to [diN-Ac-Tyr-OEt]H$^+$ (with undefined structure), **(b)** MSMS of m/z = 501.2204 assigned to [diN-Ac-Tyr-OEt]H$^+$, **(c)** MSMS of m/z = 501.2215 assigned to [diN-Ac-Tyr-OEt]H$^+$, **(d)** MSMS of m/z = 501.2221 assigned to [diN-Ac-Tyr-OEt]H$^+$, and **(e)** MSMS of m/z = 501.2215 assigned to [diN-Ac-Tyr-OEt]H$^+$ both with undefined structures*

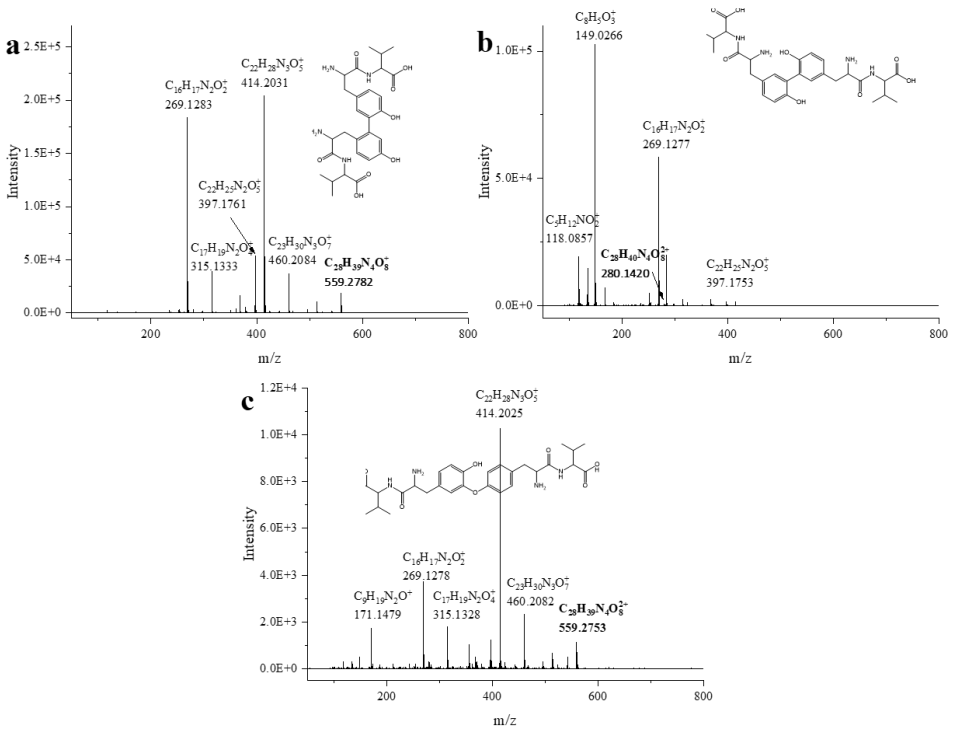

Figure TYR.SI11 *MS/MS spectra of products **7**, **8,** and **12** derived from Tyr-Val irradiated with 3CB in aqueous solution, Ar-saturated: a) MSMS of m/z = 559.2782 assigned to [diTyrVal]H$^+$, **(b)** MSMS of m/z = 280.1420 assigned to [diTyrVal]2H^{2+}, **(c)** MSMS of m/z = 559.2753 assigned to [diTyrVal]H$^+$*

Tryptophan:

Table TRP.SI1 *Gradient elution methods for samples*

Trp		Trp-OEt		N-Ac-Trp		N-Ac-Trp-OMe		Lys-Trp		Trp-Tyr		Ala-Trp-Ala	
time	%B	**time**	%B	**time**	%B	**time**	%B	**time**	%B	**Time**	%B	**time**	%B
-1.00	5	**-1.00**	5	**-1.00**	5	**-1.00**	10	**-1.00**	1	**-1.00**	10	**-1.00**	6
0.00	5	**0.00**	5	**0.00**	5	**0.00**	10	**0.00**	1	**0.00**	10	**0.00**	6
1.00	5	**1.00**	10	**2.00**	20	**2.00**	20	**1.50**	1	**2.00**	10	**3.00**	6
30.00	60	**14.00**	25	**14.00**	20	**14.00**	20	**15.00**	25	**3.00**	12	**4.00**	20
36.00	60	**28.00**	75	**24.00**	40	**24.00**	40	**20.00**	25	**6.00**	12	**15.00**	20
37.00	5	**36.00**	75	**29.00**	60	**29.00**	60	**31.00**	60	**7.00**	14	**18.00**	60
42.00	5	**37.00**	5	**36.00**	60	**36.00**	60	**36.00**	60	**16.00**	14	**28.00**	60
		42.00	5	**37.00**	5	**37.00**	10	**37.00**	1	**18.00**	18	**30.00**	6
				42.00	5	**42.00**	10	**42.00**	1	**20.00**	18	**32.00**	6
										31.00	60		
										36.00	60		
										37.00	10		
										42.00	10		

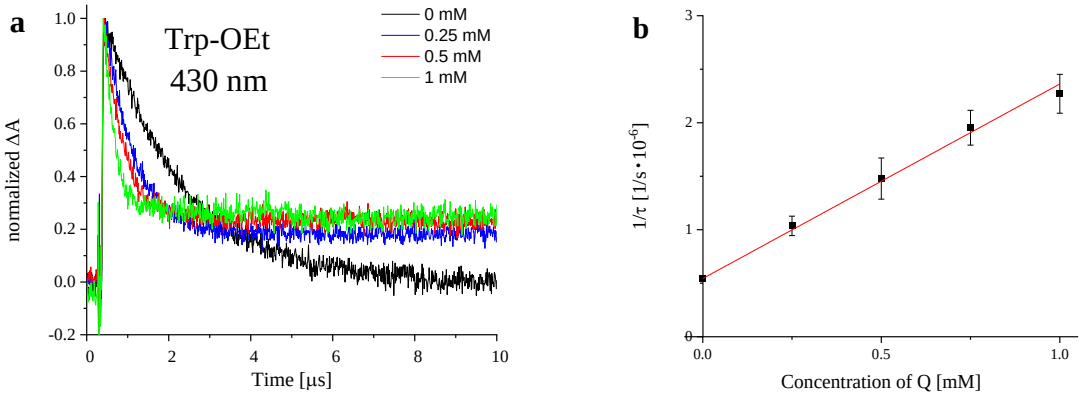

Figure TRP.SI1 ***(a)*** *Kinetic traces for the ^{3}3CB* decay at 430 nm in the presence of varying concentrations of Trp-OEt (0-1 mM) at pH 7* ***(b)*** *The Stern-Volmer plots according to* ***Equation 2*** *for the quenching of ^{3}3CB* by Trp-OEt at pH 7 in aqueous solution for 3CB (4 mM)*

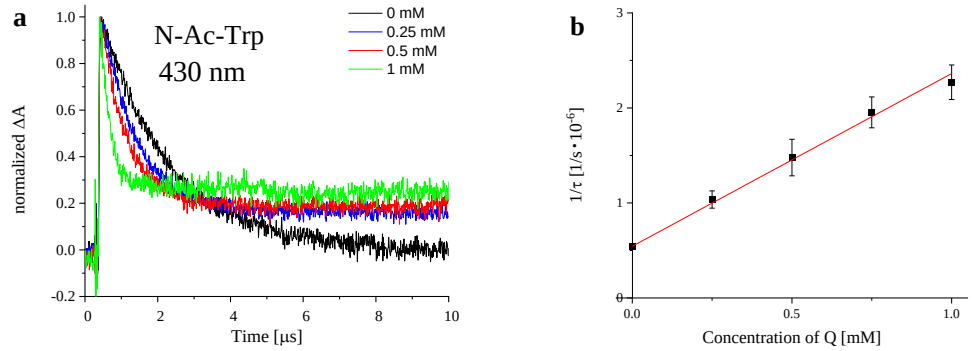

Figure TRP.SI2 ***(a)*** *Kinetic traces for the ^{3}3CB* decay at 430 nm in the presence of varying concentrations of N-Ac-Trp (0-1 mM) at pH 7* ***(b)*** *The Stern-Volmer plots according to* ***Equation 2*** *for the quenching of ^{3}3CB* by N-Ac-Trp at pH 7 in aqueous solution for 3CB (4 mM)*

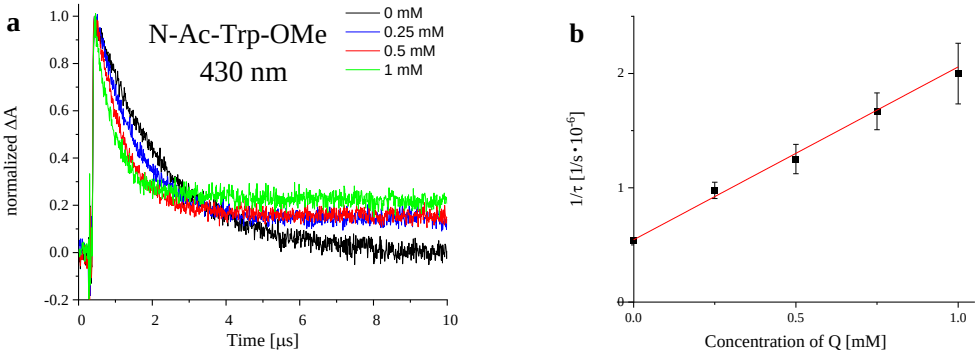

Figure TRP.SI3 ***(a)*** *Kinetic traces for the ^{3}3CB* decay at 430 nm in the presence of varying concentrations of N-Ac-Trp-OMe (0-1 mM) at pH 7* ***(b)*** *The Stern-Volmer plots according to* ***Equation 2*** *for the quenching of ^{3}3CB* by N-Ac-Trp-OMe at pH 7*

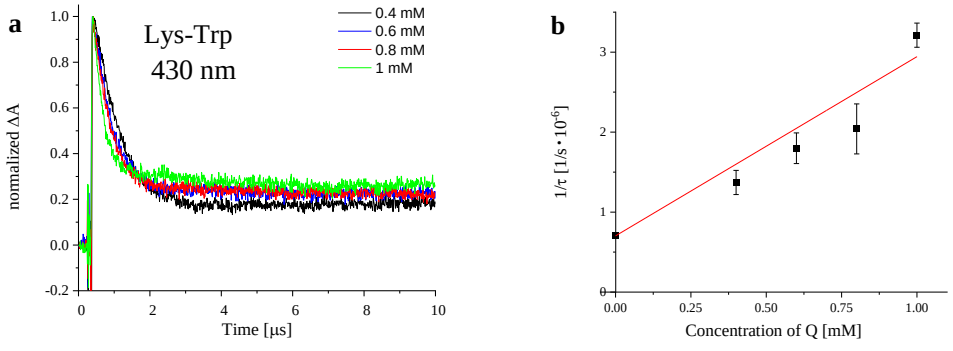

Figure TRP.SI4 ***(a)*** *Kinetic traces for the ^{3}3CB* decay at 430 nm in the presence of varying concentrations of Lys-Trp (0.4-1 mM) at pH 7* ***(b)*** *The Stern-Volmer plots according to* ***Equation 2*** *for the quenching of ^{3}3CB* by Lys-Trp at pH 7*

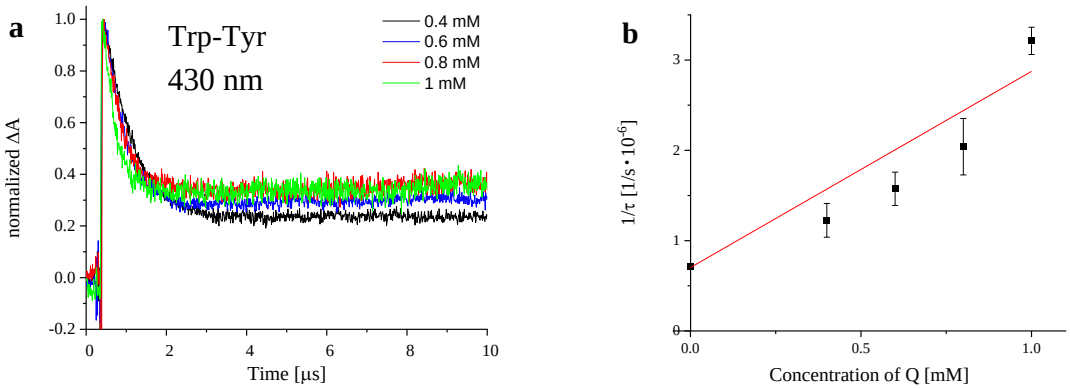

Figure TRP.SI5 ***(a)*** *Kinetic traces for the* ^{3}*3CB* decay at 430 nm in the presence of varying concentrations of Trp-Tyr (0.4-1 mM) at pH 7* ***(b)*** *The Stern-Volmer plots according to* ***Equation 2*** *for the quenching of* ^{3}*3CB* by Trp-Tyr at pH 7*

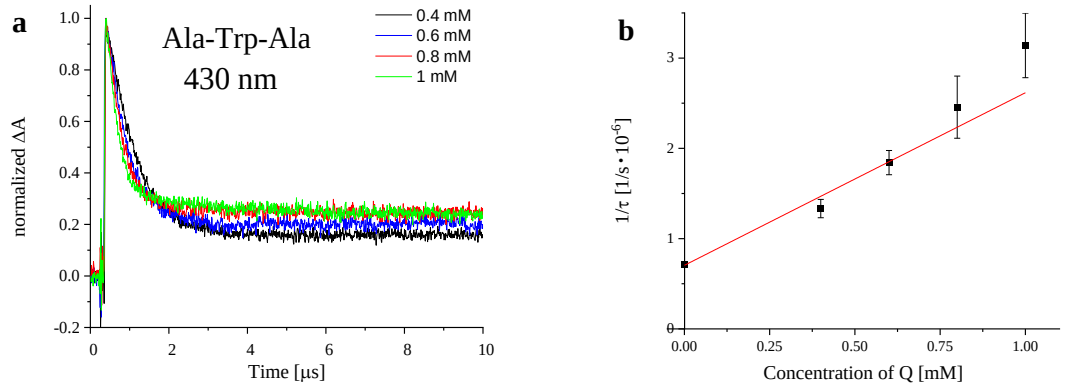

Figure TRP.SI6 ***(a)*** *Kinetic traces for the* ^{3}*3CB* decay at 430 nm in the presence of varying concentrations of Ala-Trp-Ala (0.4-1 mM) at pH 7* ***(b)*** *The Stern-Volmer plots according to* ***Equation 2*** *for the quenching of* ^{3}*CB* by Ala-Trp-Ala at pH 7*

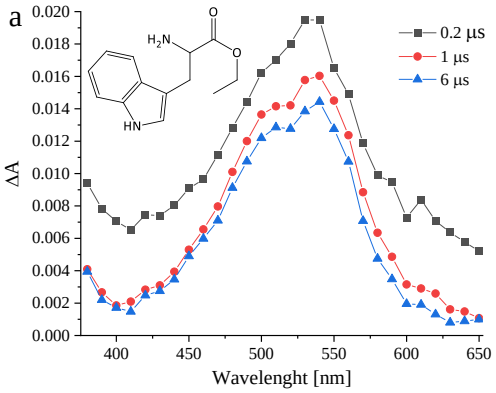
a
0.2 µs
1 µs
6 µs
ΔA
Wavelenght [nm]

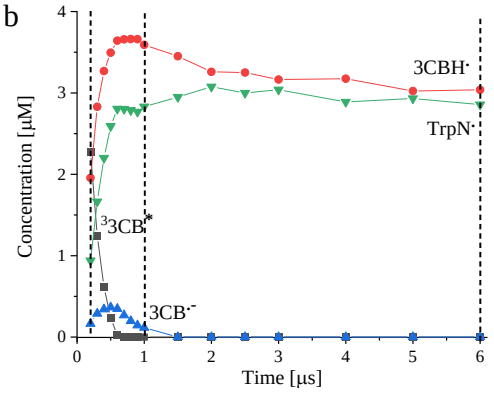
b
3CBH·
TrpN·
3CB*
3CB·⁻
Concentration [µM]
Time [µs]

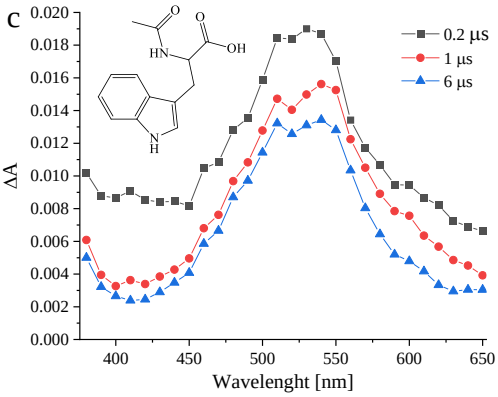
c
0.2 µs
1 µs
6 µs
ΔA
Wavelenght [nm]

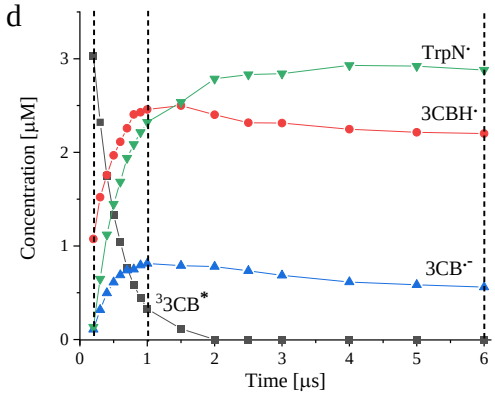
d
TrpN·
3CBH·
3CB·⁻
3CB*
Concentration [µM]
Time [µs]

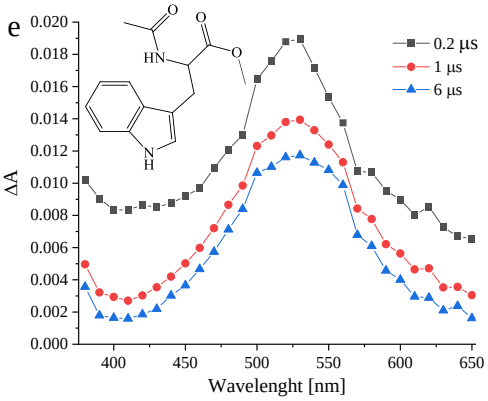
e
0.2 µs
1 µs
6 µs
ΔA
Wavelenght [nm]

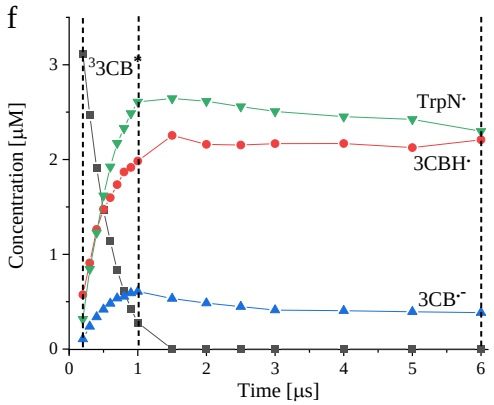
f
3CB*
TrpN·
3CBH·
3CB·⁻
Concentration [µM]
Time [µs]

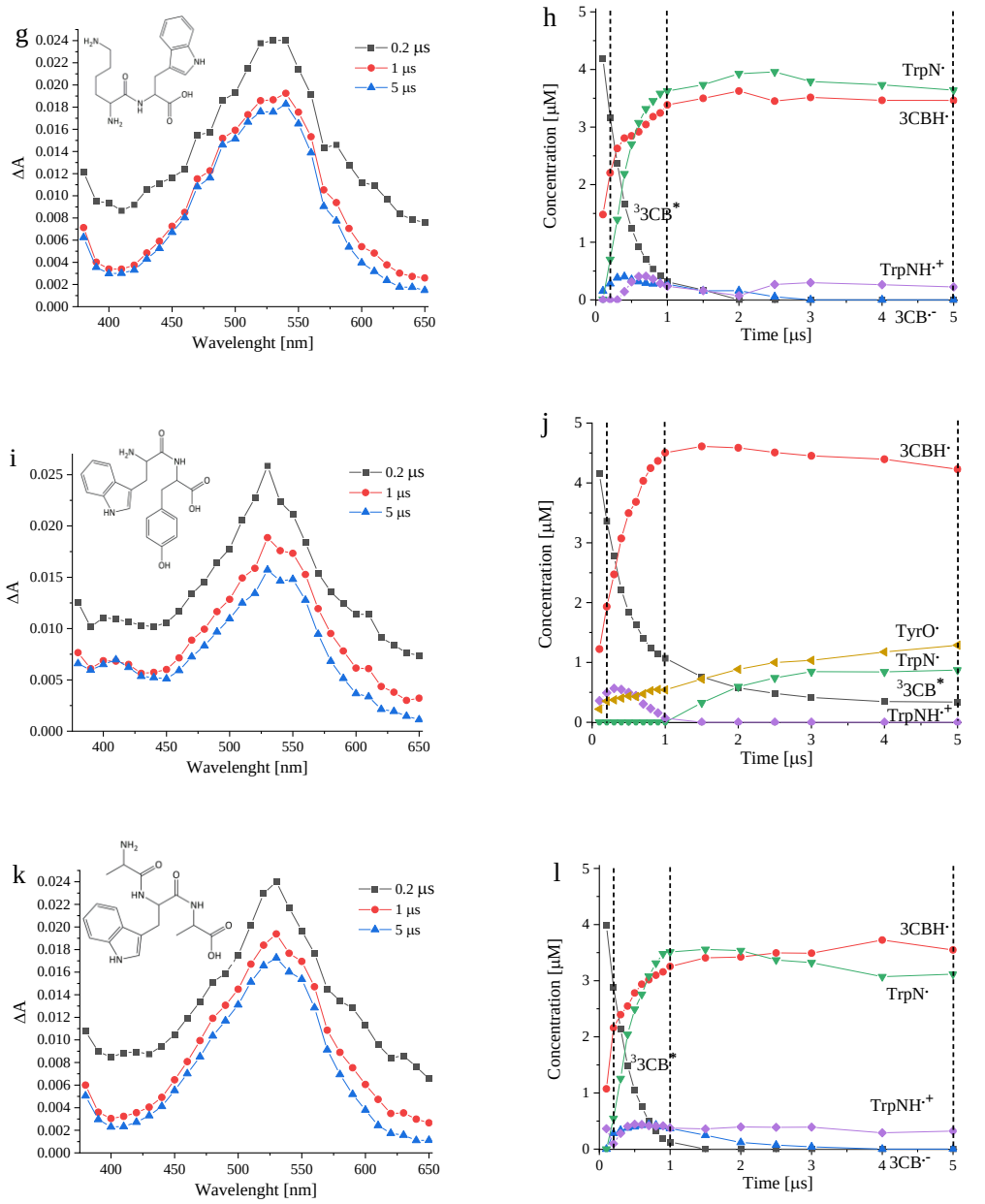

Figure TRP.SI7 *Evolution of transient absorption spectra from 3CB-sensitized oxidation of* ***(a)*** *Trp-OEt;* ***(c)*** *N-Ac-Trp;* ***(e)*** *N-Ac-Trp-OMe;* ***(g)*** *Lys-Trp;* ***(i)*** *Trp-Tyr;* ***(k)*** *Ala-Trp-Ala all at pH 7. Spectra were recorded at different delays following laser pulse 0.2 (black ■), 1 (red ●), 6 or 5 µs (blue ▲). Concentration profiles of transients identified in the laser flash photolysis of an aqueous solution of* ***(b)*** *Trp-OEt;* ***(d)*** *N-Ac-Trp;* ***(f)*** *N-Ac-Trp-OMe;* ***(h)*** *Lys-Trp;* ***(j)*** *Trp-Tyr;* ***(l)*** *Ala-Trp-Ala (1 mM) and 3CB (4 mM) at pH 7 where (black ■) is ^{3}3CB*, (red ●) is 3CBH$^{\bullet}$, (blue ▲) is 3CB$^{\bullet-}$, (green ▼) is TrpN$^{\bullet}$, (purple ♦) is TrpNH$^{\bullet+}$, and (dark yellow ◀) is TyrO$^{\bullet}$. Dotted lines represent points at which concentrations were measured on spectra represented in respective figure to the left. Dotted lines represent times at which respective spectra were presented in* ***(a)***, ***(c)***, ***(e)***, ***(g)***, ***(i)***, *and* ***(k)***

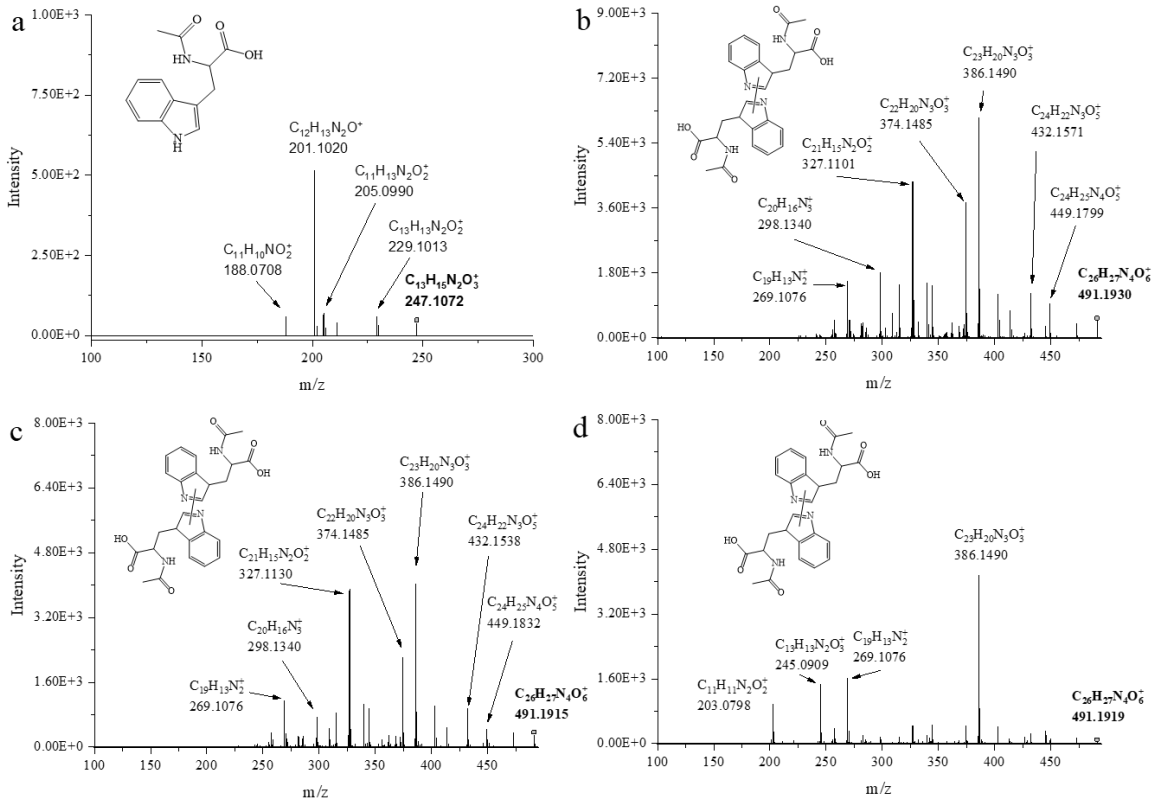

Figure TRP.SI8 *MS/MS spectra of N-Ac-Trp and dimers derived from N-Ac-Trp irradiated with 3CB in aqueous solution, Ar-saturated*

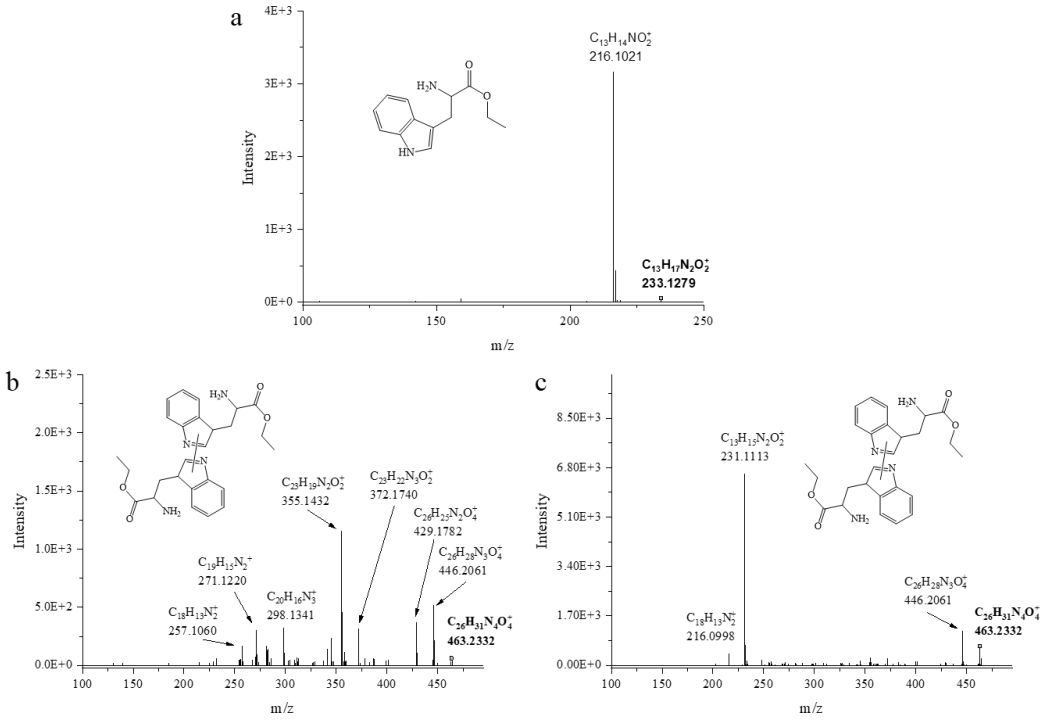

Figure TRP.SI9 *MS/MS spectra of Trp-OEt and dimers derived from Trp-OEt irradiated with 3CB in aqueous solution, Ar-saturated*

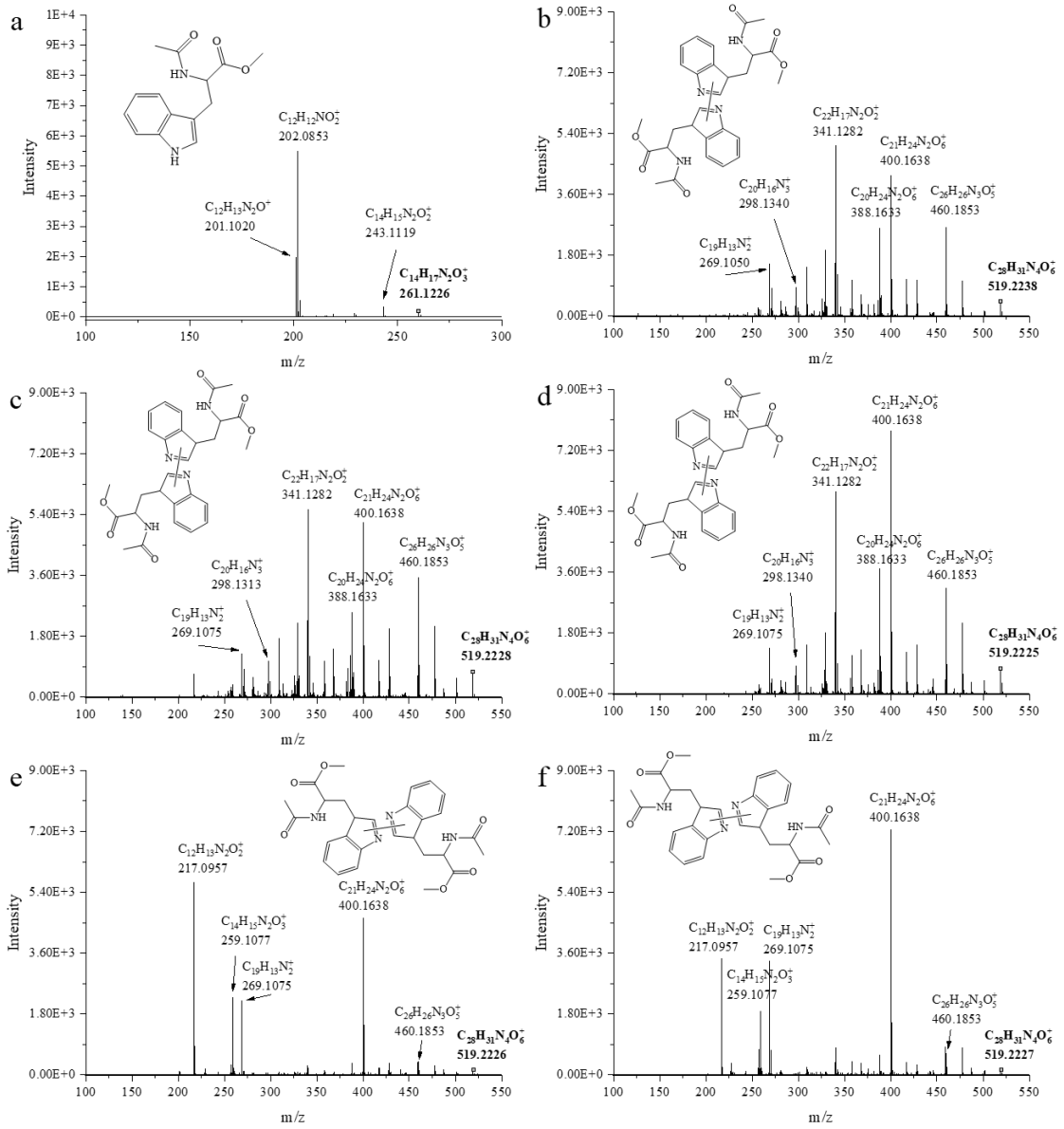

Figure TRP.SI10 *MS/MS spectra of N-Ac-Trp-OMe and dimers derived from N-Ac-Trp-OMe irradiated with 3CB in aqueous solution, Ar-saturated*

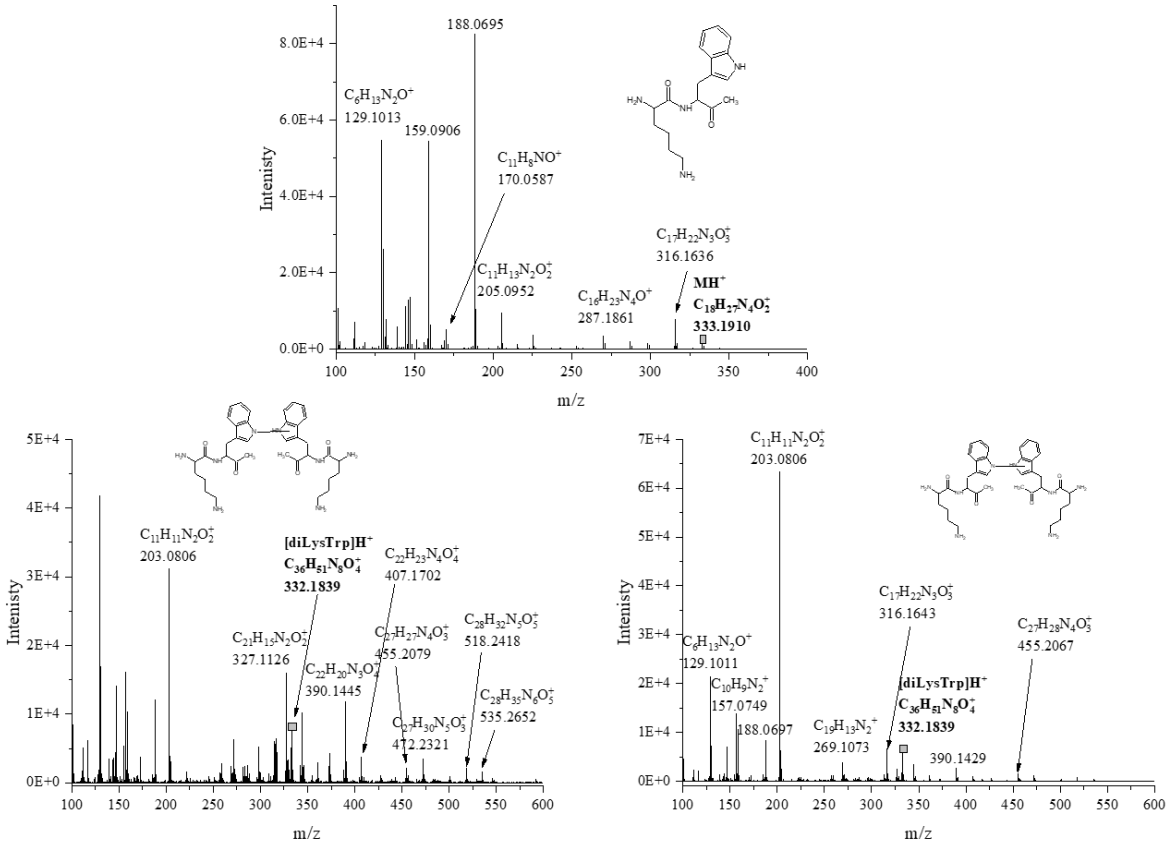

Figure TRP.SI11 *MS/MS spectra of Lys-Trp and dimers derived from Lys-Trp irradiated with 3CB in aqueous solution, Ar-saturated*

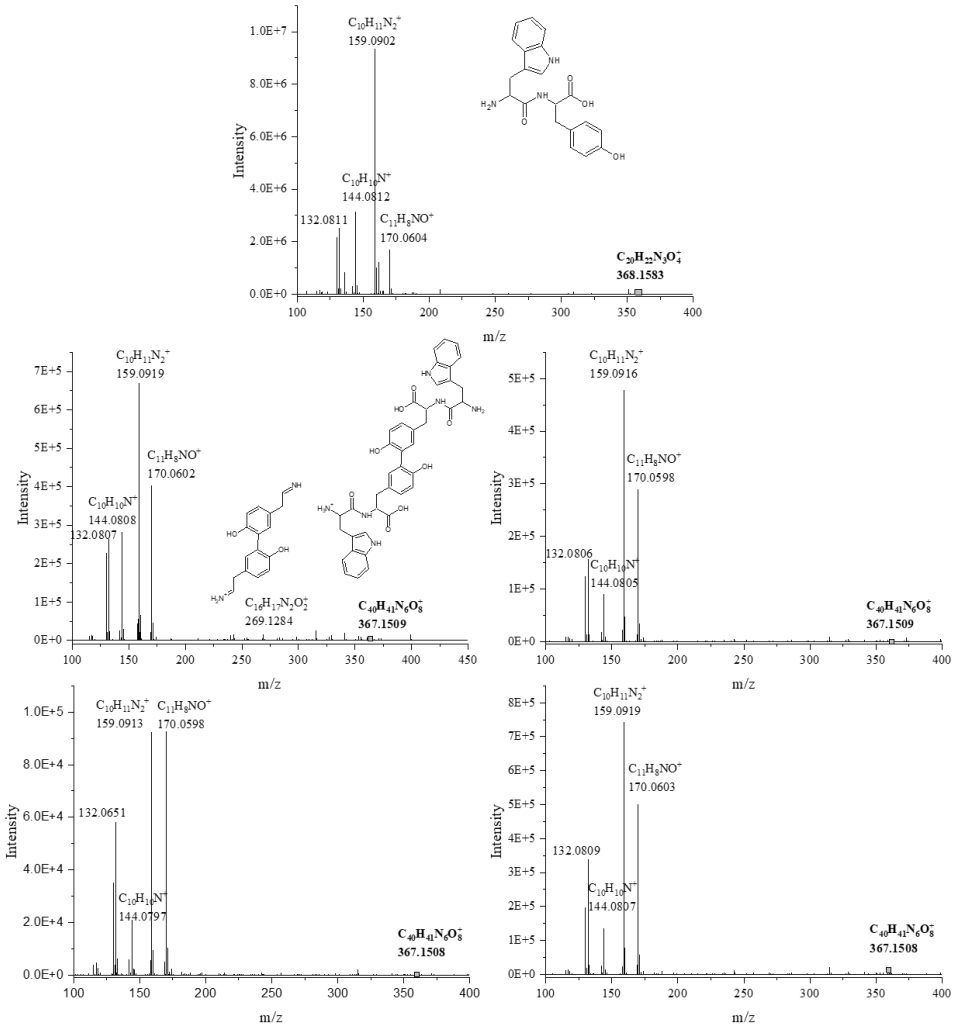

Figure TRP.SI12 *MS/MS spectra of Trp-Tyr dimers derived from Trp-Tyr irradiated with 3CB in aqueous solution, Ar-saturated*

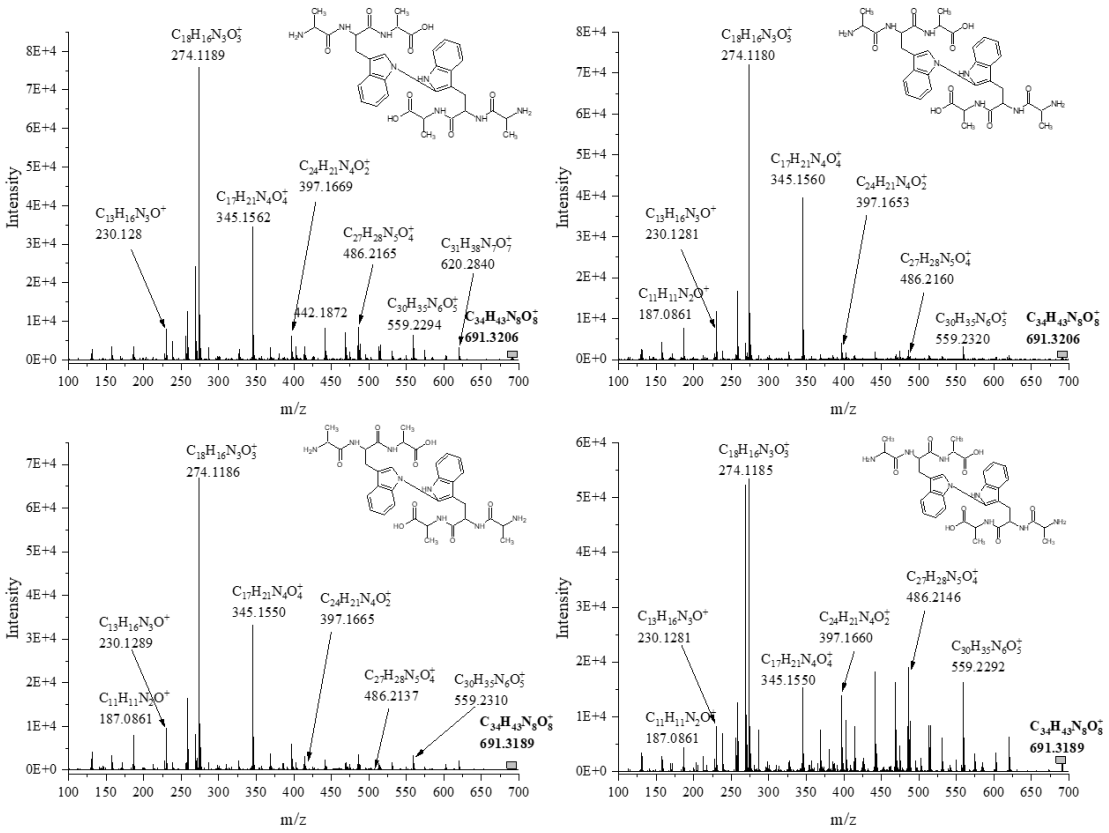

Figure TRP.SI13 *MS/MS spectra of various dimeric products derived from Ala-Trp-Ala irradiated with 3CB in aqueous solution, Ar-saturated*

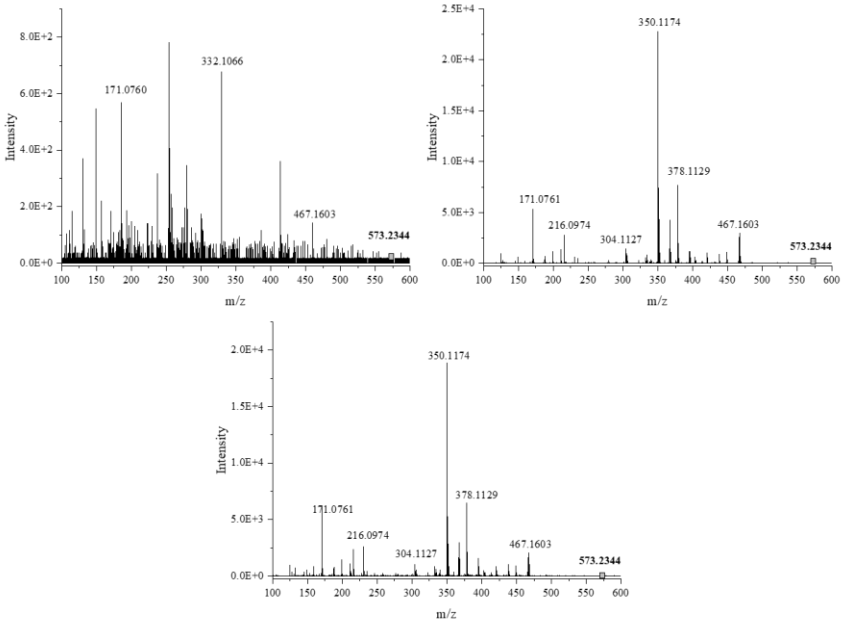

Figure TRP.SI14 *MS/MS spectra of various covalent adducts of 3CB and Ala-Trp-Ala derived from Ala-Trp-Ala irradiated with 3CB in aqueous solution, Ar-saturated*

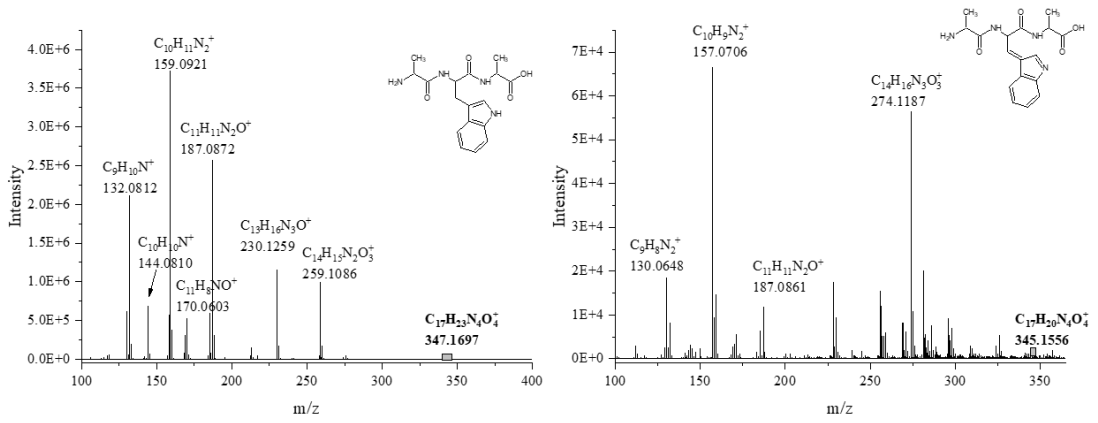

Figure TRP.SI15 *MS/MS spectra of Ala-Trp-Ala and Ala-Trp-Ala(-2H) derived from Ala-Trp-Ala irradiated with 3CB in aqueous solution, Ar-saturated*

Histidine:

Table HIS.SI1 *Gradient elution methods for samples*

His; 1-Me-His		**His-OMe; His-NH_2; N-Ac-His**		**Ala-His; His-Ala; His-Phe; Gly-His-Gly**	
time	%B	**time**	%B	**time**	%B
-1.00	1	**-1.00**	1	**-1.00**	2
0.00	1	**0.00**	1	**0.00**	2
1.50	1	**1.50**	1	**3.00**	15
5.00	12	**15.00**	25	**8.00**	15
15.00	25	**25.00**	25	**10.00**	90
25.00	25	**30.00**	40	**22.00**	2
30.00	40	**31.00**	60	**25.00**	2
31.00	60	**36.00**	60		
36.00	60	**37.00**	1		
37.00	1	**42.00**	1		
42.00	1				

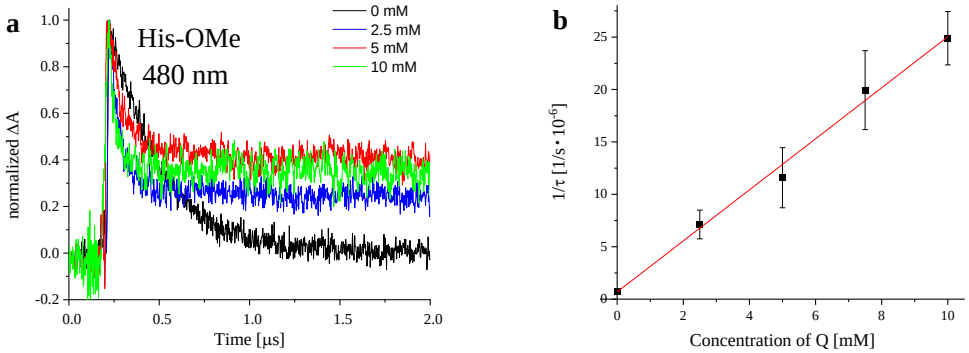

Figure HIS.SI1 ***(a)*** *Kinetic traces for the ^{3}3CB* decay at 480 nm in the presence of varying concentrations of His-OMe at pH 7* ***(b)*** *The Stern-Volmer plots according to* ***Equation 2*** *for the quenching of ^{3}3CB* by His-OMe at pH 7 in aqueous solution for 3CB (5 mM)*

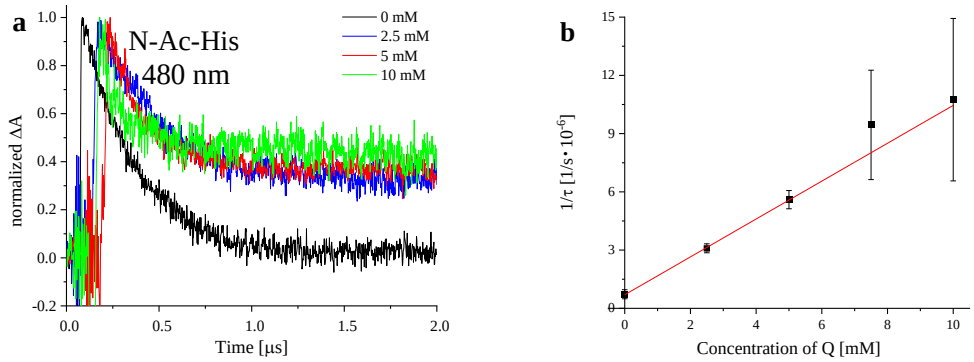

Figure HIS.SI2 ***(a)*** *Kinetic traces for the ^{3}3CB* decay at 480 nm in the presence of varying concentrations of N-Ac-His at pH 7* ***(b)*** *The Stern-Volmer plots according to* ***Equation 2*** *for the quenching of ^{3}3CB* by N-Ac-His at pH 7 in aqueous solution for 3CB (5 mM)*

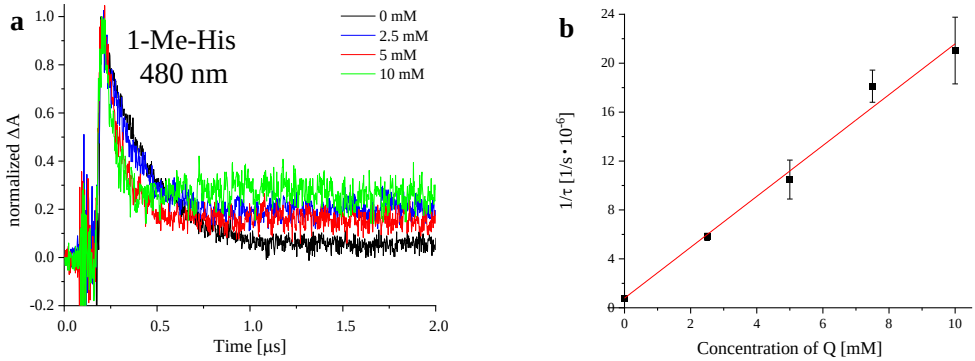

Figure HIS.SI3 ***(a)*** *Kinetic traces for the ^{3}3CB* decay at 480 nm in the presence of varying concentrations of 1-Me-His at pH 7* ***(b)*** *The Stern-Volmer plots according to* ***Equation 2*** *for the quenching of ^{3}3CB* by 1-Me-His at pH 7 in aqueous solution for 3CB (5 mM)*

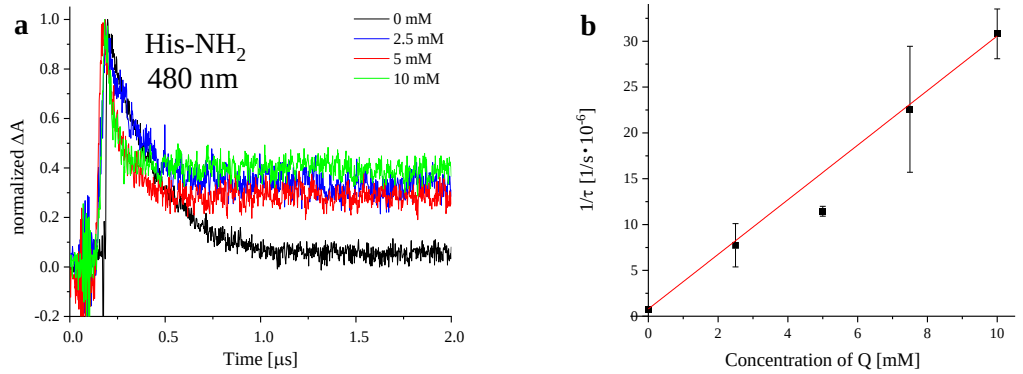

Figure HIS.SI4 ***(a)*** *Kinetic traces for the ^{3}3CB* decay at 480 nm in the presence of varying concentrations of His-NH_2 at pH 7* ***(b)*** *The Stern-Volmer plots according to* ***Equation 2*** *for the quenching of ^{3}3CB* by His-NH_2 at pH 7 in aqueous solution for 3CB (5 mM)*

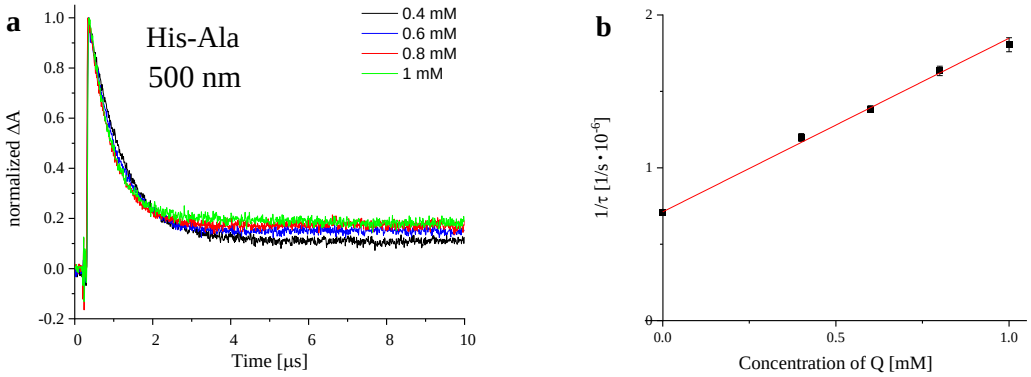

Figure HIS.SI5 ***(a)*** *Kinetic traces for the ^{3}3CB* decay at 500 nm in the presence of varying concentrations of His-Ala at pH 7* ***(b)*** *The Stern-Volmer plots according to* ***Equation 2*** *for the quenching of ^{3}3CB* by His-Ala at pH 7 in aqueous solution for 3CB (5 mM)*

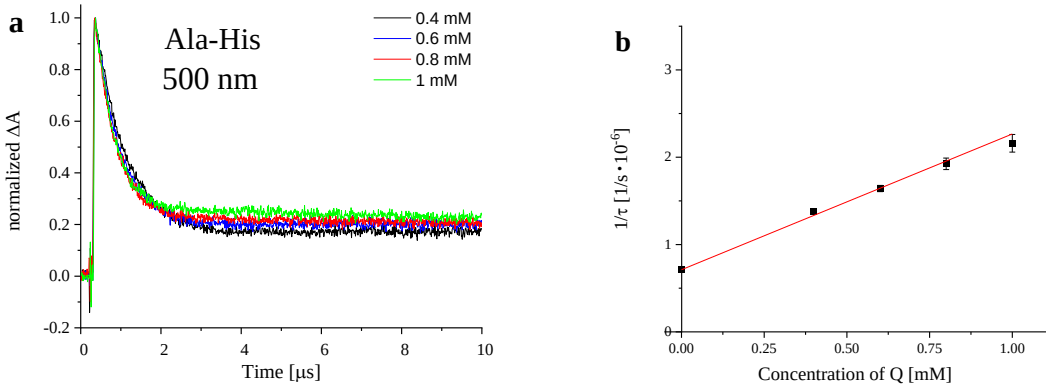

Figure HIS.SI6 ***(a)*** *Kinetic traces for the ^{3}3CB* decay at 500 nm in the presence of varying concentrations of Ala-His at pH 7* ***(b)*** *The Stern-Volmer plots according to* ***Equation 2*** *for the quenching of ^{3}3CB* by Ala-His at pH 7 in aqueous solution for 3CB (5 mM)*

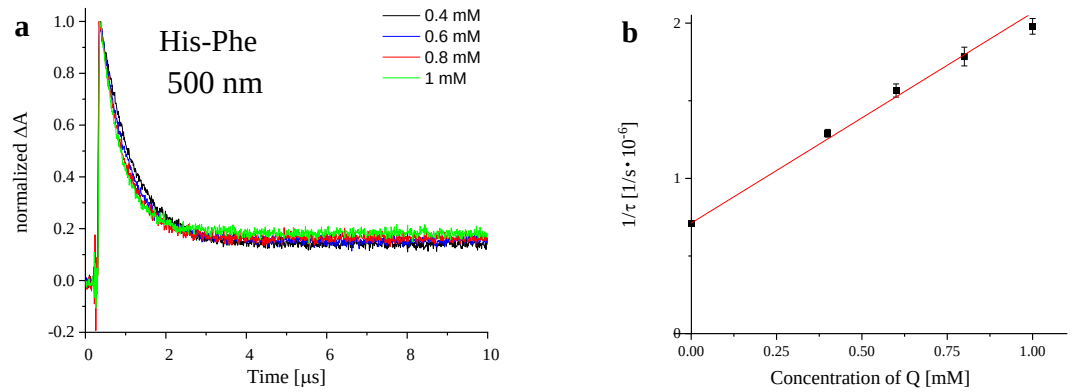

Figure HIS.SI7 ***(a)*** *Kinetic traces for the ^{3}3CB* decay at 500 nm in the presence of varying concentrations of His-Phe at pH 7* ***(b)*** *The Stern-Volmer plots according to* ***Equation 2*** *for the quenching of ^{3}3CB* by His-Phe at pH 7 in aqueous solution for 3CB (5 mM)*

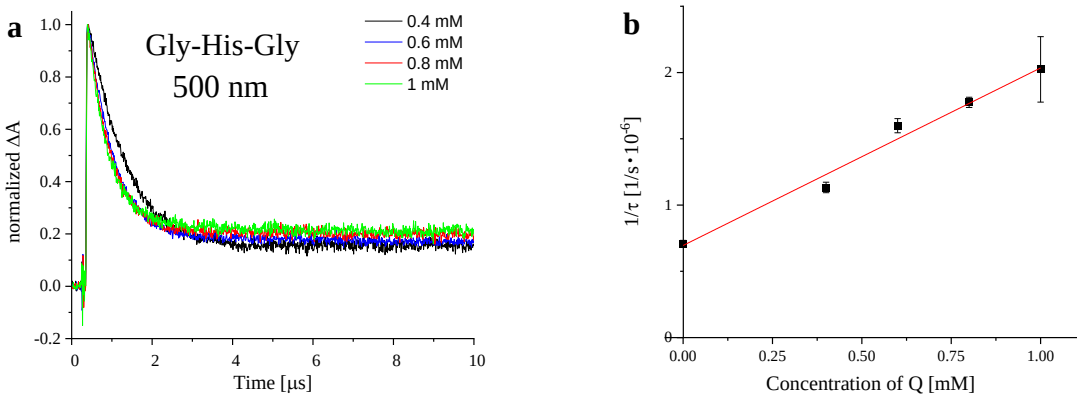

Figure HIS.SI8 ***(a)*** *Kinetic traces for the ^{3}3CB* decay at 500 nm in the presence of varying concentrations of Gly-His-Gly at pH 7* ***(b)*** *The Stern-Volmer plots according to* ***Equation 2*** *for the quenching of ^{3}CB* by Gly-His-Gly at pH 7 in aqueous solution for 3CB (5 mM)*

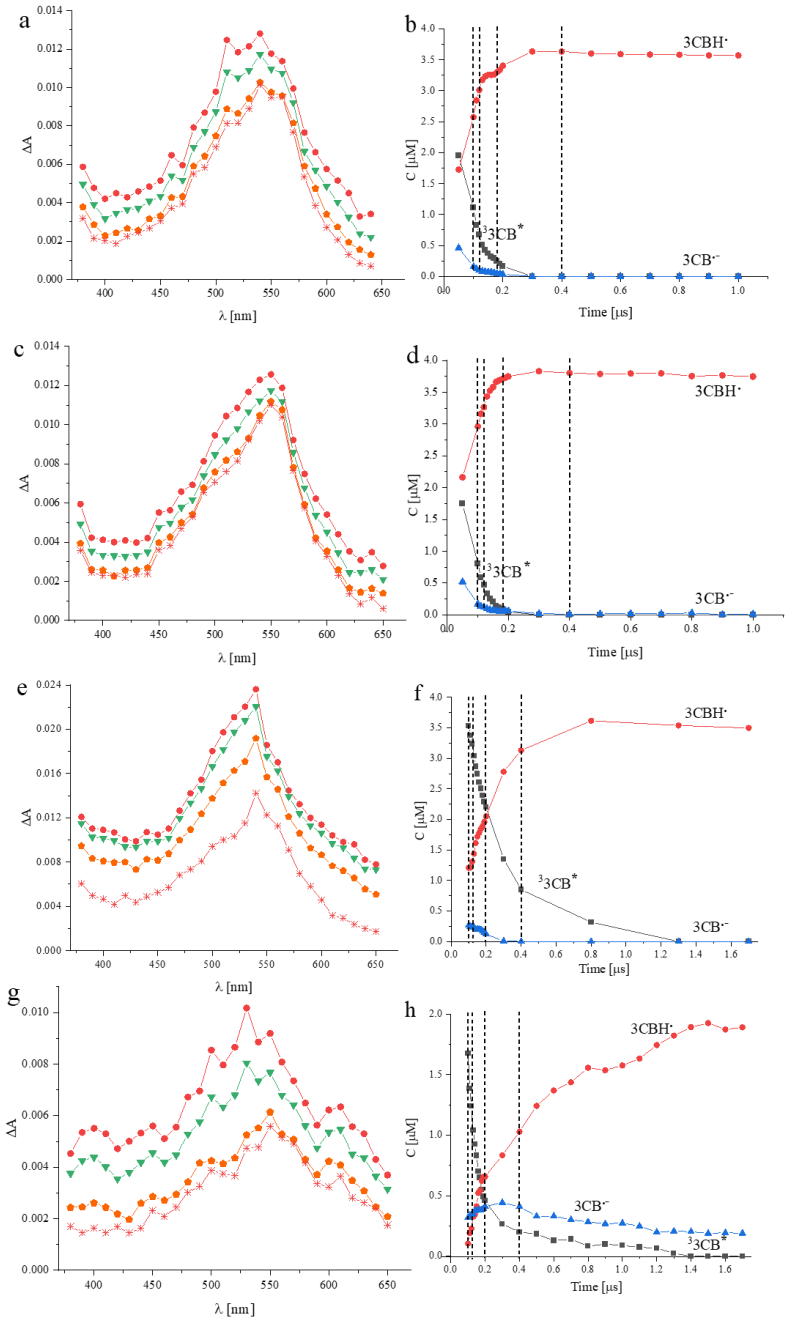

Figure HIS.SI9 *Transient absorption spectra recorded for* ***(a)*** *His-OMe (10 mM),* ***(c)*** *His-NH₂ (10 mM),* ***(e)*** *N-Ac-His (10 mM),* ***(g)*** *1-Me-His (10 mM) and 3CB (5 mM) at pH around 7 in aqueous solution, Ar-saturated: (●) 0.1 μs, (▲) 0.12 μs, (●) 0.18 μs, (*) 0.4 μs after the laser pulse. Concentration profiles for* ***(b)*** *His-OMe,* ***(d)*** *His-NH₂,* ***(f)*** *N-Ac-His, and* ***(h)*** *1-Me-His representing short-lived species used in spectra deconvolution in DECOM software: (▪) ^{3}3CB*, (●) 3CBH·, (▲) 3CB·⁻. Dotted lines represent times at which respective spectra were presented in* ***(a)***, ***(c)***, ***(e)***, *and* ***(g)***

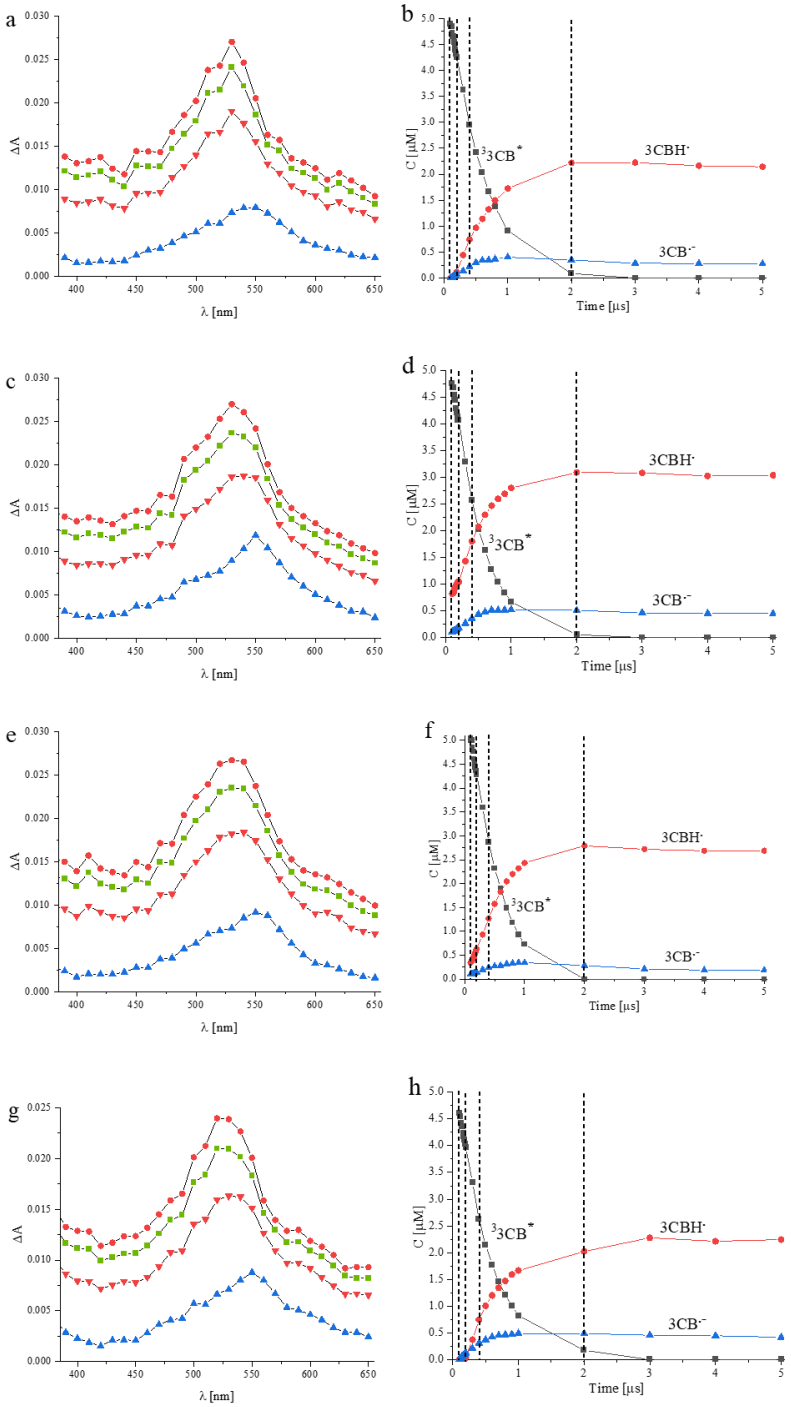

Figure HIS.SI10 *Transient absorption spectra recorded for **(a)** His-Ala (1 mM), **(c)** Ala-His (1 mM), **(e)** His-Phe (1 mM), **(g)** Gly-His-Phe (1 mM) and 3CB (5 mM) at pH around 7 in aqueous solution, Ar-saturated: (●) 0.1 μs, (■) 0.2 μs, (▼) 0.4 μs, (▲) 2.0 μs after the lase pulse. Concentration profiles for **(b)** His-Ala (1 mM), **(d)** Ala-His (1 mM), **(f)** His-Phe (1 mM), **(h)** Gly-His-Phe (1 mM) with short-lived species used in spectra deconvolution in DECOM software: (▪) ^{3}3CB*, (●) 3CBH$^\bullet$, (▲) 3CB$^{\bullet-}$. Dotted lines represent times at which respective spectra were presented in **(a)**, **(c)**, **(e)**, and **(g)***

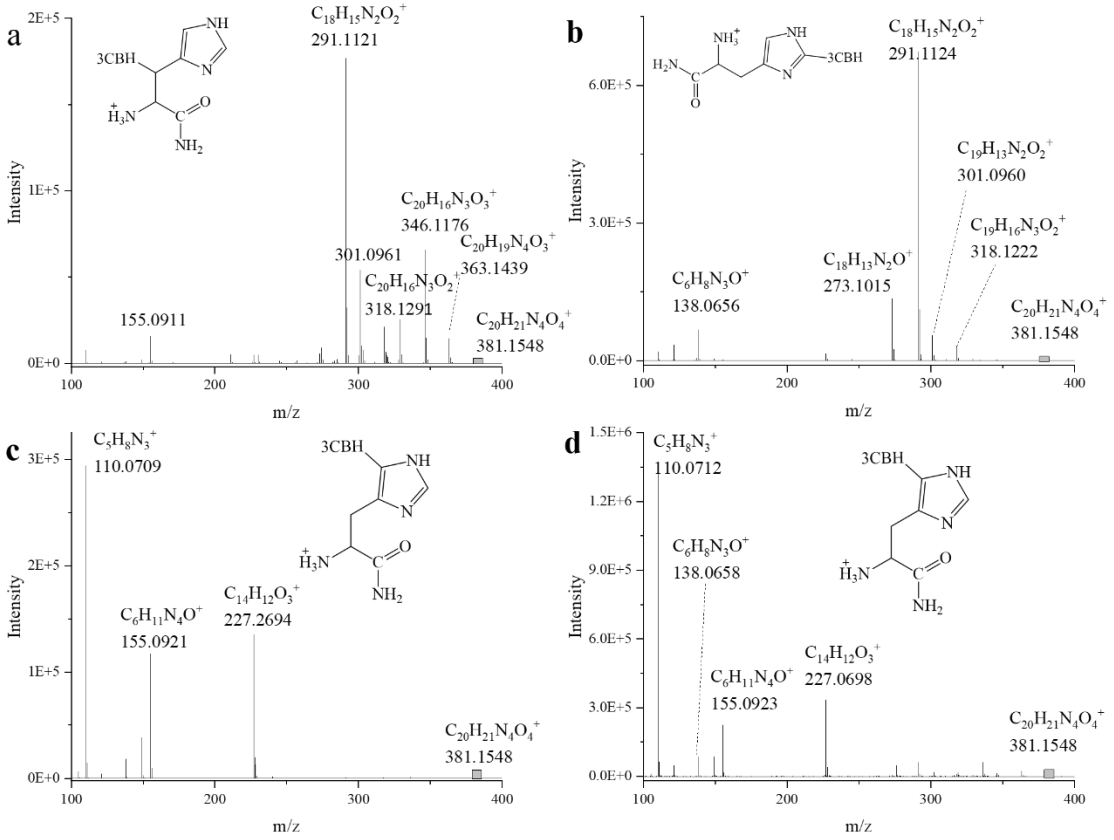

Figure HIS.SI11 *MS/MS spectra of identified [His-NH_2-3CBH]H^+ adducts with m/z 381 (product **7 a-d**)*

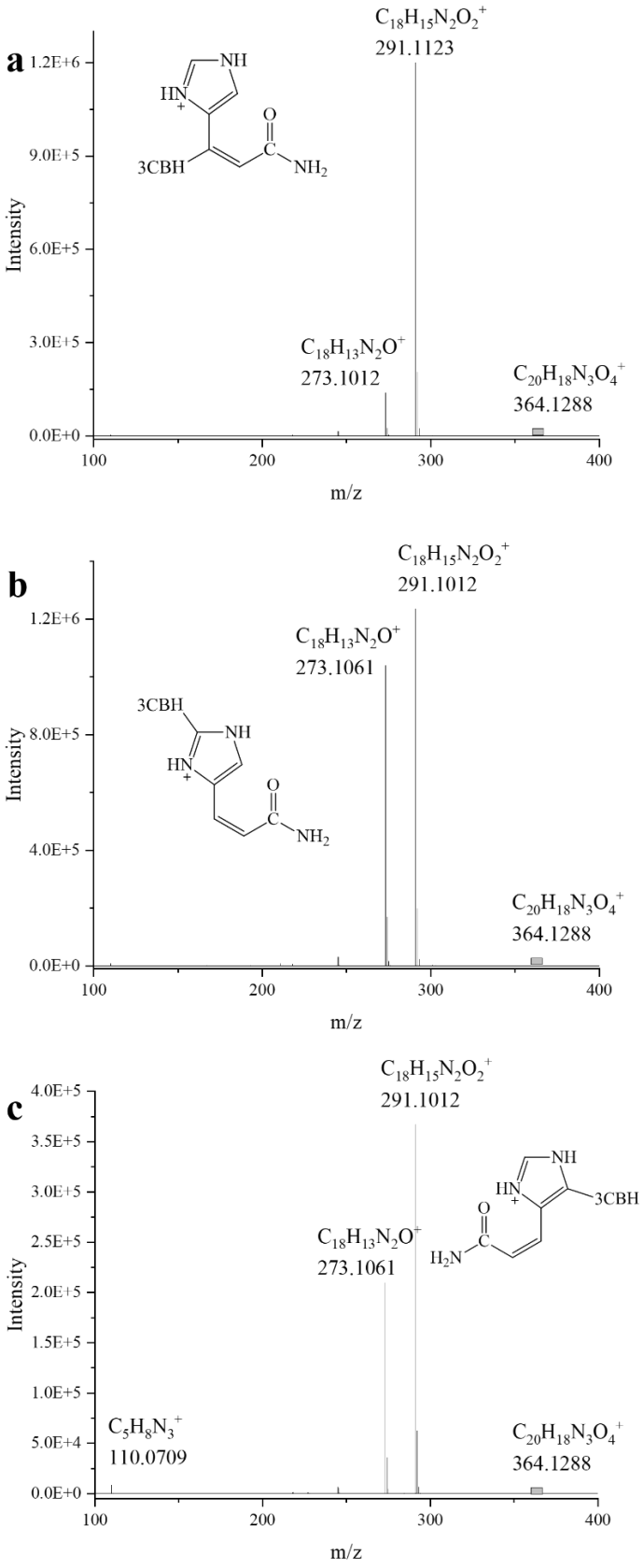

Figure HIS.SI12. *MS/MS spectra of identified [His-NH_2-3CBH$_{-NH2}$]H^+ adducts with m/z 364 (product **8 a-c, Table HIS.2**)*

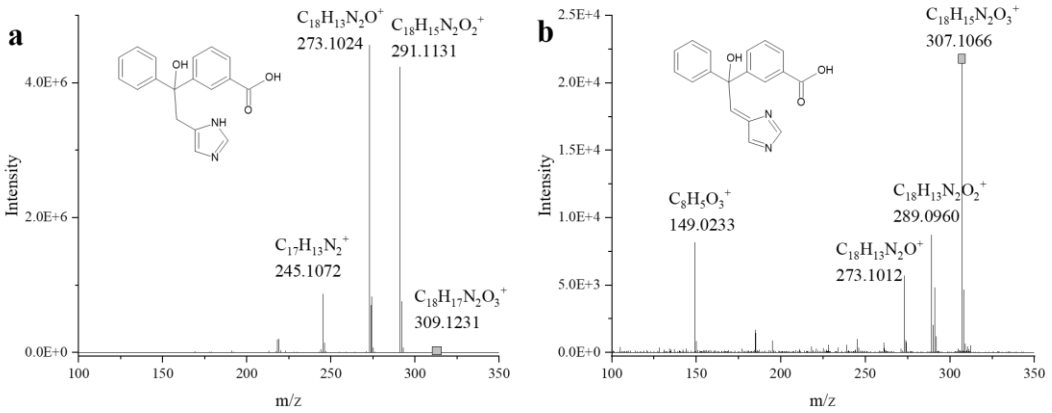

Figure HIS.SI13 *MS/MS spectra of identified products* ***(a)*** *[Im-CH_2-3CBH]H^+ and* ***(b)*** *[Im-CH_2-3CBH-$_{2Da}$]H^+ (product* ***5*** *and* ***6***, ***Table HIS.2*** *respectively) from His-NH_2.*

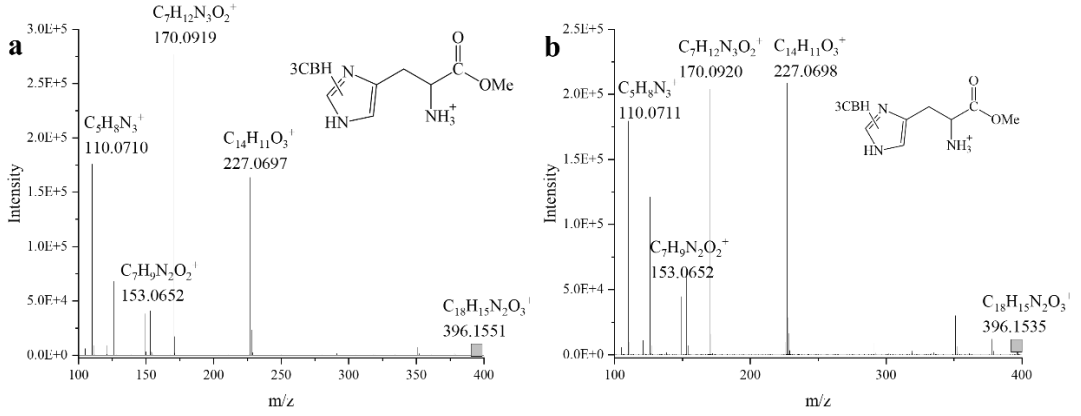

Figure HIS.SI14 *MS/MS spectra of identified His-OMe-3CBH adducts*

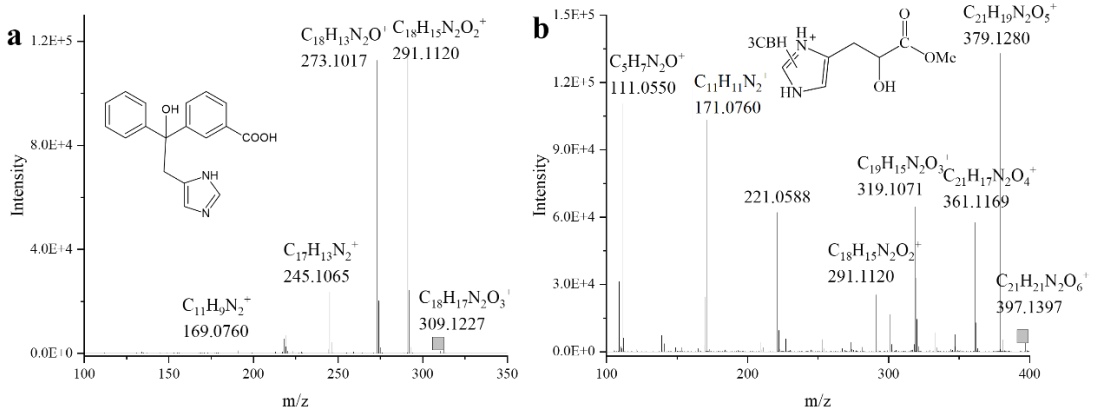

Figure HIS.SI15 *MS/MS spectra of identified products* ***(a)*** *[Im-CH_2-3CBH]H^+ and* ***(b)*** *[His-OMe-3CBH]H^+ identified from His-OMe oxidized in the presence of light and sensitizer (products* ***5*** *and* ***10 a-b****, respectively,* ***Table HIS.2****)*

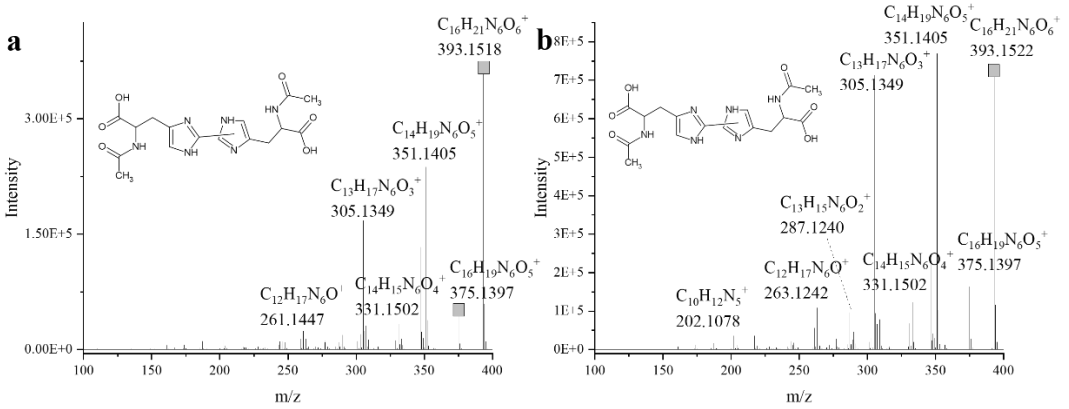

Figure HIS.SI16 *MS/MS spectra of identified [di-N-Ac-His]H$^+$ formed during sensitized oxidation of N-Ac-His (products **11 a-b**, respectively, **Table HIS.2**)*

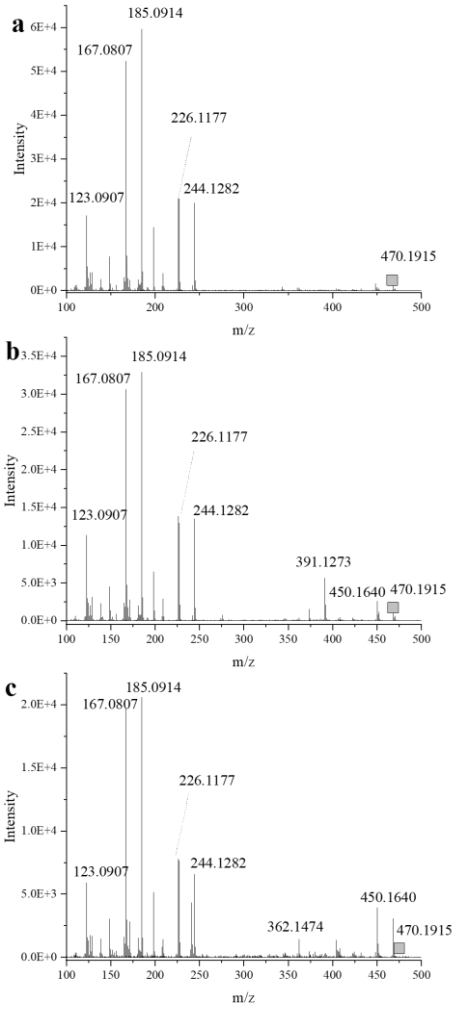

Figure HIS.SI17. *MS/MS spectra of identified products from sensitized photo-oxidation of N-Ac-His. Isomers of adducts between 3CBH$^\bullet$ and N-Ac-HisN$^\bullet$ after loss of ethanol to give [di-N-Ac-His$_{-EtOH}$-3CBH]H$^+$ with different retention time: **(a)** 12.7 min, **(b)** 13.3 min and **(c)** 13.9 min (products **12 a-c**, respectively, **Table HIS.2**)*

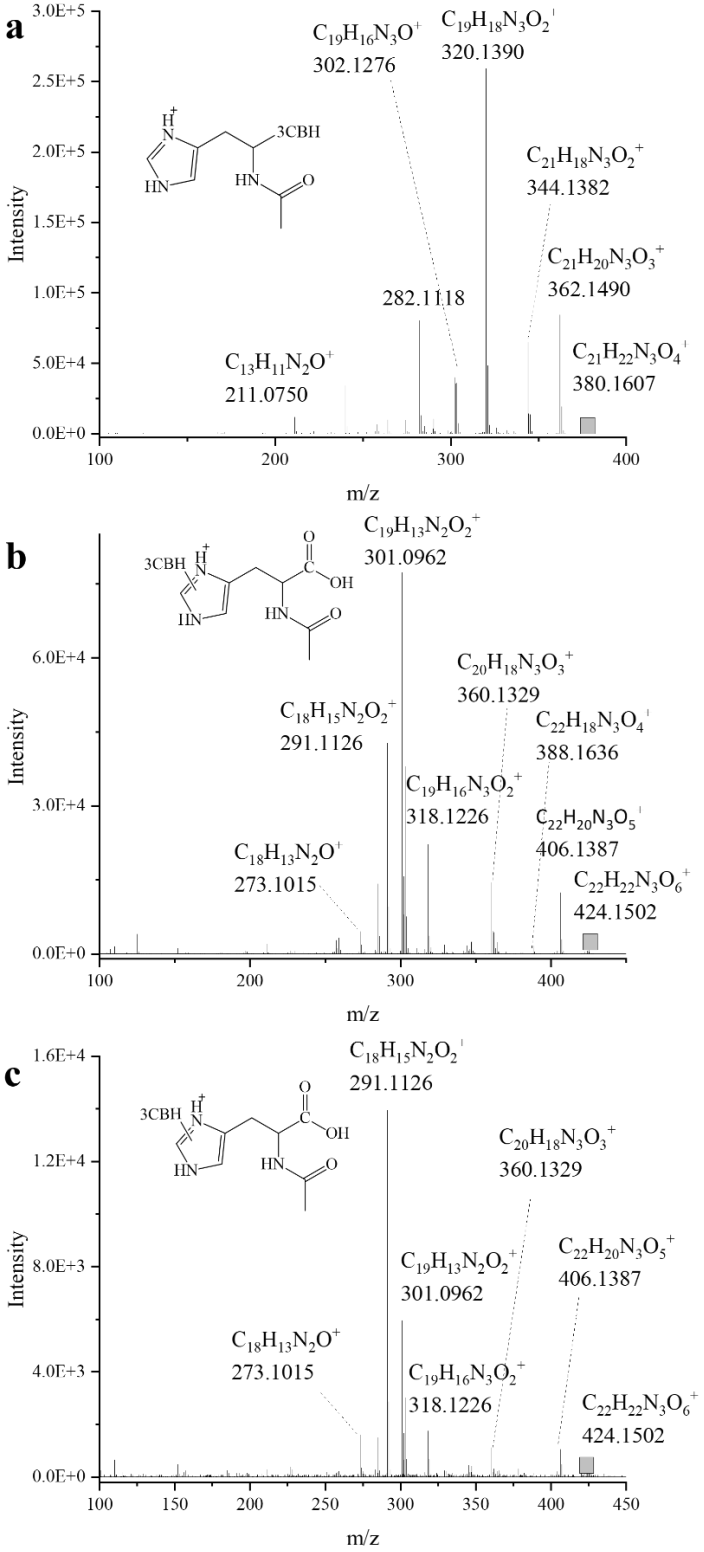

Figure HIS.SI18. *MS/MS spectra of identified CBH-adducts to N-Ac-His formed during sensitized photo-oxidation of N-Ac-His:* ***(a)*** *[N-Ac-His-3CBH$_{-CO2}$]H$^+$,* ***(b)*** *[N-Ac-His-3CBH]H$^+$, and* ***(c)*** *[N-Ac-His-3CBH]H$^+$ (products* ***13****,* ***14 a****, and* ***14 b*** *respectively from* ***Table HIS.2****)*

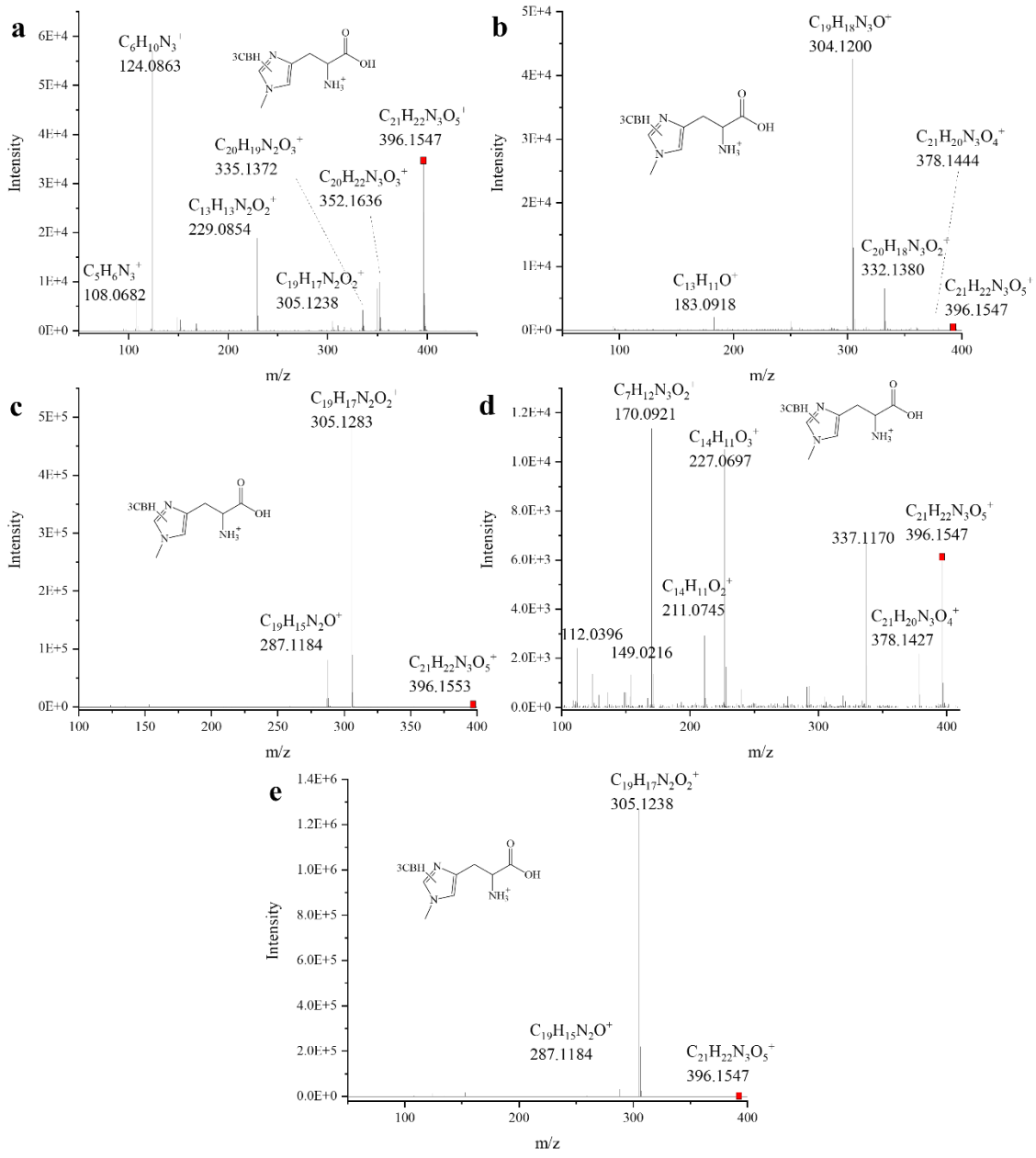

Figure HIS.SI19. *MS/MS spectra of identified 1-Me-His-3CBH adducts formed during sensitized photo-oxidation of 1-Me-His:* ***(a)*** *[1-Me-His-3CBH]H$^+$ with retention time 8.3 min,* ***(b)*** *[1-Me-His-3CBH]H$^+$ with retention time 9.4 min,* ***(c)*** *[1-Me-His-3CBH]H$^+$ with retention time 9.7 min,* ***(d)*** *[1-Me-His-3CBH]H$^+$ with retention time 11.4 min,* ***(e)*** *[1-Me-His-3CBH]H$^+$ with retention time 11.8 min (products* ***15 a-e*** *respectively,* ***Table HIS.2****)*

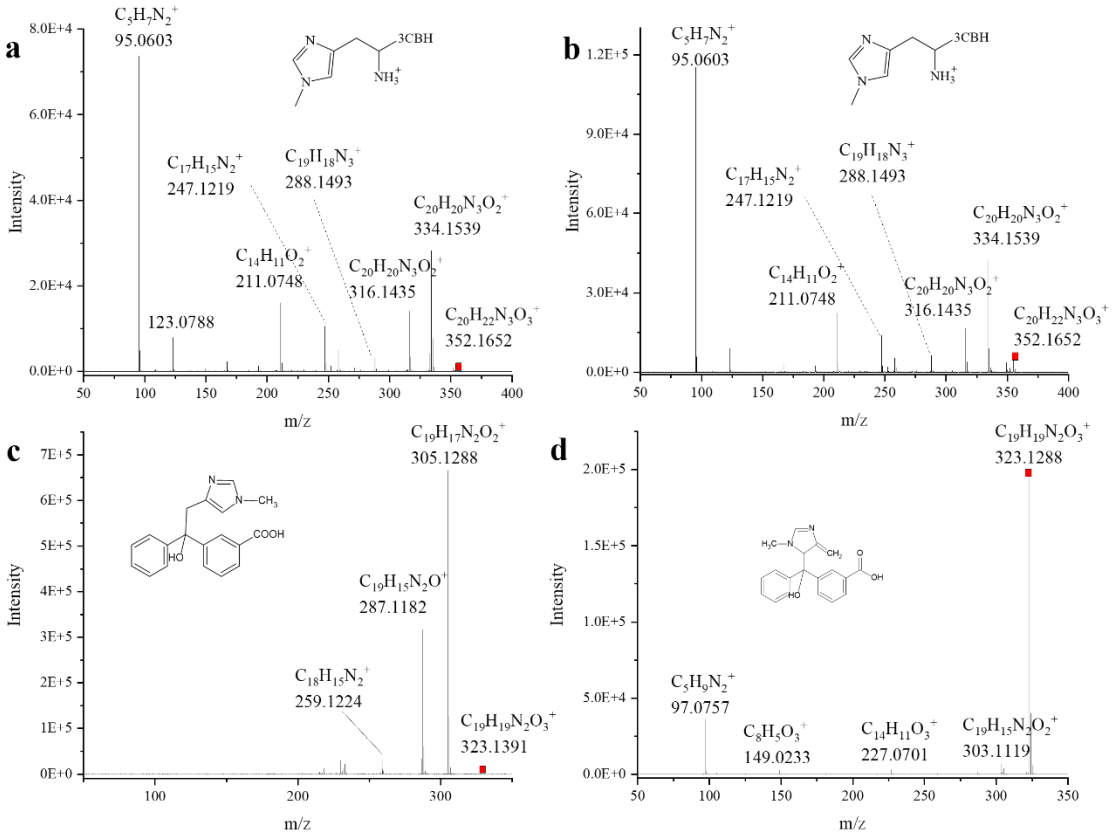

Figure HIS.SI20 *MS/MS spectra of identified 1-Me-His products from sensitized photo-oxidation of 1-Me-His:* ***(a)*** *[1-Me-His-3CBH-$_{CO2}$]H$^+$ with retention time 8.5 min,* ***(b)*** *[1-Me-His-3CBH-$_{CO2}$]H$^+$ with retention time 8.9 min,* ***(c)*** *[1-Me-Im-CH$_2$-3CBH]H$^+$ with retention time 13.2 min,* ***(d)*** *[1-Me-Im-CH$_2$-3CBH]H$^+$ with retention time 14.7 min (products* ***16 a-b*** *and* ***18 a-b****, respectively,* ***Table HIS.2****)*

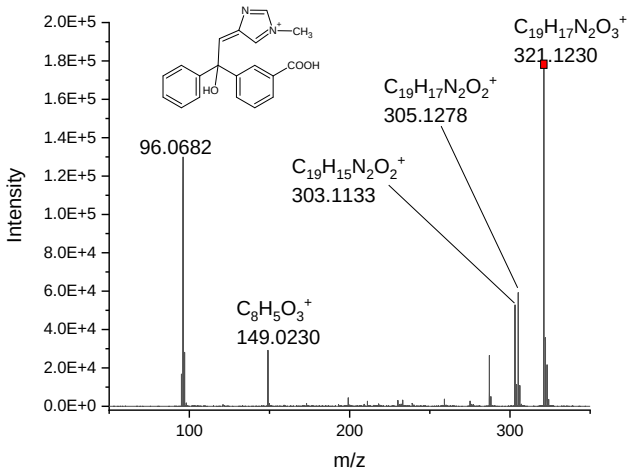

Figure HIS.SI21 *MS/MS spectra of identified [1-Me-Im-$_{2Da}$-CH$_2$-3CBH]H$^+$ derived from photo-oxidation of 1-Me-His in the presence of 3CB* (product* ***19****,* ***Table HIS.2****)*

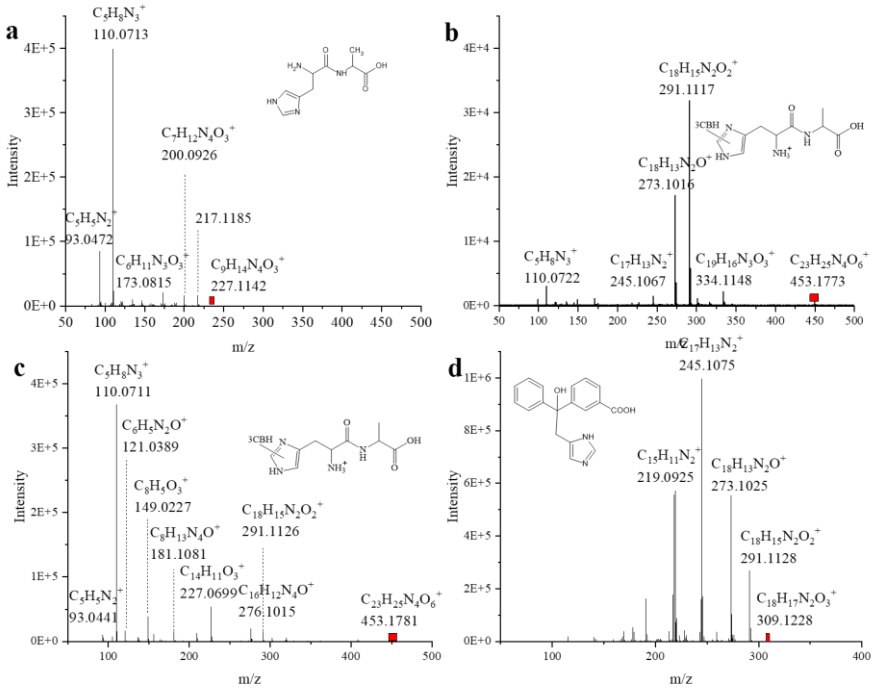

Figure HIS.SI22 *MS/MS spectra of identified products derived from sensitized photo-oxidation of His-Ala:* ***(a)*** *[His-Ala]H$^+$ (product* ***2f****),* ***(b)*** *[His-Ala-3CBH] H$^+$ (product* ***20 a****),* ***(c)*** *[His-Ala-3CBH]H$^+$, (product* ***20 b****) and* ***(d)*** *[Im-CH$_2$-3CBH]H$^+$ (product* ***5****) (****Table HIS.2****)*

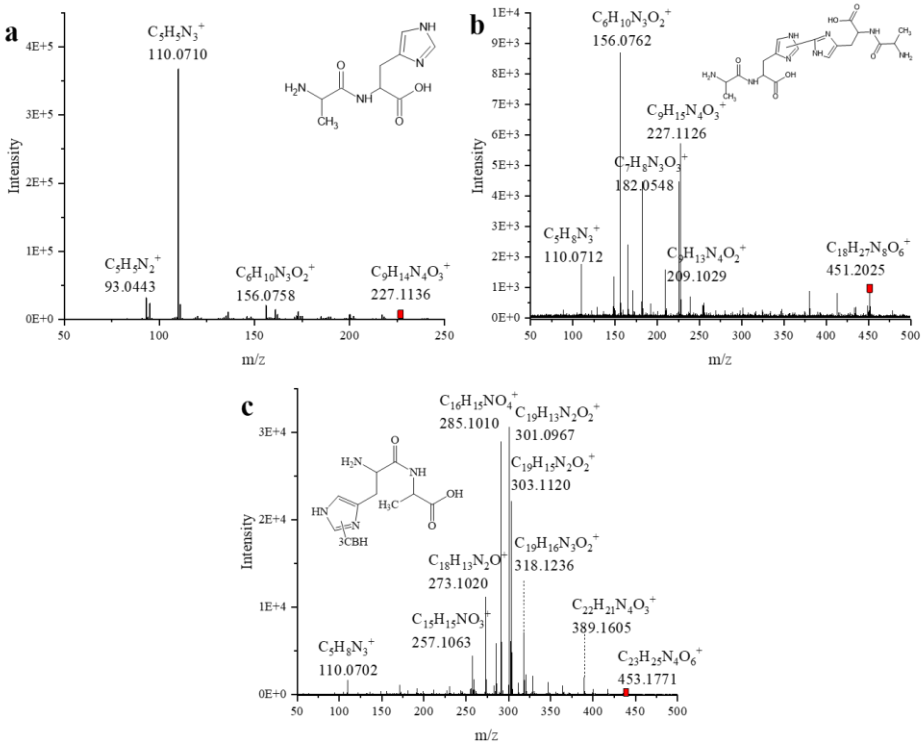

Figure HIS.SI23 *MS/MS spectra of identified products derived from sensitized photo-oxidation of Ala-His:* ***(a)*** *[Ala-His]H$^+$ (product* ***2g****),* ***(b)*** *[di-Ala-His]H$^+$ (product* ***21****),* ***(c)*** *[AlaHis-3CBH]H$^+$(product* ***22****), (****Table HIS.2****)*

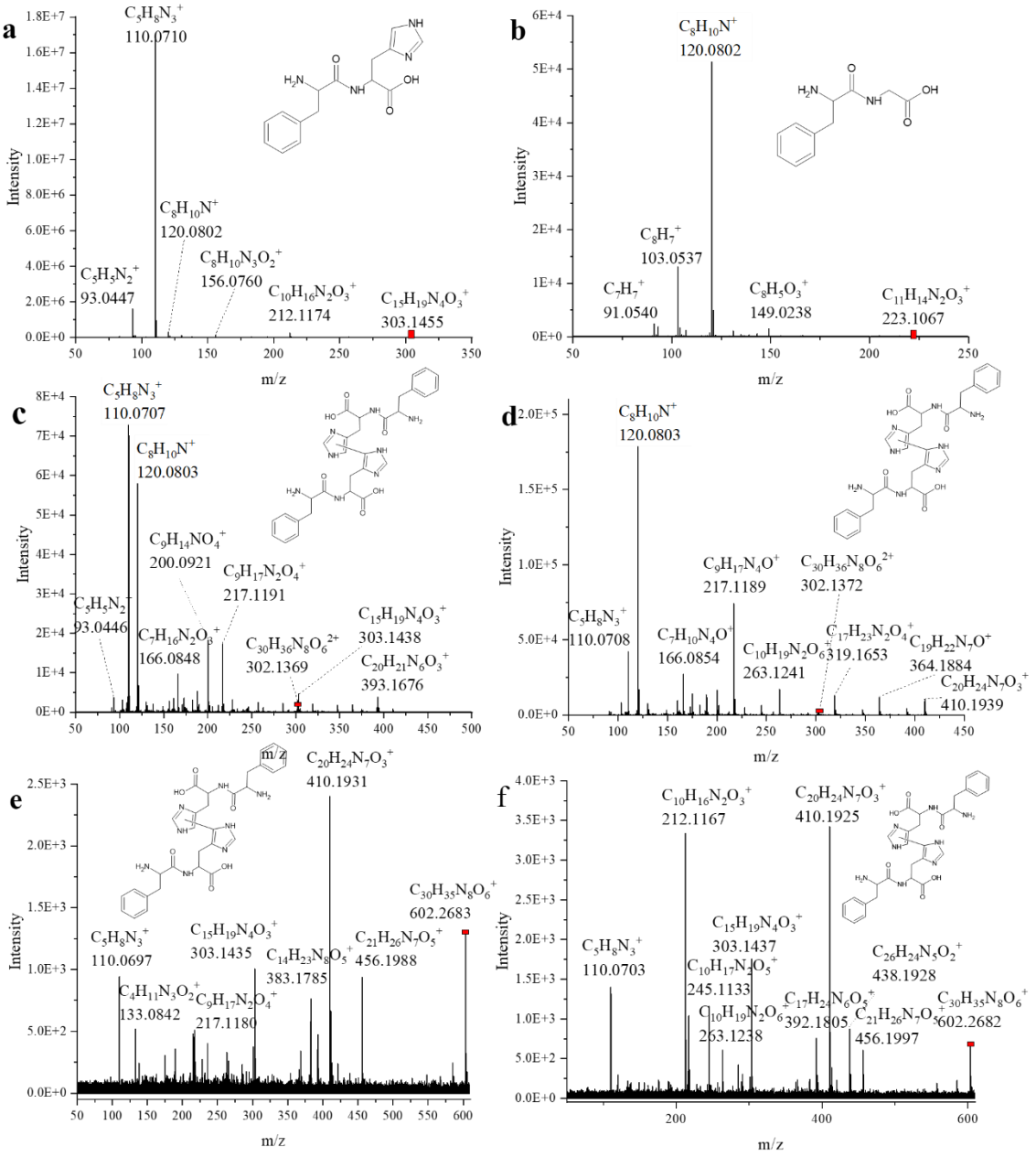
a
$C_5H_8N_3^+$ 110.0710
$C_8H_{10}N^+$ 120.0802
$C_8H_{10}N_3O_2^+$ 156.0760
$C_{10}H_{16}N_2O_3^+$ 212.1174
$C_{15}H_{19}N_4O_3^+$ 303.1455
$C_5H_5N_2^+$ 93.0447
b
$C_8H_{10}N^+$ 120.0802
$C_8H_7^+$ 103.0537
$C_7H_7^+$ 91.0540
$C_8H_5O_3^+$ 149.0238
$C_{11}H_{14}N_2O_3^+$ 223.1067
c
$C_5H_8N_3^+$ 110.0707
$C_8H_{10}N^+$ 120.0803
$C_9H_{14}NO_4^+$ 200.0921
$C_9H_{17}N_2O_4^+$ 217.1191
$C_{15}H_{19}N_4O_3^+$ 303.1438
$C_5H_5N_2^+$ 93.0446
$C_7H_{16}N_2O_3^+$ 166.0848
$C_{30}H_{36}N_8O_6^{2+}$ 302.1369
$C_{20}H_{21}N_6O_3^+$ 393.1676
d
$C_8H_{10}N^+$ 120.0803
$C_9H_{17}N_4O^+$ 217.1189
$C_{30}H_{36}N_8O_6^{2+}$ 302.1372
$C_5H_8N_3^+$ 110.0708
$C_7H_{10}N_4O^+$ 166.0854
$C_{10}H_{19}N_2O_6^+$ 263.1241
$C_{17}H_{23}N_2O_4^+$ 319.1653
$C_{19}H_{22}N_7O^+$ 364.1884
$C_{20}H_{24}N_7O_3^+$ 410.1939
e
$C_{20}H_{24}N_7O_3^+$ 410.1931
$C_{30}H_{35}N_8O_6^+$ 602.2683
$C_5H_8N_3^+$ 110.0697
$C_{15}H_{19}N_4O_3^+$ 303.1435
$C_{14}H_{23}N_8O_5^+$ 383.1785
$C_{21}H_{26}N_7O_5^+$ 456.1988
$C_4H_{11}N_3O_2^+$ 133.0842
$C_9H_{17}N_2O_4^+$ 217.1180
f
$C_{10}H_{16}N_2O_3^+$ 212.1167
$C_{20}H_{24}N_7O_3^+$ 410.1925
$C_{15}H_{19}N_4O_3^+$ 303.1437
$C_5H_8N_3^+$ 110.0703
$C_{10}H_{17}N_2O_5^+$ 245.1133
$C_{26}H_{24}N_5O_2^+$ 438.1928
$C_{10}H_{19}N_2O_6^+$ 263.1238
$C_{17}H_{24}N_6O_5^+$ 392.1805
$C_{21}H_{26}N_7O_5^+$ 456.1997
$C_{30}H_{35}N_8O_6^+$ 602.2682
Intensity
m/z

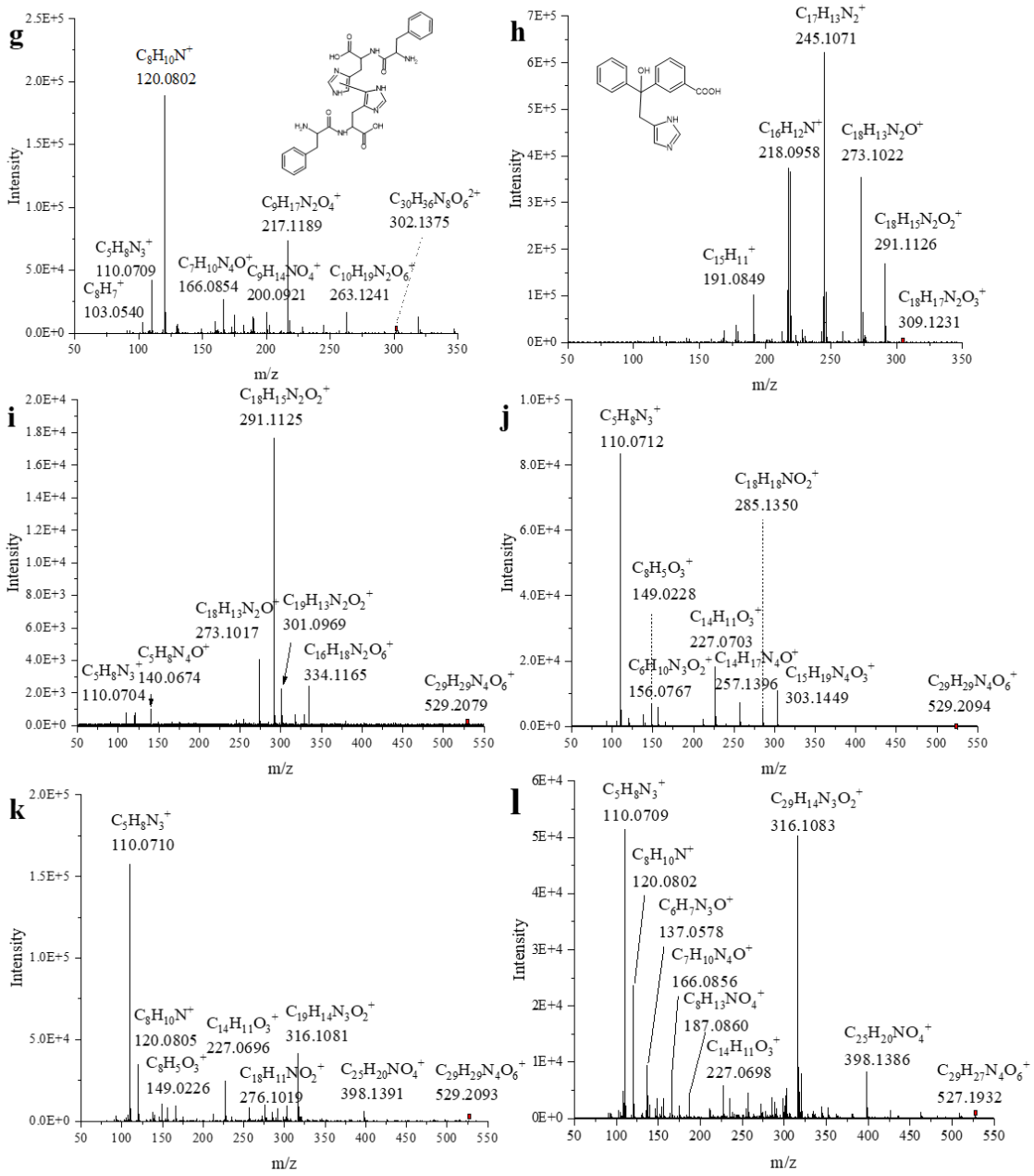

Figure HIS.SI24 *MS/MS spectra of products derived from sensitized photo-oxidation of His-Phe:* ***(a)*** *$[HisPhe]H^+$ (product* ***2f****),* ***(b)*** *$[GlyPhe]H^+$ (product* ***23****),* ***(c)*** *$[di\text{-}His\text{-}Phe]H^+$ (product* ***24a****),* ***(d)*** *$[di\text{-}His\text{-}Phe]H^+$ (product* ***24b****),* ***(e)*** *$[di\text{-}His\text{-}Phe]H^+$ (product* ***24c****),* ***(f)*** *$[di\text{-}His\text{-}Phe]H^+$ (product* ***24d****),* ***(g)*** *$[di\text{-}His\text{-}Phe]H^+$ (product* ***24e****, z = 2),* ***(h)*** *$[Im\text{-}CH_2\text{-}3CBH]H^+$ (product* ***5****),* ***(i)*** *$[His\text{-}Phe\text{-}3CBH]H^+$ (product* ***26a****),* ***(j)*** *$[His\text{-}Phe\text{-}3CBH]H^+$ (product* ***26b****),* ***(k)*** *$[His\text{-}Phe\text{-}3CBH]H^+$ (product* ***26c****),* ***(l)*** *$[His\text{-}Phe\text{-}3CBH_{\text{-}2Da}]H^+$ (product* ***27****) (****Table HIS.2****)*

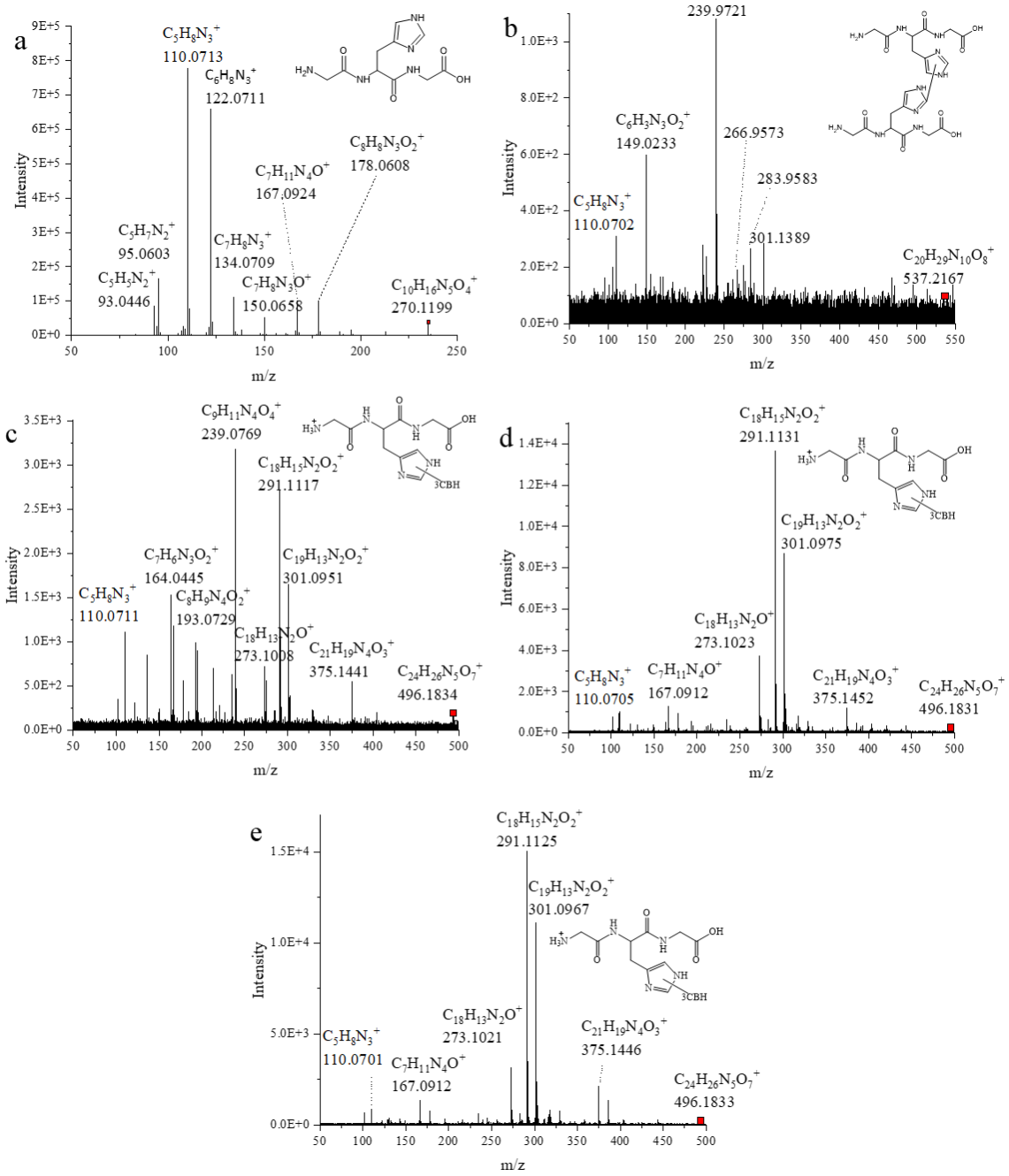

Figure HIS.SI25 *MS/MS spectra of products from Gly-His-Gly:* ***(a)*** *[Gly-His-Gly]H*$^+$, ***(b)*** *[di-Gly-His-Gly]H*$^+$, ***(c)*** *[Gly-His-Gly-3CBH]H*$^+$, ***(d)*** *[Gly-His-Gly-3CBH]H*$^+$, ***(e)*** *[Gly-His-Gly-3CBH]H*$^+$*; (products* ***2i, 28-29 c Table HIS.2*** *respectively)*

Phenylalanine:

Table PHE.SI1 Gradient elution methods for samples (flow = 0.3 mL min^{-1}; Oven temperature = 45°C)

Phe		Phe-OEt		N-Ac-Phe; N-Ac-Phe-OEt		Phe-Gly	
time	%B	**time**	%B	**time**	%B	**time**	%B
-1.00	2	**-1.00**	7	**-1.00**	7	**-1.00**	6
0.00	2	**0.00**	7	**0.00**	7	**0.00**	6
6.00	2	**6.00**	7	**6.00**	7	**5.00**	6
7.00	23	**7.00**	23	**7.00**	26	**7.50**	20
20.00	23	**20.00**	23	**20.00**	26	**20.00**	30
23.00	40	**23.00**	40	**23.00**	40	**30.00**	40
30.00	40	**30.00**	40	**30.00**	40	**31.00**	60
31.00	60	**31.00**	60	**31.00**	60	**36.00**	60
36.00	60	**36.00**	60	**36.00**	60	**37.00**	6
37.00	2	**37.00**	7	**37.00**	7	**42.00**	6
42.00	2	**42.00**	7	**42.00**	7		

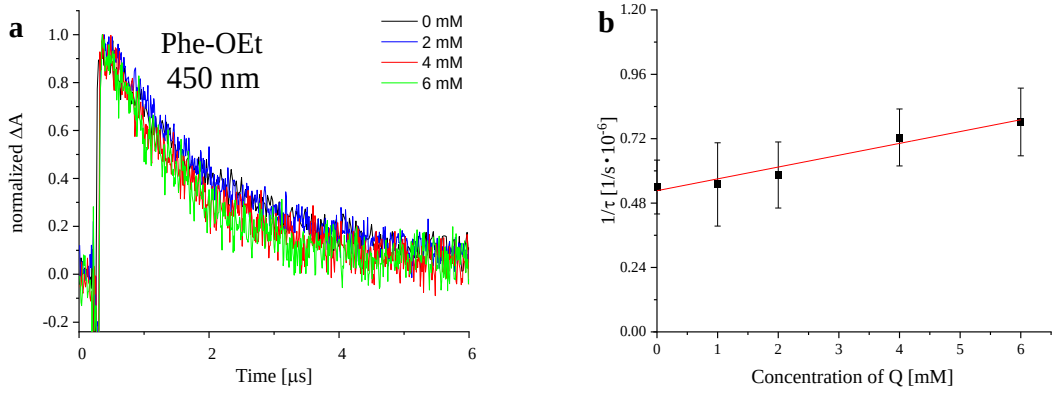

Figure PHE.SI1 ***(a)*** *Kinetic traces for the ^{3}3CB* decay at 450 nm in the presence of varying concentrations of Phe-OEt at pH 7* ***(b)*** *The Stern-Volmer plots according to* ***Equation 2*** *for the quenching of ^{3}3CB* by Tyr at pH 7 in aqueous solution for 3CB (4 mM)*

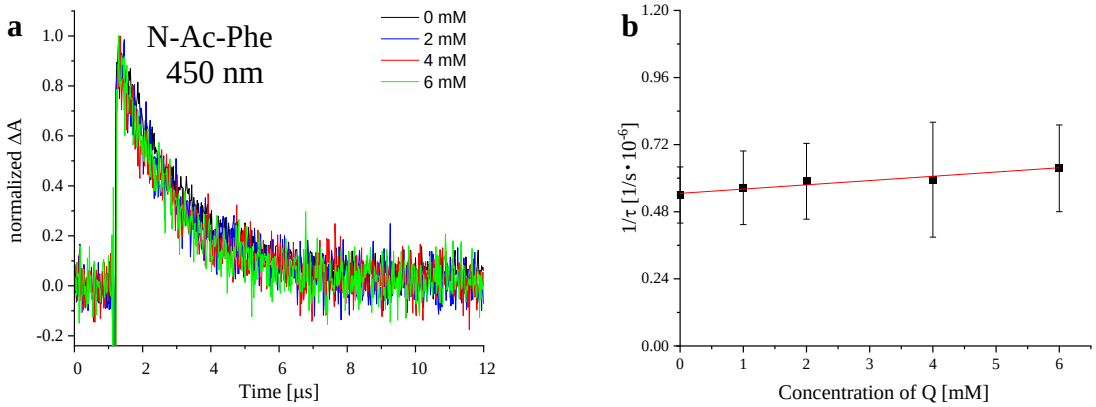

Figure PHE.SI2 ***(a)*** *Kinetic traces for the ^{3}3CB* decay at 450 nm in the presence of varying concentrations of N-Ac-Phe at pH 7* ***(b)*** *The Stern-Volmer plots according to* ***Equation 2*** *for the quenching of ^{3}3CB* by N-Ac-Tyr at pH 7 in aqueous solution for 3CB (4 mM)*

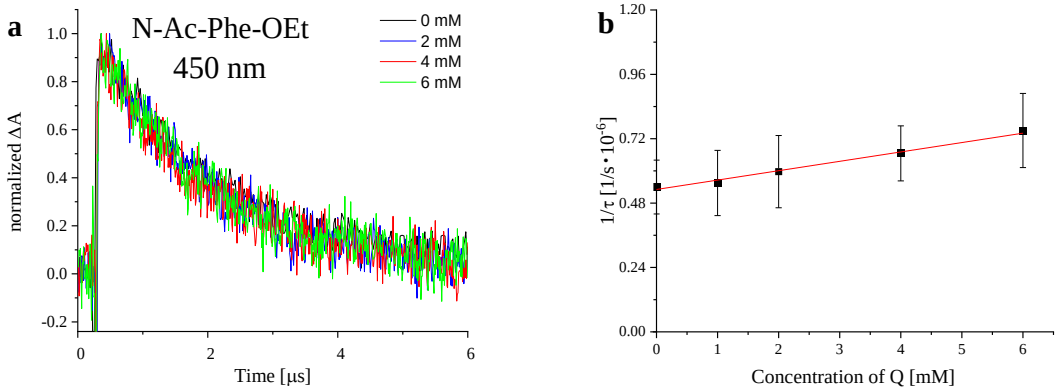

Figure PHE.SI3 ***(a)*** *Kinetic traces for the ^{3}3CB* decay at 450 nm in the presence of varying concentrations of N-Ac-Phe-OEt at pH 7* ***(b)*** *The Stern-Volmer plots according to* ***Equation 2*** *for the quenching of ^{3}3CB* by N-Ac-Phe-OEt at pH 7 in aqueous solution for 3CB (4 mM)*

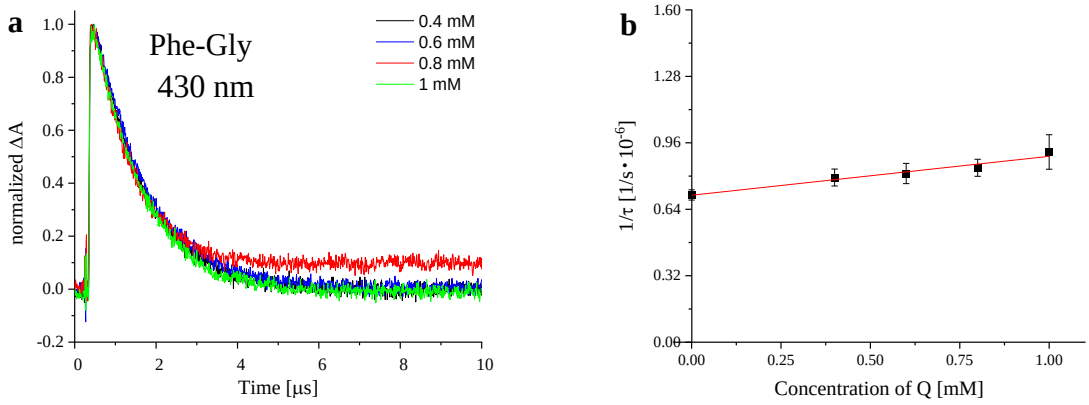

Figure PHE.SI4 ***(a)*** *Kinetic traces for the ^{3}3CB* decay at 430 nm in the presence of varying concentrations of Phe-Gly at pH 7* ***(b)*** *The Stern-Volmer plots according to* ***Equation 2*** *for the quenching of ^{3}3CB* by Phe-Gly at pH 7 in aqueous solution for 3CB (5 mM)*

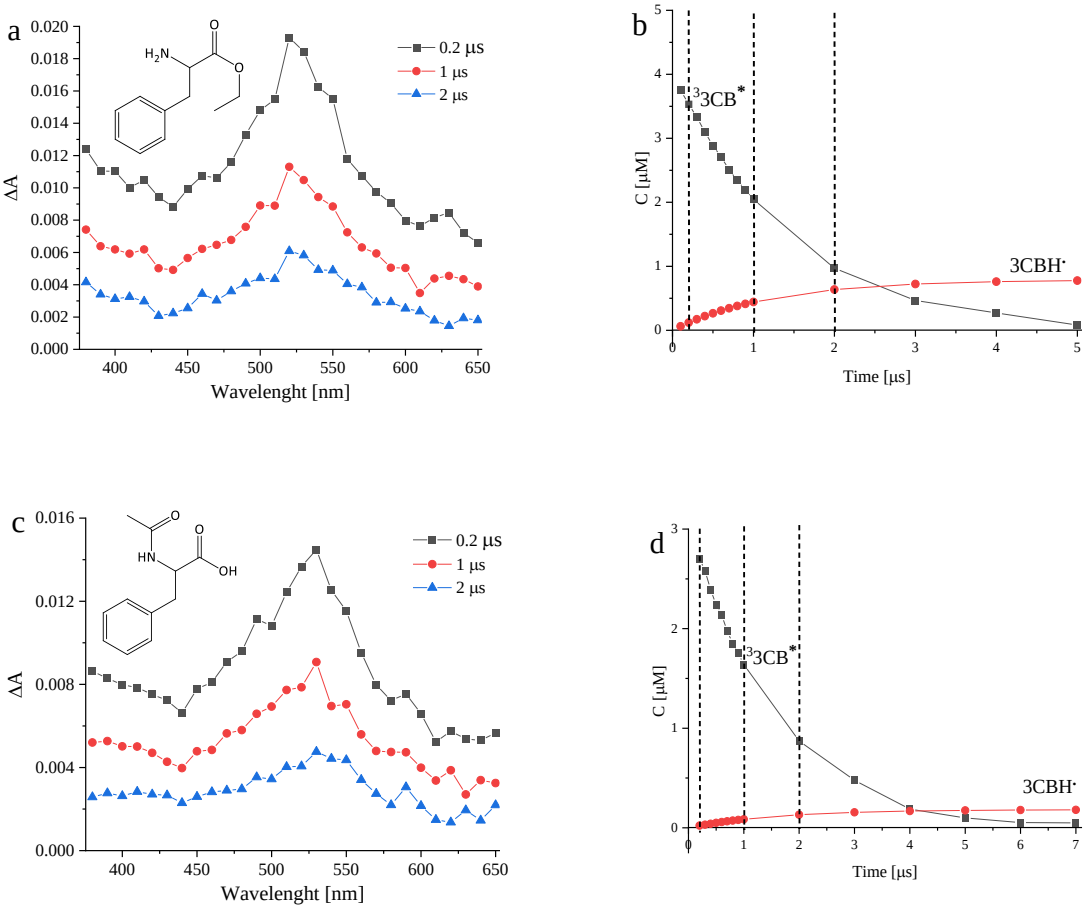

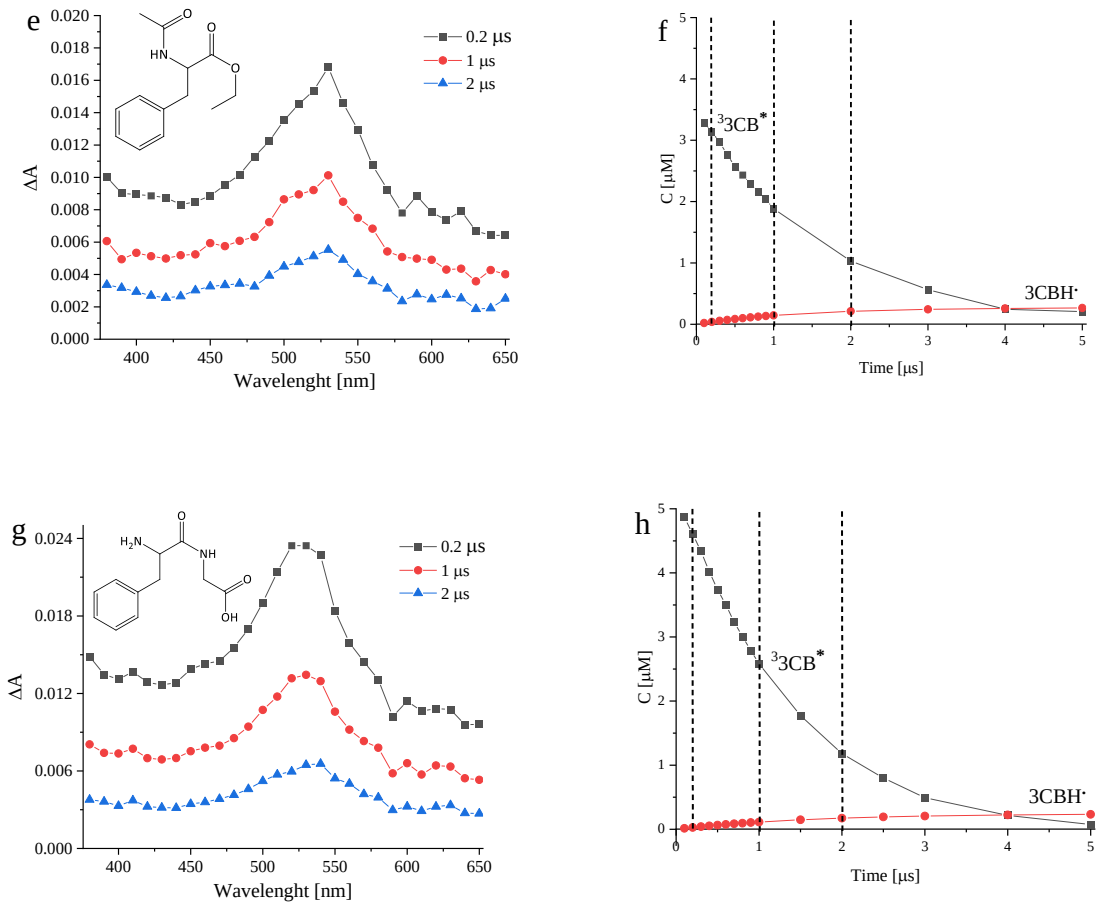

Figure PHE.SI5 *Evolution of transient absorption spectra from 3CB-sensitized oxidation of* ***(a)*** *Phe-OEt;* ***(c)*** *N-Ac-Phe;* ***(e)*** *N-Ac-Phe-OEt;* ***(g)*** *Phe-Gly at pH 7. Spectra were recorded at different delays following laser pulse 0.2 (black ■), 1 (red ●), 2 µs (blue ▲). Concentration profiles of transients identified in the laser flash photolysis of an aqueous solution of* ***(b)*** *Phe-OEt;* ***(d)*** *N-Ac-Phe;* ***(f)*** *N-Ac-Phe-OEt;* ***(h)*** *Phe-Gly and 3CB (4 mM) at pH 7 where (black ■) is ^{3}3CB*, and (red ●) is 3CBH$^\bullet$. Dotted lines represent points at which concentrations were measured on spectra represented in respective figure to the left. Dotted lines represent times at which respective spectra were presented in* ***(a)***, ***(c)***, ***(e)***, *and* ***(g)***

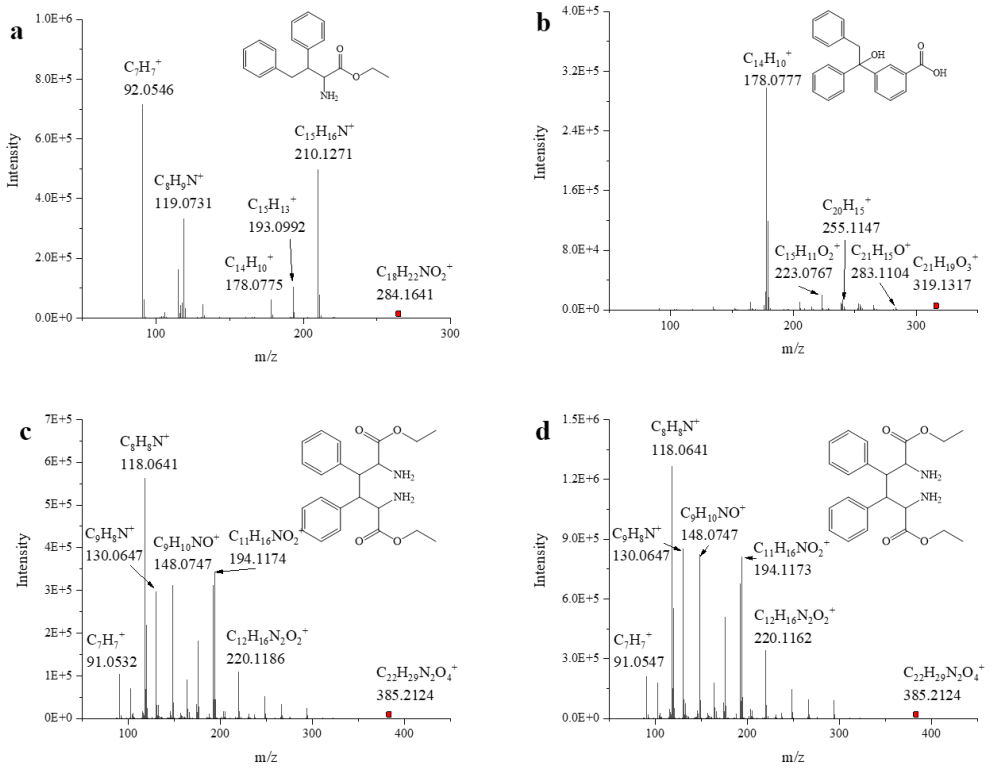

Figure PHE.SI6 *MS/MS spectra of products* ***(a) 7***, ***(b) 6***, ***(c) 8a***, *and* ***(d) 8b***, *derived from Phe-OEt irradiated with 3CB in aqueous solution, Ar-saturated*

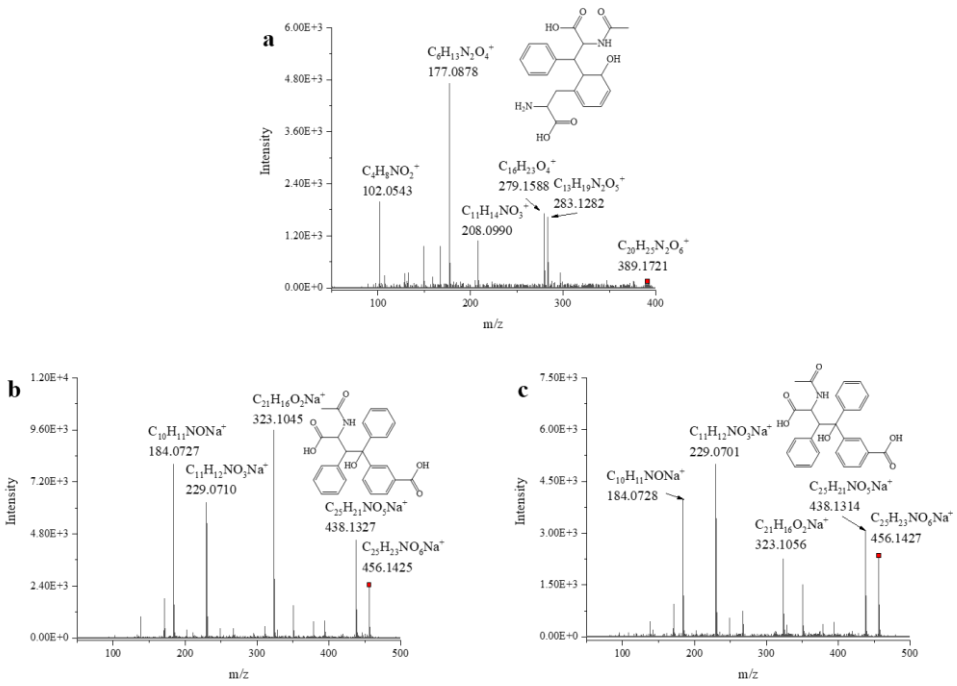

Figure PHE.SI7 *MS/MS spectra of products* ***(a) 9***, ***(b) 10a***, *and* ***(c) 10b*** *derived from N-Ac-Phe irradiated with 3CB in aqueous solution, Ar-saturated*

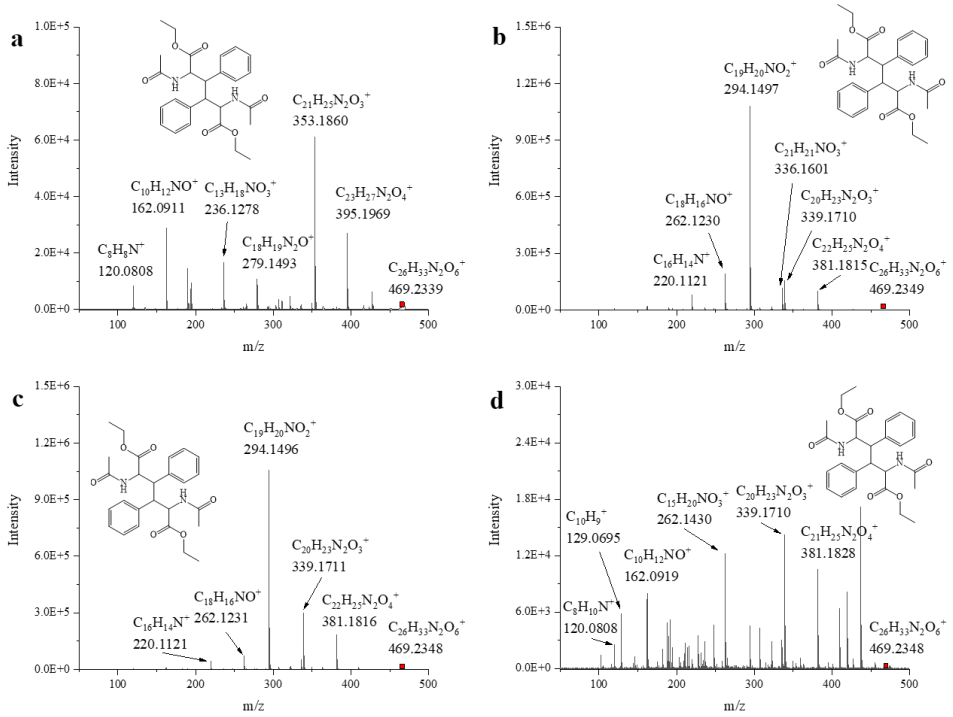

Figure PHE.SI8 *MS/MS spectra of products **11a-d** derived from N-Ac-Phe-OEt irradiated with 3CB in aqueous solution, Ar-saturated*

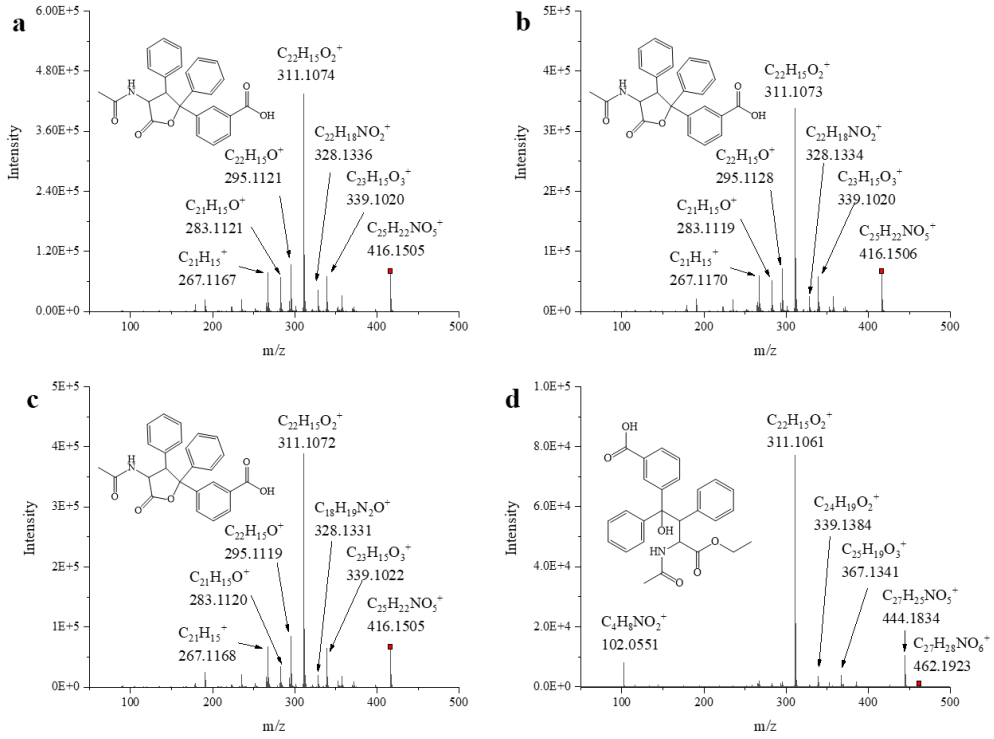

Figure PHE.SI9 *MS/MS spectra of products **12a-c**, and **(d) 13** derived from N-Ac-Phe-OEt irradiated with 3CB in aqueous solution, Ar-saturated*

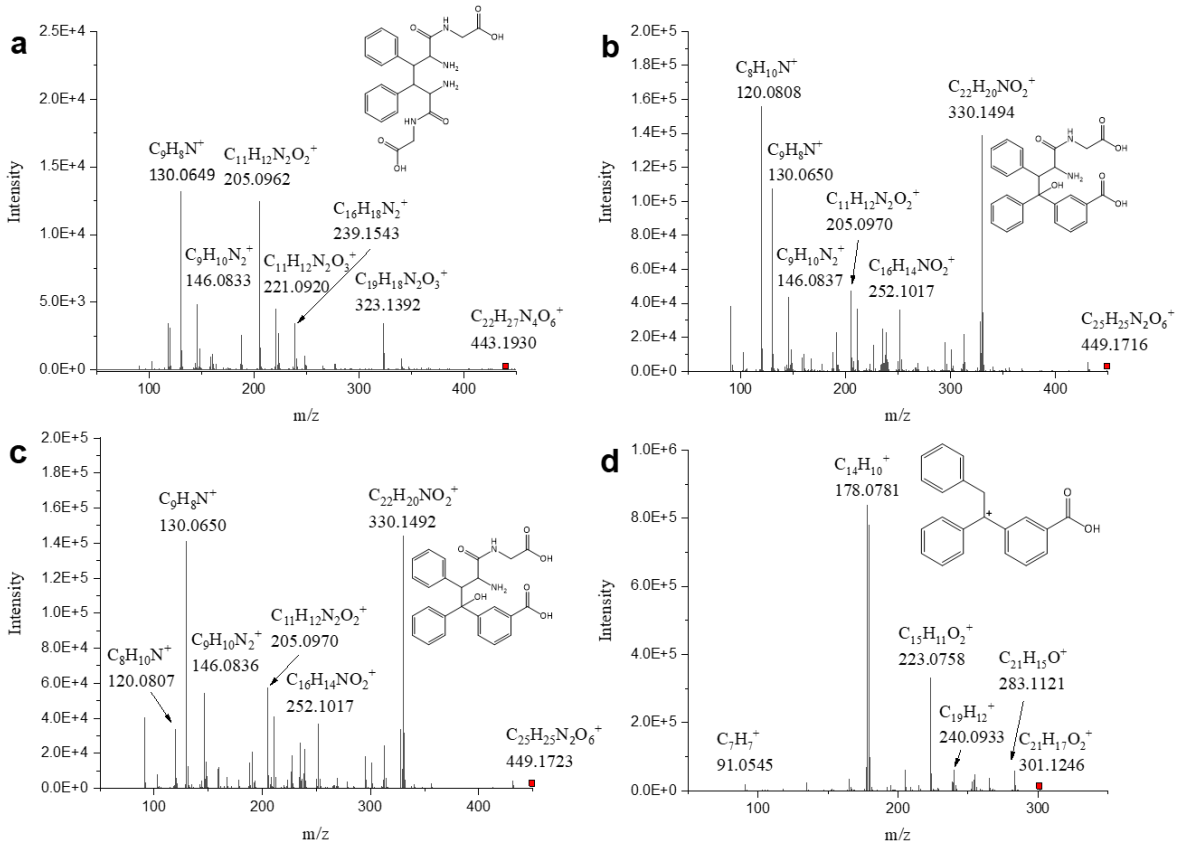

Figure PHE.SI10 *MS/MS spectra of products* ***(a) 14***, ***(b) 15a***, ***(c) 15b***, *and* ***(d) 6*** *derived from Phe-Gly irradiated with 3CB in aqueous solution, Ar-saturated*

GAPDH:

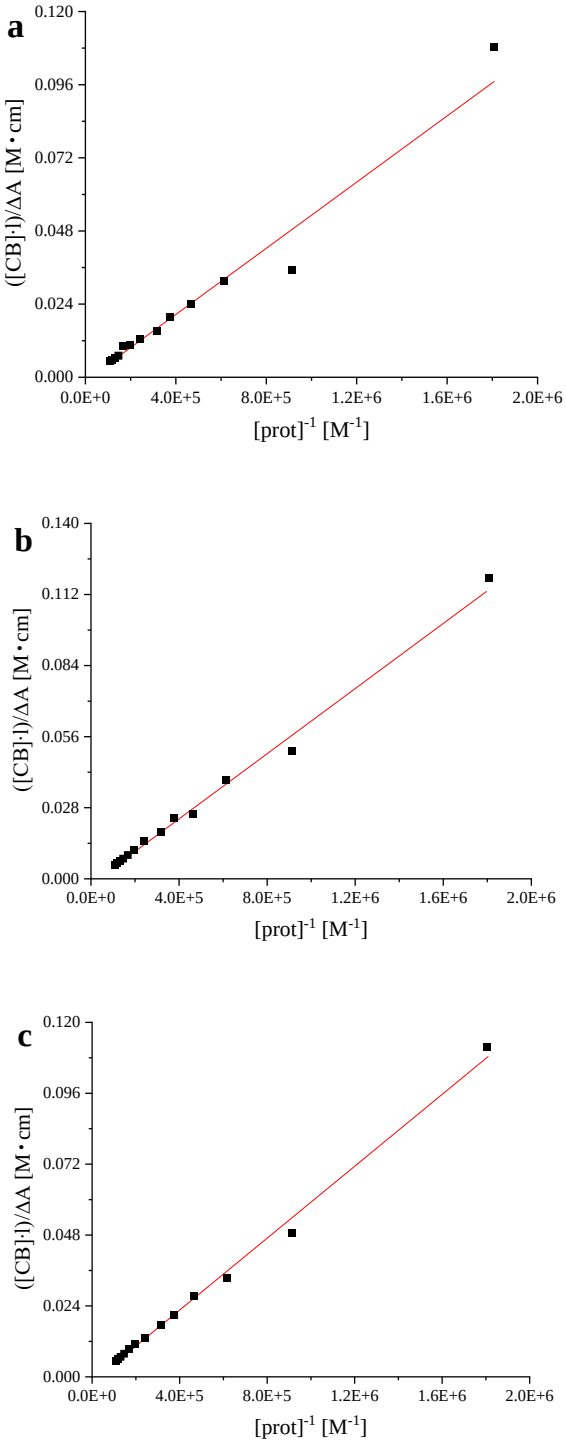

Figure GAPD.SI1. *Linear regressions of concentration of 3CB multiplied by optical length and divided by differences in absorption versus reciprocal of protein concentration that allowed for measurement of K*

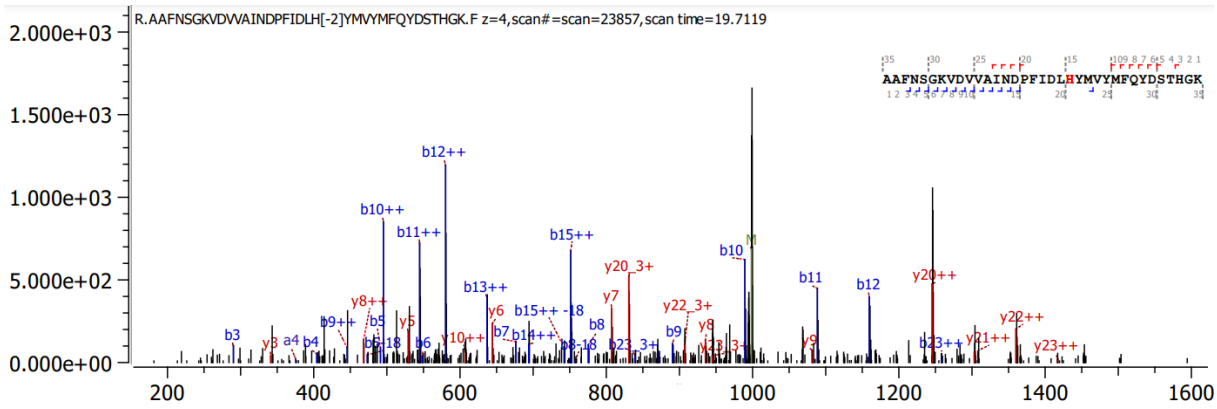

Figure GAPD.SI2. *The MS/MS spectrum of P1 of in-solution digested sample of 5 min irradiated solution of GAPDH with 3CB*

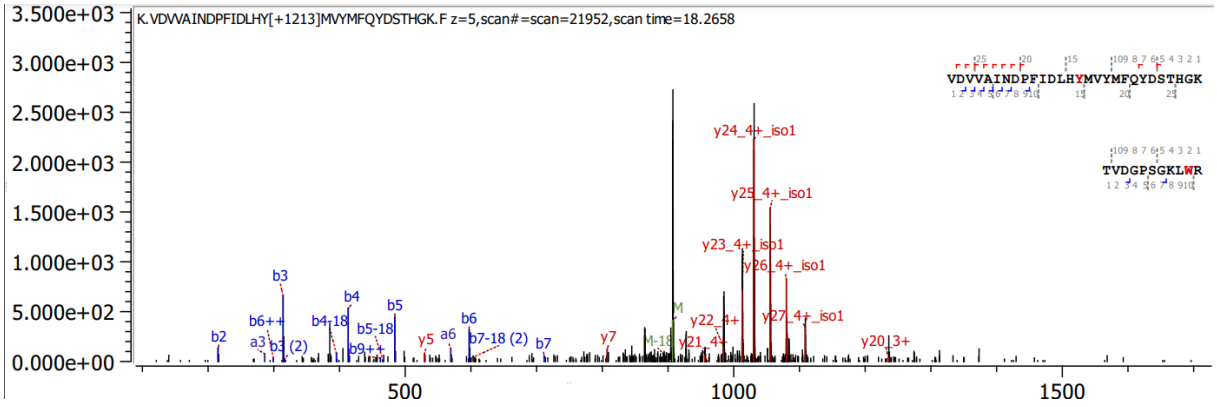

Figure GAPD.SI3. *The MS/MS spectrum of P2 of in-solution digested sample of 5 min irradiated solution of GAPDH with 3CB*

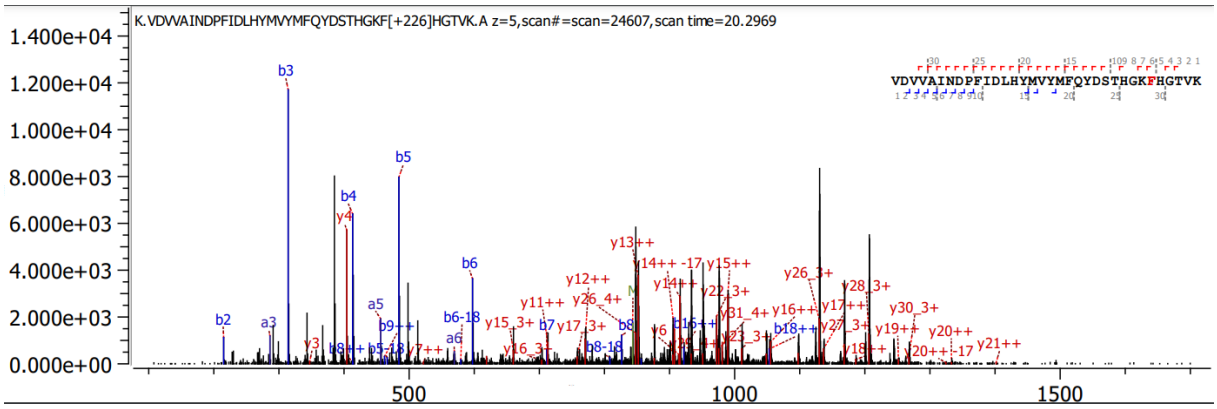

Figure GAPD.SI4. *The MS/MS spectrum of P3 of in-solution digested sample of 5 min irradiated solution of GAPDH with 3CB*

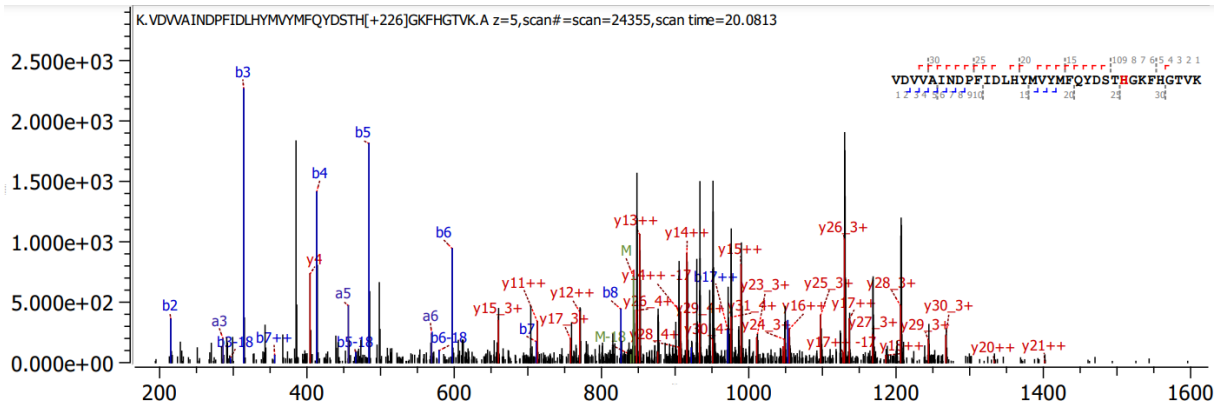

Figure GAPD.SI5. *The MS/MS spectrum of P4 of in-solution digested sample of 5 min irradiated solution of GAPDH with 3CB*

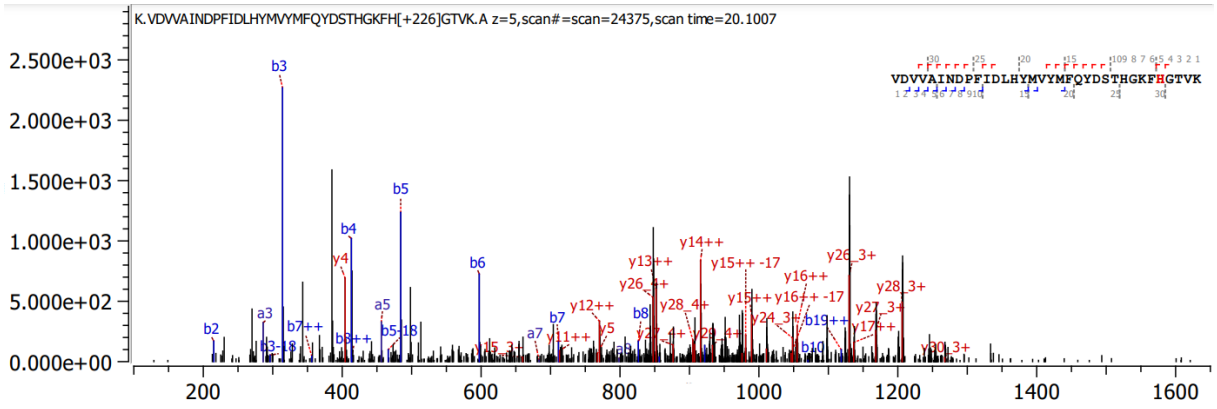

Figure GAPD.SI6. *The MS/MS spectrum of P5 of in-solution digested sample of 5 min irradiated solution of GAPDH with 3CB*

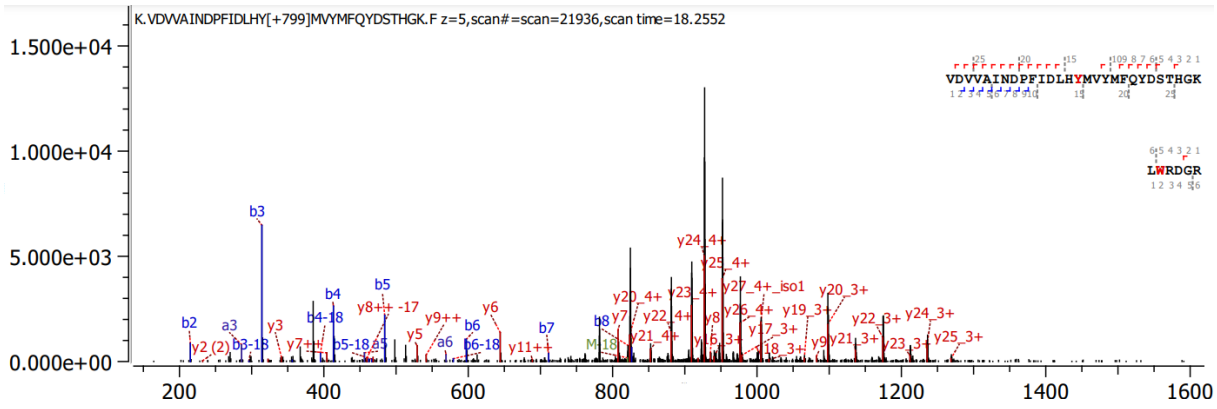

Figure GAPD.SI7. *The MS/MS spectrum of P6 of in-solution digested sample of 5 min irradiated solution of GAPDH with 3CB*

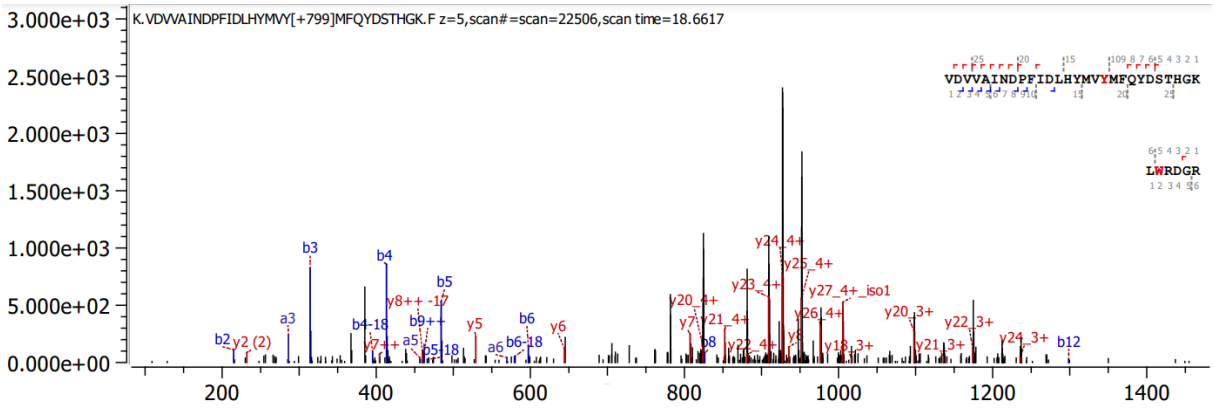

Figure GAPD.SI8. *The MS/MS spectrum of P7 of in-solution digested sample of 5 min irradiated solution of GAPDH with 3CB*

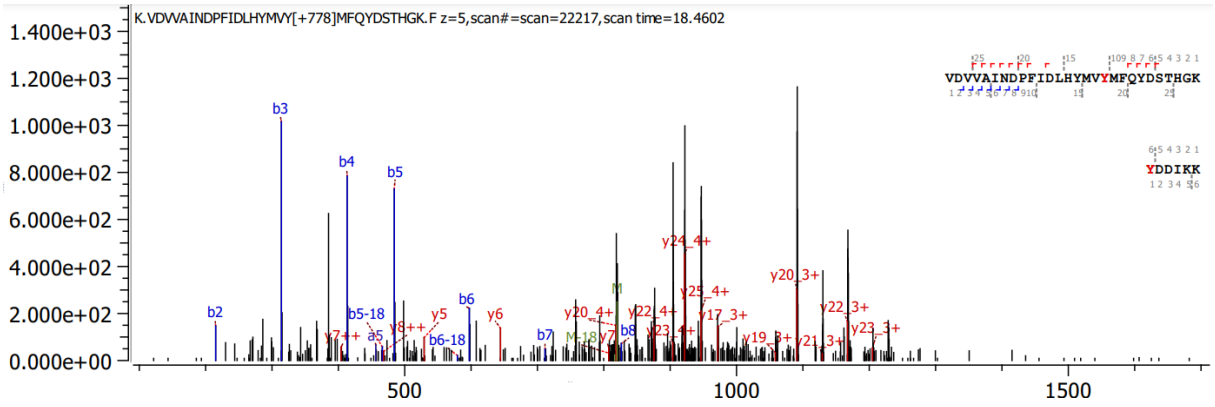

Figure GAPD.SI9. *The MS/MS spectrum of P8 of in-solution digested sample of 5 min irradiated solution of GAPDH with 3CB*

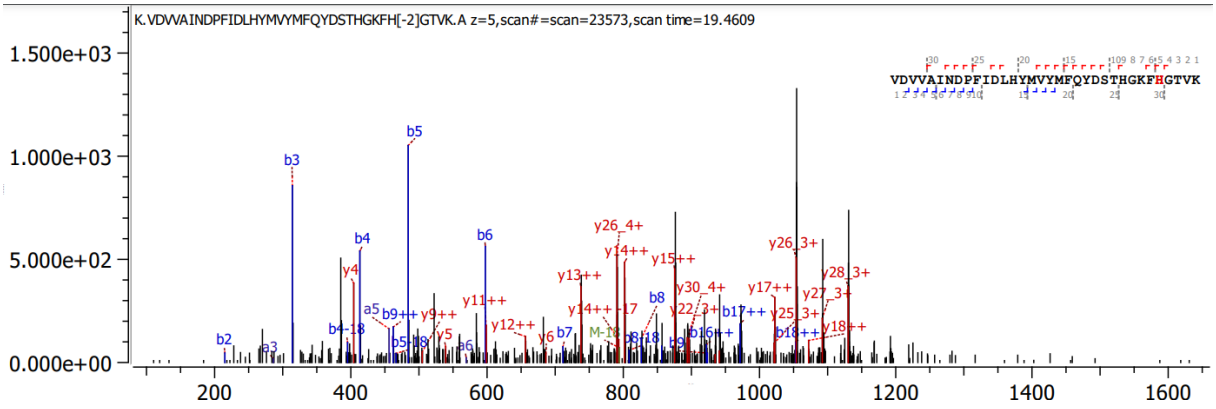

Figure GAPD.SI10. *The MS/MS spectrum of P9 of in-solution digested sample of 5 min irradiated solution of GAPDH with 3CB*

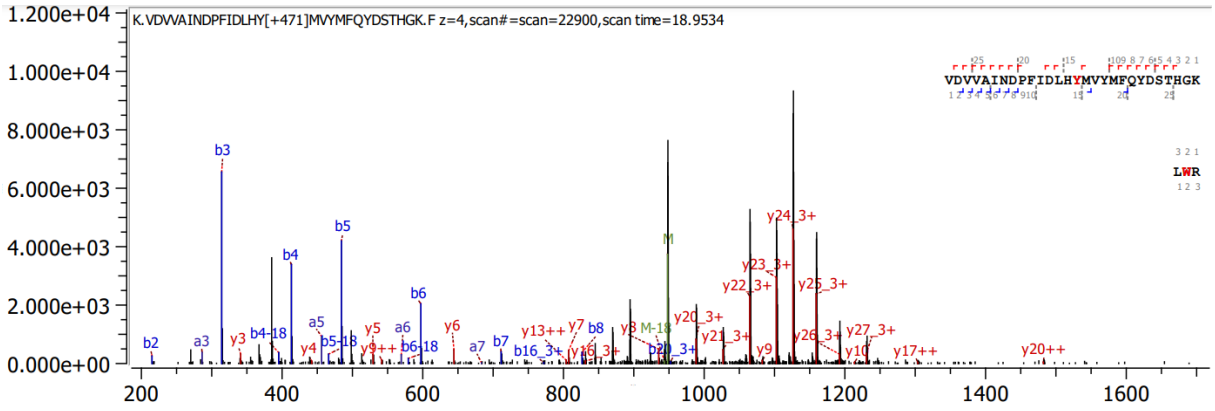

Figure GAPD.SI11. *The MS/MS spectrum of P10 of in-solution digested sample of 5 min irradiated solution of GAPDH with 3CB*

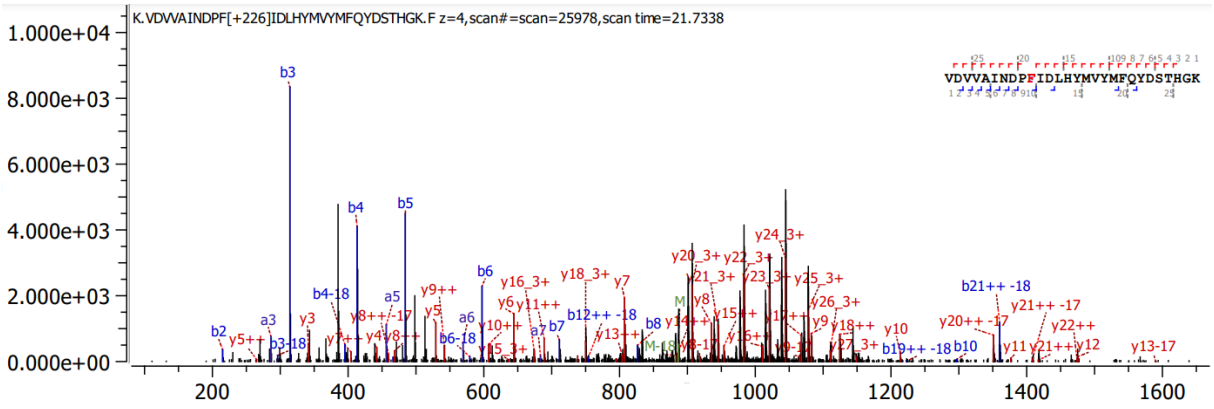

Figure GAPD.SI12. *The MS/MS spectrum of P11 of in-solution digested sample of 5 min irradiated solution of GAPDH with 3CB*

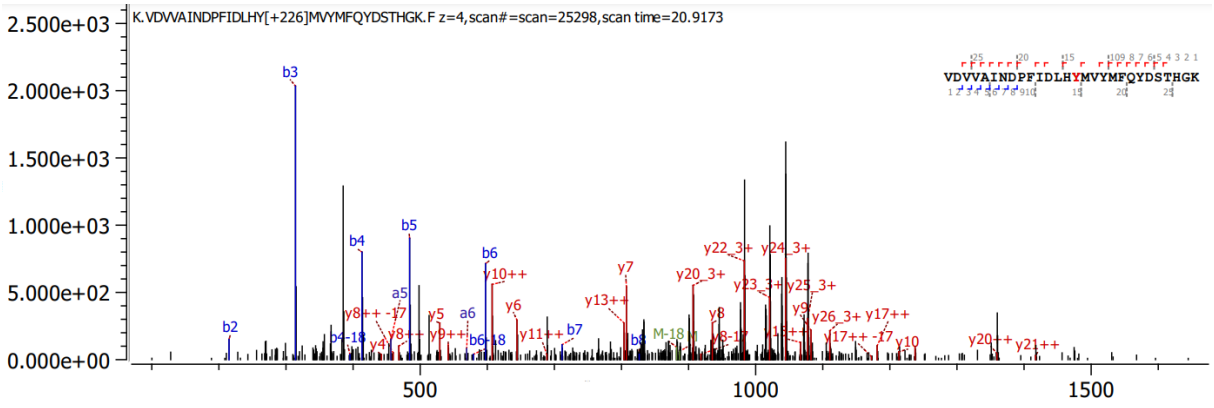

Figure GAPD.SI13. *The MS/MS spectrum of P12 of in-solution digested sample of 5 min irradiated solution of GAPDH with 3CB*

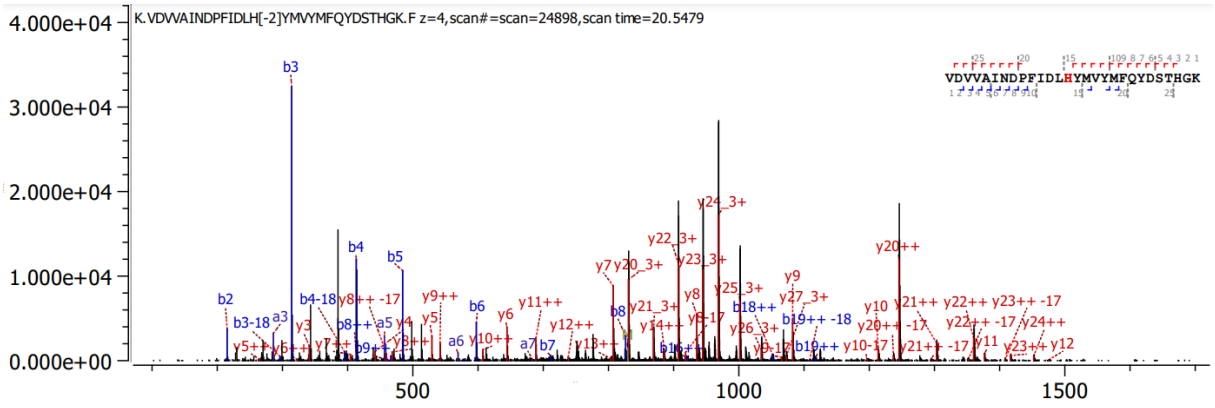

Figure GAPD.SI14. *The MS/MS spectrum of P13 of in-solution digested sample of 5 min irradiated solution of GAPDH with 3CB*

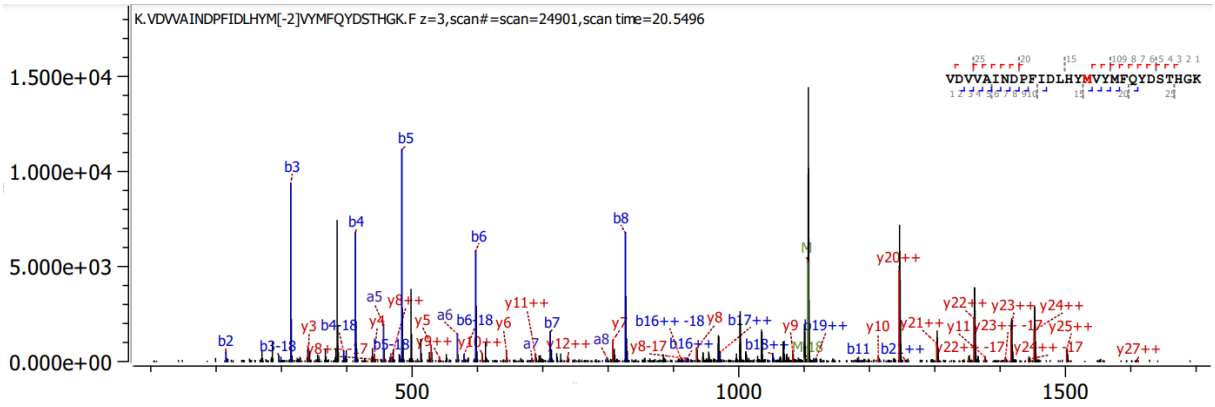

Figure GAPD.SI15. *The MS/MS spectrum of P14 of in-solution digested sample of 5 min irradiated solution of GAPDH with 3CB*

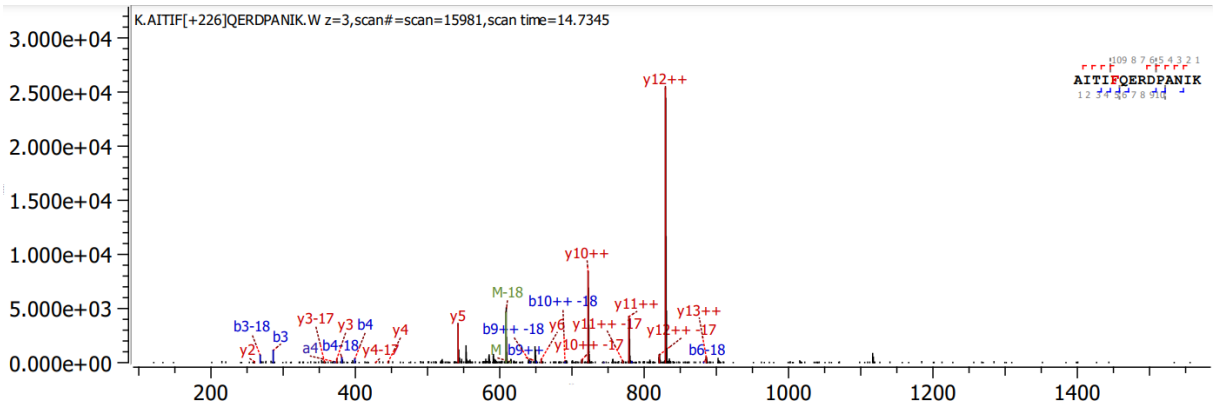

Figure GAPD.SI16. *The MS/MS spectrum of P15 of in-solution digested sample of 5 min irradiated solution of GAPDH with 3CB*

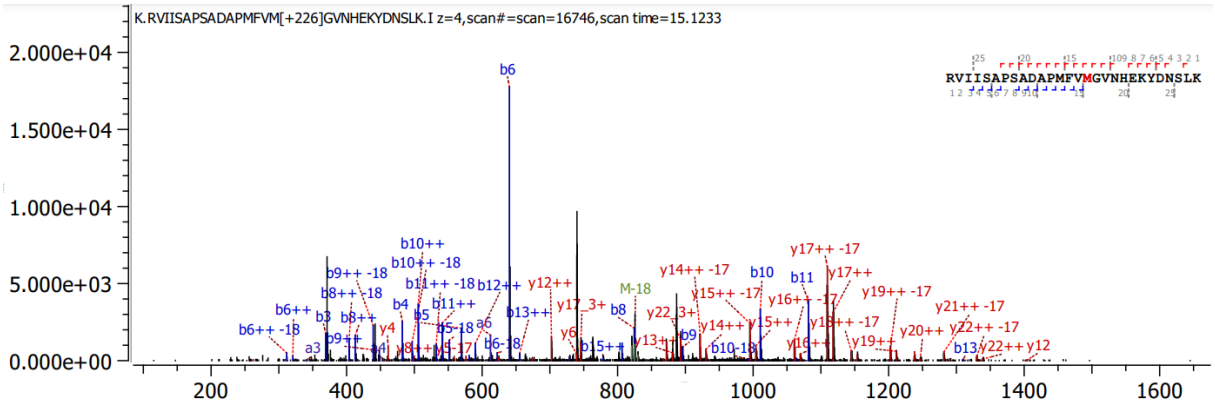

Figure GAPD.SI17. *The MS/MS spectrum of P16 of in-solution digested sample of 5 min irradiated solution of GAPDH with 3CB*

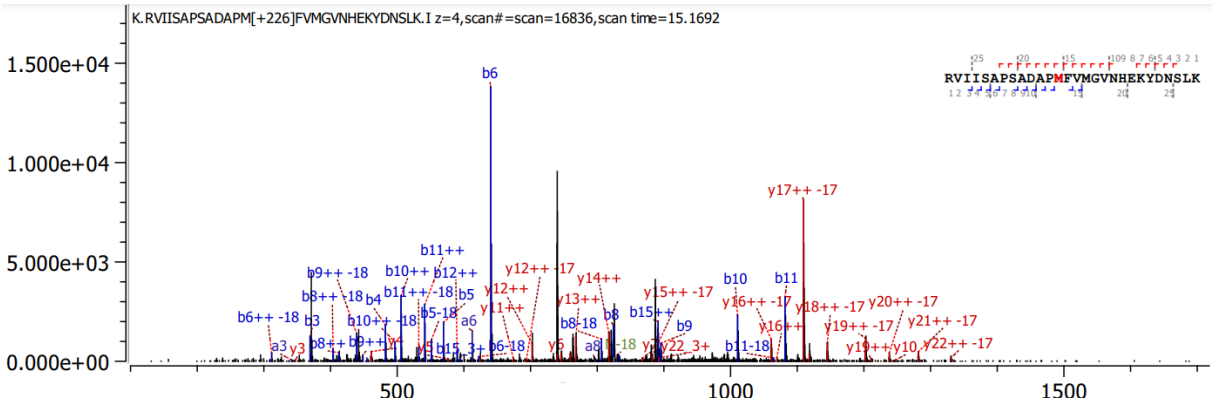

Figure GAPD.SI18. *The MS/MS spectrum of P17 of in-solution digested sample of 5 min irradiated solution of GAPDH with 3CB*

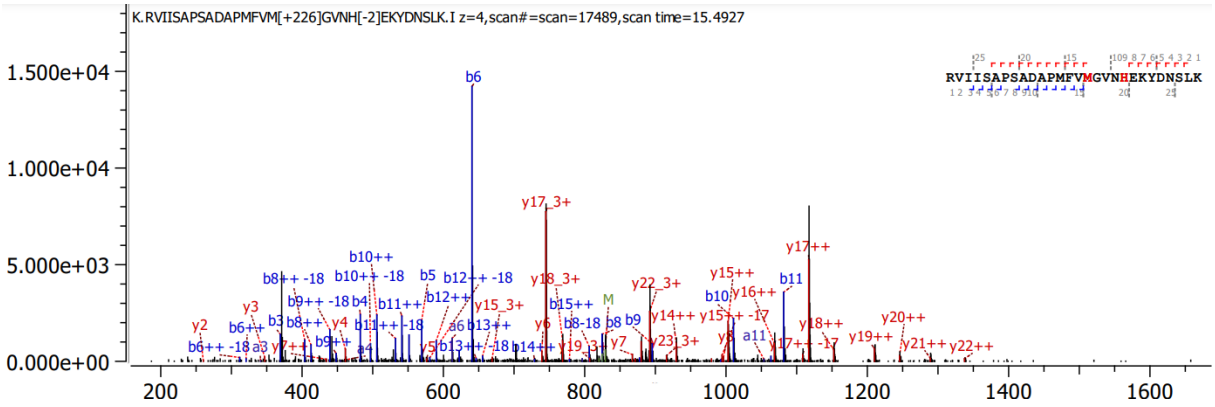

Figure GAPD.SI19. *The MS/MS spectrum of P18 of in-solution digested sample of 5 min irradiated solution of GAPDH with 3CB*

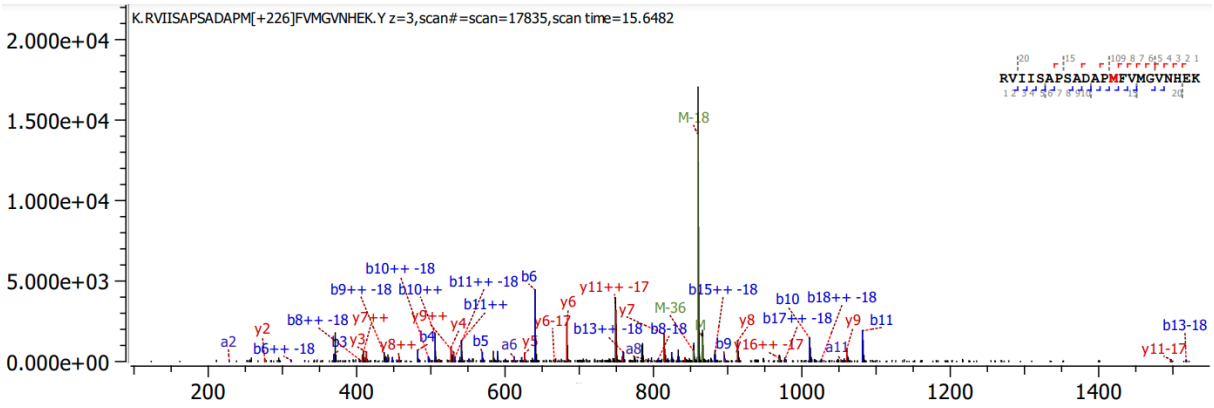

Figure GAPD.SI20. *The MS/MS spectrum of P19 of in-solution digested sample of 5 min irradiated solution of GAPDH with 3CB*

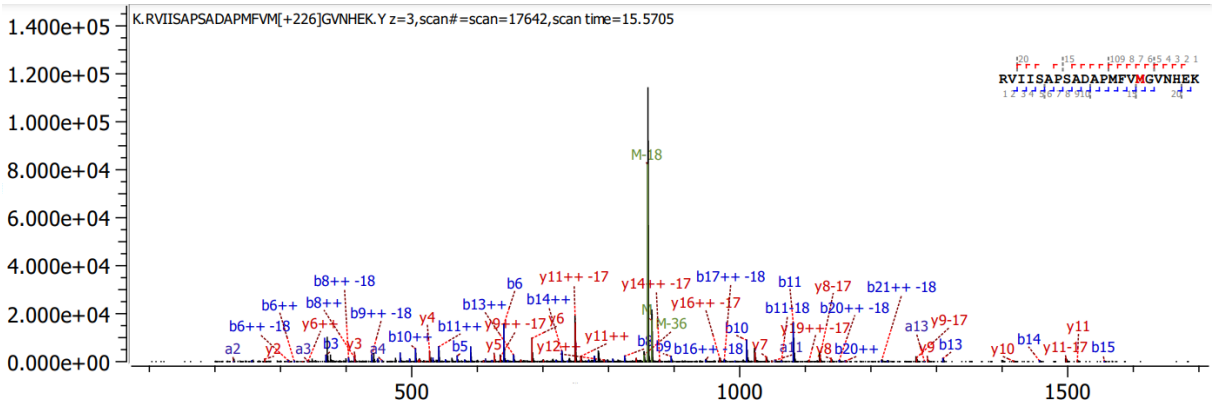

Figure GAPD.SI21. *The MS/MS spectrum of P20 of in-solution digested sample of 5 min irradiated solution of GAPDH with 3CB*

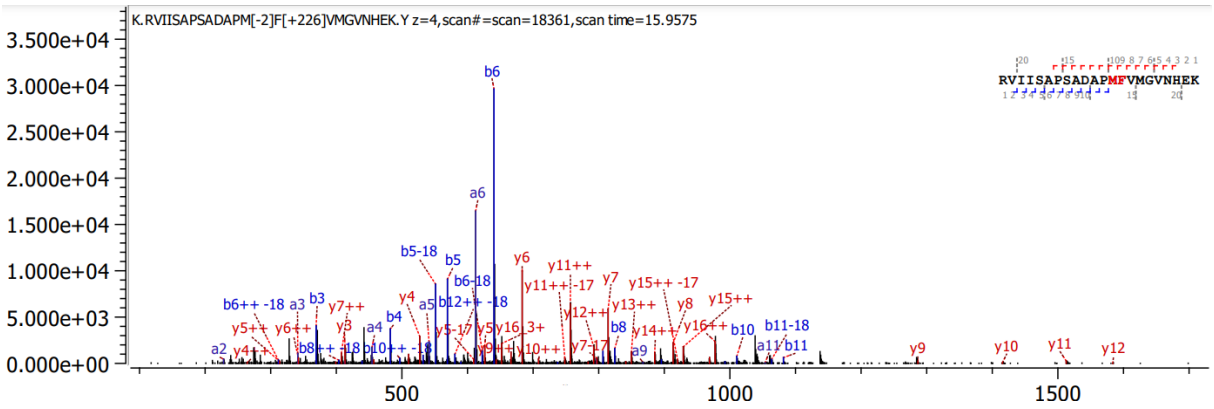

Figure GAPD.SI22. *The MS/MS spectrum of P21 of in-solution digested sample of 5 min irradiated solution of GAPDH with 3CB*

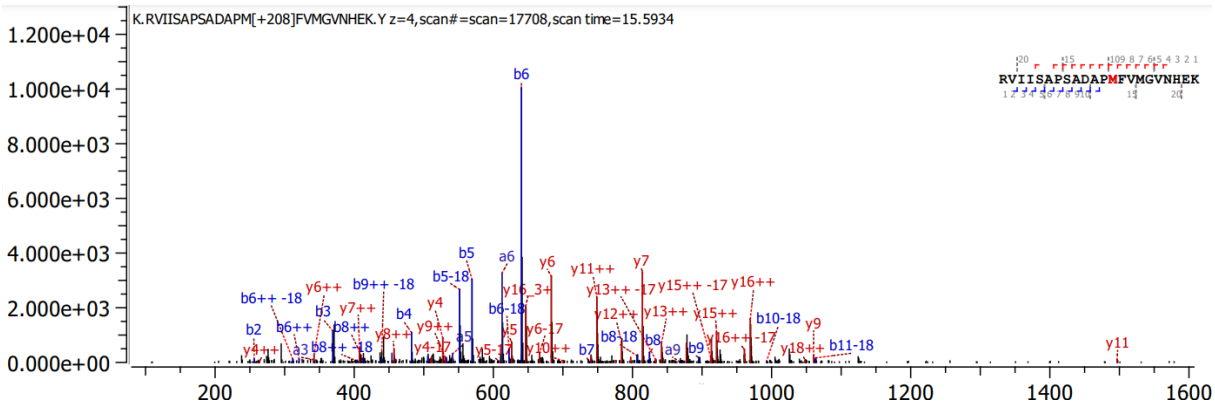

Figure GAPD.SI23. *The MS/MS spectrum of P22 of in-solution digested sample of 5 min irradiated solution of GAPDH with 3CB*

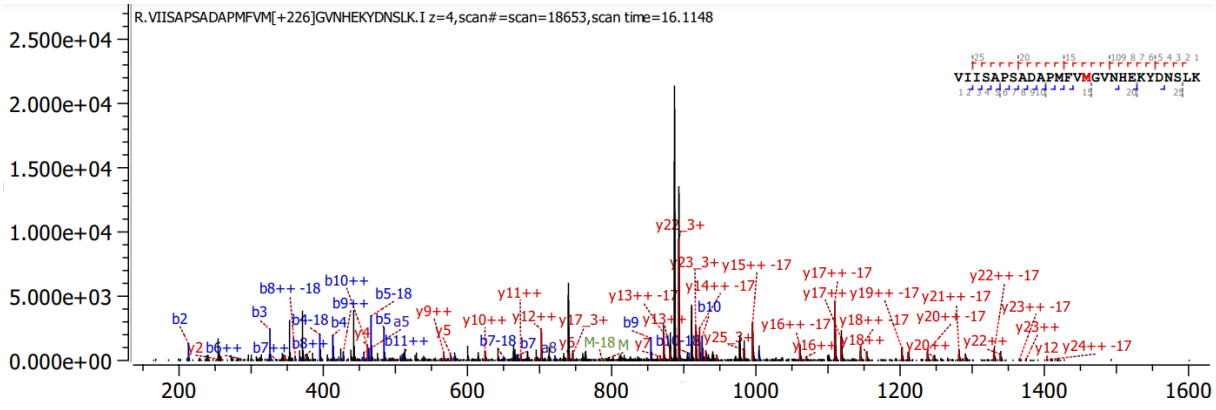

Figure GAPD.SI24 *The MS/MS spectrum of P23 of in-solution digested sample of 5 min irradiated solution of GAPDH with 3CB*

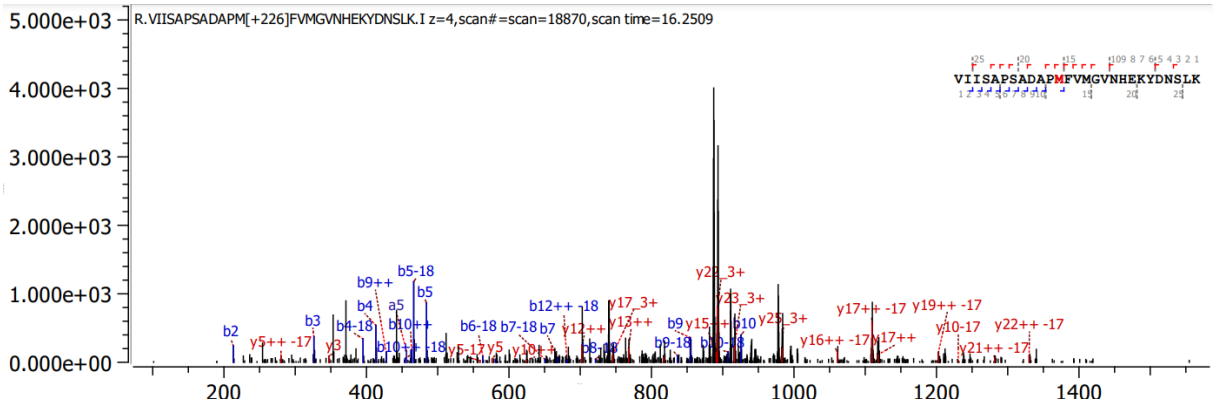

Figure GAPD.SI25. *The MS/MS spectrum of P24 of in-solution digested sample of 5 min irradiated solution of GAPDH with 3CB*

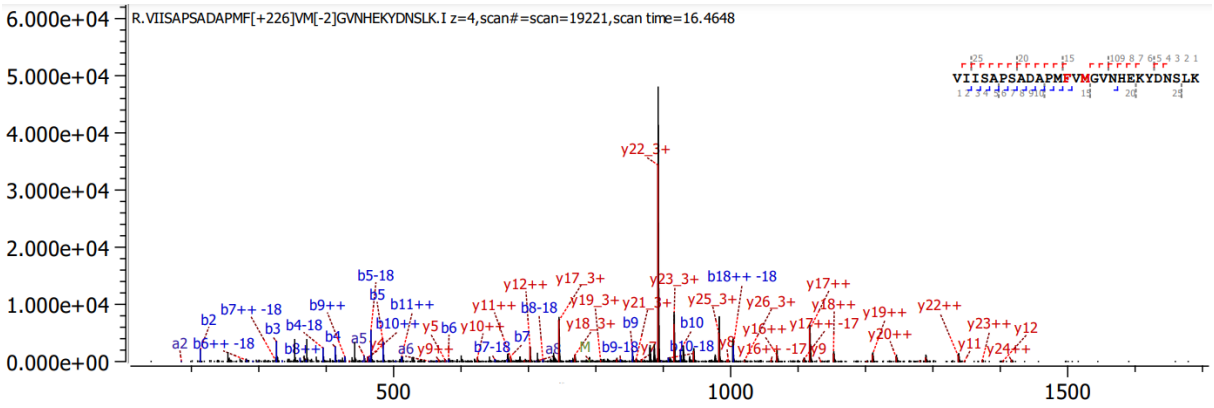

Figure GAPD.SI26. *The MS/MS spectrum of P25 of in-solution digested sample of 5 min irradiated solution of GAPDH with 3CB*

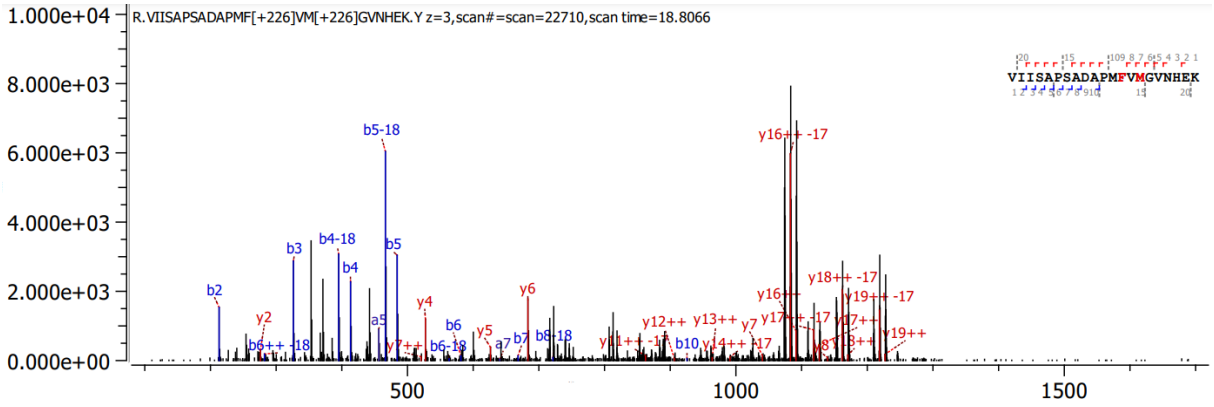

Figure GAPD.SI27. *The MS/MS spectrum of P26 of in-solution digested sample of 5 min irradiated solution of GAPDH with 3CB*

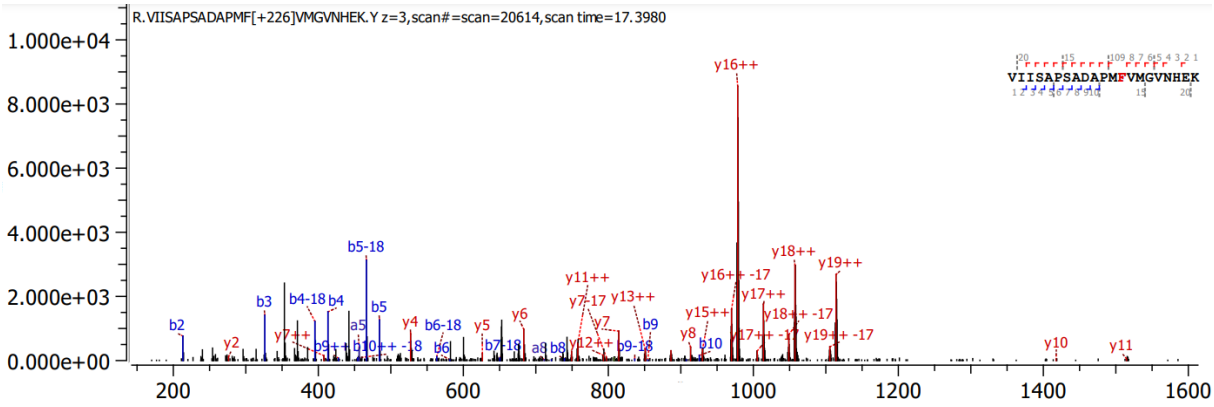

Figure GAPD.SI28. *The MS/MS spectrum of P27 of in-solution digested sample of 5 min irradiated solution of GAPDH with 3CB*

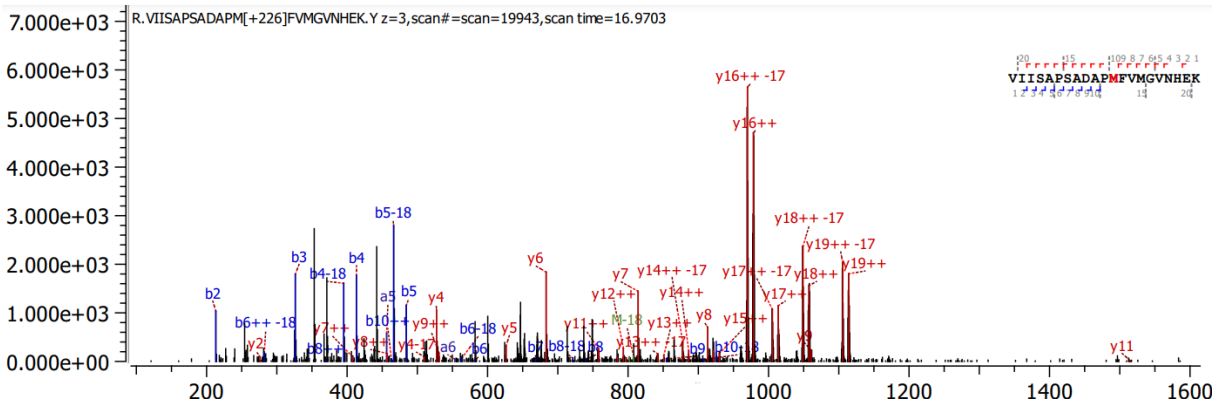

Figure GAPD.SI29. *The MS/MS spectrum of P28 of in-solution digested sample of 5 min irradiated solution of GAPDH with 3CB*

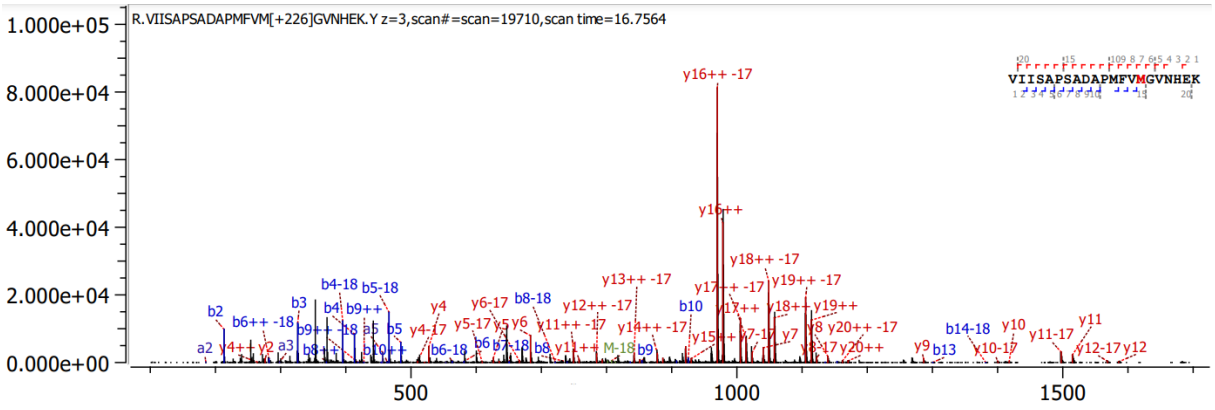

Figure GAPD.SI30. *The MS/MS spectrum of P29 of in-solution digested sample of 5 min irradiated solution of GAPDH with 3CB*

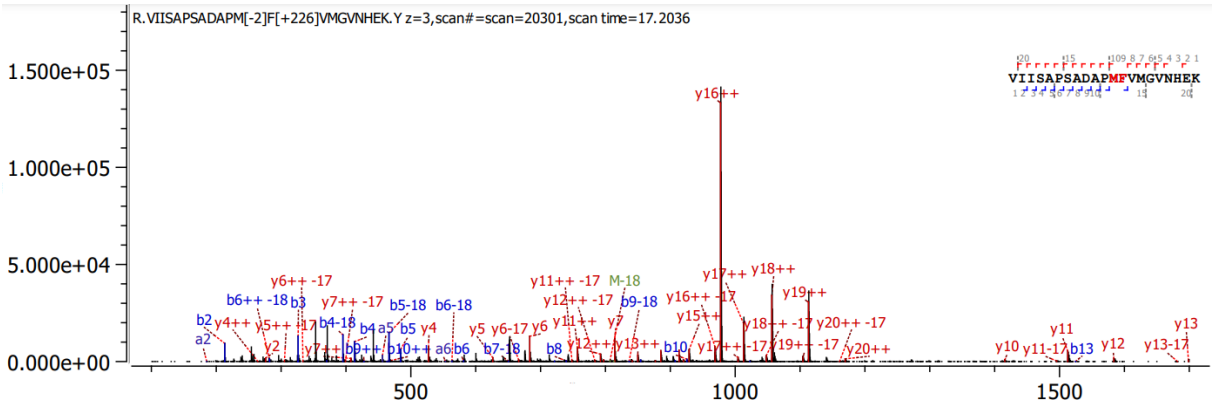

Figure GAPD.SI31. *The MS/MS spectrum of P30 of in-solution digested sample of 5 min irradiated solution of GAPDH with 3CB*

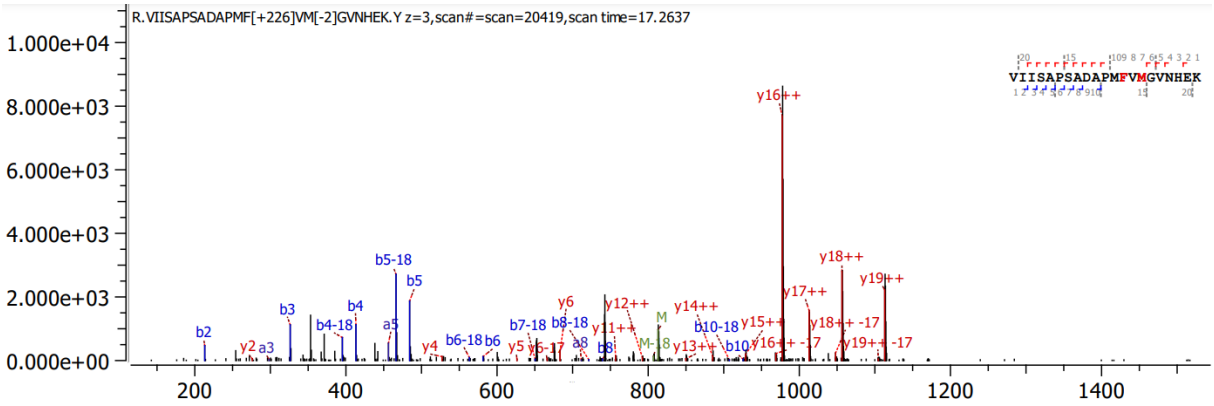

Figure GAPD.SI32. *The MS/MS spectrum of P31 of in-solution digested sample of 5 min irradiated solution of GAPDH with 3CB*

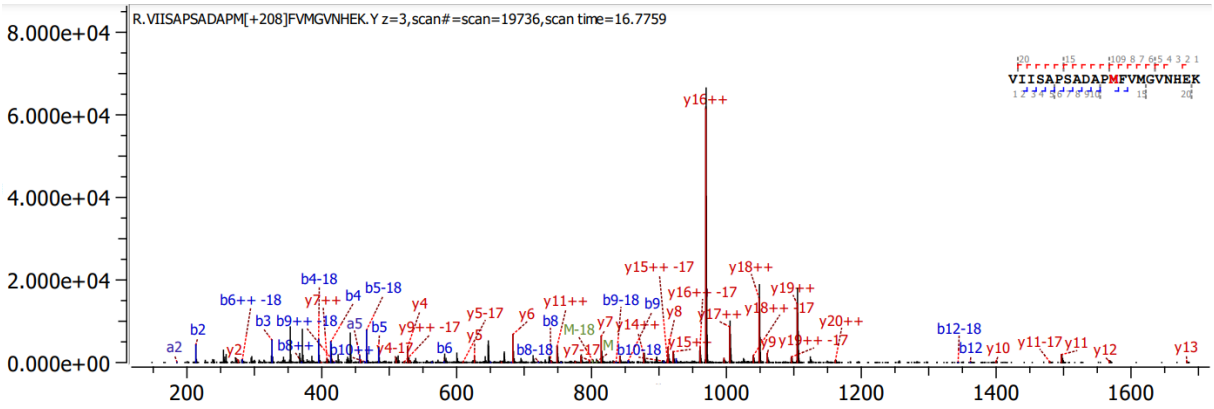

Figure GAPD.SI33. *The MS/MS spectrum of P32 of in-solution digested sample of 5 min irradiated solution of GAPDH with 3CB*

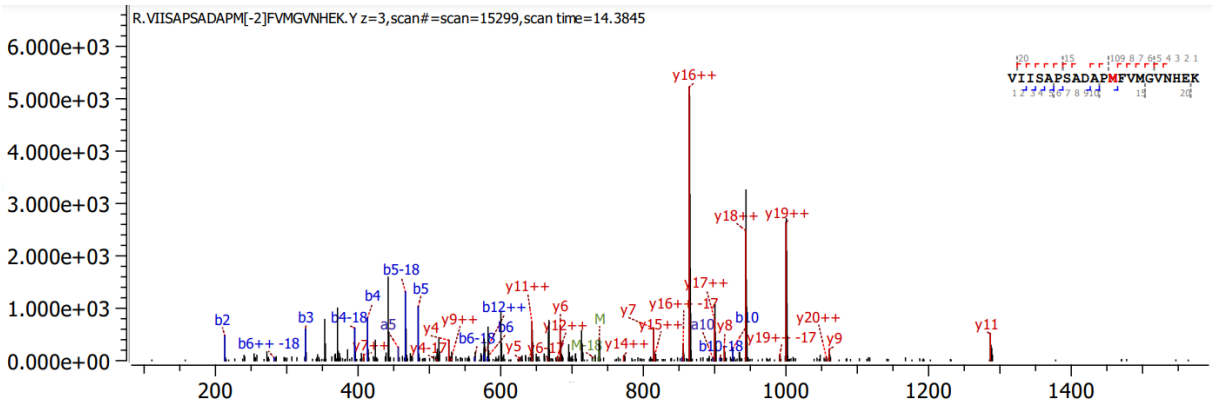

Figure GAPD.SI34. *The MS/MS spectrum of P33 of in-solution digested sample of 5 min irradiated solution of GAPDH with 3CB*

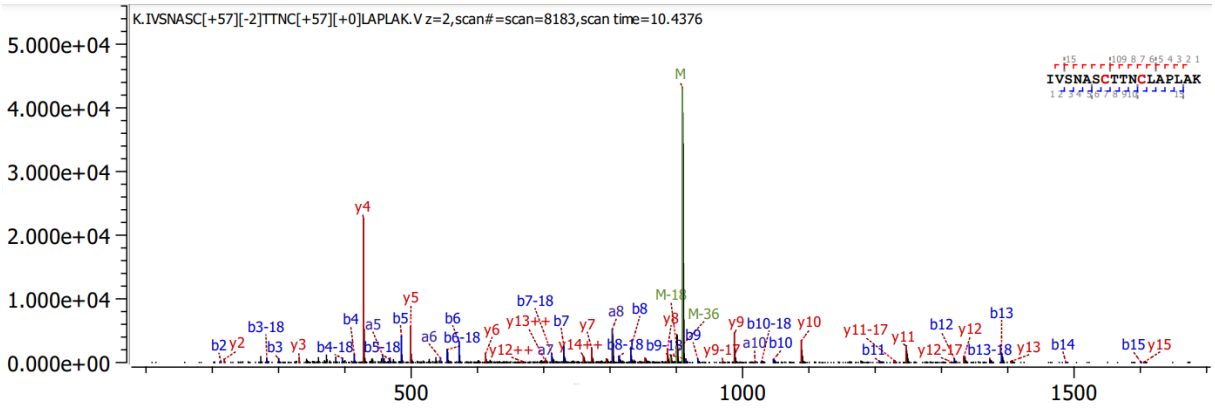

Figure GAPD.SI35. *The MS/MS spectrum of P34 of in-solution digested sample of 5 min irradiated solution of GAPDH with 3CB*

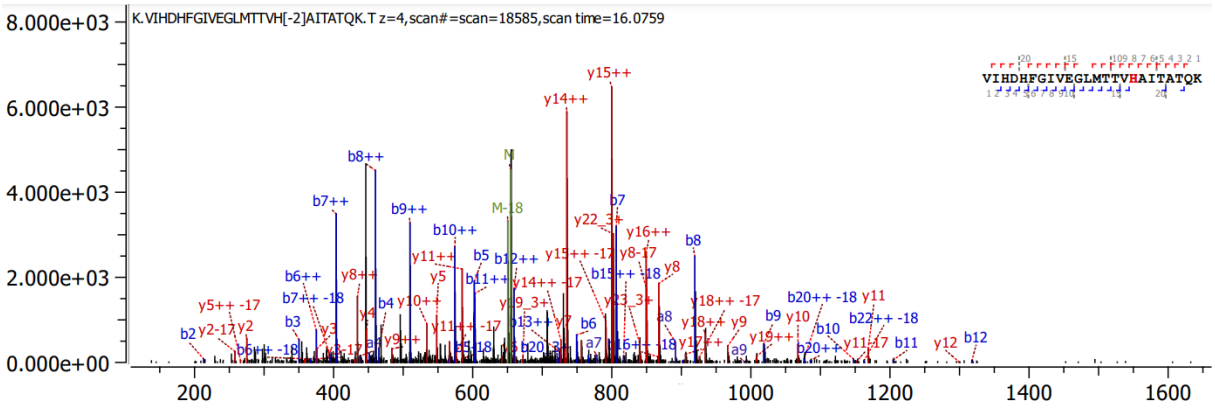

Figure GAPD.SI36. *The MS/MS spectrum of P35 of in-solution digested sample of 5 min irradiated solution of GAPDH with 3CB*

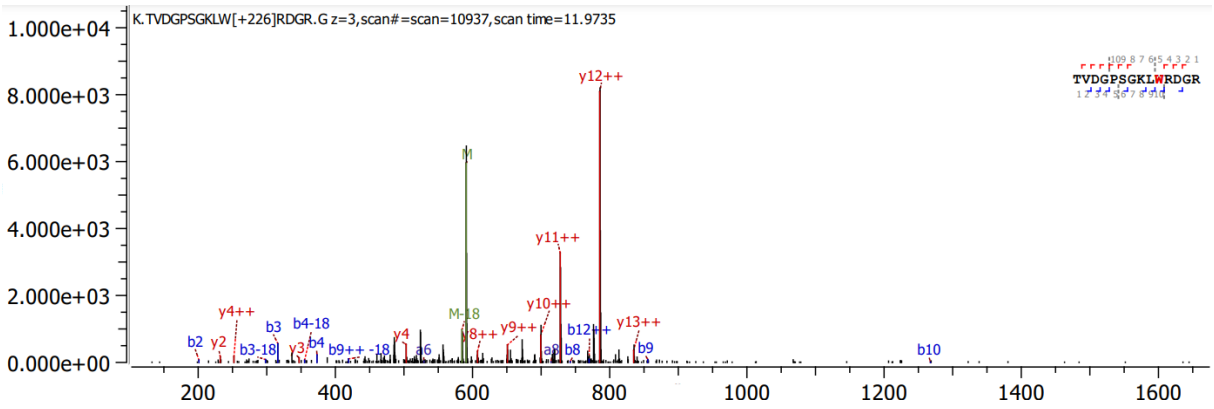

Figure GAPD.SI37. *The MS/MS spectrum of P36 of in-solution digested sample of 5 min irradiated solution of GAPDH with 3CB*

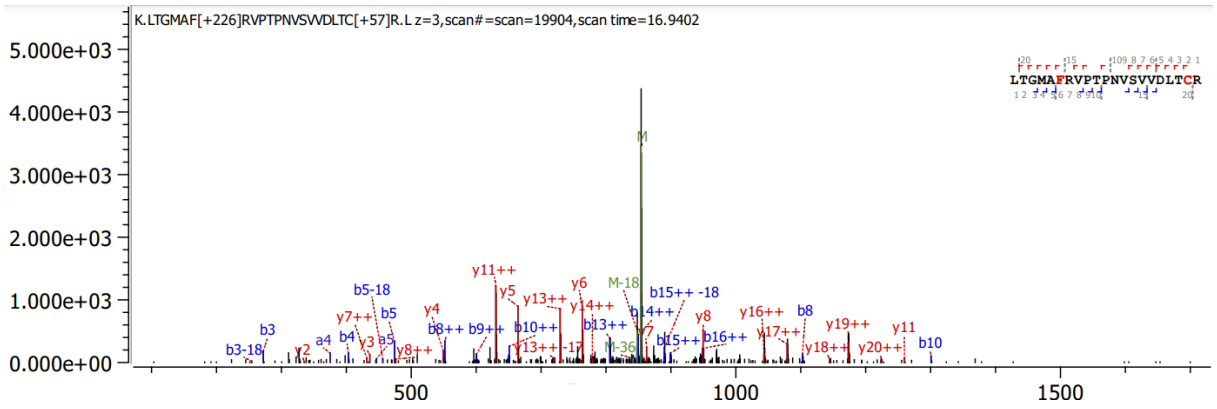

Figure GAPD.SI38. *The MS/MS spectrum of P37 of in-solution digested sample of 5 min irradiated solution of GAPDH with 3CB*

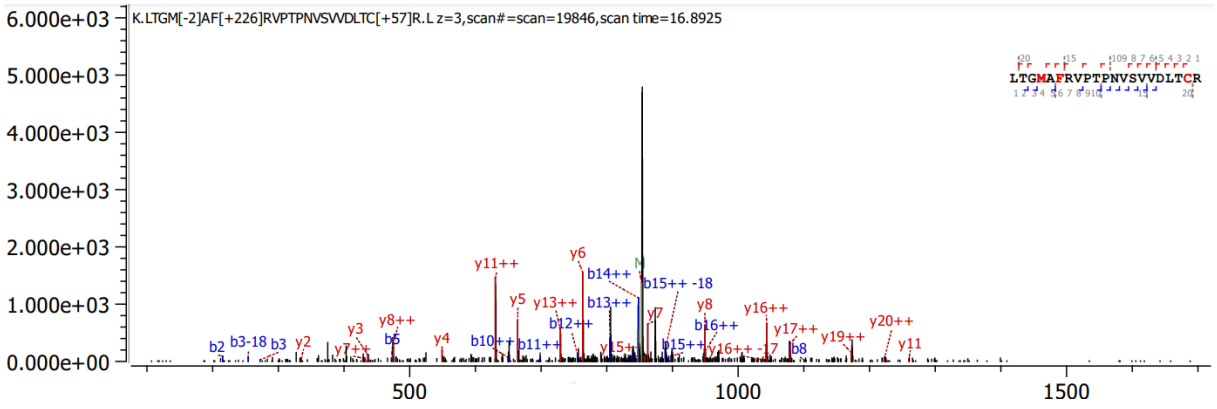

Figure GAPD.SI39. *The MS/MS spectrum of P38 of in-solution digested sample of 5 min irradiated solution of GAPDH with 3CB*

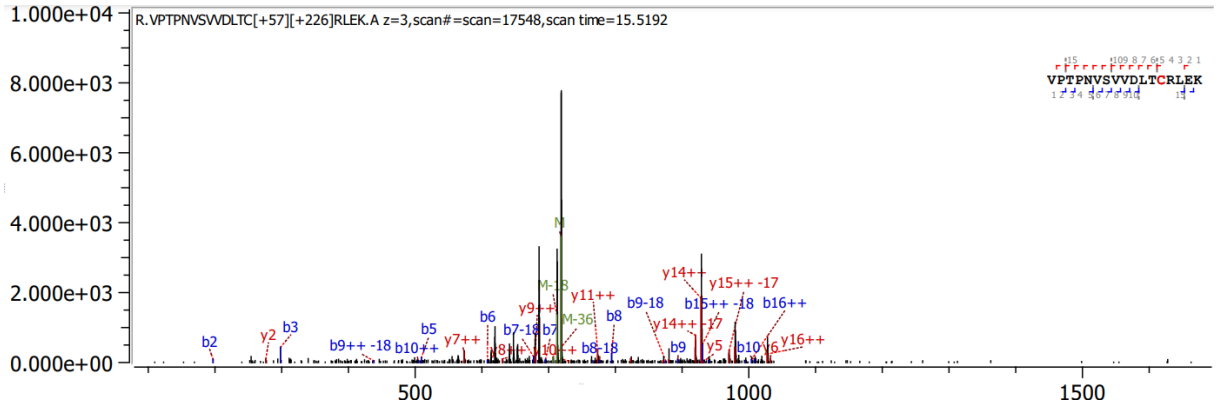

Figure GAPD.SI40. *The MS/MS spectrum of P39 of in-solution digested sample of 5 min irradiated solution of GAPDH with 3CB*

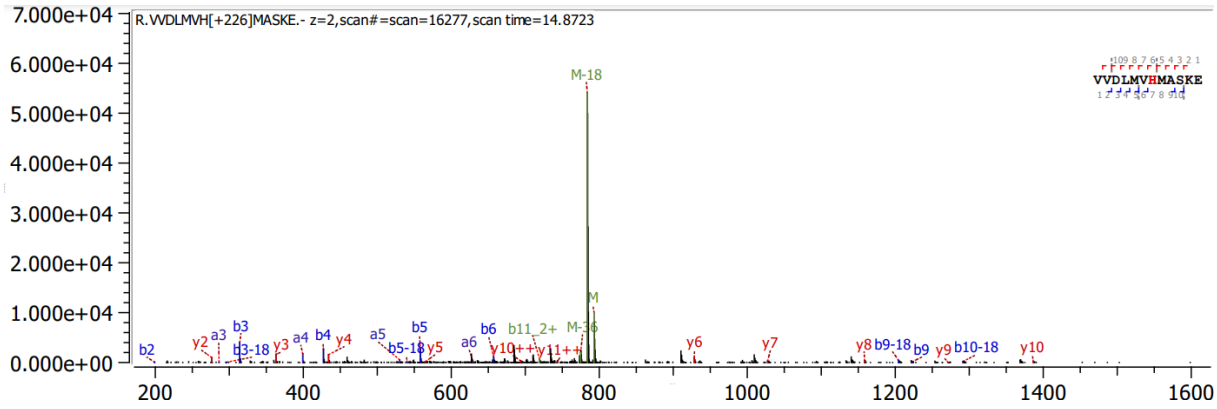

Figure GAPD.SI41. *The MS/MS spectrum of P40 of in-solution digested sample of 5 min irradiated solution of GAPDH with 3CB*

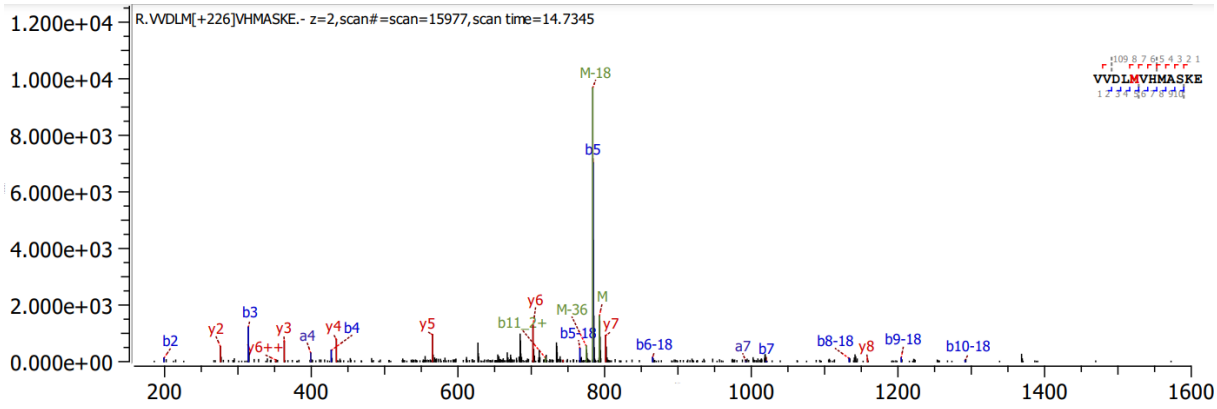

Figure GAPD.SI42. *The MS/MS spectrum of P41 of in-solution digested sample of 5 min irradiated solution of GAPDH with 3CB*

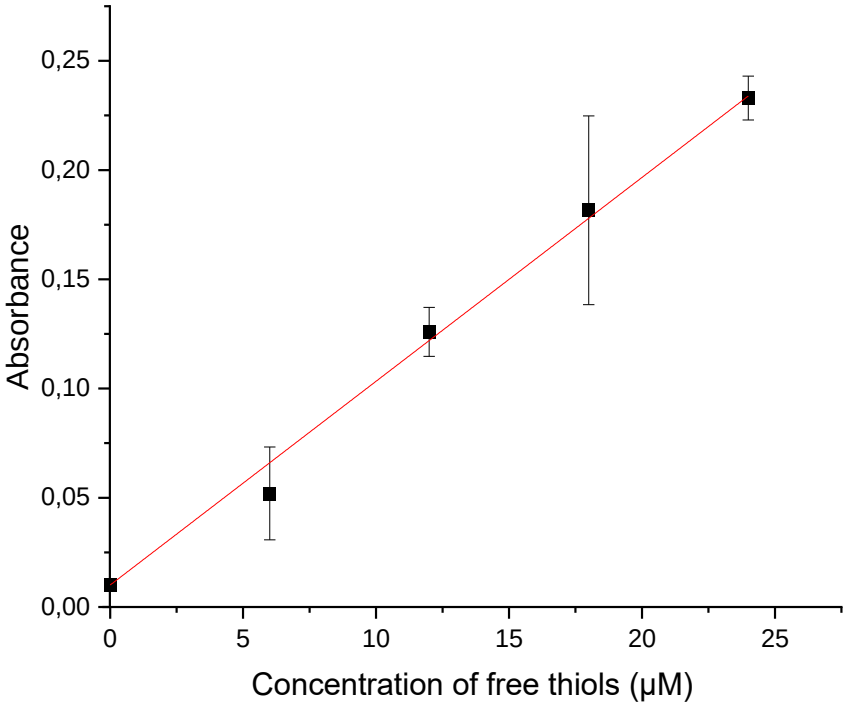

Figure GAPD.SI43. *Calibration curve that allowed for calculation of the concentration of free thiols*

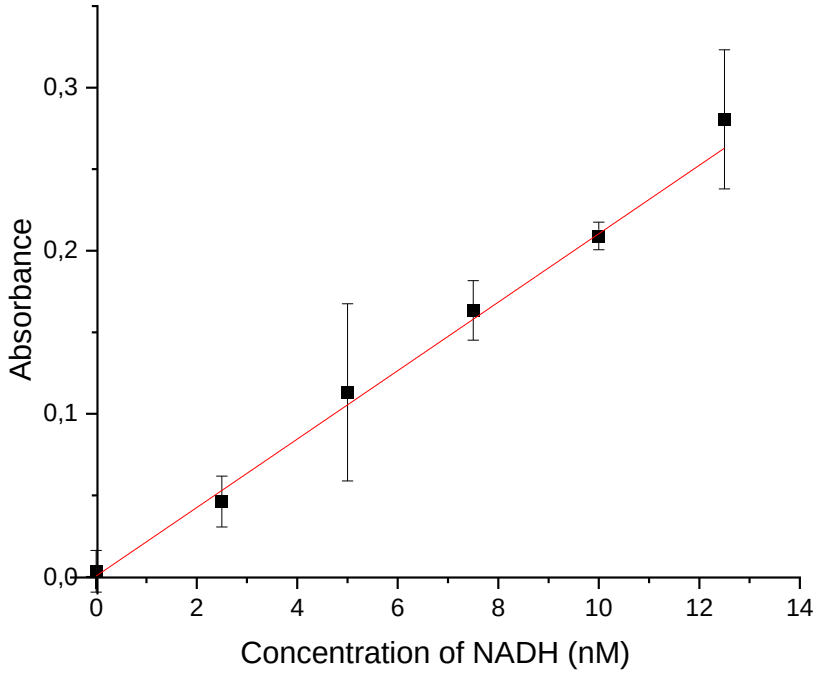

Figure GAPD.SI44. *Standard curve from which activities for each respective sample were calculated*